

**THEORETICAL AND EXPERIMENTAL INVESTIGATION ON
HEAT PIPE SOLAR COLLECTOR INTEGRATED WITH
LATENT HEAT THERMAL ENERGY STORAGE**

MOHAMMAD SAJAD NAGHAVI SANJANI

**THESIS SUBMITTED IN FULFILMENT OF THE
REQUIREMENTS FOR THE DEGREE OF DOCTOR OF
PHILOSOPHY**

**FACULTY OF ENGINEERING
UNIVERSITY OF MALAYA
KUALA LUMPUR**

2016

UNIVERSITY OF MALAYA
ORIGINAL LITERARY WORK DECLARATION

Name of Candidate: **Mohammad Sajad Naghavi Sanjani**

Registration/Matric No.: **KHA110052**

Name of Degree: **Doctor of Philosophy**

Title of Project Paper/Research Report/Dissertation/Thesis (“this work”):

Theoretical and experimental investigation on heat pipe solar collector integrated with latent heat thermal energy storage

Field of study: **ENERGY**

I do solemnly and sincerely declare that:

- (1) I am the sole author/writer of this work;
- (2) This work is original;
- (3) Any use of any work in which copyright exists was done by way of fair dealing and for permitted purposes and any excerpt or extract from, or reference to or reproduction of any copyright work has been disclosed expressly and sufficiently and the title of the work and its authorship have been acknowledged in this work;
- (4) I do not have any actual knowledge nor do I ought reasonably to know that the making of this work constitutes an infringement of any copyright work;
- (5) I hereby assign all and every rights in the copyright to this work to the University of Malaya (“UM”), who henceforth shall be owner of the copyright in this work and that any reproduction or use in any form or by any means whatsoever is prohibited without the written consent of UM having been first had and obtained;
- (6) I am fully aware that if in the course of making this work I have infringed any copyright whether intentionally or otherwise, I may be subject to legal action or any other action as may be determined by UM.

Candidate signature:

Date: 31/08/2016

Subscribed and solemnly declared before,

Witness’s Signature:

Date: 31/08/2016

Name:

Designation:

ABSTRACT

The purpose of this research is to evaluate theoretically and experimentally the thermal performance of a compact design of an evacuated tube heat pipe solar collector integrated with a latent heat storage tank. Paraffin wax is used as phase change material in the latent heat storage tank. In this design, solar energy incident on the solar tubes is collected and stored in the latent heat storage tank via the heat pipe with fins attached to the condenser ends inside the latent heat storage tank. The stored heat is then transferred to the supply water via a set of finned pipes located inside the tank. The phase change material acts as an intermediate heat storage medium between the solar collector and the hot water supply.

This design is studied in two steps. Primarily, the simplified design of the proposed system is theoretically modeled by applying sets of mathematical equations to have a basic estimation on the performance of the system. Then, after preparing the technical design of the system and constructing the experimental setup in the actual size, the field tests are carried out in two cases. First, is for charging only and discharging only modes and second, is for simultaneous charging-discharging mode.

The significances of this design could be expected in three cases. First, the prevention of overheating of the supplied water at times that the solar radiation is very strong and second is extending the performing time of the system in the evening when the system is on second mode. Third, to increase the absorbed solar energy fraction.

The results of the primary analysis show that for a large range of flow rates, the thermal performance of this design is higher than of a similar system without latent heat storage. Furthermore, the analysis shows that the efficiency of the new design is less sensitive to the hot water load than the conventional model. The field tests of the experimental setup are taken for different weather conditions, supply water flow rates and hot water draw off time. The results indicated that this design is able to perform satisfactorily in different climatic condition and water flow rates. In addition, this design makes the solar water

heater system able to collect the heat at the midday time with highest solar radiation intensity and deliver it to the supply water at the same time or hours later, while the outlet hot water is in the operating temperature range. According to the experimental results, depending on the daily solar radiation, the efficiency of the system varies in the range of 36% to 42%. Daily solar radiation and hot water load are directly proportional to the efficiency of the system. The experimental tests for simultaneous charging-discharging indicated that the system is able to produce hot water in day time and night time for domestic use in a tropic climatic region like Malaysia. Generally, it could be concluded that this design is suitable for use as a stand-alone system for hot water demands at night as part of a configuration with conventional solar water heater systems to produce hot water in duration of day and night for different patterns of hot water demand.

ABSTRAK

Tujuan kajian ini adalah untuk menilai secara teori dan uji kaji mengenai prestasi haba daripada satu pengumpul solar paip haba tiub kosong yang direka bentuk kompak bersepadu dengan tangki penyimpanan haba pendam. Parafin lilin digunakan sebagai bahan perubahan fasa untuk tangki penyimpanan haba pendam. Dalam reka bentuk ini, kejadian tenaga solar pada tiub solar dikumpul dan disimpan di dalam tangki penyimpanan haba pendam melalui paip haba dengan sirip bersambung ke kondenser berakhir ke dalam tangki penyimpanan haba pendam. Haba yang disimpan kemudiannya dipindahkan ke bekalan air melalui satu set paip bersirip terletak di dalam tangki. Bahan perubahan fasa bertindak sebagai medium penyimpanan haba perantaraan antara pengumpul solar dan bekalan air panas.

Reka bentuk ini dikaji dalam dua langkah. Terutamanya, reka bentuk yang dipermudahkan sistem yang dicadangkan itu secara teori dimodelkan dengan menggunakan set persamaan matematik untuk mempunyai anggaran asas kepada prestasi sistem. Kemudian, selepas menyediakan reka bentuk teknikal sistem dan membina persediaan eksperimen dalam saiz sebenar, ujian lapangan dijalankan dalam dua kes. Pertama, adalah untuk mod mengecas sahaja dan menyahcas dan kedua, adalah untuk memasuki mod mengecas - menyahcas secara serentak.

Signifikan reka bentuk ini boleh dijangkakan dalam tiga kes. Pertama, pencegahan bekalan air secara panas melampau pada masa-masa yang radiasi solar adalah sangat kuat dan kedua melanjutkan sistem pelaksanaan masa pada waktu petang apabila sistem berada dalam mod kedua. Ketiga, untuk meningkatkan pecahan tenaga solar yang diserap.

Keputusan analisis utama menunjukkan bahawa untuk pelbagai kadar aliran besar, prestasi haba reka bentuk ini adalah lebih tinggi daripada sistem yang sama tanpa penyimpanan haba pendam. Tambahan pula, analisis menunjukkan bahawa keberkesanan reka bentuk baru adalah kurang sensitif kepada beban air panas daripada model

konvensional. Ujian lapangan untuk persediaan eksperimen diambil dalam keadaan yang berbeza cuaca, kadar aliran air bekalan dan masa pengaliran air panas. Keputusan menunjukkan bahawa reka bentuk ini dapat melaksanakan prestasi yang memuaskan dalam keadaan iklim dan kadar aliran air yang berbeza. Di samping itu, reka bentuk ini membolehkan sistem pemanas air solar dapat menyimpan haba pada masa tengah hari dengan intensiti sinaran solar yang tertinggi dan menyalurkan kepada bekalan air pada masa yang sama atau beberapa jam kemudian manakala air panas yang keluar dipraktikkan dalam kadar suhu operasi. Menurut hasil eksperimen, bergantung kepada sinaran suria harian, keberkesanan sistem adalah berbeza-beza dalam lingkungan 36% hingga 42%. Sinaran suria harian dan beban air panas adalah berkadar terus dengan kecekapan sistem. Secara umumnya, ia boleh disimpulkan bahawa reka bentuk ini dapat menjadi sebagai satu sistem yang berdiri sendiri untuk permintaan air panas pada waktu malam atau sebahagian daripada konfigurasi dengan sistem pemanas air solar konvensional untuk menghasilkan air panas pada waktu siang dan malam untuk pola permintaan air panas yang berbeza.

ACKNOWLEDGEMENTS

I would like to thank the University of Malaya for financial support from the High Impact Research Grant (HIRG) scheme (UM-MoHE). Without this grant, I defiantly could not do my PhD.

I would like to greatly thank my supervisor, Dr. Hendrik Simon Cornelis Metselaar, for giving me the opportunity of working with his research team and creating a calm research environment. If I did not have his constant companion and great tolerance in the entire duration of the research period, without a doubt, I could not complete my PhD program. Apart from the scientific points, I learned from him that to be successful in other aspects of life, I should also have unremitting efforts while being patient. Thank him for believing in me.

I must thank my second supervisor, Dr. Irfan Anjum Badruddin, for his unlimited supports. He always was supportive and attempted to push me forward to do higher quality of the works. His office door was always open to me. I never forget his kind helps when I faced problems.

If I say my best luck in these years was getting to know Professor Kok Seng Ong, it is nothing less than truth. Prof. Ong guided me in the right direction when I was facing the hardest time. Our deep and challenging discussions about the technical issues of the research work will always remain in my mind as one of the sweetest memories. William A. Ward the American writer said “The good teacher explains; The superior teacher demonstrates; The great teacher inspires.”. I believe Dr. Ong is a great teacher.

I would like to thank my friends and colleagues Specially Mohammad Mehrali and Mahdi Mehrali, for their supports and backing. Now, it is more than seven years that we are friend and I hope it never stops.

I would like to express my gratitude to my uncle Behrooz Agharazi. He is much more than an uncle for me; he is like my elder brother and a very close friend. He always had a confidence in me. I thank him from the deep of my heart.

Finally, last but the most important, my parents, Mojtaba Naghavi and Zohreh Agharazi. They gave me my name, they gave me my life, and everything else in between. I deeply appreciate all the efforts they have put into giving me the life I have now. Success is in my stride, because I have parents like them by my side. I always pray for you to have long life in health and happiness.

University of Malaya

TABLE OF CONTENTS

Abstract	iii
Abstrak	v
Acknowledgements	vii
Table of contents	ix
List of figures	xiv
List of tables	xviii
List of symbols and abbreviations.....	xx
List of appendices	xxiv
CHAPTER 1: INTRODUCTION.....	1
1.1 Background.....	1
1.2 Research gaps	2
1.3 Research objectives	4
1.4 Research methodology.....	4
1.5 Scope of the study.....	5
1.6 Structure of the thesis	5
CHAPTER 2: LITERATURE REVIEW.....	7
2.1 Introduction.....	7
2.2 SWH systems.....	7
2.2.1 Conventional SWH systems	7
2.2.2 SWH-LHS integrated configurations	8
2.3 PCM Heat exchanger devices	13
2.3.1 Fins enhancement technique.....	13
2.3.1.1 Melting process	13

2.3.1.2	Solidification process	18
2.3.2	HP enhancement technique	20
2.4	Theoretical approaches	27
2.4.1	PCM.....	28
2.4.2	HP 33	
 CHAPTER 3: MATERIALS AND METHODS		36
3.1	Introduction.....	36
3.2	Model description	36
3.2.1	Background Art	36
3.2.2	Conceptual design	37
3.3	Theoretical model	38
3.3.1	Solar energy.....	39
3.3.2	Heat pipe surface temperature	39
3.3.3	Charging mode	40
3.3.3.1	PCM sensible heating.....	41
3.3.3.2	PCM latent heating.....	42
3.3.4	Discharging mode.....	43
3.3.4.1	Heat transfer to finned HWSHE pipe.....	45
3.3.4.2	PCM solidifying	45
3.3.5	System performance and efficiency	46
3.3.5.1	Thermal analysis of the ETHPSC baseline system	46
3.3.5.2	Usable hot water and efficiency	47
3.4	HPSC-LHS design.....	49
3.4.1	HPSC selection.....	49
3.4.2	PCM selection	51

3.4.3	Design of fin on the HPC	53
3.4.4	Design of fins on the pipe.....	54
3.5	Experimental investigation	56
3.5.1	The apparatus	56
3.5.2	Experimental procedure	59
3.5.3	Efficiency calculations	59
3.5.4	Uncertainty analysis	62
 CHAPTER 4: THEORETICAL MODEL OF THE HPSC-LHS DESIGN.....		63
4.1	Introduction.....	63
4.2	Conceptual design arrangement.....	63
4.3	Model validation.....	65
4.4	Absorbable solar energy	66
4.5	Charging mode.....	67
4.6	Discharge mode	71
4.7	Comparison with baseline system	74
4.8	Summary.....	77
 CHAPTER 5: EXPERIMENTAL STUDY PART I: CHARGING ONLY AND DISCHARGING ONLY MODES		79
5.1	Introduction.....	79
5.2	Experimental investigation	79
5.2.1	The apparatus	79
5.3	Results and discussion	80
5.3.1	Charging only mode	84
5.3.2	Discharging only mode	89

5.4	System efficiency.....	95
5.4.1	Estimation of the melted fraction of the PCM	96
5.4.2	System thermal efficiency	98
5.5	Summary.....	101
CHAPTER 6: EXPERIMENTAL STUDY PART II: SIMULTANEOUS CHARGING-DISCHARGING MODE		102
6.1	Introduction.....	102
6.2	Hot water load profile	102
6.3	Results and discussion	104
6.3.1	Nonconsecutive runs	104
6.3.2	Consecutive runs	108
6.4	Summary.....	110
CHAPTER 7: CONCLUSIONS AND RECOMMENDATIONS		112
7.1	Conclusions	112
7.2	Recommendations.....	115
	References	117
	List of publications and papers presented	129
	Appendix A: Absorbable solar energy calculation	130
	Appendix B: Theoretical solution algorithm.....	132
	<i>B.1. HPSC-PCM system – Charging mode</i>	<i>132</i>
	<i>B.2. HPSC-PCM system – discharging model.....</i>	<i>133</i>
	<i>B.3. Baseline HPSC system</i>	<i>134</i>
	Appendix C: MATLAB code for theoretical analysis	135
	Appendix D: CAD drawings of Fins and LHS tank	149

Appendix E: Tables of data of Chapter 5.....	156
Appendix F: Tables of data of Chapter 6.....	180

University of Malaya

LIST OF FIGURES

Figure 1.1: Distribution of the newly installed capacity by collector type in 2012 – WORLD (Mauthner, 2012).....	2
Figure 2.1: A: Layout of the domestic SWH-PCM system; B: Arrangement of the PCM cylinders in the Tank (Talmatsky & Kribus, 2008).	9
Figure 2.2: Schematic presentation of the integrated solar collector storage system with PCM (Eames & Griffiths, 2006).	10
Figure 2.3: Water-PCM storage for use with conventional SWH system (Al-Hinti et al., 2010).	11
Figure 2.4: Cross-sectional view of the TES tank design (Canbazoglu et al., 2005).....	12
Figure 2.5: Optimum design for fin distance as a function of Rayleigh number (Lacroix & Benmadda, 1998).	16
Figure 2.6: Shell and tube LHS unit with the PCM on the shell side and the HTF flowing inside (Lacroix, 1993).	17
Figure 2.7: Effect of different fin material and thickness on its thermal enhancement (Zhang & Faghri, 1996).	19
Figure 2.8: Models of finned heat pipe heat exchanger elements (Abhat, 1978).	20
Figure 2.9: The HP-LHS heat exchanger system (Horbaniuc et al., 1996).	22
Figure 2.10: PCM unit configuration during charging and discharging (Shabgard et al., 2012).	23
Figure 2.11: Two HP-PCM heat exchanger configurations; (a) module 1, (b) in module 1 the PCM surrounds the HTF tubes, (c) module 2, (d) in module two the PCM is placed inside the tubes and the HTF flows perpendicular to the tube (Shabgard et al., 2010). .	24
Figure 2.12: Physical model of the HP-PCM system; (A) when PCM is in condenser region (Sharifi et al., 2012), (B) when PCM is in condenser region with foil (Sharifi et al., 2014), (C) when PCM is in middle of the heat pipe (Sharifi et al., 2015).	26
Figure 2.13: A network system for the heat pipe operation. (a) A sketch of the heat pipe heat transfer. (b) A network analogy of the heat pipe heat transfer (Zuo & Faghri, 1998).	34
Figure 3.1: ETHPSC-PCM system.	37
Figure 3.2: Simplified model of conventional and introduced HPSC systems.....	38

Figure 3.3: Heat pipe cross section.	40
Figure 3.4: Arrangement of PCM slabs.	44
Figure 3.5: Passive Tracking by solar tube collector.	49
Figure 3.6: Glass tube and HP with aluminum fin.....	50
Figure 3.7: FT-IR analysis of the paraffin wax provided by Sigma Aldrich co.	52
Figure 3.8: DSC curves for melting and solidification of the paraffin wax.....	52
Figure 3.9: Fin shell on HPC (side view and 3D view).	53
Figure 3.10: CAD drawing of the spring circular fins on the pipe.	54
Figure 3.11: Schematic of piping design.....	55
Figure 3.12: Schematic of experimental setup.	57
Figure 3.13: a. Photo of HPSC-LHS experimental setup, b. Photo of inside of the LHS tank.....	57
Figure 3.14: The thermocouples locations.	58
Figure 4.1: Heat transfer process in LHS tank.....	64
Figure 4.2: Fins designs for the HPC (top) and the HWSHE (bottom).	64
Figure 4.3: Comparison of the interface location.....	66
Figure 4.4: Recorded solar radiation and ambient temperature.	67
Figure 4.5: PCM temperature history for high (a) and low (b) daily solar radiation days.	68
Figure 4.6: Liquid-solid interface in charging mode.	69
Figure 4.7: HPE, HPC and PCM temperatures.	70
Figure 4.8: Outlet supply water temperature in HPSC-LHS design for different flow rates.	72
Figure 4.9: Progression of solid-liquid interface in slabs 1, 5, 10, 15 and 20 for different flowrates.	73
Figure 4.10: Outlet water temperature (T_w, b, o) for baseline HPSC system.	74

Figure 4.11: Comparison of efficiency and usable hot water volume for different flow rates.	75
Figure 4.12: Comparison of HPE and the HPC temperature at two supply water flow rates.	76
Figure 5.1: Solar radiation and ambient temperature in day time for runs in case 1.	82
Figure 5.2: Solar radiation and ambient temperature in day time for runs in case 2.	83
Figure 5.3: The PCM temperature increase in the middle and bottom of the tank in charging mode for runs 1-3 and 4-6.	85
Figure 5.4: The PCM temperature growth in middle and bottom of the tank in charging mode for runs 7-9 and 10-12.	86
Figure 5.5: The HP sections wall temperatures versus the PCM temperature at the middle of the tank for runs 1-6.	87
Figure 5.6: The HP sections wall temperatures versus the PCM temperature at the middle of the tank for runs 7-12.	88
Figure 5.7: The hot water outlet temperature for three flow rates.	90
Figure 5.8: The hot water outlet temperature for three flow rates.	91
Figure 5.9: The PCM temperature change at the middle of the tank during the discharge operation.	92
Figure 5.10: The PCM temperature change at the middle of the tank during discharging.	93
Figure 5.11: The HP sections wall temperatures versus the PCM temperature at the middle of the tank in discharging operation for runs 1-6.	94
Figure 5.12: The HP sections wall temperatures versus the PCM temperature at the middle of the tank in discharging operation for runs 7-12.	95
Figure 5.13: The PCM maximum temperature in the bottom and the middle of the tank versus total daily radiation.	97
Figure 5.14: The PCM mean temperature and melted fraction.	98
Figure 5.15: Overall thermal efficiency variations of the system with uncertainty range.	100
Figure 6.1: Hot water draw off profiles.	103

Figure 6.2: The experimental results for run N-H-100.	105
Figure 6.3: The experimental results for run N-L-100.....	106
Figure 6.4: The experimental results for run N-H-150.	107
Figure 6.5: The experimental results for run N-L-150.....	107
Figure 6.6: The experimental results for run Y-H-100.	109
Figure 6.7: The experimental results for run Y-L-100.....	109
Figure 6.8: The experimental results for run Y-H-150.	111
Figure 6.9: The experimental results for run Y-L-150.....	111
Figure D.1: CAD design of the fin shell, which HP condenser will be inserted into that.	149
Figure D.2: CAD drawing of the LHS tank.	150
Figure D.3: CAD drawing of the LHS tank cover.	151
Figure D.4: CAD drawing of the discharging valve cover.	152
Figure D. 5: Isotropic view of the HPSC-LHS system.	153
Figure D. 6: side view of the HPSC-LHS system.....	153
Figure D. 7: Heat exchange arrangement of the TES tank of the HPSC-LHS system (Side view).....	154
Figure D. 8: Heat exchange arrangement of the TES tank of the HPSC-LHS system (Isotropic view).	154
Figure D. 9: Heat pipe and its fin shell arrangement in the heat pipe condenser side heat exchanger (Isotropic view).....	155

LIST OF TABLES

Table 3.1: Specifications of the evacuated tube solar collector.	51
Table 3.2: Specifications and dimensions of the HP.	51
Table 3.3: Physical properties of the Paraffin Wax.	52
Table 4.1: Dimensions of LHS tank and fins for theoretical analysis.	65
Table 5.1: Dimensions of the experimental setup.	80
Table 5.2: Summary of the runs.	81
Table 5.3: The PCM initial and maximum temperature.	97
Table 5.4: Cumulative energy and efficiencies from runs 1-6.	99
Table 5.5: Cumulative energy and efficiencies from runs 7-12.	99
Table 6.1: Summary of the runs.	104
Table E. 1: Data of run 1.	156
Table E. 2: Data of run 2.	158
Table E. 3: Data of run 3.	160
Table E. 4: Data of run 4.	162
Table E. 5: Data of run 5.	164
Table E. 6: Data of run 6.	166
Table E. 7: Data of run 7.	168
Table E. 8: Data of run 8.	170
Table E. 9: Data of run 9.	172
Table E. 10: Data of run 10.	174
Table E. 11: Data of run 11.	176
Table E. 12: Data of run 12.	178

Table F. 1: Data for run 1.....	180
Table F. 2: Data for run 2.....	182
Table F. 3: Data for run 3.....	184
Table F. 4: Data for run 4.....	186
Table F. 5: Data for run 5.....	188
Table F. 6: Data for run 6.....	190
Table F. 7: Data for run 7.....	192
Table F. 8: Data for run 8.....	194

University of Malaya

LIST OF SYMBOLS AND ABBREVIATIONS

Symbols

$A_{c,c}$:	Cross section area of the fin on HPC
$A_{f,c}$:	Face area of the fin on the HPC
A_p	:	Pipe inner surface area
A_{tank}	:	LHS tank Surface area
A_{sc}	:	Solar collector apparatus area
$c_{p,l}$:	Specific heat of liquid PCM
$c_{p,s}$:	Specific heat of solid PCM
$c_{p,w}$:	Specific heat of water
$d_{p,i}$:	Pipe inner diameter
$d_{t,o}$:	HPSC glass outer diameter
$d_{t,i}$:	HPSC glass inner diameter
d_w	:	Mesh wire diameter
d_t	:	Glass tube outer diameter
E_d	:	Total delivered energy
F_{melt}	:	Molten PCM fraction
g	:	Gravity
G_{sc}	:	Extraterrestrial radiation
$h_{f,c}$:	Fin height on the condenser
$h_{f,p}$:	Fin height on pipe
h_{pcm}	:	Heat transfer coefficient in PCM
h_{st}	:	Storage tank height
h_w	:	Heat transfer coefficient in water
I_b	:	Beam solar radiation
I_d	:	Diffuse solar radiation
I_g	:	Solar radiation diffusely
I_T	:	Total incident radiation
k_{eff}	:	Effective thermal conductivity of wick
$k_{f,c}$:	Thermal conductivity of fin on condenser
$k_{f,p}$:	Thermal conductivity of fin on pipe
k_{ins}	:	LHS tank insulation thermal conductivity
k_l	:	Thermal conductivity of liquid PCM
k_s	:	Thermal conductivity of solid PCM
k_T	:	Hourly clearness index
k_w	:	Thermal conductivity of heat pipe wall
l_a	:	Length of heat pipe adiabatic region
l_c	:	Length of heat pipe condenser region
l_e	:	Length of heat pipe evaporator region
$l_{f,c}$:	Fin length on the condenser
$l_{f,p}$:	Fin length on pipe
l_p	:	Length of solar absorber plate
l_{st}	:	Storage tank length
$l_{st,s}$:	Length of a section of the storage tank
L	:	Latent heat of PCM
Lr	:	Usable volume loss rate percentage
\dot{m}_w	:	Water mass flow rate

m_w	:	Mass of the stored hot water in water storage tank
n	:	Number of the day in year
N_a	:	Number of apertures per unit length of wick
N_c	:	Tenths cloud cover
N_f	:	Number of the fins
N_g	:	Reflective Index of glass
N_t	:	Number of HPSCs
$P_{f,c}$:	Perimeter of the fin on HPC
q	:	Heat flux
$r_{o,hpa}$:	Heat pipe adiabatic outer radius
$r_{o,hpe}$:	Heat pipe evaporator outer radius
$r_{o,hpc}$:	Heat pipe evaporator outer radius
$r_{v,hpa}$:	Vapor core radius at adiabatic section
$r_{v,hpe}$:	Vapor core radius at evaporator section
$r_{w,hpa}$:	Wick radius at adiabatic section
$r_{w,hpe}$:	Wick radius at evaporator section
R_b	:	Beam contribution ratio
R_{hp}	:	HP overall thermal resistance
$R_{hp,c,o}$:	HPC thermal resistance to surrounding
$R_{hp,c,p}$:	HPC wall thermal resistance
$R_{hp,c,w}$:	HPC wick thermal resistance
$R_{hp,i}$:	HP internal liquid resistance
$R_{hp,e,p}$:	HPE wall thermal resistance
$R_{hp,e,w}$:	HPE wick thermal resistance
S	:	Absorbed solar energy
St	:	Stefan number $[=c_l \Delta T_l / L]$
t	:	Time
t_{CHE}	:	PCM thickness in CHE mode
t_{DHE}	:	PCM slab thickness in DHE mode
$t_{f,CHE}$:	Thickness of fin on heat pipe
$t_{f,DHE}$:	Thickness of fin on water pipe
t_{hp}	:	Thickness of the heat pipe wall
t_{wck}	:	Thickness of the wick
T_{amb}	:	Ambient temperature
T_f	:	Film temperature
$T_{hp,c}$:	HPC surface temperature
$T_{hp,a}$:	HPA surface temperature
$T_{hp,e}$:	HPE surface temperature
T_m	:	PCM melting temperature
T_{pcm}	:	PCM temperature
$T_{pcm,m}$:	PCM temperature in middle of the LHS tank
$T_{pcm,b}$:	PCM temperature in the bottom of the LHS tank
\bar{T}_{pcm}	:	PCM mean temperature in the LHS tank
T_s	:	Cold water temperature
T_u	:	Water operating temperature
$T_{w,b,i}$:	Inlet water temperature in baseline system
$T_{w,b,o}$:	Outlet water temperature in baseline system
$T_{w,c}$:	Inlet cold water temperature

$T_{w,i,i}$:	Inlet water temperature in innovative system
$T_{w,i,o}$:	Outlet water temperature in innovative system
$T_{w,h}$:	Outlet hot water temperature
$T_{w,t,i}$:	Inlet water temperature to water storage tank
$T_{w,t,o}$:	Outlet water temperature from water storage tank
V_u	:	Usable volume of hot water
$V_{u,d}$:	Destroyed usable volume of hot water
$V_{u,r}$:	Remained usable volume of hot water
w_{st}	:	Storage tank width
x_{ins}	:	LHS tank insulation thickness
X_{pcm}	:	Liquid-solid location in PCM slab
Y_{pcm}	:	Solid-liquid location in PCM slab

Greeks

α	:	Tilted incidence
α_n	:	Normal incidence of glass
α_s	:	Thermal diffusivity [= $k_s/\rho_s c_s$]
β_s	:	Slope of solar collector
β_e	:	Expansion coefficient of the PCM
γ	:	Surface Azimuth angle
δ	:	Declination
ε	:	Porosity
ε_g	:	Glass emittance
ε_p	:	Plate emittance
ε_s	:	Sky emissivity
θ	:	Angle of incidence
θ_z	:	Zenith angle
λ	:	Longitude
ρ_i	:	Diffuse reflectance of that surface
ρ_g	:	Diffuse reflectance of the ground
ρ_l	:	Liquid PCM density
ρ_s	:	Solid PCM density
ρ_w	:	Water density
μ_{pcm}	:	Dynamic viscosity of the PCM
μ_w	:	Dynamic viscosity of the water
v_w	:	Mean velocity of water inside the pipe
$(\tau\alpha)$:	Appropriate transmittance-absorptance
ϕ	:	Latitude
ω	:	Hour angle
η	:	Efficiency

Abbreviations

CHE	:	Charging heat exchange process
DHE	:	Discharge heat exchange process
ETHPSC	:	Evacuated tube heat pipe solar collector
HP	:	Heat pipe
HPA	:	Heat pipe adiabatic section
HPC	:	Heat pipe condenser section
HPE	:	Heat pipe evaporator section
HPSC	:	Evacuated tube heat pipe solar collector
HPSC-B	:	Evacuated tube heat pipe solar collector-Baseline model
HTF	:	Heat transfer fluid
HWSHE	:	Hot water supply heat exchanger
IPSWH	:	Integrated passive solar water heater
LHS	:	Latent heat storage
PCM	:	Phase change material
PSWH	:	Passive solar water heater
SHS	:	Sensible heat storage
SEA	:	Solar energy absorption
SWH	:	Solar water heater
TES	:	Thermal energy storage

University of Malaya

LIST OF APPENDICES

Appendix A: Absorbable solar energy calculation.....	130
Appendix B: Theoretical solution algorithm.....	132
Appendix C: MATLAB code for theoretical analysis.....	135
Appendix D: CAD drawings of Fins and LHS tank.....	149
Appendix E: Tables of data of Chapter 5.....	156
Appendix F: Tables of data of Chapter 6.....	180

University of Malaya

CHAPTER 1: INTRODUCTION

1.1 Background

Thermal energy transport and conversion play a very significant role in more than 90% of energy technologies (Mathur, 2011). This fact increased attraction of researchers to investigate on thermal performance improvement of all applications such as space and water heating, waste heat utilization, cooling and air-conditioning (Regin et al., 2008). These years, one of the major research topics in this field is finding and improving the techniques and mechanisms for effective thermal energy storage (TES). The TES systems must be able to play their role in thermal energy transmission management of various mechanisms. A majority of the researches on TES are closely connected to utilization of the renewable energy sources like solar energy and the storage of the absorbed energy.

The necessity of using solar energy in recent years has become a popular belief. Energy potential of this renewable energy source has proven to be the most accessible worldwide, simplicity of technology, and manageability of the energy consumption. By the end of 2012, the installed capacity of solar thermal systems in 58 countries was 269.3 GWh, corresponding to a total of 384.7 million square meters of collector area (Mauthner, 2012). Solar water heating (SWH) is one of the major applications for low temperature solar thermal systems. SWH systems are mostly available in two forms of flat plate and evacuated tube collectors. Most evacuated tube collectors in use in middle Europe use heat pipes (HPs) for their core instead of passing liquid directly through them (Mahjouri, 2004). As shown in Figure 1.1, with a share of 81%, evacuated tube collectors are by far the most important solar thermal collector technology worldwide (Mauthner, 2012).

Beside SWS techniques, efficient storage and time-wise usage of the hot water is an important issue. To reach to the highest possible fraction of the solar thermal energy absorption, it is necessary to collect the heat continuously in day time and store it for

longer periods of time. Hot water storage in form of sensible heat requires large volumes of space and additional devices such as immersed electrical heater, agitator to reduce stratification effect in water storage tank and controllers. Moreover, healthy and cleanness of the stored water and the tank become a considerable issues. Alternative storage technologies, such as latent heat storage (LHS) systems with phase change materials (PCMs) could be a new way to store the heat.

1.2 Research gaps

In contrast to a sensible heat storage (SHS) material which absorbs and releases energy essentially uniformly over a broad temperature range, a PCM absorbs and releases a large quantity of energy in the vicinity of its melting/freezing point. In addition to their LHS capacity, the PCMs also store and release sensible energy as well. Thus, the latent heat capacity of PCMs is always augmented to a significant extent by their sensible heat capacity. The TES in latent heat form is capable to store two to four times as much energy as sensible heat in a temperature range of 49°C to 60°C during the daytime (Sharma et al., 2009). This would also increase the collector energy absorption fraction by reducing energy losses and also omits the stratification effect in hot water tank. However, poor thermal conductivity (usually 0.1–0.6 W/(m.K)) of PCMs drastically affects their thermal performance, which in turn limits their practical application (Zalba et al., 2003). Hence,

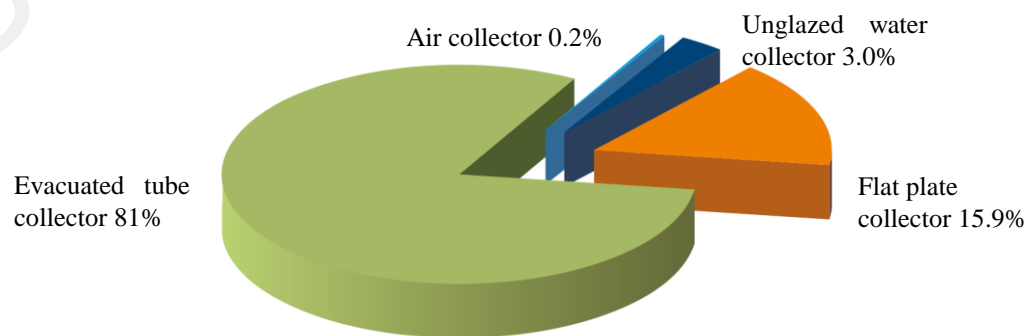


Figure 1.1: Distribution of the newly installed capacity by collector type in 2012 – WORLD (Mauthner, 2012).

several models and techniques have been applied to improve thermal conductivity and optimize the performance of LHS systems, like including finned tubes of different configurations, bubble agitation, shell and tube (multi tubes), micro-encapsulating the PCM, insertion of metal matrix into the PCM and heat pipe (HP). The HP, as one of these techniques, is a highly effective passive device for transmitting heat at high rates over considerable distances with extremely small temperature drops, exceptional flexibility, simple construction, and easy control with no external pumping power (Faghri, 2014).

Several configurations of SWH systems, which were integrated with PCMs have been developed and analyzed theoretically or experimentally within the past few years (Benli & Durmuş, 2009; Buckles & Klein, 1980; Eames & Griffiths, 2006; Koca et al., 2008; Kousksou et al., 2011; Lenel & Mudd, 1984; Malvi et al., 2011; Mazman et al., 2009; Saman et al., 2005; Varol et al., 2010; Wu & Fang, 2011; Zeng et al., 2009). The overwhelming of all proposed systems is the integration of the PCM to the SHS tank. In these researches, the PCMs were added as immersed rectangular or cylindrical slabs inside the SHS tank.

From the reviews on recent relevant researches, the most notable shortcomings that reveals from the literature survey are as below:

1. To the author' knowledge, although there are few research works on the combination of heat pipe solar collectors and PCM in storage tanks (Horbaniuc et al., 1999; Nithyanandam & Pitchumani, 2011; Sharifi et al., 2014), there is no work done on a compact design of a SWH-LHS systems such that the PCM is the only TES and acts as an intermediate heat exchanger between the solar collector and the supply water.
2. There is little work on performance of evacuated tube heat pipe solar water heater systems in direct integration with PCM.
3. Finding a new technique/design for SWH system with LHS unit is still a challenge for researchers. Minimizing the effects of hot water overheating at time with strong

radiation and increasing the solar heat absorption fraction are some of the contents of this challenge.

1.3 Research objectives

The objectives of this research are:

1. To design and develop a system of heat pipe solar collector (HPSC), which includes latent heat storage (LHS)
2. To model mathematically the performance of the proposed HPSC-LHS system
3. To experimentally test the proposed system for different water flowrates, different solar intensity etc.

1.4 Research methodology

According to the objectives, the first part of the study is the feasibility examination of the system by modelling the simplified model of the proposed design. For this purpose, a set of mathematical equations for modeling the solar absorption process, heat pipe operation, heat storage to and release from the PCM and heat transfer to the hot water is prepared. Then, the computations are performed by programming the solution in MATLAB.

Next step is design and fabrication the LHS tank and preparation of the experimental setup for field tests. The design of the LHS tank is covered all the previous findings of other researchers regarding the effective design of the fins for HP-PCM configuration, the effective design of the fins for heat transfer between PCM and water pipelines and the most suitable PCMs for heat storage.

The test is carried out in two steps. One, is for charging only mode in the day time and discharging only mode in the night time. The effect of the weather conditions (days with high/low solar radiation intensity), flow rates and discharge time on the thermal

performance and efficiency of the system will be assessed. In second step, the simultaneous charging-discharging operation of the system will be tested. Parameters such as the hot water consumptions pattern in domestic patterns, weather conditions and hot water production capacity are taken into account.

1.5 Scope of the study

The study was limited to an investigation of the development of a new design of a SWH system by employing an evacuated tube heat pipe solar collector (HPSC), which is directly integrated with the a LHS tank. This study explores the performance of the proposed system as a compact design of the HPSC-LHS system.

1.6 Structure of the thesis

This dissertation comprises seven chapters.

Chapter 1 provides a basic introduction to the study and briefly presents the motivation for the study, its focus, goals and objectives and research approaches.

Chapter 2 provides a context for the research by study the relevant literature on previous developments on HPSC-LHS systems, HP-PCM configurations, effective fin designs and suitable PCMs for this work.

Chapter 3 provides the detail expressions of the proposed model as well as the theoretical modelling method and the experimental test procedures.

Chapter 4 contains the results and discussions relevant to the theoretical study of the HPSC-LHS system.

Chapter 5 contains the experimental tests of the HPSC-LHS system for charging only mode and discharging only mode.

Chapter 6 contains the experimental tests of the HPSC-LHS system for simultaneous charging-discharging mode.

Chapter 7 provides a conclusion of the research and prepares a list of recommendations for further studies and opportunities.

University of Malaya

CHAPTER 2: LITERATURE REVIEW

2.1 Introduction

According to objectives of this research, studies are limited to fields of SWH systems integrated with LHS units (SWH-LHS), techniques to improve the melting/solidification rates in the PCM, and analytical/numerical simulation methods.

2.2 SWH systems

In this section, first, an overview of the various SWH systems will be considered and then, in second part, SWH systems which were integrated with PCM as LHS unit will be assessed.

2.2.1 Conventional SWH systems

Normally, SWH systems categorizes in two forms: one is open/close loop systems and two is active/passive systems. Direct or open loop systems circulate potable water through the collectors, while indirect or closed loop systems use a heat exchanger that separates the potable water from the fluid, known as the heat transfer fluid (HTF) that circulates through the collector. After being heated in the panels, the HTF flows to the heat exchanger, where its heat is transferred to the potable water. Open loop systems are relatively cheap but they have mainly two drawbacks, which are no overheat protection - unless they have a heat export pump - and collectors accumulate scale in hard water areas - unless an ion-exchange softener is used.

In other form, active SWH systems use one or more pumps to circulate water and/or heating fluid in the system, while passive SWH systems (PSWH) rely on heat-driven convection or heat pipes (HPs) to circulate water or heating fluid in the system. PSWH systems – in comparison with active ones - are usually more simple, reliable, and cost-

effective method of harnessing the sun's thermal energy to provide required hot water of households. Similar to the open loop mode, overheating is also a drawback of these systems. The key factor in design of a PSWH is its ability to collect, store and release the solar heat in demanded time. In either classes of conventional PSWH systems, the thermal energy stores as hot water in the form of the sensible heat.

Several comparative studies have indicated that the average efficiency of HPSC system is higher than flat plate SWH system (Ayompe et al., 2011; Kim & Seo, 2007; Zambolin & Del Col, 2010). Although, Nkwetta and Smyth (2012) reported that in most climates, flat-plate collectors will generally be more cost-effective than evacuated tubes, but the optical efficiency of the flat plate collector in the morning and in the afternoon hours decreases due to more reflection losses. Zambolin and Del Col (2010) reported that in the daily tests the HPSC displays a higher efficiency for a larger range of operating conditions, as compared to the flat plate collector.

2.2.2 SWH-LHS integrated configurations

The main advantages of PCMs are high storage density, high energy security for supplying of energy, isothermal operation, and easy construction to the system (Akgün et al., 2007). Within the past few years, several researches have been conducted theoretically and experimentally to incorporate the advantages of the PCM as a TES units on SWH systems (Benli & Durmuş, 2009; Buckles & Klein, 1980; Eames & Griffiths, 2006; El Qarnia & Adine, 2010; Jegadheeswaran et al., 2011; Jung & Boo, 2014; Koca et al., 2008; Kousksou et al., 2011; Lenel & Mudd, 1984; Malvi et al., 2011; Mazman et al., 2009; Saman et al., 2005; Sharma et al., 2000; Talmatsky & Kribus, 2008; Varol et al., 2010; Wu & Fang, 2011). In almost all of these researches, the PCM was placed inside the hot water storage tank or in the position of the heat exchange devices with macro-encapsulated packs (Al-Hinti et al., 2010; Ibáñez et al., 2006; Khalifa et al., 2013;

Nallusamy et al., 2007). Overall, reports showed that under certain conditions such as system configuration, PCM type, inlet fluid temperature, inlet flow rate and discharge process, there might be improvement on the performance of the system.

In a research work by Talmatsky and Kribus (2008) on the performance enhancement of a SWH system, which the PCM was arranged in cylindrical containers spaced apart in each layer, in order to increase the surface area for convection between the PCM and hot water (Figure 2.1). They concluded that integrating PCM as a container in the water storage tank of the domestic SWH system may not be substantially beneficial, because the system is very sensitive to the PCM parameters. Therefore, it may lead to unreliable results or failure in the system. Although, later, Kousksou et al. (2011) argued this conclusions by over studying the same model. They attempted to find out some possibilities for using PCMs in SWH systems. They concluded that the high sensitivity of the SWH system to the choice of first order design parameters such as the PCM melting temperature may open the perspective of successfully designing of a SWH-LHS system.

Esen et al. (1998) investigated on the effect of various PCM cylindrical package on the thermal performance of a SHS tank in an arrangement similar to the model of (Kousksou et al.). In their model, the SHS tank was linked to a solar assisted heat pump by means of a chiller for use as a heat source. At day time, the heat collects and transfers

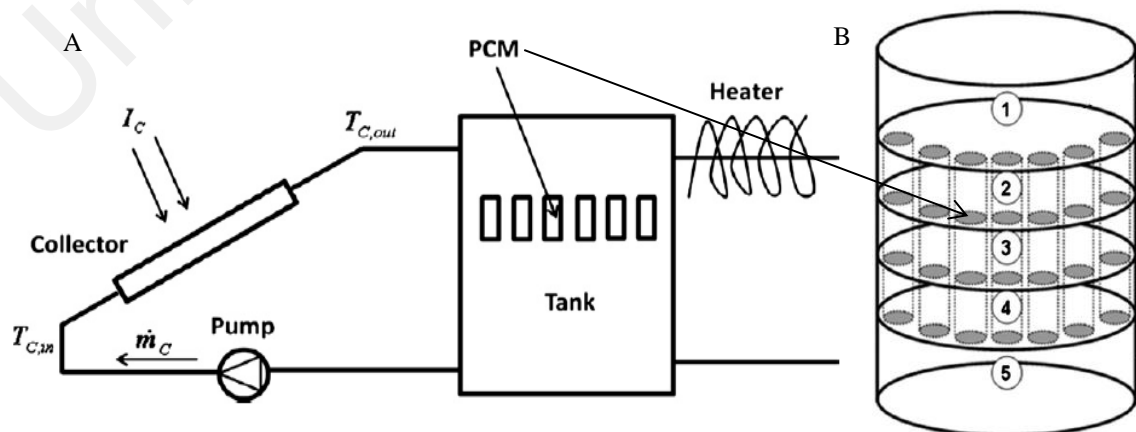


Figure 2.1: A: Layout of the domestic SWH-PCM system; B: Arrangement of the PCM cylinders in the Tank (Talmatsky & Kribus, 2008).

to the SHS tank. Then, the stored heat provides the space-heating load. It was found, theoretically, that calcium chloride hexahydrate stores heat much faster than other type of the PCMs.

Eames and Griffiths (2006) developed a solar collector with storage system which was filled with water and various concentrations of PCM slurries with melting point of 65°C (Figure 2.2). It was found that the PCM slurry system collected heat marginally less effectively than water. Due to the lower specific heat capacity of the water than the water-PCM slurries and the high energy of phase transition in the 58–60°C temperature range more energy is stored for a longer period above 58°C, which improves the solar saving fraction.

Zeng et al. (2009) introduced a new configuration for a SWH for floor heating. They developed a novel structure of integrated water pipe floor heating system using shape-stabilized PCM instead of using a conventional big hot water tank.

Al-Hinti et al. (2010) reported an experimental investigation on the performance of a SWH system, which PCM slabs inserted into the hot water storage tank (Figure 2.3). The tank contained many thin walled, cylindrical, aluminum containers. Each container had a

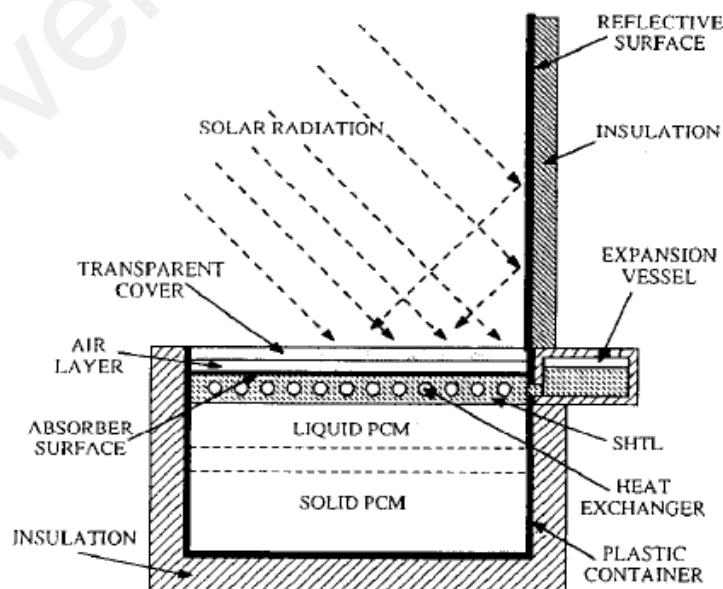


Figure 2.2: Schematic presentation of the integrated solar collector storage system with PCM (Eames & Griffiths, 2006).

volume of water and paraffin wax. The suitability of the melting temperature of paraffin wax enabled the storage of excess energy available in daytime hours as latent heat, and then the release of this stored heat to maintain the water temperature in an acceptable range for most domestic applications. Various tests indicated that the water-PCM storage succeeded in keeping the water temperature over 45°C under most of operational and climatic conditions. They found that daytime consumption of moderate amounts of hot water withdrawn from the hot water tank on sufficiently spaced time intervals does not adversely affect the final water temperature or the overall performance of the system. In addition, it was demonstrated that in cases of extreme consumption during evening hours, the existence of PCM could partially recover the temperature of water, and thus resulting in extending the effective operational time of the system.

In another similar research work, Canbazoglu et al. (2005) experimentally investigated on the performance enhancement of a SWH which PCM cylinders were integrated inside the water storage tank (Figure 2.4). The time variations of the water temperature at the

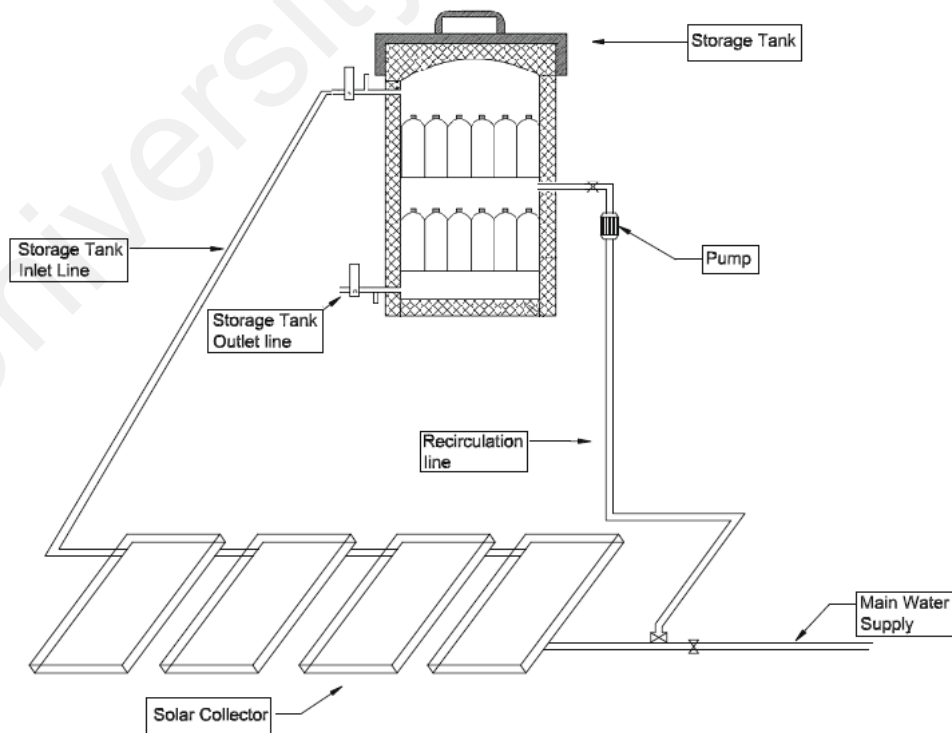


Figure 2.3: Water-PCM storage for use with conventional SWH system (Al-Hinti et al., 2010).

midpoint of the heat storage tank and at the outlet of the collector in a conventional and the introduced design were compared. They found that the produced hot water mass and total heat accumulated in the hot water tank were approximately 2.6–3.5 times more than the conventional system.

Nallusamy et al. (2007) experimentally investigated on the thermal behavior of a packed bed design of a combined sensible and latent heat storage unit. The PCM filled in spherical capsules, which were packed in an insulated cylindrical storage tank. Charging experiments were carried out at constant and varying (solar energy) inlet fluid temperatures to examine the effects of inlet fluid temperature and flow rate of heat transfer fluid on the performance of the storage unit. Discharging experiments were carried out by both continuous and batch wise processes to recover the stored heat. One of the findings of this research was that the batch wise discharging of hot water from the storage tank was best suited for applications where the requirement is intermittent.

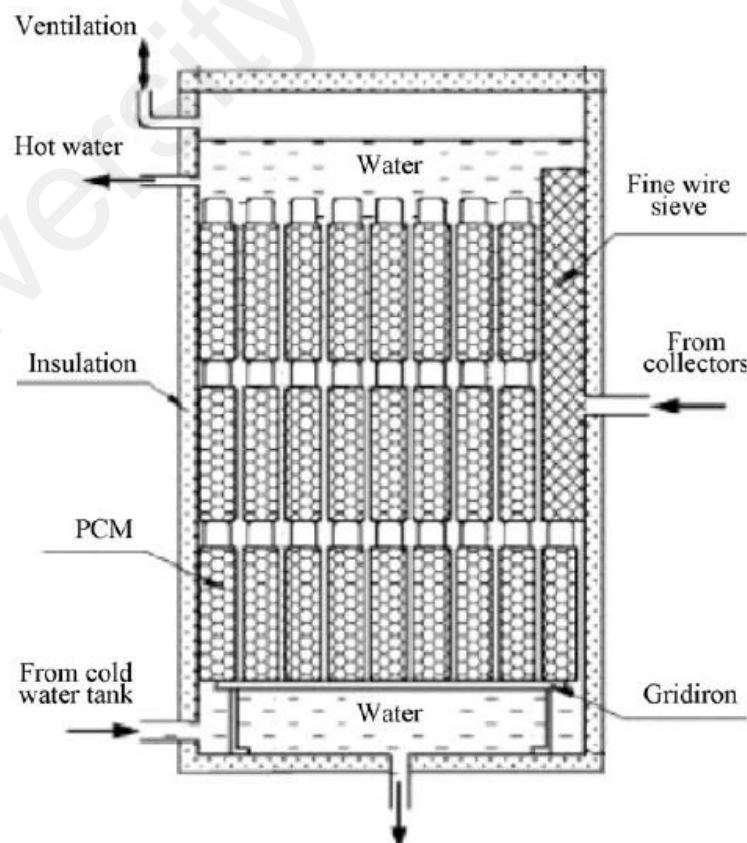


Figure 2.4: Cross-sectional view of the TES tank design (Canbazoglu et al., 2005).

2.3 PCM Heat exchanger devices

According to aforementioned research reports, beside many influential factors in the SWH system and the LHS device configuration, the heat transfer mechanism and configuration play the most important role in performance of a SWH-LHS system. Designing an effective LHS unit involves two challenging aspects: one is to select a suitable PCM and the other is to maximize the heat transmission between the PCM and the heat source (Liu et al., 2012). The thermal performance of LHS design is limited by the poor thermal conductivity of PCMs employed. Therefore, successful large-scale utilization of the LHS device completely depends on the influence of it on the overall performance of the heat transmission system (Jegadheeswaran & Pohekar, 2009). Regarding this matter, in PCM charging/discharging (melting/solidification) processes, many techniques were employed to increase heat storage/release capacity and rates, like including finned tubes of different configurations, bubble agitation, shell and tube (multi tubes), micro-encapsulating the PCM, insertion of metal matrix into the PCM and HP.

According to the general view of this research project, HP and fins are two techniques that are used for heat transmission enhancement to/from the PCM.

2.3.1 Fins enhancement technique

In thermal systems, fins provide extra heat transfer surface. Many studies have investigated effect of different fin configurations in LHS systems. The majority of studies were focused on the fins' thermal behavior in solidification and melting phases. These studies are presented in two subsections below.

2.3.1.1 Melting process

During the phase change processes, the heat transfer mechanisms are contingent on the orientation and configuration of the fins within the PCM storage unit. Heat is moved

to the solid PCM during melting through conduction and once the melting begins, the heat is transferred by natural convection. Because the liquid PCM has a lower thermal conductivity compared to the solid PCM as the melting progresses, the heat transfer by conduction becomes almost insignificant. The additional melting is typically by natural convection because of the gradient of density inside the liquid PCM. Consequently, for nearby fins, the PCM is not essential to enhance the conduction rate, but is an important natural convection improvement.

A numerical study was conducted by Reddy (2007) on the melting process in a tilted rectangular cavity, which is integrated to a SWH. The top wall was used as a solar radiation receiver and the stored heat was provided through the bottom wall from the melted PCM to the cold water. The simulation was done with (4, 9 and 19) and without fins. After 24 h, the PCM's liquid fraction was checked. While all the finned systems exhibited decent melting rate than the unfinned system, 95% of melting was observed only in a system with 9 fins. That is the 9-fin system offered the highest performance.

Akhilesh et al. (2005) heated the top wall of a rectangular PCM container in a numerical study. They studied the changes in melting process after increasing number of fins per unit length. The heat transfer area was increased by adding more fins per unit length and consequently higher energy was stored. Nevertheless, they found that increasing number of fins beyond a certain value (critical value) did not improve the performance significantly. The effect of the natural convection was disregarded in this study.

Gharebaghi and Sezai (2008) studied the performance improvement in the rectangular container by adding horizontal fins to the heated vertical walls. The temperature of walls was held constant and it was higher than the PCM's melting point. It was observed that the heat transfer rate increased because of the fins. Moreover, vertical walls with horizontal fins were advised to be favored to horizontal ones with vertical fins. The

conductivity of heat transfer showed increase by the decrease in the distance between the neighboring fins (consistent with system with more fin numbers). Thus, it can be concluded that increasing the number of fins beyond some value may only result in marginal upsurge in heat transfer rate. The reason is that when the number of fins is increased, the buoyancy driven flows experience a hampering effect and the melting process becomes conduction dominated.

Lacroix and Benmadda (1997) studied the influence of horizontal fins coming from vertical heated wall in the melting process in a rectangular enclosure. The effect of length and number of fins on the melting rate was studied. The melting rate for shorter fins was more or less independent of number of fins. Moreover, the melting process got similar to the condition of no fins once the melting front passed the fin tips. Therefore, the presence of fins was barely noticed. On the other hand, increase in number of longer fins in all cases progressively improved the melting rate. At higher heated wall temperature, higher number of fins resulted in only minor improvement in melting rate. This is because of the hampering influence on the buoyancy driven flows. As such, temperature of heated wall determines the optimum number of fins. Thus, lower number (4 fins of 0.03 m) of longer fins is much more effective in improving the melting rate than the shorter ones (19 fins of 0.01 m). Longer fins enhanced the melting rate considerably even with small difference of temperature between melting point and heated wall, which was more efficient than increasing the of heated wall temperature beyond the melting point. Lacroix and Benmadda (1998) also reported that the onset of natural convection was slowly prevented once the distance between the fins was reduced. Consequently, it can be said that if the less number of fins used, natural convection would happen. Nevertheless, they observed that too much distance reduced the total heat transfer surface area. That is for a constant size of the module, the distance between the fins (fin number) should be optimized.

Lamberg (2003) and Lamberg et al. (2004) studied similar system. They compared a system with two fins with a system without any fin. The findings showed that in a rectangular enclosure with horizontal fins, significant improvement in the melting rate is true. Reddy (2007) had earlier found that increasing the fins slowed the melting. Even though the optimum number of fins was reported, it cannot be generalized because non-dimensional analysis was not done. As Lacroix and Benmadda (1998) mentioned, the optimum distance between the fins drops once the Rayleigh number increases.

Shatikian et al. (2008) indicated that thick fins stayed in the heated surface temperature consistently along the length. In contrast, thin fins experienced temperature gradient for the same length. From heat transfer perspective, it is necessary that fins perform at fixed state. But too thick fins can reduce the number of fins. Thus, the fin thickness should also be enhanced together with fin number for the best performance.

Lacroix (1993) created a 3-D model for melting process in shell and tube LHS system with the HTF flowing inside and the PCM on the shell side. As shown in Figure 2.6, annular fins were used around the tube. Natural convection was incorporated by effective thermal conductivity as a function of the Rayleigh number in the conduction equation. As a result, the fins conducted great heat along the radial direction. Significant increase in stored energy was seen for all ranges of inlet temperature of HTF and mass flow rate owing to the presence of fins. Increasing the fin numbers increased the rate of heat transfer and stored energy in all conditions. Yet, the enhancement factor was reliant on inlet

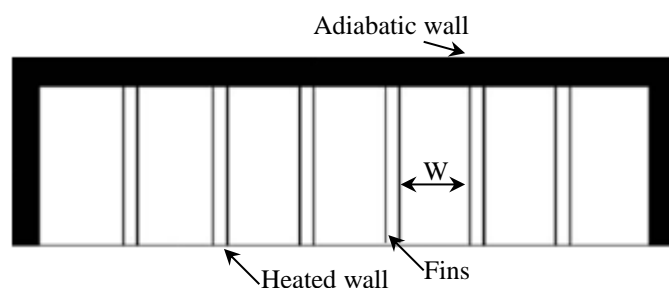


Figure 2.5: Optimum design for fin distance as a function of Rayleigh number (Lacroix & Benmadda, 1998).

temperature of HTF and mass flow rate, because the maximum enhancement was seen for small inlet temperature and moderate flow rates. Conversely, for a larger inlet temperature of HTF and mass flow rate, the enhancement factor was not substantial even with higher number of fins.

Zhang and Faghri (1996) studied similar configuration by examining the effect of fin height. At any time during the melting, the liquid fraction of PCM could be increased by adding the fin height. It can be attributed to the fact that the melting fronts on both sides of the fins were significantly affected by the fin height even though the effect of fins on the melt front was barely seen between the fins. The study also concentrated on the effect of early subcooling on the liquid fraction and the position of the melt front. They reported substantial decrease in performance because of the subcooling. On both sides of the fins, the effect of the subcooling was nearly zero on the performance. This obviously demonstrates that fins are very effective in countering the performance reduction as a result of the PCM's subcooling effect. Normally, inorganic PCMs exhibit a significant amount of the subcooling, which in turn badly affects the system performance (Günther et al., 2007).

Seeniraj et al. (2002) studied the transient behavior of stored high temperature PCMs in tube heat exchanger and finned shell. They showed that some quantity of PCM closer to the tube exit remains in the solid state when unfinned tube are used. A few number of

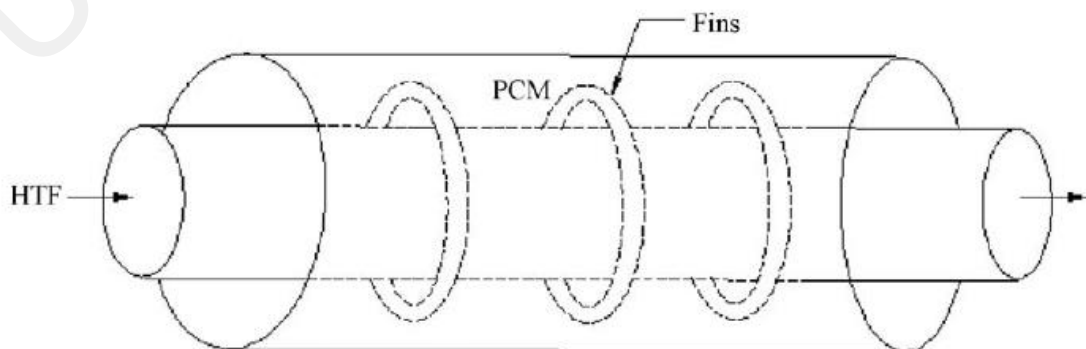


Figure 2.6: Shell and tube LHS unit with the PCM on the shell side and the HTF flowing inside (Lacroix, 1993).

annular fins can keep fairly high temperature difference between the melting point and the HTF. Therefore, the melting is found everywhere in the axial direction. A substantial increment in the energy stored was seen for a fixed size of LHS unit because of the presence of the fins.

2.3.1.2 Solidification process

Opposing to the melting process, solidification is mostly led by conduction. According to Lamberg (2004), natural convection is present only in the beginning during solidification and as the time passes, natural convection exerts almost zero effect in comparison to the effect of conduction. The PCM heat transfer characteristics have studied during solidification. Ettouney et al. (2004) investigated the solidification in a tube and shell heat exchanger. Similar results were found by Ettouney et al. (2005) in spherical storage device. It can be said that during solidification in all LHS configurations the solidified layers develop from heat transfer surface and stay parallel to it. Even though natural convection happens in the liquid PCM at earlier stages, it reduces quickly as the solidification goes on because the liquid volume gets smaller and smaller.

Stritih (2004) estimated the fin effectiveness to compare the heat transfer in a rectangular module filled with PCM, with and without fins. The effectiveness is defined as the ratio between heat flux with and that without fins. Results showed that the fin effectiveness was significantly high and causes to 40% reduction in solidification time. Guo and Zhang (2008) simulated the effect of vertical fins attached to horizontal constant temperature wall on solidification of high temperature PCM. The results indicated that the discharge time with fins was almost $1/30^{\text{th}}$ of that without fins. The time required for complete solidification was found to be decreasing almost linearly with number and thickness of the fins.

In a quite similar study, Shatikian et al. (2008) observed that the solidification was not only initiated at the horizontal wall but also at the vertical fins attached to the wall. It is also added that at any time heat transfer from the fin to the wall was much higher than that coming directly from the PCM to the wall. Moreover, as the time elapsed, direct heat transfer from the PCM to the wall became negligible. This shows that fins increase the heat transfer rate from the PCM. However, the numerical study by Gharebaghi and Sezai (2008) has revealed that heat flux is higher for system with horizontal fins than that of system with vertical fins for any number of fins.

The effect of radial fins on enhancement has also been examined by Liu et al. (2005). They designed spiral twisted fins attached to the tube carrying HTF. It was reported that during solidification, fins not only increase the conduction heat transfer, but also natural convection, which prevails at earlier stages. Because of this, employing fins were found to be more effective at earlier stages than at latter stages. Nevertheless, the enhancement factor was as high as 250% due to fins. It was also recommended to use less width fins as they produce more effective enhancement.

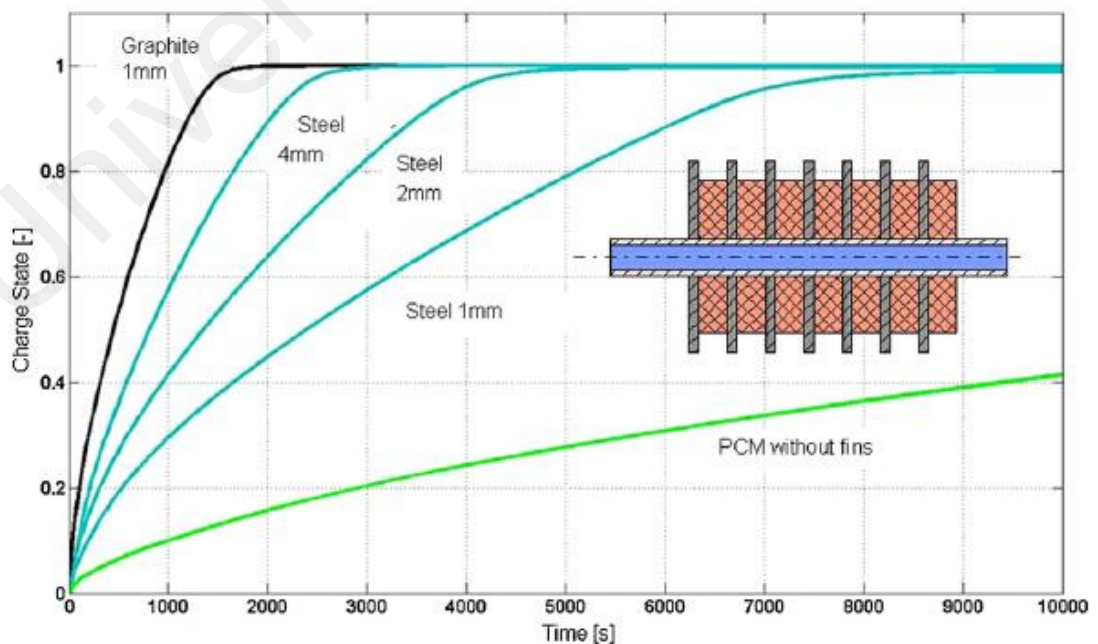


Figure 2.7: Effect of different fin material and thickness on its thermal enhancement (Zhang & Faghri, 1996).

Zhang and Faghri (1996) studied the effect of different fin material on its thermal enhancement in the LHS system by using the finned tube. Both graphite foil and aluminum show no galvanic corrosion in contact with steel since the pipe is generally made of steel. As shown in Figure 2.7, in order to have the same heat transport performance, fins made of steel demand much more volume than those made of graphite foil. Therefore, the cost for steel fins is significantly higher.

2.3.2 HP enhancement technique

This section overviews papers incorporated HPs in LHS units, which HP is acting as an intermediate device between the heat source and the PCM. The HP, as one of these techniques, is a highly effective passive device for transmitting heat at high rates over considerable distances with extremely small temperature drops, exceptional flexibility, simple construction, and easy control with no external pumping power (Faghri, 2014). The HP uses to amplify the charging/discharging processes rate.

Probably, for the first time, Abhat (1978) took into account the idea of the amplification of the melting-freezing process rate of the PCM by incorporating HP. He studied vastly, the performance of a finned HP inserted into a PCM container for solar

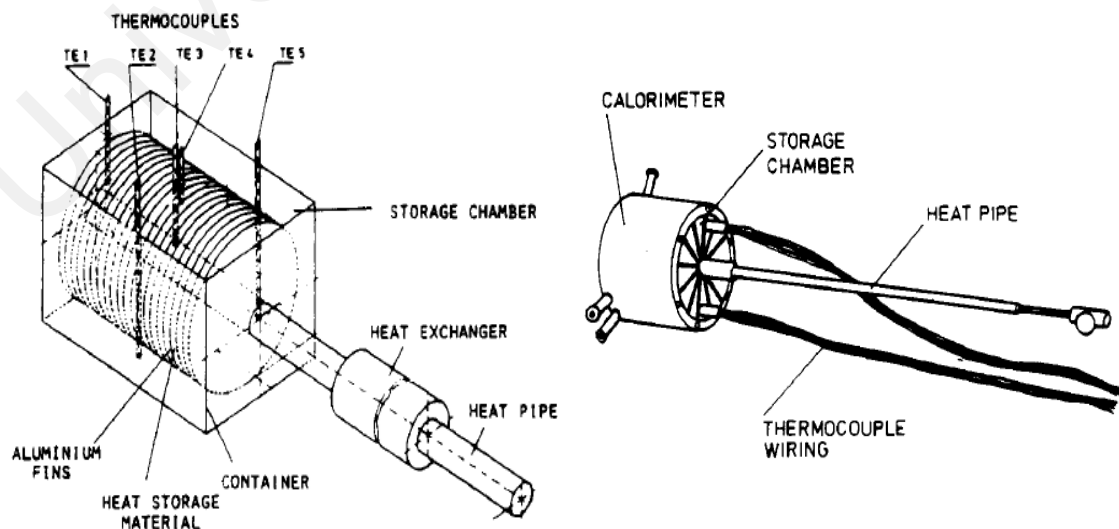


Figure 2.8: Models of finned heat pipe heat exchanger elements (Abhat, 1978).

heating applications (Figure 2.8). The charging time and temperature gradients between HP and PCM for two different storage substances were been investigated. The experimental tests were done for a small 1:6 model filled with paraffin as the PCM. Results indicated the capability of the heat exchanger concept to operate within small temperature swings (less than 10°C) for realistic heat input rates.

Few years later, in another research, Abhat (1980) reviewed the essential parameters that need to be undertaken for a low temperature solar thermal system and also studied different configurations of the hybrid HP-PCM for low temperature solar heating applications in many aspects. Many parameters like suitable PCM and heat exchanger design for higher thermal conductivity, SHS and LHS and importance of stratification in hot water storage tanks have been reviewed; then, the influence of various geometrical parameters such as fin height, fin thickness, fin spacing, and void fraction on the thermal performance of a system was discussed. He concluded that the use of the HP offers several advantages and renders flexibility in operations and applications such as: (i) the HP transports heat under very low temperature gradients so that an almost isothermal heat source in contact with the fins and the thermal storage medium within the storage chamber is attained; (ii) the heat flux transformation capability of the HP can be utilized to give low heat flux densities within the storage chamber for large heat flow rates in the heat source/heat sink sections; (iii) The HP can operate uni-directionally as a diode.

Horbaniuc et al. (1996) introduced a design for the HP-PCM heat exchanger, shown in Figure 2.9, which (1) HP heat transfer surface is extended with some (2) longitudinal fins; inside (3) the storage chamber, (4) the PCM is placed at the adiabatic side of the HP, while the cold flow passes around (5) the condenser side and the hot flow passes around (6) the evaporator side. The operation modes of the heat exchanger are (i) Charging: when the hot fluid flows through the evaporator region and heat is transferred to the melting PCM (the finned region of the HPs plays the role of a condenser); (ii) Discharging: when

the stored heat is removed from the PCM and transferred to the cold fluid that flows through the upper part of the PCM (during this operation mode the finned region of the HP plays the role of an evaporator and the upper end represents the condenser); (iii) Simultaneous charging/discharging: when both the cold and the hot agents simultaneously flow through the PCM, the heat is at the same time stored and transferred to the cold fluid. They evaluated the effect of solid-liquid interface by considering the radial heat transfer (due to the HP wall) and the angular one (due to the fin). The research undertaken parameters like number of fins, the difference between the melting temperature of the PCM and the boiling temperature of the heat transfer agent of the HP. In the other research by this team (1999), they studied the solidification of a PCM within a finned HP-PCM system by the radial heat propagation toward the HP wall and the angular propagation toward the fins. They concluded that the solidification time decreases with more fins.

Few years later, Liu et al. (2006a) experimentally studied the model that was introduced by Horbaniuc et al. (1996) in charging only and discharging only modes and later, they (2006b) studied simultaneous charging-discharging modes, too. They observed that the system is able to operate in different modes and it provides more flexible operation to makes it suitable for systems of time and/or weather dependent energy,

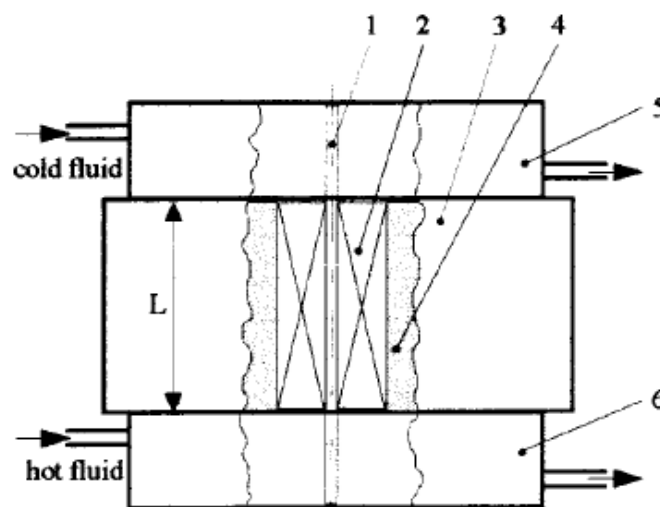


Figure 2.9: The HP-LHS heat exchanger system (Horbaniuc et al., 1996).

especially solar energy and other renewable energies. In addition, they found out that several variables such as the initial temperature of the PCM, cold and hot flow temperatures and rates and the HP specifications and fins geometries must be designed carefully to make the device able to function well.

Shabgard et al. (2012) performed an energy and exergy study on the LHS model that was introduced by B. Horbaniuc *et al.*, with two changes in the design; one is that this time instead of one module of HP-PCM, a set of modules have been considered and two the system is considered to be in vertical position. As it is shown in Figure 2.10, the PCM is cascaded and embedded to HPs in which thermal energy of inlet HTF is stored in the PCMs during charging, and recovered during discharging. The HTF that leaves the LHS during charging returns to the collector field. Multiple gravity-assisted HPs or thermosiphons, with their ends penetrating into the HTF channels, pass through the PCM in each unit. The LHS is occurring in three layers of different PCMs. Hence, each PCM unit contains a single PCM. The PCM units also act as heat exchangers, transferring thermal energy between the HTF and the PCM during the charging and discharging cycles. The thermal operation is considered for a high temperature PCM applications (280–390°C). Thermal processes of the heat exchanger system were planned similar to the work by Liu et al. (2006a). The energy analysis was determined by a thermal network

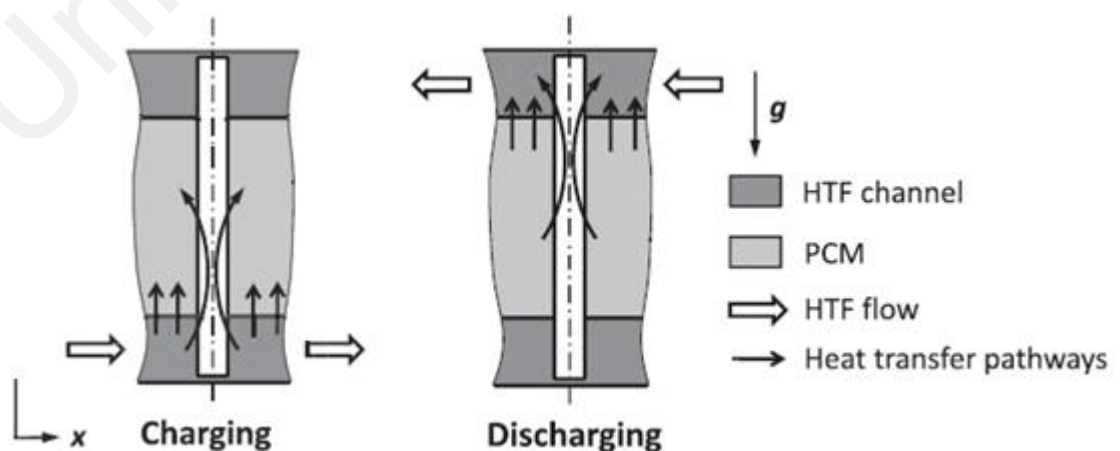


Figure 2.10: PCM unit configuration during charging and discharging (Shabgard et al., 2012).

model which will be explained later in the section 2.4.3. It was found that when the PCM was cascaded, the LHS recovers about 10% more exergy during a 24 hour charging-discharging cycle compared to the best non-cascaded LHS considered in this work.

In the other work by same research team (2010), they studied a different model of HP-PCM heat exchanger with a similar method. The research investigated on the benefits of inserting multiple HPs between the HTF and the PCM in two configurations as presented in Figure 2.11. In module 1, the HTF is passing through the tube while tubes were surrounded by the PCM. In module 2, inversely, the PCM was placed inside the tubes and the HTF was perpendicularly passing around the tubes. HPs are inserted through the surface of tubes. The influence of the number of HPs as well as their orientation relative to the HTF flow direction and the gravity vector were investigated. They observed adding HPs enhances thermal performance of both modules in charging or discharging processes. Regarding the orientation of the HPs, in module 1, the HP orientation plays a minor role in determining the system's thermal response, while in module 2, the HP orientation is an

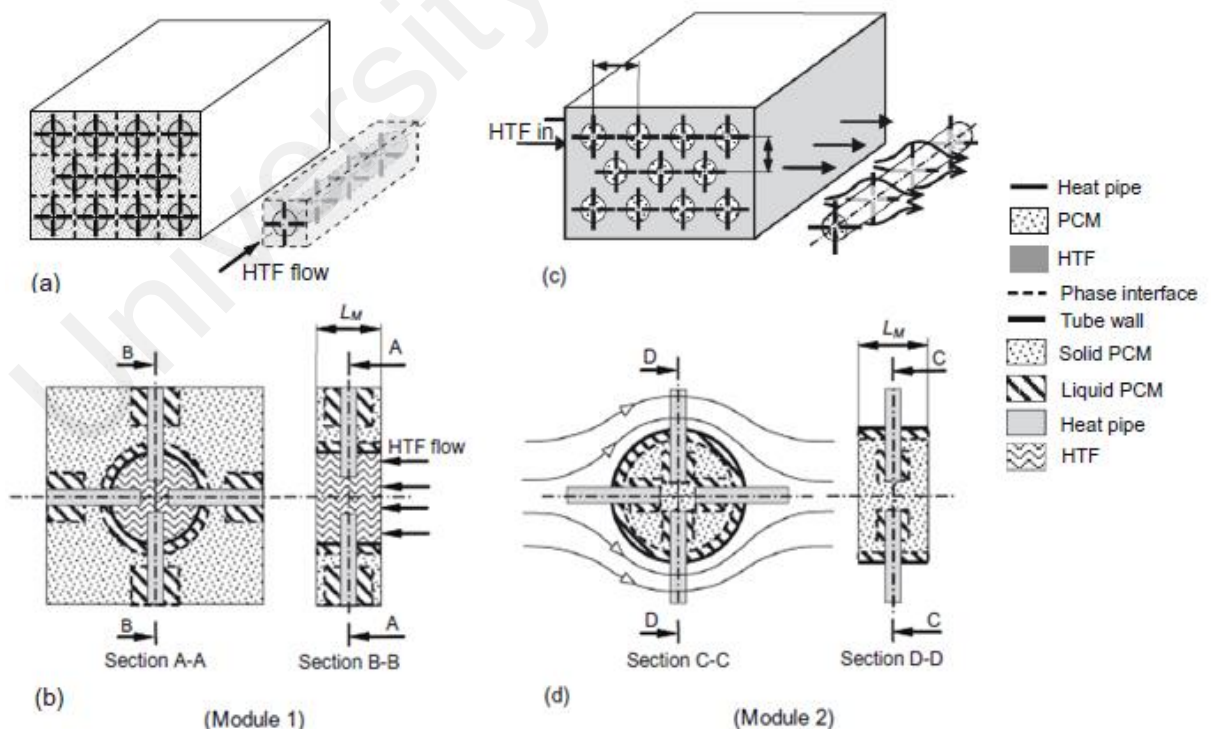


Figure 2.11: Two HP-PCM heat exchanger configurations; (a) module 1, (b) in module 1 the PCM surrounds the HTF tubes, (c) module 2, (d) in module two the PCM is placed inside the tubes and the HTF flows perpendicular to the tube (Shabgard et al., 2010).

important factor. They, also, described the thermal behavior of the hybrid HP-PCM system by HP effectiveness and a generalized HP effectiveness factors.

Nithyanandam and Pitchumani (2011) used a numerical optimization scheme to maximize the energy transfer rate and the HP effectiveness in the model introduced by Shabgard et al. (2010) shown in Figure 2.11. They found that increment in the HTF mass flow rate, module length and tube radius reduced the effectiveness of the HPs; while increment in the length of the condenser section, the length of the evaporator section and the vapor core radius enhanced its effectiveness. It was observed that in module 2, the discharging effectiveness decreased when the HTF mass flow rate increased, due to the significant improvement of the heat transfer rate between the vertical HPs and HTF. Optimum design conditions indicated that the effectiveness of the HPs in augmenting the thermal performance of the LHS is significantly higher for module 1, while the effective charging/discharging rate of the PCM was found to be higher in module 2.

Sharifi et al. (2012) conducted numerical study on the heat transfer characterization of a HP-PCM unit, when the PCM is in vicinity of condenser section and when metal foils were protruded from the HP and sunk to the PCM container to increase heat transfer area between HP and PCM (Figure 2.12.A & 2.12.B). For the first model, a comparison study between melting induced by heating from a HP, an isothermal surface, a solid rod and a hollow tube were simulated. In physical model, the PCM was contained in a vertical cylindrical annulus, which surrounds the condenser section of the HP. The isothermal surface, rod and tube each have the same exterior dimensions as the HP. The parametric study revealed that in all cases considered in this study, the HP provides the largest PCM melting enhancement, relative to either the rod or tube; and approach the maximum attainable rates associated with the isothermal surface. Melting rates are enhanced as either the condenser length or the diameter of the HP is increased. Melting rates were governed by transient heat transfer equations and coupled with heat transfer effects of (i)

conduction in the HP walls, rod and tube, (ii) vaporization, condensation and compressible flow of the HP working fluid, and (iii) natural convection in the PCM melt.

In the second model, they (2014) studied the influence of the HP evaporator-to-condenser length ratio, as well as the overall temperature difference between the working fluid and the PCM melting temperature. They found that using foils on HP or rods leads to increased phase change rates when it compared with the baseline model. For a small (approximately 1%) volume fraction of foil in the PCM-foil matrix, melting (solidification) rates associated with HP-foil configurations were increased by approximately 300% (900%) relative to configurations involving the rod with no foil. Melting (solidification) rates relative to configurations involving the HP with no foil were increased by approximately 200% (600%). Superior phase change rates were achieved by utilizing only 1.21% foil volume fraction within the PCM in conjunction with the HP, permitting nearly the same total amount of latent energy to be stored within a fixed storage volume.

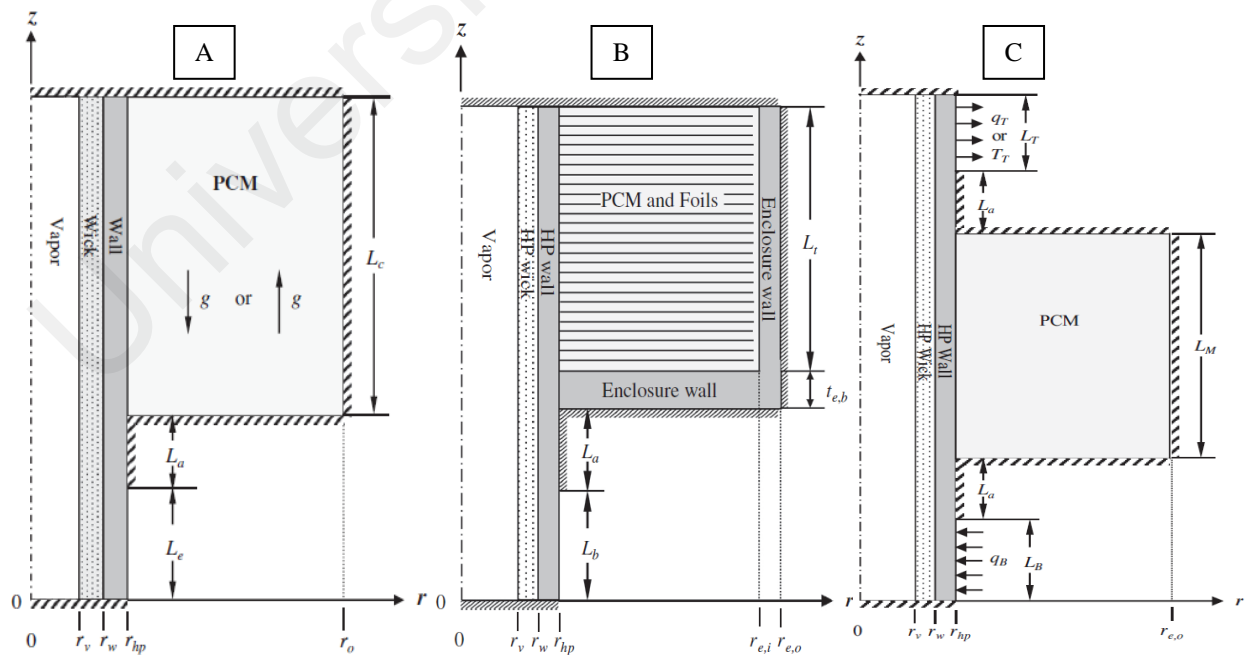


Figure 2.12: Physical model of the HP-PCM system; (A) when PCM is in condenser region (Sharifi et al., 2012), (B) when PCM is in condenser region with foil (Sharifi et al., 2014), (C) when PCM is in middle of the heat pipe (Sharifi et al., 2015).

In the other work by this team (2015), similar analysis process is done for the model that the PCM was positioned at the adiabatic side of the HP (Figure 2.12.C). The HP is heated from the bottom to melt (charge) the PCM that is positioned in the middle of the HP length, and is cooled from the top to solidify (discharge) the PCM. They defined three modes of operations as (i) charging only, (ii) simultaneous charging/discharging, and (iii) discharging only. All modes of operation were handled with a single HP-PCM of which the top and bottom sections are inactivated during charging only and discharging only modes, respectively. The parametric study of the influence of the PCM enclosure height and input/output heat transfer rates showed that for the same mass of PCM, a longer enclosure exhibits a lower HP bottom average wall temperature and relatively more PCM melting during simultaneous charging and discharging. Increasing either of the input, output or both heat transfer rates had a significant effect on the temperature of the HP bottom and top sections, but only a minor impact on the temperature of the HP middle section.

Overall, it could be understood that beyond different methods, which have been used for charging/discharging rate enhancement in the PCM, HP is a reliable and manageable choice. Interestingly, advantages of the HP and PCM cover their disadvantages like overheating of the HP and low thermal conductivity of the PCM. Finned HP and HP with Foil/Foam techniques showed more advantages rather than simple HP. Using HP solar collectors integrated with low temperature LHS are capable to be considered for more investigation.

2.4 Theoretical approaches

Regarding the objectives of this research project, analytical approach is required to determine a rough estimation of a simplified model.

2.4.1 PCM

Several mechanisms are at work when a solid melts or a liquid solidifies. Such a change phase involves heat transfer, possible supercooling, absorption or release of latent heat, changes in thermodynamic properties, surface effects, etc. According to the definition, before a solid can melt a certain amount of energy is needed to overcome the binding forces that maintain its solid structure. This energy is referred to as the latent heat (heat of fusion) of the material and represents the difference in thermal energy (enthalpy) levels between liquid and solid states, when all other things being equal. The characteristics of phase change problems are temperature field and the location of the interface. Problems of this kind arise in the fields such as molecular diffusion, friction and lubrication, combustion, etc.

Overviews of the origins of such problems can be found to as “moving boundary problems” or “free boundary problems” (Crank, 1984; Wilson et al., 1978; Wrobel & Brebbia, 1991, 1993; Zerroukat & Chatwin, 1994). Moving boundary problem named Stefan problem is another issue to develop simulation methods of PCMs (Hasnain, 1998; Zongqin & Bejan, 1989). The simplest solution for Stefan problems is the one-phase Stefan problem. The term of ‘one-phase’ designates only the liquid phases active in the transformation and the solid phase stay at its melting temperature. The Stefan problem was extended to the two-phase problem, the so-called Neumann problem which is more realistic (Özişik, 1993). In Neumann problem, the initial state of the PCM is assumed solid, during the melting process, its initial temperature does not equal to the phase change temperature, and the melting temperature does not maintain at a constant value.

The formulation of the Stefan problems as models of basic phase-change processes was presented in several textbooks (Alexiades & Solomon, 1993; Hahn & Ozisik, 2012; Kaviany, 2002). Under certain restrictions on the parameters and data, such problems admit explicit solutions in closed form. Unfortunately, closed-form explicit solutions may

be found only under the following very restrictive conditions: 1-dimensional, semi-infinite geometry, uniform initial temperature, constant imposed temperature at the boundary and thermophysical properties constant in each phase. References relevant to the one-phase Stefan problem were well documented in the book by Hill (1987). Specifically, various techniques and approximations have been attempted to study the problem of an inward solidification with spherical symmetry. These include the power-series approximation method of Kreith and Romie (2002); the closed-form solution by Langford (1966) under the assumption of constant solidification rate; the approximate integral method of Poots (1962); the numerical solution by Tao (1967), Li (1995), and Caldwell and Chan (1998); the perturbation method by Huang and Shih (1975); the small parameter expansion solution by Pedroso and Domoto (1973); the strained coordinates method by Riley et al. (1974); the matched asymptotic expansions solution by Stewartson and Waechter (1976); the asymptotic solution (near the final stage of complete solidification) of ; the small-time expansion solutions by Davis and Hill (1982), and Hill and Kucera (1983).

B. Horbaniuc (1999; 1996) used a 1-D transient conduction exact solution for solidification process in the PCM. Solid-liquid interface was calculated by superpositioning radial and angular thickness growth rates. Mathematical expressions were determined based on exponential and parabolic solutions and then the results of both were compared. This method used as sizing tools for the proposed system. In this method, HP is simply assumed as a heat source with a uniform imposed temperature on the surface and the fins, which this causes to over estimating of the solidification time. In other word, the physical phenomenon of the HP was not considered.

Using one-phase Stefan problem in many various cases have been considered by researchers. Wu et al. (2002) followed the one-phase Stefan problem without neglecting the thermal effect of the surface tension at the interface. Surface tension affects the

equilibrium temperature (melting temperature) at the interface of the two phases via the Gibbs–Thomson law. In this approach, the latent heat liberated from the solidifying front is assumed to be carried away by the solidified phase only. This simplification leads to the familiar unsteady heat-diffusion equation for the solid phase with moving interfacial boundary. The equation describing the progression of the interface is derived from equating the amount of heat released per increase of the freezing layer to that diffused into the solidified field (Stefan condition).

Briozzo and Tarzia (2010) considered one-phase non-classical one-dimensional Stefan problems for a source function F , which depends on the heat flux, or the temperature on the fixed face $x=0$. In the first case, they assumed a temperature boundary condition, and in the second case they assumed a heat flux boundary condition or a convective boundary condition at the fixed face. Exact solutions of a similarity type were obtained in all cases. In other similar work, Blank et al. (2007) presented existence, uniqueness and regularity of the free boundary in the Hele-Shaw problem with a degenerate phase. The Hele-Shaw model describes the flow of a viscous fluid being injected into a slot between two nearby plates. It is used in injection molding for the production of packaging materials and the interior plastic parts of cars and airplanes, in electromechanical machining, and to study the diffusion of nutrients and medicines within certain tumors. They obtained the unique weak solution to the Hele-Shaw problem with a mushy zone as the (point wise) “Mesa” type limit of solutions to one-phase Stefan problems with increasing diffusivities, and fixed initial and boundary data.

Naaktgeboren (2007) presented the classical one-phase Stefan problem in dimensionless form with a time-varying heat-power flux boundary condition. The formulating parameters are the Stefan number, Ste , and a generalized form of the Biot number, Bi . The asymptotic solution for $Bi \rightarrow 0$ of the governing equations is of an isothermal phase change material domain, simplifying the model into a moving boundary

zero-phase type problem. Exact solutions to the zero-phase model can be found for finite domains in Cartesian, cylindrical and spherical coordinates in one dimension with sign-switching boundary conditions in terms of moving boundary location, or, conversely, melting times.

Alexiades and Solomon (1993) remarked that explicit solutions exist only for semi-infinite problems and with parameters constant in each phase and constant initial and imposed temperatures. This leaves out even problems with constant flux. The most methods that commonly referred to as an analytical approximation methods are quasi-stationary approximation, the Megerlin method, and heat balance integral and perturbation methods. Their applicability depends on being able to simplify the problem to a form that fits the method. Such simplifications are achieved by making various physical and/or mathematical assumptions on the underlying process and the mathematical problem modelling the process. The resulting solution may turn out to be quite accurate, especially for standard, simple, laboratory type processes. The fundamental difficulty is that there is no way to know a priori how accurate the solution will be because, on the one hand, there is no way to check the validity of the physical simplifications and, on the other hand, there is no error estimates for the mathematical approximations. Consequently, the usefulness of analytical approximation method is restricted to providing qualitative and “order-of-magnitude” information rather than precise quantitative information. In fact, such simple methods are necessary as both “system sizing” tools and debugging tools for numerical codes. Driven by this philosophy and attitude, which grew out of actual experience in the field, it is required to stress the usefulness of the quasi-stationary approximation as a tool to estimating, for example melt times and heat absorbed by simple “back-of-the-envelope” calculations. The main usefulness of analytic approximations lies in the fact that, being analytic expressions, they reveal qualitative behavior (such as dependence of parameters) in ways that numerical

solutions cannot. In continue some relevant research papers, which used approximation method will be presented.

Alexiades and Solomon (1993) expressed that the quasi-stationary approximation method plays a key role in modeling of PCM systems to determine reasonable tradeoffs between charge and discharge parameters to store all available heat and totally discharge the heat during a discharge process.

Some other research works also attempted to use simplified one-phase analytical solution to simulate their models. Lamberg and Sirén (2003) presented a simplified 1-D one-phase analytical model which predicts the solid–liquid interface location and temperature distribution of the fin in the solidification process with a constant end-wall temperature in the finned two-dimensional PCM storage. The analytical results were compared to numerical results and they showed that the analytical model was more suited to the prediction of the solid–liquid interface location than the temperature distribution of the fin in the PCM storage.

Xiao et al. (2009) presented a simplified theoretical model established to optimize an interior PCM for energy storage in a lightweight passive solar room. Analytical equations were presented to calculate the optimal phase change temperature and the total amount of latent heat capacity and to estimate the benefit of the interior PCM for energy storage. Further, as an example, the analytical optimization is applied to the interior PCM panels in a direct-gain room with realistic outdoor climatic conditions of Beijing. The analytical results agree well with the numerical results.

Sobotka et al. (2013) presented a parametric model for the analytical determination of the solidification and cooling times of semi-crystalline polymers. This work presents an efficient method to quickly calculate with good accuracy (to 5%) the solidification time of an injected semi-crystalline polymer slab. The knowledge of this ratio enables to predict analytically the solidification time in a 1-D finite medium. This ratio can be

parameterized as a function of characteristic numbers in phase change problems: Stefan numbers and the ratio of thermal diffusivities of both phases.

Mosaffa et al. (2012b) presented an analytical approach for the prediction of temperature during the solidification in a two-dimensional rectangular latent heat storage using a PCM with internal plate fins. The basic energy equation was formulated accounting for the presence of a HTF on the walls. The developed analytical model estimates satisfactorily the solidification time of PCM in storage, which could be useful in the design of PCM-based TESs. In other relevant research work by Mosaffa et al. (2012a), the development of an approximate analytical model for the solidification process in a shell and tube finned thermal storage was reported. A comparative study was presented for solidification of the PCM in cylindrical shell and rectangular storages having the same volume and heat transfer surface area. It was found that the PCM solidification rate in the cylindrical shell storage exceeds the rectangular storage.

Bauer (2011) considered a quasi-stationary approximation solution based on the approach that includes effective boundary conditions and material parameters and geometry. Based on analytical and numerical computations, time of freezing for two basic geometries was examined. These geometries are the flat wall and a single tube which have flat fins and radial fins on the outside, respectively.

2.4.2 HP

Defining accurate boiling/condensing processes in HP is also one of the difficult challenges. Most of the detailed analytical and numerical research on HPs has been done on the vapor core region and wall heat conduction, since the liquid flow is difficult to describe with an exact theoretical model (Faghri, 2014).

After reviewing several papers, two analytical methods had been found that are mathematically strong and were validated by experimental works. One is by Zhu and Vafai (1999), which is a 1-D analytical model for low-temperature cylindrical HPs. They

developed a closed-form solution, which incorporates liquid-vapor interfacial hydrodynamic coupling and non-Darcian transport through the porous wick. The solution is able to predict the vapor and liquid velocity and pressure distributions. In addition, the steady-state vapor and wall temperatures for a given input heat load in the evaporator region and a convective boundary condition in the condenser region, are obtained.

The second method - which was first introduced by Zuo and Faghri (1998) - is using a thermal network model - based on lumped resistance method - to analyze heat transfer in HP. This method provides a unique view into the physics behind the HP operation, which was considered a thermal network of various components. Transient HP behavior was described by first order, linear, ordinary differential equations. Figure 2.13 shows the thermal elements related to heat transfer through the HP. Process descriptions of the system are: (1) Radial heat conduction through the evaporator wall, (2) Radial heat conduction through the evaporator liquid-wick, (3) Vapor flow (heat convection), (4) Axial heat conduction through the adiabatic section wall, (5) Axial heat conduction

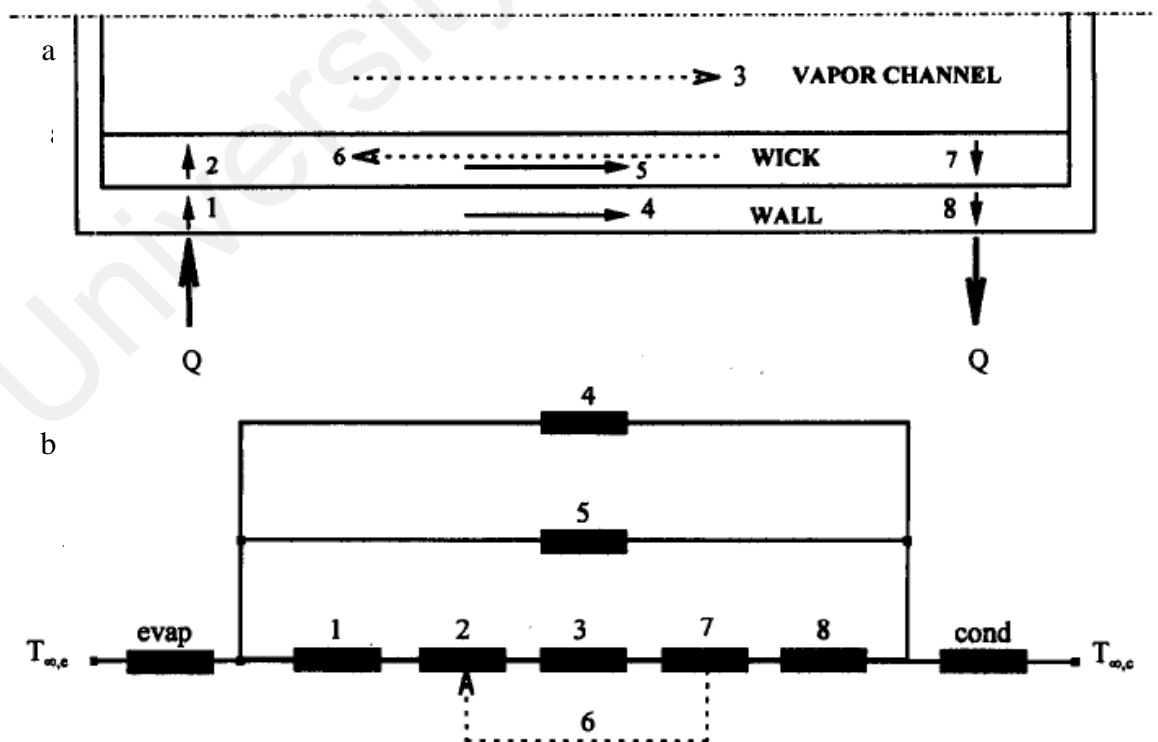


Figure 2.13: A network system for the heat pipe operation. (a) A sketch of the heat pipe heat transfer. (b) A network analogy of the heat pipe heat transfer (Zuo & Faghri, 1998).

through the adiabatic section liquid-wick, (6) Liquid flow (heat convection), (7) Radial heat conduction through the condenser liquid-wick, (8) Radial heat conduction through the condenser wall.

H. Shabgard *et al.* (2010) used this method to analysis a high temperature LHTES system with HP and HTF tube. Authors used a same concept to model the PCM. In this way, thickness of the PCM is divided to equal segments (five discrete in this work) and then, an energy balance will be applied to each one of them to find the temperature at center node. Finding temperature variations of the nodes specifies the solid-liquid interface in the material.

University of Malaysia

CHAPTER 3: MATERIALS AND METHODS

3.1 Introduction

This chapter consists of three sections. The first part is the description of the conceptual design of the proposed model; the second part is the expression of the mathematical equations for theoretical modelling; and the third part is the expression of the experimental setup and test procedures.

3.2 Model description

This section presents a full description of the investigated model. After a short review on the background of the SWH model, the conceptual design of the model is expressed. Then, by referring to the findings from the relevant literature review in Chapter 2, essential logics for design of the system are collected and regarding to these the actual design of the fins, PCM tank and other components of the setup are presented.

3.2.1 Background Art

As understood from the literature reviews, passive solar water heating (PSWH) is a simple, reliable, and cost-effective method of harnessing the sun's thermal energy to provide required hot water of households. PSWHs can be further subdivided into two classes: systems in which the functions of heat collection and storage are separate (the HP collector systems), and systems with combined collection and storage systems, which could be called the integral passive solar water heater (IPSWH). The key factor in design of an IPSWH is its ability to collect and release the solar thermal energy.

In baseline IPSWH systems, the absorbed solar energy stores as hot water in the form of sensible heat. This report introduces a new configuration of a compact design of an IPSWH system by using HPSC system integrated with LHS tank (HPSC-PCM), to be

able to incorporate advantages of heat pipes and PCMs to improve the HPSC performance.

3.2.2 Conceptual design

In a baseline HPSC-B, the end of the HP condenser section (HPC) is inserted into a shell welded into the manifold. Solar energy absorbed by the HP evaporator section (HPE) and transfers to the HPC. The supply water heats up as it passes over the HPC. The solar energy is then circulates to and stores in a large insulated water tank.

According to the schematic diagram in Figure 3.1, in the proposed HPSC-LHS system, the manifold is reshaped as a tank and is filled with the PCM. In order to increase efficiency, the HPC end shell is provided with fins welded on. Another finned pipe is provided in the manifold to exchange the heat from the PCM to the supply water. The domestic hot water supply is heated up as it passes into the supply heat exchanger pipe to the hot water supply point. The proposed system consists of three heat transfer processes - solar energy absorption, PCM charging process and PCM discharging process to the cold supply water. Solar energy incident on the solar collector transfers to the HPC.

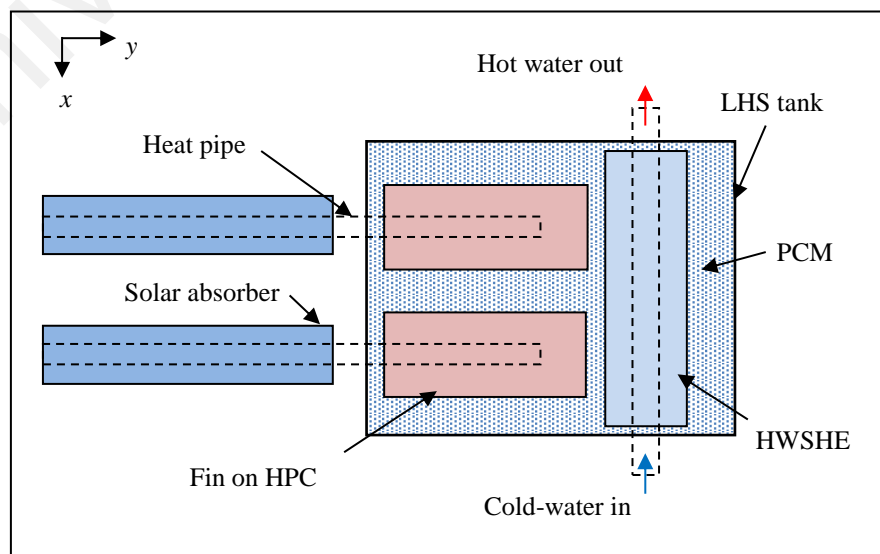


Figure 3.1: ETHPSC-PCM system.

Figure 3.2 presents the structural details of the baseline and introduced models: (1) Cold water inlet, (2) Hot water outlet, (3) Manifold, (4) HP, (5) Evacuated tube, (6) LHS Tank, (7) Hot water supply heat exchanger (HWSHE) pipe, (8) Fin on HWSHE pipe, (9) Fin on HPC, (10) The PCM.

3.3 Theoretical model

In mathematical textbooks, the quasi-stationary approximation method plays a key role in modeling of PCM models to determine reasonable tradeoffs between charge and discharge parameters to store all available heat and totally discharge the heat during a discharge process (Alexiades & Solomon, 1993). This section presents equations for mathematical modelling of the heat transfer processes. The aim of the following mathematical modeling is to obtain a sizing estimation of the thermal characteristics of the proposed design.

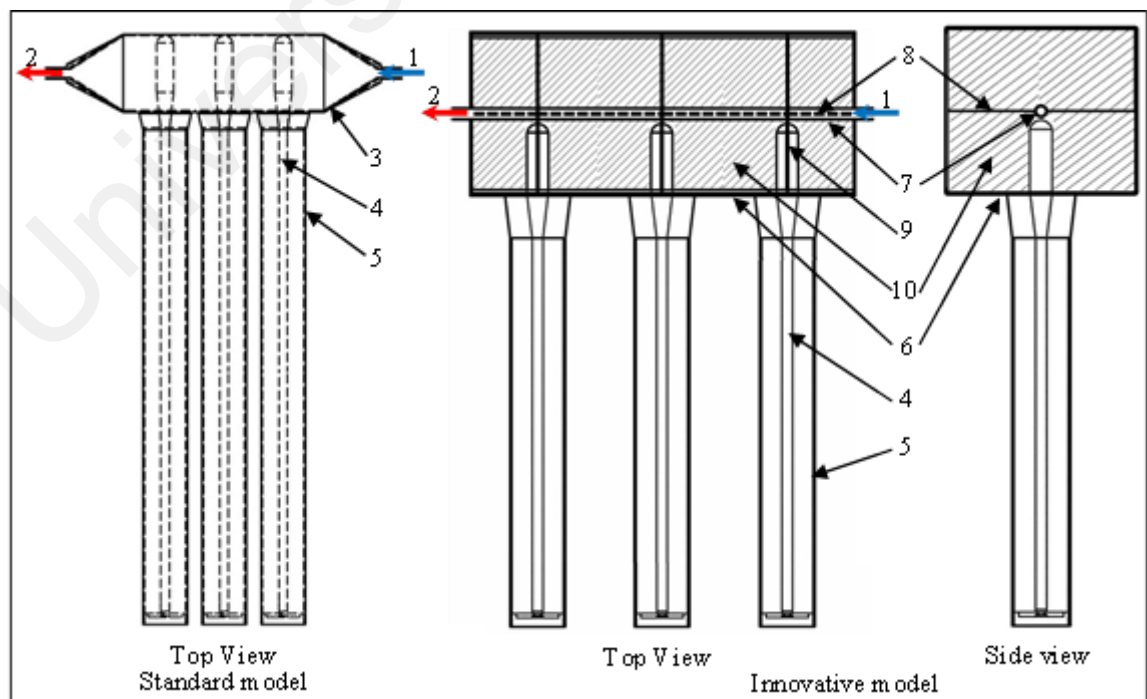


Figure 3.2: Simplified model of conventional and introduced HPSC systems.

3.3.1 Solar energy

Solar radiation incident on and absorbed by a tilted collector surface depends upon several variables like surface material properties, convection from the surface and reflectance factors. Beckman et al. (1977) proposed a theoretical method for a tilted collector:

$$S(t) = I_b(t) \cdot R_b \cdot (\tau\alpha)_b + I_d(t) \cdot (\tau\alpha)_d \cdot \left(\frac{1+\cos\beta_s}{2}\right) + I_T(t) \cdot \rho_g \cdot (\tau\alpha)_g \cdot \left(\frac{1-\cos\beta_s}{2}\right) \quad (3.1)$$

A complete set of equations provided in appendix A. The latitude and longitude of the Kuala Lumpur International Airport meteorological station is 2.44° and 101.42°.

3.3.2 Heat pipe surface temperature

A schematic diagram of a cylindrical heat pipe is shown in Figure 3.3. Zhu and Vafai (1999) introduced a set of mathematical equations, which provides an analytical solution for surface temperature along the length of a low temperature heat pipe. For steady state operation, the axial temperature distribution is obtained from:

$$T_{hp}(x, t) = \begin{cases} T_{pcm}(t) + \frac{S(t)}{2\pi l_c} \left[\left(\frac{\ln(r_{o,hpe}/r_{w,hpe})}{k_w} + \frac{\ln(r_{w,hpe}/r_{v,hpe})}{k_{eff}} \right) \left(1 + \frac{l_c}{l_e} \right) + \frac{1}{h_{pcm,c} r_{o,hpe}} \right] & 0 \leq x \leq l_e \\ T_{pcm}(t) + \frac{S(t)}{2\pi l_c} \left[\frac{\ln(r_{o,hpa}/r_{w,hpa})}{k_w} + \frac{\ln(r_{w,hpa}/r_{v,hpa})}{k_{eff}} + \frac{1}{h_{pcm,c} r_{o,hpa}} \right] & l_e \leq x \leq l_e + l_a \\ T_{pcm}(t) + \frac{S(t)}{2\pi h_{pcm,c} r_{o,hpc} L} & l_e + l_a \leq x \leq l \end{cases} \quad (3.2)$$

It is assumed that there is no radial heat transfer across the HPE and the HPC. Conduction along the length of heat pipe is negligible. The surface temperatures of solar absorber plate and HPE are assumed equal.

Multiple wire mesh screen is considered as wick type of the heat pipe. The effective thermal conductivity of the liquid-saturated wick and working fluid is calculated according to Peterson (1994):

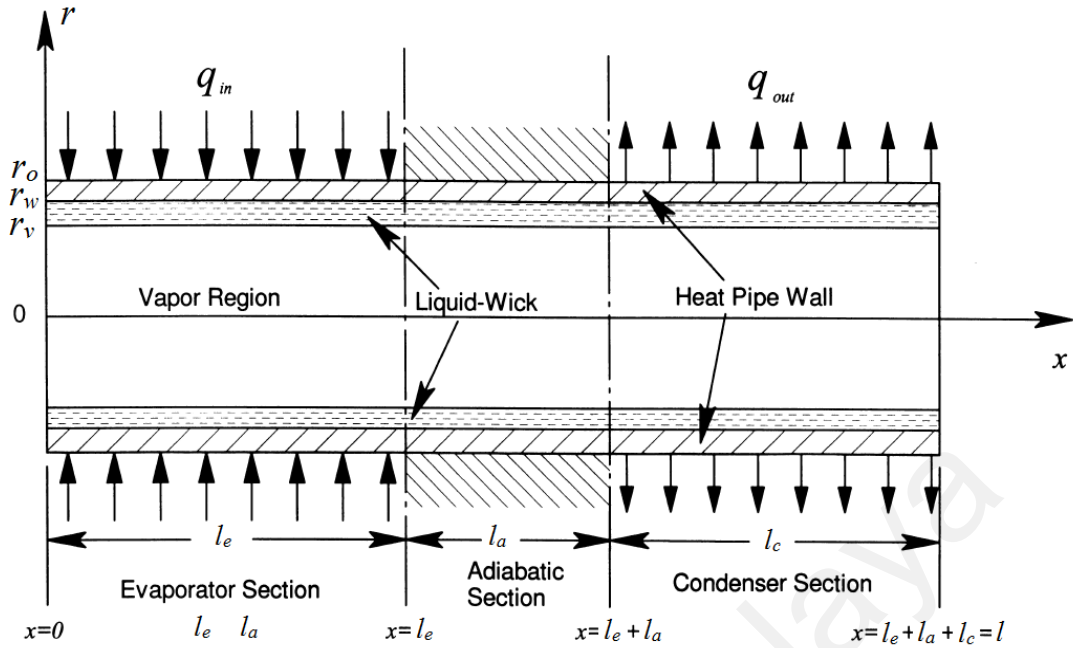


Figure 3.3: Heat pipe cross section.

$$k_{\text{eff}} = \frac{k_e[k_e + k_s - (1 - \varepsilon)(k_e - k_s)]}{k_e + k_s + (1 - \varepsilon)(k_e - k_s)} \quad (3.3)$$

where, $\varepsilon = 1 - (\pi N_a d_w)/4$ in equation 3.3.

Natural convection coefficient in a rectangular cavity containing paraffin wax during melting is prepared by Marshall (1979):

$$h_{pcm,c}(t) = 0.072 \times \left\{ [g \times \rho_l^2 \times c_{pl} \times k_l^2 \times \beta_e \times (\theta/2)] / \mu \right\}^{1/3} \quad (3.4)$$

where, $\theta = (T_{hpc}(t) - T_m)$ in equation 3.4.

3.3.3 Charging mode

During the charging mode, the heat transferred from the HP will be stored in the PCM. The PCM temperature distribution and the interface location need to be determined. The heat equation in the PCM is a 2nd order linear partial differential equation with non-homogeneous boundary conditions. According to the Figure 3.4, the heat transfer from the HPC to the PCM is symmetric on the both sides. Therefore, calculations are determined only for the PCM on one side of the finned PCM. One important assumption in the quasi-stationary one-phase Stefan problem is that the imposed temperature on the

hot plate must be uniform. The hot plate is the finned HPC. Another assumption is that the heat transfer from the HPC fin to the PCM occurs in one dimension. The PCM is initially at ambient temperature. Heat storage in PCM is sensible storage before it reaches its melting point and after that is latent storage. The charging mode contains of both sensible and latent heating. A flowchart of the calculations for charging mode is provided in Appendix B.

3.3.3.1 PCM sensible heating

One of the basic conditions in the Neumann solution for the quasi-stationary one-phase Stefan problem is that the PCM must be at its melting point. Therefore, to achieve an accurate result, transient sensible heating calculations need to be done separately. The PCM temperature is a function of position and time, $T(x, t)$. A slab of the PCM, $0 \leq x \leq l$, is considered to be solid at uniform temperature. Heat transfer through the PCM is by the imposed temperature at the interface of the PCM and the HPC fin. The other three edges are assumed insulated. The mathematical model of the one-dimensional transient heating process can be expressed as:

$$\rho_s c_s \frac{\partial T}{\partial t} = k_s \frac{\partial^2 T}{\partial x^2}, \quad (3.5)$$

The method of separation of variables is used to solve the equation with the following initial and boundary conditions (Ozisik, 1993):

$$T(x, 0) = T_{amb} < T_m, \quad (3.6a)$$

$$T(0, t) = T_{hpc}(t), \quad (3.6b)$$

$$\frac{\partial T}{\partial t} \Big|_{x=l_{CHE}} = 0 \quad (3.6c)$$

The solution of this heat conduction problem is as below:

$$T(x, t) = \left(\frac{T_{hpc}(t) - T_{amb}}{L} x + T_{amb} \right) + \sum_{n=1}^{\infty} C_n e^{-\frac{\alpha_s^2 n^2 \pi^2 t}{L^2}} \sin\left(\frac{n\pi x}{L}\right), \quad (3.7)$$

where, x denotes the position of the PCM in distance from the hot plate (HPC) and $C_n =$

$$\frac{2}{l_{pcm}} \int_0^{l_{pcm}} \frac{T_{hpc}(t) - T_{amb}}{l_{pcm}} \text{Sin} \left(\frac{n\pi x}{l_{pcm}} \right) dx, n = 1, 2, 3, \dots$$

3.3.3.2 PCM latent heating

During melting, one more boundary condition at the interface location, $X(t)$, will be added to the problem. Therefore, the equation 3.5 must be solved by the following initial and boundary conditions for the range of $0 < x < X(t)$:

$$T_{pcm}(0, t) = T_{hp}(t), \quad (3.8a)$$

$$T_{pcm}(X_{pcm}(t), t) = T_m, \quad (3.8b)$$

$$\rho_l L X_{pcm}'(t) = -k_l \frac{\partial T_{pcm}}{\partial t} \Big|_{x=X_{pcm}(t)}, \quad (3.8c)$$

$$X_{pcm}(0) = 0 \quad (3.8d)$$

The values of the PCM properties are in the liquid phase. Existence of boundary condition 3.8c makes the heat equation very complicated. According to the Neumann solution for the one-phase Stefan problem (Alexiades & Solomon, 1993), the quasi-stationary solution for expression of the interface location and temperature distribution in the PCM in terms of the original physical variables for charging process takes the form:

$$X_{pcm}(t) = \eta_{f,c} \sqrt{(2k_l S t_1 t) / (\rho c_l)} \quad (3.9)$$

$$T_{pcm}(x, t) = T_{hpc}(t) - \Delta T_l \frac{x}{X_{pcm}(t)}, 0 \leq x \leq X_{pcm}(t), \quad (3.10)$$

where, $\Delta T_l = T_{hpc}(t) - T_m$.

Existence of fins on the HPC increases the rate of the heat transfer rate from the object to surrounding material. It was assumed that the temperature distribution in the fin surface is uniform. To include the influence of this assumption in the calculation process, the efficiency of the fin is determined from the following equations (Bergman & Incropera, 2011):

$$\eta_{f,c}(t) = \frac{q_f(t)}{q_{max}(t)}, \quad (3.11)$$

$$q_f(t) = \sqrt{h_{pcm,c}(t)P_{f,c}k_{f,c}A_{c,c}}\theta(t) \frac{(\cosh(mh_{f,c})-1)}{\sinh(mh_{f,c})} \quad (3.12)$$

and

$$q_{max}(t) = h_{pcm}(t)A_{f,c}\theta(t) \quad (3.13)$$

where, $\theta(t) = (T_{hpc}(t) - T_{pcm}(t))$, $m(t) = \sqrt{h_{pcm,c}(t)P_{f,c}/k_{f,c}A_{f,c}}$. The value of the efficiency of the fin will be multiplied to the equation 3.9, which causes to slow down the interface growth rate.

3.3.4 Discharging mode

The PCM inside the LHS tank is divided into a finite number of slabs (j), as shown in Figure 3.6. Energy balance is applied to each slab. Outlet water temperature of each slab is equal to the inlet water temperature of the next slab. The solidification rate of the PCM in each slab depends on the inlet water temperature. The finned HWSHE pipe is placed at the middle of the tank, so the PCM in each slab is divided to two equal parts on the upper side and lower side of the finned HWSHE pipe. Heat transfer occurs from both sides of the fin. The flowchart of the discharging mode is shown in Appendix B.

The PCM solidifies due to the cold supply water entering at velocity v and temperature $T_{w,i,i}$ into the storage tank. The unknown variables are the solid-liquid interface progression rate in each slab and the outlet water temperature after each slab. The determination of these variables must be done simultaneously. It is assumed that in a physical process of discharging - when Stefan number is small ($St < 2$) - the PCM temperature remains constantly in the range of melting point, while the solid-liquid interface is progressing (Alexiades & Solomon, 1993). Thus, the supply water temperature is rising while the slab j is solidifying. After the slab j fully solidified, it has effectively lost its thermal inertia, and its temperature will rapidly fall to the inlet water

temperature at its location, and the water will quickly respond to one less slab. It means that supply water initially was warming up by N slabs, but after the earliest PCM slabs solidified, the supply water will be warmed up by $(N-1)$ slabs. For this method of solution, few assumptions must be considered. As indicated in Figure 3.4, it is assumed that in discharging mode the thermal energy transmission from the PCM to the finned HWSHE pipe occurs only in one direction (on the y axis). In addition, heat transmission in the direction of x can be ignored, when the axial temperature drop is not too substantial. It is assumed that heat conduction is negligible inside the water, which is thermally at the steady state, so that its temperature depends merely on the pipe direction, which is reasonable for fairly rapid flow, after an initial transient, if the pipe is not too narrow and not as well long. Another assumption is that the latent heat of the PCM is so large that the surface temperature of the PCM at fins, and the pipe walls can be taken as essentially equal to T_m during the entire solidification process. This assumption implies a uniform temperature of T_m in the PCM throughout the solidification. Large latent heat (small Stefan number) implies that the front will not penetrate very far into the PCM, and a large conductivity will tend to level up the temperature, so the assumption is plausible at least. If in charge process the PCM is not fully melted, then, in discharging process, only molten mass fraction of the PCM is considered as an active mass of the PCM slab.

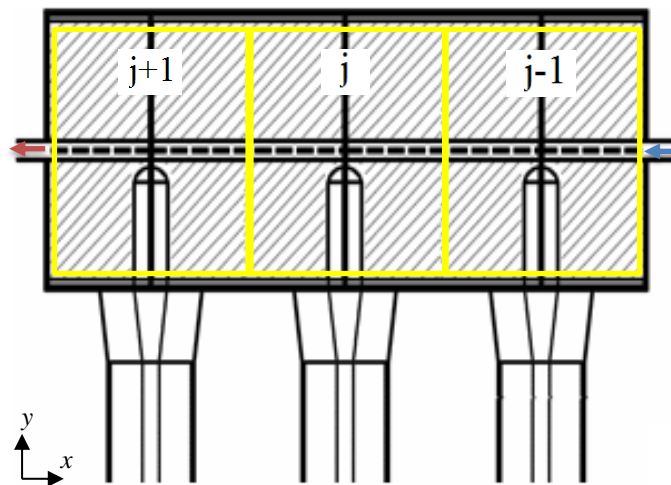


Figure 3.4: Arrangement of PCM slabs.

3.3.4.1 Heat transfer to finned HWSHE pipe

The rate of change of the stored thermal energy in the PCM slab obtains by:

$$\dot{q}(t) = \dot{q}_p(t) + \dot{q}_{f,p}(t) \quad (3.14)$$

where $\dot{q}_p(t)$ is the heat flux to the pipe and $\dot{q}_{f,p}(t)$ is the heat flux through the fins. Total heat transfer to the supply water via the pipe wall and fins can be calculated as:

$$\dot{q}(t) = A_p h_w(t) \theta(t) + N_f \eta_{f,p} \sqrt{h_{pcm,d}(t) P_{f,p} k_{f,p} A_{c,f}} \theta(t) \frac{(\cosh m l_{f,p} - 1)}{\sinh m l_{f,p}} \quad (3.15)$$

where, $m = \sqrt{h_{pcm,d}(t) P_{f,p} / k_{f,p} A_{c,f}}$. $h_{pcm,d}$ is calculated from equation 3.4 while $\theta = (T_m - T_{w,i,i}(t))$. Efficiency of the fin on the pipe, $\eta_{f,p}$, is calculated by placing related variables to the equation (11). Then, by taking into account all parameters, outlet water temperature from each slab of the PCM will be obtained by:

$$T_{w,i,o}(x, t) = T_{w,i,i}(x, t) + \dot{q}(t) / c_{p,w} \dot{m} \quad (3.16)$$

The convective heat transfer coefficient of the water could be estimated based on the thermal behavior of the flow in an isothermal pipe when the thermal entrance region is not fully developed and $Re_D < 2500$ (Lienhard, 2011):

$$h_w = \left(\frac{k_w}{d_{p,i}} \right) \times \left(3.657 + \frac{0.0018 Gz^{1/3}}{(0.04 + Gz^{-2/3})^2} \right), \quad (3.17)$$

where, $Gz = (Re_D Pr d_{i,p}) / x$, $Re_D = (\rho_w v_w d_{p,i}) / \mu_w$ and $Pr = (c_{p,i} \mu_w) / k_w$.

3.3.4.2 PCM solidifying

To find out the solidification time of the PCM slabs, the equation 3.5 in the PCM must be solved again with different initial and boundary conditions. In this case, the heat equation must be solved based on the imposed heat flux ($\dot{q} < 0$):

$$T_{pcm}(x, 0) = T_m, \quad (3.18a)$$

$$\rho_s \bar{L} Y_{pcm}'(t) = -k_s \frac{\partial T_{pcm}}{\partial t} \Big|_{y=Y_{pcm}(t)}, \quad (3.18b)$$

$$-k_s \frac{\partial T_{pcm}}{\partial t} \Big|_{y=0} = \dot{q}(t), \quad (3.18c)$$

$$Y_{pcm}(0) = 0 \quad (3.18d)$$

Values of variable are in liquid phase. In this method, the case of a melted slab at its melt temperature T_m is being solidified by an imposed flux $\dot{q}(t)$ at the fin faces. According to the Neumann solution method for a one-phase quasi-stationary Stefan problem, by including their initial and boundary conditions, the equation for the solid-liquid interface location takes the form:

$$Y_{pcm}(t) = \dot{q}(t) t / \rho_s \bar{L} \quad (3.19)$$

If the melted PCM slabs are at a temperature higher than the melting temperature, to be able to include the effect of stored sensible heat, the latent heat magnitude can be modified by following equation (Alexiades & Solomon, 1993):

$$\bar{L} = L + \frac{1}{2} c_l (T_L - T_m) \quad (3.20)$$

where, $T_L = \text{mean}(T_{pcm}(x = 0: l_{pcm}, t_{end}))$ is the mean temperature of the PCM at the end of the melting time.

3.3.5 System performance and efficiency

This section compares the thermal performance of the proposed system with a conventional system. In the latter one, the hot water is stored in the storage tank without water draw-off. This system is considered as a baseline system. By considering the effects of stratification, efficiencies and potential of delivering hot water could be computed.

3.3.5.1 Thermal analysis of the ETHPSC baseline system

In the baseline HPSC, cold water passes directly over the HPC in the manifold and the heated water stored in an insulated storage tank. By considering the same equations for heat pipe surface temperature mentioned in section 3.3.2, the heat transfers from the HPC

to the supply water are determined. The flowchart of the baseline HPSC system is provided in appendix B.

Each unit of solar panel consists of an array of HPSCs. Therefore, the thermal performance of the array of the HPCs can be analyzed based on external forced convection over a tube. Churchill and Bernstein (Lienhard) presented correlations for heat transfer from a cylinder to the environment:

$$\overline{h_w} = \frac{d_{p,i}}{k_w} \times \left(0.3 + \frac{0.62Re_D^{1/2}Pr^{1/3}}{[1+0.4/Pr^{2/3}]^{1/4}} \left[1 + \left(\frac{Re_D}{282000} \right)^{5/8} \right]^{4/5} \right) \quad (3.21)$$

Heat transfer rate is determined from:

$$T_{w,b,o} = T_{w,b,i} + \overline{h_w}A_p(T_{hpc} - T_{w,b,i})/\dot{m}c_{p,w} \quad (3.22)$$

All properties are determined at a film temperature $T_f = (T_{hpc} + T_{w,b,i})/2$.

3.3.5.2 Usable hot water and efficiency

During the day, solar heat is collected and stored in the LHS tank. No water is drawing off during the day. The primary objective of the storage tank is to maintain the hot water temperature. The extent to which temperature is degraded over time needs to be quantified. Effective operation of hot water stored in a water tank relies on natural thermal stratification (Armstrong et al., 2014a). Destratification arises due to both heat convection from the hot water layer to lower temperature layers and vertical conduction in storage tank wall, even when there is no water draw-off (Fernandez-Seara et al., 2007).

A recent research by Armstrong et al. (2014b), determined the loss rate of usable hot water in a standby hot water tank due to the effect of the destratification. They found that for a tank with a 74 liter capacity and 0.7mm thickness made of copper, which is clad with an external 50 mm thick layer of rigid polyurethane insulating foam (0.028 W/mK) (Standard, 2013), hot water usable volume loss rate over 12 hour is 2.1 liters/hour. In other words, by dividing the usable volume loss rate to the tank capacity, 3% of the usable

hot water will be destroyed in the tank. It is also assumed that the heat losses from the tank wall to the environment are negligible compared to the conjugate exchange with the water.

Armstrong et al. (2014a) defined usable hot water volume as equal to the volume of fluid from a tank that can be mixed to a useful final operating temperature, T_u . The usable hot water volume could be computed by:

$$V_u(t) = m_w \times \sum_{hr=1}^{12} \frac{T_{w,t,o}(t) - T_u}{T_u - T_{w,t,i}(t)} \quad (3.23)$$

Since the tank is considered to be in unused mode, based on the usable volume loss rate percentage (Lr), the usable volume destruction per hour could be computed as follows:

$$V_{u,d}(t) = V_u(t) \times Lr \times (12 - t) \quad (3.24)$$

The term of $(12 - t)$ presents the time that the produced hot water in the solar collector will be on standby in the tank. Therefore, the total remaining usable hot water after 12 hours can be determined by:

$$V_{u,r} = \sum_{hr=1}^{12} V_u(t) - V_{u,d}(t) \quad (3.25)$$

Destratification does not occur in the PCM tank, so there is no destructive energy in the PCM tank ($V_{u,d}(t) = 0$). According to equations 3.23 and 3.25 the usable hot water and total usable hot water volume produced by the PCM tank could be computed.

The total delivered energy by usable hot water from the water tank and from the PCM tank can be calculated by

$$E_d = V_{u,r} c_{p,w} (T_u - T_{w,t,i}(t)) \quad (3.26)$$

The energy efficiency of the systems is determined by:

$$\eta_{tot} = \frac{E_d}{I} \quad (3.27)$$

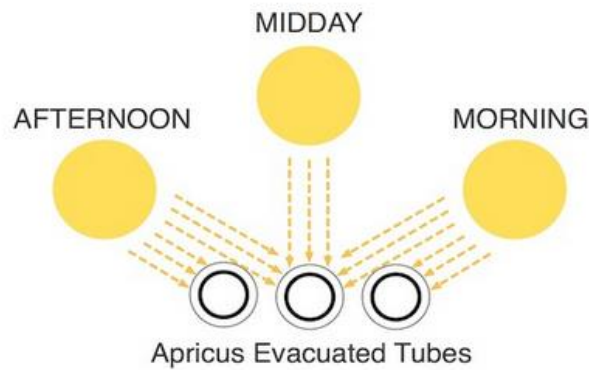


Figure 3.5: Passive Tracking by solar tube collector.

3.4 HPSC-LHS design

For a professional design of the actual model of the proposed system several steps must be executed accurately. There are four critical parameters that have direct influence on the performance of the system, which are proper solar collector, effective fins design for heat sink side, effective fins design for pipe and LHS tank size. To be able to incorporate the findings of previous research works, important findings of relevant to each items must to be extracted.

3.4.1 HPSC selection

Several comparative studies have shown that the performance of SWH systems utilizing HPSC is better than those using conventional flat plate collectors (Ayompe et al., 2011; Kim & Seo, 2007; Wei-Sheng, 2013; Zambolin & Del Col, 2010).

For solar collector tubes, a set of 20 pieces of ETHPSC is chosen. This is produced in a Malaysian company named Thermo Renewable SDN BHD. Specifications of evacuated glass tube solar collectors are listed in Table 3.1. Glass tube consists of two layers, which between the layers is evacuated to insulate it against heat loss. As shown in Figure 3.5, the round absorber surface of the evacuated tubes passively tracks the sun throughout the day, so no mechanical tracking device is required. This allows optimum surface area

exposure, which covers the majority of the solar radiation every day. The evacuated tubes receive >20% more solar exposure compared to a flat absorber, allowing more solar energy conversion to heat each day.

As shown in Figure 3.6, the evacuated glass tube and HP are assembled with insertion of an aluminum fin, which connects these two parts together. The aluminum heat transfer fin is tightly held against the inner wall of the evacuated tube as well as the HP. This is an important design feature as over time with the high temperature, aluminum will soften, and so the clips ensure long term tight contact, which is essentially for optimal performance. Specifications and dimensions of the copper HP is listed in Table 3.2.



Figure 3.6: Glass tube and HP with aluminum fin.

Table 3.1: Specifications of the evacuated tube solar collector.

Item	Value
Number of heat pipes	20
Glass tube outer diameter, D_t (mm)	58
Glass tube thickness, t_c (mm)	3
Absorber plate thickness, t_p (mm)	1
Evacuated tube length, l_p (mm)	1800
Glass emittance, ε_g	0.88
Plate emittance, ε_p	0.95
Reflective Index of glass, N	1.53

Table 3.2: Specifications and dimensions of the HP.

Item	Value
HPE length, l_e (mm)	1675
HPA length, l_a (mm)	30
HPC length, l_c (mm)	70
HPE outer diameter, $d_{o,hpe}$ (mm)	8
HPC outer diameter, $d_{o,hpc}$ (mm)	24
HP wall thickness, t_{hpe} (mm)	1
Wick thickness, t_{wick} (mm)	1
Vapor core cross-sectional radius, r_v (mm)	0.054
HPE wick capillary radius, $r_{c,eva}$ (mm)	0.04
Thermal conductivity of liquid, k_e (W/mK)	0.63
Thermal conductivity of wall, k_s (W/mK)	385
Porosity, ε	0.5
Permeability, K (m ²)	1.5×10^{-9}
Fiber thickness, d (m)	2×10^{-5}
Mesh number per unit length, N	40

3.4.2 PCM selection

Desired properties of a suitable PCM need to be studied in thermodynamic, kinetic, chemical, and economic criteria. For low temperature heat exchanger and solar applications, Paraffin with melting temperature in the range of 40-60°C received more attractions. This material contains in them one major component called alkanes, characterized by C_nH_{2n+2} (Abhat, 1983). Paraffin is white, odorless, tasteless, waxy solid with a heat of fusion of 180 –220 kJ/kg. Based on the vast study on the previous relevant researches, a Paraffin wax with melting temperature in the range of 53-57°C (ASTM D87) is chosen. Company of Sigma-Aldrich manufactures this material. The FTIR and DSC

tests of this product are shown in Figures 3.7 and 3.8. Thermal properties of the PCM is listed in Table 3.3.

Table 3.3: Physical properties of the Paraffin Wax.

Property	Value
Melting point, T_m (°C)	53-58
Density solid / liquid at 15/70°C, ρ_s/ρ_l (kg/m ³)	990 / 916
Thermal conductivity of solid / liquid, k_s/k_l (W/mK)	0.349 / 0.167
Specific heat solid / liquid, c_s/c_l (kJ/kgK)	2.76 / 2.48
Volume expansion at $\Delta T=20^\circ\text{C}$, β_{PCM} (%)	0.293
Heat storage capacity, L (kJ/kg)	163
Dynamic viscosity, μ (kg/ms)	0.00385

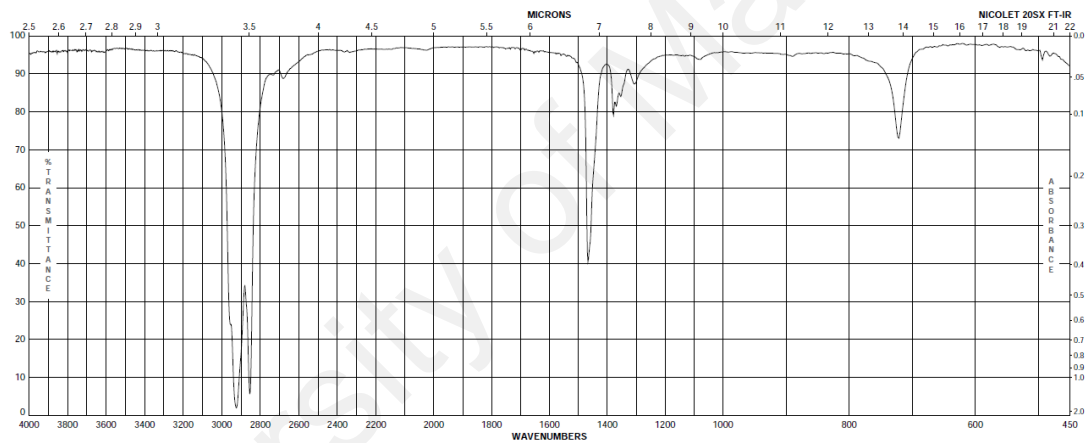


Figure 3.7: FT-IR analysis of the paraffin wax provided by Sigma Aldrich co.

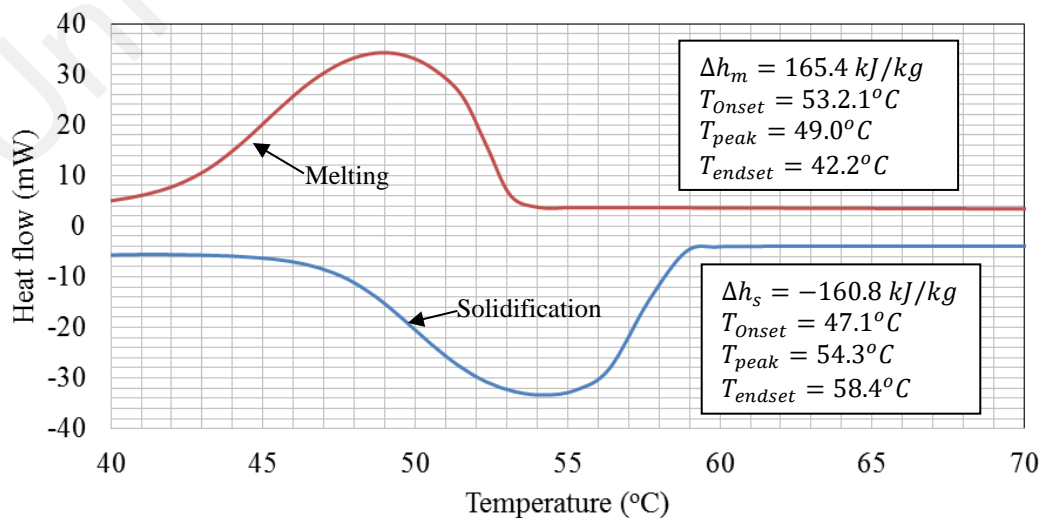


Figure 3.8: DSC curves for melting and solidification of the paraffin wax.

3.4.3 Design of fin on the HPC

Besides the material of the fin, there are three parameters that have high influences on the performance of the fin, which are orientation, length, and spacing (distance between the fins). Following bullet points are extracted from the studied references:

- Horizontal fins provide higher melting rate than the vertical fins.
- Decreasing distance between adjacent fins increases the heat transfer conductivity and decreases thermal resistance between the surface and the PCM.
- The onset of natural convection was gradually prevented when the distance between the fins was decreased.
- Too large distance between the fins led to the reduction in total heat transfer surface area.
- Few longer fins are far more efficient in enhancing the melting rate than more number of shorter fins.
- More number of longer fins could steadily enhance the melting rate.
- Longer fins provide more uniformed temperature distribution within the PCM.

Although, none of the researcher provides any simplified method for optimized design of the fins, but with respect to the findings of the references, a design for fins on HPC is prepared (Figure 3.9). Cylindrical and horizontal shape of the condenser leads to use of

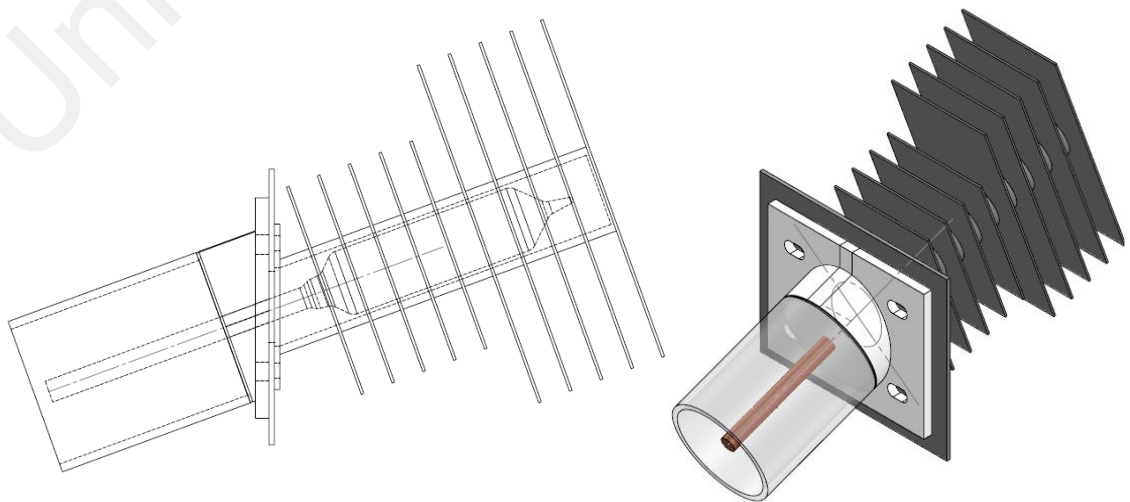


Figure 3.9: Fin shell on HPC (side view and 3D view).

vertical fins. The material is considered for this part is stainless steel. In this design the HPC inserts into the shell.

3.4.4 Design of fins on the pipe

Similar to previous section, research works on using fins in the solidification process revealed following bullet points that can indicate the design conditions:

- Fin effectiveness is significantly high and causes less solidification time and thus, the heat recovery is much faster due to fins.
- The time required for complete solidification was found to be decreasing almost linearly with number of fins.
- At any time heat transfer from the fin to the wall was much higher than that coming directly from the PCM to the wall. This will promote for longer radial fins.
- As the time elapsed, direct heat transfer from PCM to wall became negligible. It indicates that, probably, employing fins are more effective at earlier stages than at latter stages.
- Using less width fins produces more effective heat transfer enhancement.

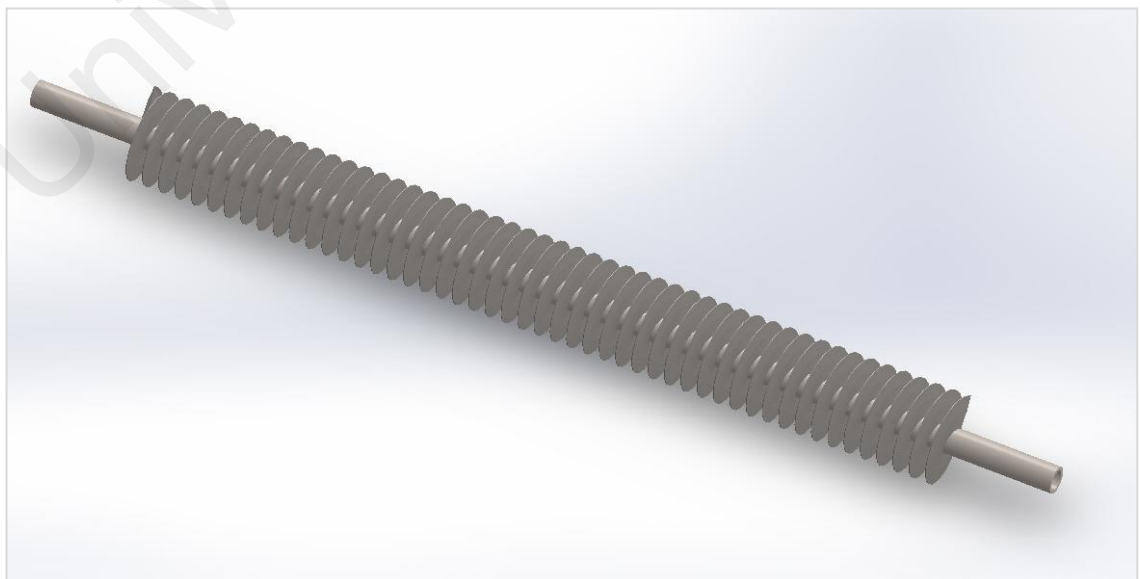


Figure 3.10: CAD drawing of the spring circular fins on the pipe.

According to these points and with consideration of limitations in fabrication, a spring circular fin around the pipe for the finned HWSHE pipe is designed (Figure 3.10).

To be able to test different supply water flow rates and flow patterns, three pipes are considered to be placed inside the LHS tank. Then, by placing valves in inlet and outlet sides of the pipes, different flow patterns could be tested. The schematic CAD design of this piping system is shown in the Figure 3.11.

3.4.4.1 PCM Tank design

Average daily solar radiation in the tropical region like Malaysia is about 4.5 kWh/day. Absorbable solar radiation is about %60. Aperture area for one row of the evacuated tube solar collector is 98,890 mm² and for 20 tubes is 1,977,800 mm². Therefore, total absorbable solar energy is:

$$Q_{solar} = 1977800/1000000 * 4.5 * \%60 = 5.34 \frac{kWh}{day} = 19224 \frac{kJ}{day}$$

Refer to specifications of the chosen PCM in Table 3.3, the total required energy to melt the PCM could be calculated by two following equations for sensible (Q_s) heat and latent heat (Q_l):

$$Q_s = m_{PCM} \cdot c_p \cdot \Delta T \quad (3.28)$$

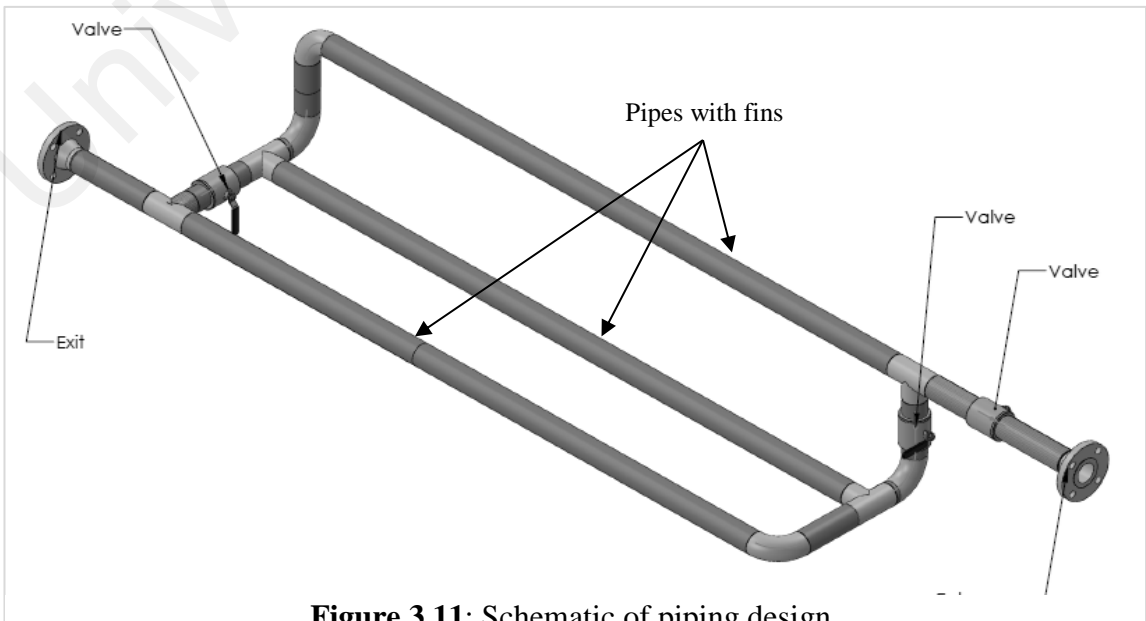


Figure 3.11: Schematic of piping design.

$$Q_l = m_{PCM} \cdot l_{f,PCM} \quad (3.29)$$

If we assume total daily solar energy absorption stores in PCM, then following equality must be remained:

$$Q_{solar} = Q_s + Q_l \quad (3.30)$$

$$Q_{solar} = m_{PCM} * (c_p \cdot \Delta T + l_{f,PCM}) \quad (3.31)$$

If $T_{initial} = 25^\circ C$ & $T_{melt} = 53^\circ C$, then:

$$m_{PCM} = \frac{19224}{2.14 \cdot (53 - 25) + 189} = 76.57 \text{ kg}$$

By considering the possible energy losses, solar energy fluctuation and safety factors, perhaps the magnitude of the PCM must be considered 75% of the calculated mass above, which the mass of PCM will be between ~57kg.

To calculate the required capacity of the LHS tank, volumes of the PCM, heat pipe condenser fin shell, and finned pipe must be calculated and then, with respect to the knowledge from previous research works, about the effective geometry of the container in charging/discharging rates of the PCM, the most proper dimensions for the tank be estimated.

- Volume of the 20 pieces of the condenser fin shells: 0.00324 m³
- Supply water finned pipe channel: 0.00448 m³
- PCM volume in melt mode: 0.06223 m³

Therefore, the required tank capacity is 0.06995 m³. CAD drawing of the LHS tank is shown in Appendix C. According to the considered dimensions of the tank, the capacity is 0.07303 m³, which is 5% more than calculated capacity.

3.5 Experimental investigation

3.5.1 The apparatus

The Schematic of experimental set-up the HPSC-LHS system is shown in Figure 3.12. A photograph of the experimental setup and the LHS tank are shown in Figure 3.13.

The dimensions of the experimental setup is charted in Table 5.1. The inlet cold water is from an overhead water supply tank. A low power magnetic water pump and a needle valve placed in the pipe line between the water tank and LHS tank enabled the water flow rate to be controlled. The LHS tank is insulated with 50 mm rockwool and the connecting pipe with K-FLEX cool insulation. Temperatures are measured using copper-constantan (Type T) thermocouples (TCs). Locations of the TCs are shown in Figure 3.14. Ten TCs (TC1-TC10) are immersed in the middle of the LHS tank from the top and the side. Two

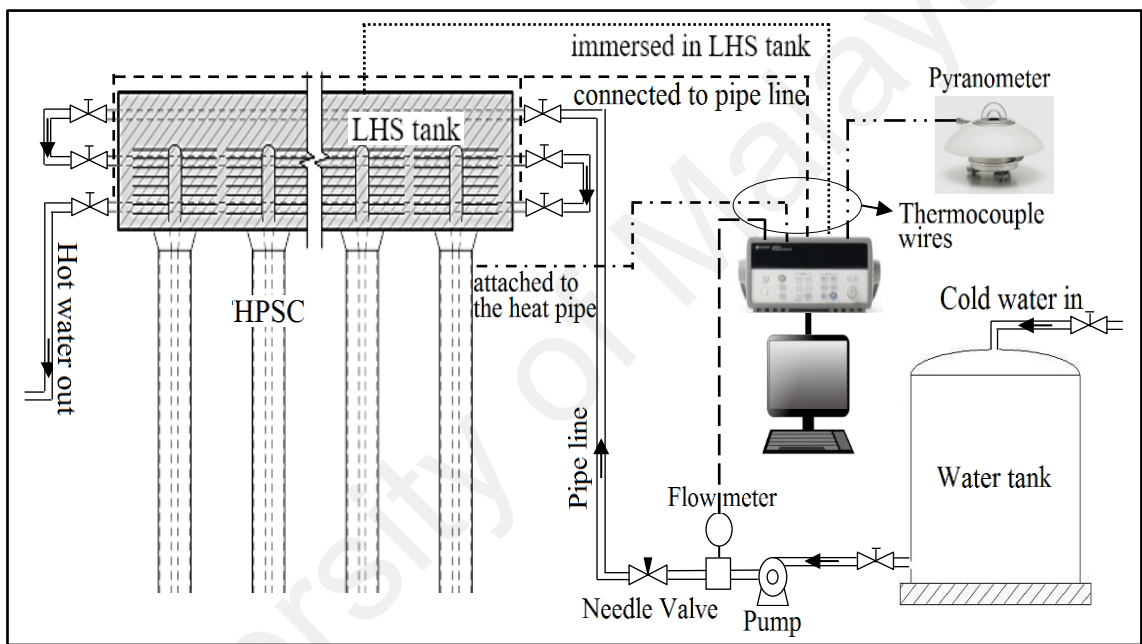


Figure 3.12: Schematic of experimental setup.



Figure 3.13: a. Photo of HPSC-LHS experimental setup, b. Photo of inside of the LHS tank.

TCs (TC11-TC12) are placed at the bottom of the LHS tank. Water inlet and outlet temperatures were measured with six TCs (TC13-TC18)), which are placed at the beginning and the end of the finned pipes. TC19 is connected to the pyranometer. TC20 is connected to the flowmeter. TC21 is measuring the ambient air temperature. Five HPs (no. 1, 5, 10, 15 and 20) are selected to measure the condenser (TC22-TC26), adiabatic (TC27-TC31) and evaporator (TC32-TC36 and TC37-TC41) temperatures. The TCs were mechanically attached to the surfaces of the HPs by tie wires.

Solar radiation is recorded by a Kipp & Zonen Pyranometer CMP10. A Burkert inline fitting type S030 is employed for water flow rate measurement. All data were recorded on an Agilent data recorder model 34970A.

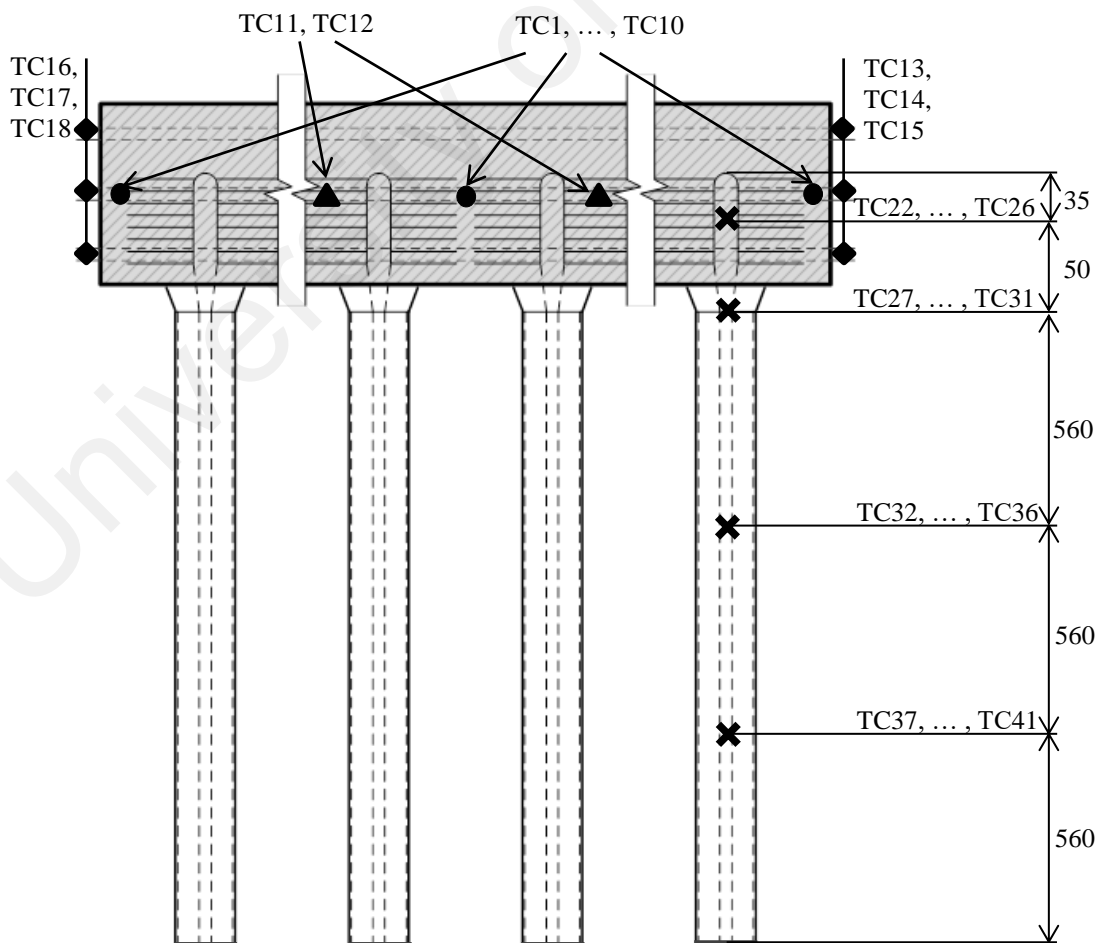


Figure 3.14: The thermocouples locations.

3.5.2 Experimental procedure

As mentioned earlier, the field tests are carried out in two types. One is charging only and discharging only and the other one is batch-wise simultaneous charging-discharging.

During the charging only mode, solar radiation incidents on the HPSC and the heat is absorbed and transferred via the HPs to the LHS tank to melt the PCM. The heat stores in the PCM in both forms of the latent and the sensible heat. In this mode, the supply water does not pass through the LHS tank. During the discharging only mode, the supply water circulate through the finned HWSHE pipes and receives heat from the molten PCM. This mode starts when the solar radiation become very weak and the heat transmission between the HPSC and the LHS tank is very low or stopped.

The batch-wise simultaneous charging-discharging mode is when both solar and supply heat transfer occurs at the same time. In actual occurrence, supply water might flow periodically throughout the day and night. In this type, the discharging time and the hot water load depend on the consumer demands. It could be at either of day time or night time.

3.5.3 Efficiency calculations

The incident solar energy (\dot{I}) is transmitted through the inner evacuated glass tube where it is absorbed (\dot{S}) by the aluminum fin. A major portion of the heat absorbed by the aluminum fin in the HPE is conveyed to the HPC (\dot{q}_{hp}). The heat flux heats up the PCM in the storage tank (q_{pcm}). Then, the stored heat will transfer to the supply water flowing in the finned pipes inside the tank (\dot{q}_w).

In the present analysis, the following assumptions are made:

- Quasi-steady state heat transfer is assumed.
- All thermal properties are assumed constant.
- There is no axial heat conduction along the length of the HPSC.

- The temperatures of the inner glass tube, aluminum fin and the HPE are assumed equal and at a uniform temperature ($T_{hp,e}$).
- The temperatures of the HPE ($T_{hp,e}$) and the HPC (T_{cond}) are assumed to be uniform in their respective sections.

The fraction of the solar radiation incident absorbed by the HPSC depends upon several variables like surface material properties, convection from the surface and reflectance factors. Duffie and Beckman (Beckman et al., 1977) proposed a theoretical method for a tilted collector:

$$\dot{S} = \dot{I}_b \cdot R_b \cdot (\tau\alpha)_b + \dot{I}_d \cdot (\tau\alpha)_d \cdot \left(\frac{1+\cos\beta_s}{2}\right) + \dot{I}_g \cdot \rho_g \cdot (\tau\alpha)_g \cdot \left(\frac{1-\cos\beta_s}{2}\right) \quad (3.32)$$

A complete set of equations for computing the \dot{S} is reported in Appendix A.

The heat transmitted from the HPE to the HPC in terms of thermal resistance is determined by the following equations:

$$\dot{q}_{hp} = (T_{hp,e} - T_{hp,c})/R_{hp} \quad (3.33)$$

where the thermal resistances are determined based on the equations reported by Brahim et al. (2014):

$$R_{hp} = R_{hp,e,p} + R_{hp,e,w} + R_{hp,i} + R_{hp,c,p} + R_{hp,c,w} + R_{hp,c,o} \quad (3.34)$$

$$R_{hp,e,p} = \ln(d_{hp,e,o}/d_{hp,e,i})/2 \cdot \pi \cdot k_{hp} \cdot l_{hp,e} \quad (3.34.a)$$

$$R_{hp,e,w} = \ln(d_{hp,ew,o}/d_{hp,ew,i})/2 \cdot \pi \cdot k_{eff} \cdot l_{hp,e} \quad (3.34.b)$$

$$R_{hp,e,i} = 2 \cdot t_w/\pi \cdot k_l \cdot d_{hp,e,i} \cdot l_{hp,e} \quad (3.34.c)$$

$$R_{hp,c,p} = \ln(d_{hp,c,o}/d_{hp,c,i})/2 \cdot \pi \cdot k_{hp} \cdot l_{hp,c} \quad (3.34.d)$$

$$R_{hp,c,w} = \ln(d_{hp,cw,o}/d_{hp,cw,i})/2 \cdot \pi \cdot k_{eff} \cdot l_{hp,c} \quad (3.34.e)$$

$$R_{hp,c,o} = 1/\pi \cdot h_{con} \cdot d_{hp,c,i} \cdot l_{hp,c} \quad (3.34.f)$$

The condensing film heat transfer coefficient is obtained from (Hussein, 2003):

$$h_{con} = 0.728 \left[\frac{g\rho_l(\rho_l-\rho_v)k_l^3 L_f g}{d_i \mu_l T_i} \right]^{1/4} \quad (3.34.g)$$

The effective thermal conductivity of the liquid-saturated wick and working fluid is calculated according to Peterson (1994):

$$k_{\text{eff}} = \frac{k_e[k_e+k_s-(1-\varepsilon)(k_e-k_s)]}{k_e+k_s+(1-\varepsilon)(k_e-k_s)} \quad (3.35)$$

where, $\varepsilon = 1 - (\pi N_a d_w)/4$ in equation (3.35).

A portion of the stored heat in the PCM tank is lost through the walls of the tank to the surrounding:

$$\dot{q}_{\text{lost}} = k_{\text{ins}} \cdot A_{\text{tank}} \cdot (\bar{T}_{\text{pcm}} - T_{\text{amb}}) / x_{\text{ins}} \quad (3.36)$$

The stored heat in the PCM tank is determined by:

$$q_{\text{pcm}} = F_{\text{melt}} \cdot m_{\text{pcm},l} \cdot (L_{\text{pcm}} + c_{p,\text{pcm}} \cdot (\bar{T}_{\text{pcm}} - T_m)) - \sum \dot{q}_{\text{lost}} \quad (3.37)$$

Heat transfer to the stream of supply water can also be calculated from

$$\dot{q}_w = \sum \dot{m}_w \cdot c_{p,w} \cdot (\dot{T}_{w,h} - \dot{T}_{w,c}) \quad (3.38)$$

The overall efficiency of the HP is determined from

$$\eta_{\text{hp}} = \left(\frac{\sum \dot{q}_{\text{hp}}}{\sum \dot{i} \times A_{\text{sc}}} \right) \cdot \%100 \quad (3.39)$$

where, solar collector area is:

$$A_{\text{sc}} = d_{t,i} \times (l_{\text{hp},a} + l_{\text{hp},e}) \times N_t \quad (3.40)$$

The total heat storage efficiency in the LHS tank is determined from

$$\eta_{\text{pcm}} = \left(\frac{q_{\text{pcm}}}{\sum \dot{i} \times A_{\text{sc}}} \right) \cdot \%100 \quad (3.41)$$

The proportion of the energy transferred to the supply water and the recorded total solar radiation express the total thermal efficiency of the system which could be determined from

$$\eta_w = \left(\frac{\sum \dot{q}_w}{\sum \dot{i} \times A_{\text{sc}}} \right) \cdot \%100 \quad (3.42)$$

3.5.4 Uncertainty analysis

Errors can arise from various factors for instance calibration errors, individual instrument uncertainty, data acquisition errors, and data reduction errors. Thus, to assign credible limits to the accuracy of the presented results, an uncertainty analysis was performed by including the calibration errors of each one of the most effective parameters. It is considered that the overall thermal efficiency of the systems mainly depend on the reading of the following parameters:

$$\eta_w = f(\dot{I}, T_{hp,e}, T_{hp,c}, T_{pcm}, T_{amb}, T_m, L_{pcm}, T_{w,h}, T_{w,c}, \dot{m}_w) \quad (3.43)$$

The uncertainty associated with each measurement can be mathematically expressed as:

$$\frac{\delta\eta_w}{\eta_w} = \sqrt{\left(\frac{\delta X_1}{X}\right)^2 + \left(\frac{\delta X_2}{X}\right)^2 + \dots + \left(\frac{\delta X_n}{X}\right)^2} \quad (3.44)$$

where n is the number of parameters, $\frac{\delta X_1}{X}$ corresponds to the standard uncertainty of the parameters.

All the TCs were calibrated and the estimated error of temperatures were recorded in the range of 30-150°C. The measured errors of the TCs for HPE, HPC, PCM, ambient temperature and inlet/outlet supply water pipes are $\pm 4.7\%$, $\pm 3.7\%$, $\pm 0.4\%$, $\pm 3.7\%$ and $\pm 0.4\%$, respectively. Same data for flowmeter and pyranometer are, $\pm 0.2\%$ and $\pm 1.4\%$ of reading of ampere in the range of 4-20 mA, respectively. The uncertainties of the melting temperature and latent heat capacity of the PCM are $\pm 4.7\%$ and $\pm 1.4\%$, respectively. According to these values, by using the equation (16), the uncertainty of the overall thermal efficiency of the system can be determined to be about $\pm 8.7\%$.

CHAPTER 4: THEORETICAL MODEL OF THE HPSC-LHS DESIGN

4.1 Introduction

This chapter examines the feasibility of the HPSC-LHS design based on actual meteorological data in a tropical region of Malaysia. The main goal that was pursued in this analysis is the theoretical evaluation of storage capacity of the proposed system of merged HPSC and LHS tank. In the analysis arrangement, during the daytime water will not pass through the manifold, and the system is only in charging mode and after sunset, the system controller lets water flow through the pipe built into the tank. A combination of mathematical algorithms is used to model a complete processes of the heat absorption, storage and release modes of the proposed system. The performance of a conventional HPSC is compared with this new design. Calculations are done by a computational code developed in Matlab.

4.2 Conceptual design arrangement

As expressed earlier in chapter 3, the conceptual configuration of the proposed model is simpler than actual one. In the simplified design, the domestic cold water supplied via a finned HWSHE pipe is heated up as it flows through the LHS tank. Single-row vertical fin is assumed welded onto the HPC shell and also to the HWSHE pipe line to enhance heat transfer as shown in Figure 4.1.

Three different heat transfer processes occur during charging and discharging of the heat within the PCM are illustrated in Figure 4.2. Solar energy absorbed by the glass tube is conducted to the condenser section (SEA) via the HP. The heat is then transferred to the PCM and represents the charging heat exchange (CHE) process. The stored heat is discharged to the finned HWSHE pipe line and represents the discharge heat exchange

(DHE) process. These processes are calculated independently based on the methodology described in section 3.3. Dimensions of the LHS tank, HP and fins are shown in Table 1.

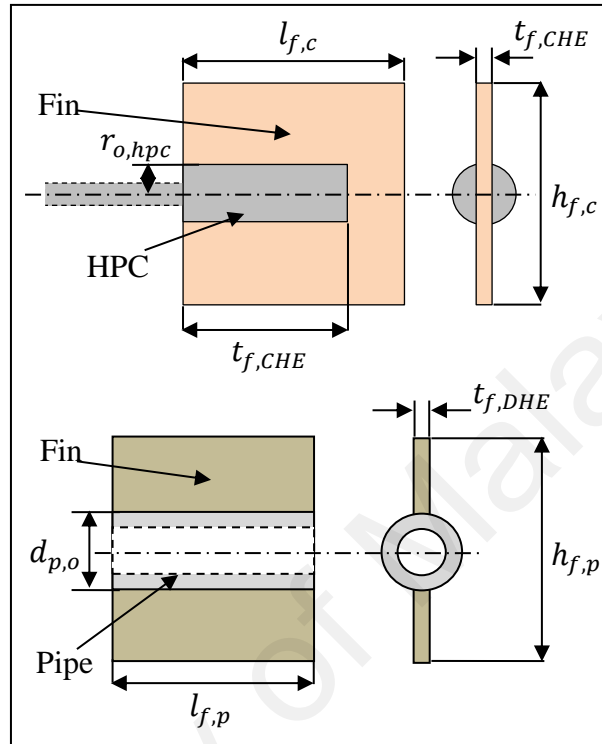


Figure 4.1: Fins designs for the HPC (top) and the HWSHE (bottom).

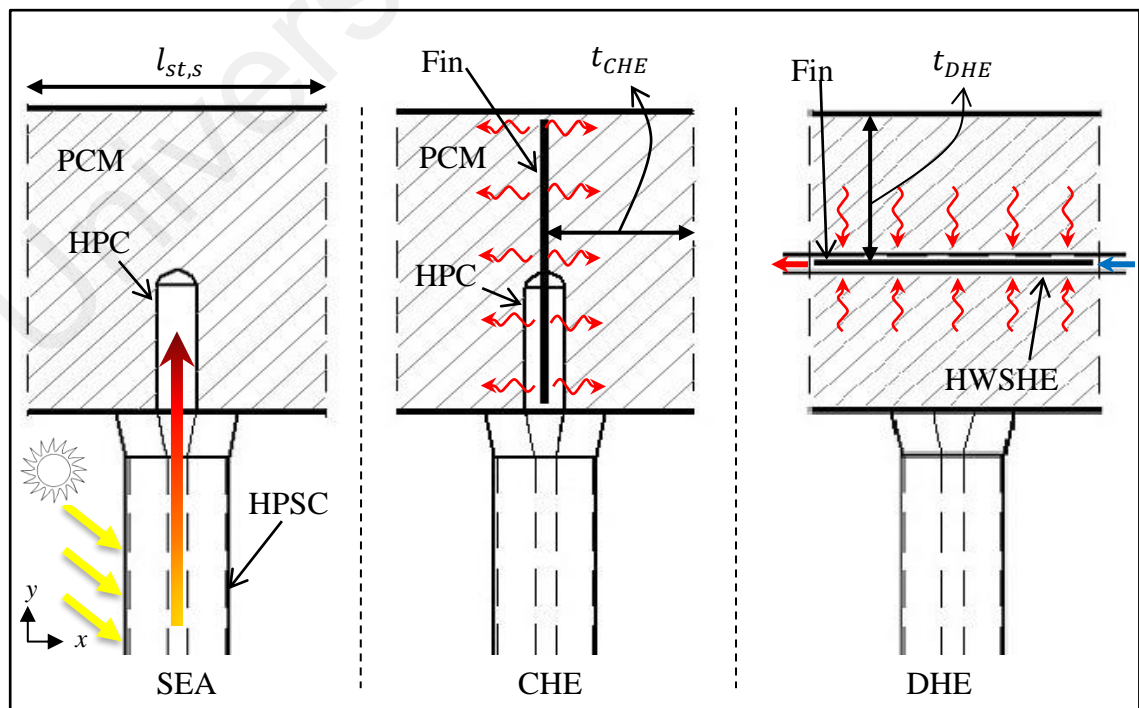


Figure 4.2: Heat transfer process in LHS tank.

Table 4.1: Dimensions of LHS tank and fins for theoretical analysis.

Item	Value
Number of heat pipes	20
Glass tube outer diameter (mm)	58
Glass tube inner diameter (mm)	52
Absorber plate thickness (mm)	1
Evacuated tube length (mm)	1675
LHS tank height (mm)	204
LHS tank width (mm)	204
LHS tank length (mm)	1725
Fin thickness on the CHE (mm)	2
Fin height on the CHE (mm)	200
Fin length on the CHE (mm)	200
Fin thickness on the pipe (mm)	2
Fin height on the pipe (mm)	91
Pipe outer diameter (mm)	18
Length of a section (mm)	142
Slope of solar collector (°)	20
Glass emittance	0.88
Plate emittance	0.95
Reflective Index of glass	1.53

4.3 Model validation

Accuracy of the theoretical modeling of a system depends on the validity of the equations employed all assumptions made. Duffie and Beckman (2013) provided a set of mathematical equations to determine absorbable incident solar energy (equation 3.1). This equation is validated by De Soto et al. (2006). Equation 3.4 determines the natural convection coefficient of melted PCM in a rectangular cavity was experimentally obtained by Marshall (1979). Zhu and Vafai (1999) developed equation 3.2 for the heat pipe surface temperature and showed that they were in very close agreement with experimental measurement. Equations 3.17 and 3.21 are used to obtain the heat transfer coefficient of supply water for flow inside a pipe and for flow across a circular cylinder. The highest error for the former equation is proven experimentally to be less than 7% (Shah & Bhatti, 1987), which for the latter equation is completely coincident with experimental data reported by Churchill and Bernstein (1977). In mathematical textbooks,

the quasi-stationary approximation method is a well-known modeling method to determine reasonable tradeoffs between charge and discharge parameters to store all available heat and totally discharge the heat during a discharge process. Alexiades and Solomon (1993) showed that for a Stefan number of $St_L < 2$, the error of this method is less than 10%. Prior analysis shows that the highest Stefan numbers in charging and discharging modes are 1.19 and 0.46, respectively. The result by phase-change interface equation introduced in section 3.3 is compared with the numerical method introduced by Cheng (2000). In Figure 4.3 the interface progression of a material with latent heat of 100MJ/kg, density of 1kg/m^3 and melting point of 0°C with a constant imposed temperature 2°C inside a rectangular chamber in duration of the two million seconds. The developments of the interface from both methods are very close.

4.4 Absorbable solar energy

Actual meteorological data for two typical days with high and low daily solar radiations in Kuala Lumpur, Malaysia are chosen for this simulation. Figure 4.4 shows the recorded solar radiation and the ambient temperature for these two days. The total daily solar radiation in low and high intensity solar radiation days are 12.6 MJ and 19.1

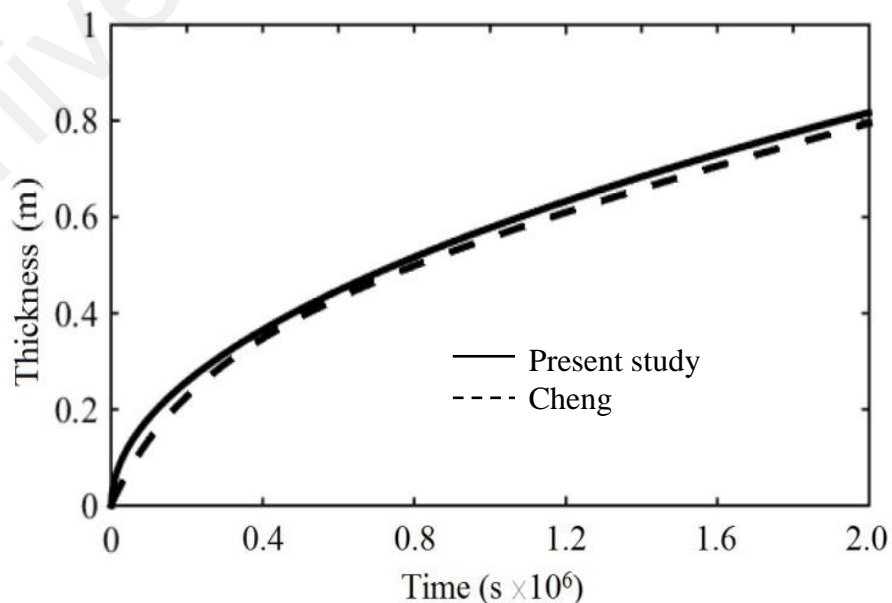


Figure 4.1: Comparison of the interface location.

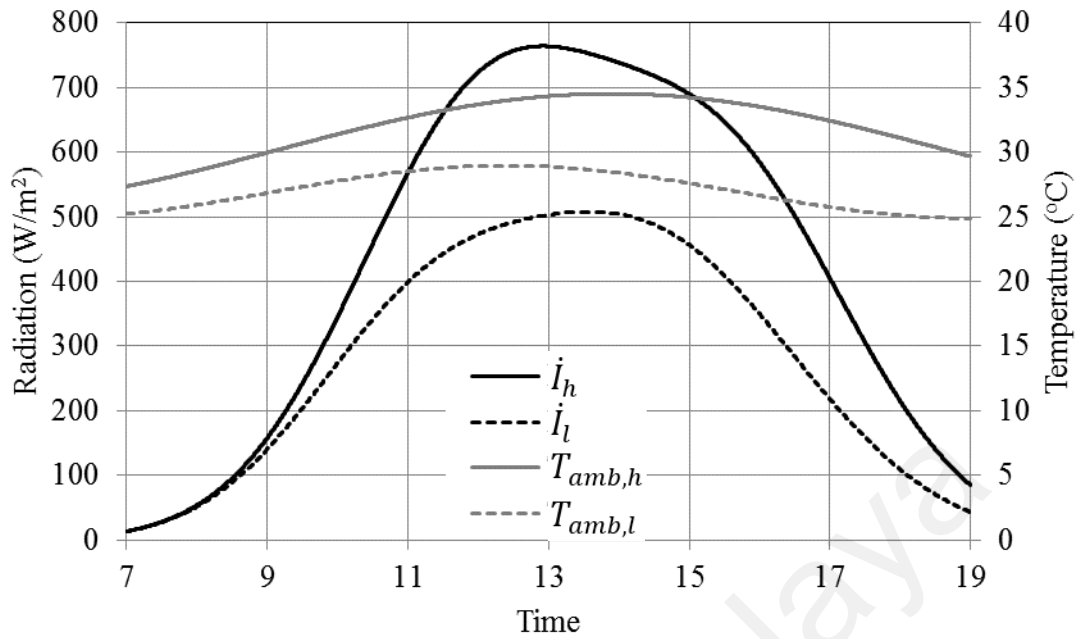


Figure 4.2: Recorded solar radiation and ambient temperature.

MJ, respectively. According to calculation, with respect to the properties of the collector, the absorbable solar radiation is approximately 60% of total radiation. The percentage of absorbed energy depends on several factors such as longitude and latitude of the place, the angle of the solar collector, glass and plate emittance and irradiation, cloudiness and ambient temperature.

4.5 Charging mode

Storing energy in the PCM is initially as sensible heat and later, after reaching the melting temperature is as latent heat, as the temperature rises again. It is assumed that the PCM is initially at the melting point. According to the primary calculation and later in experimental tests, it was found that this assumption is acceptable. Figure 4.5 presents the temperature gradient of the PCM in both days, in duration of the charging mode (day time), which varies in time and in the thickness of the PCM slab placed on one side of the HPC fins. Indeed, in charge mode, the heat flux transfers symmetrically to the PCM slab on both sides, by the fin on HPC. In a typical sunny day, the maximum temperature of the PCM adjacent to the fin reaches to above 90°C, while this amount for a cloudy/rainy

day is less than 80°C. According to equations in the section 3.3.3.2, fin efficiency is about 90% of copper material.

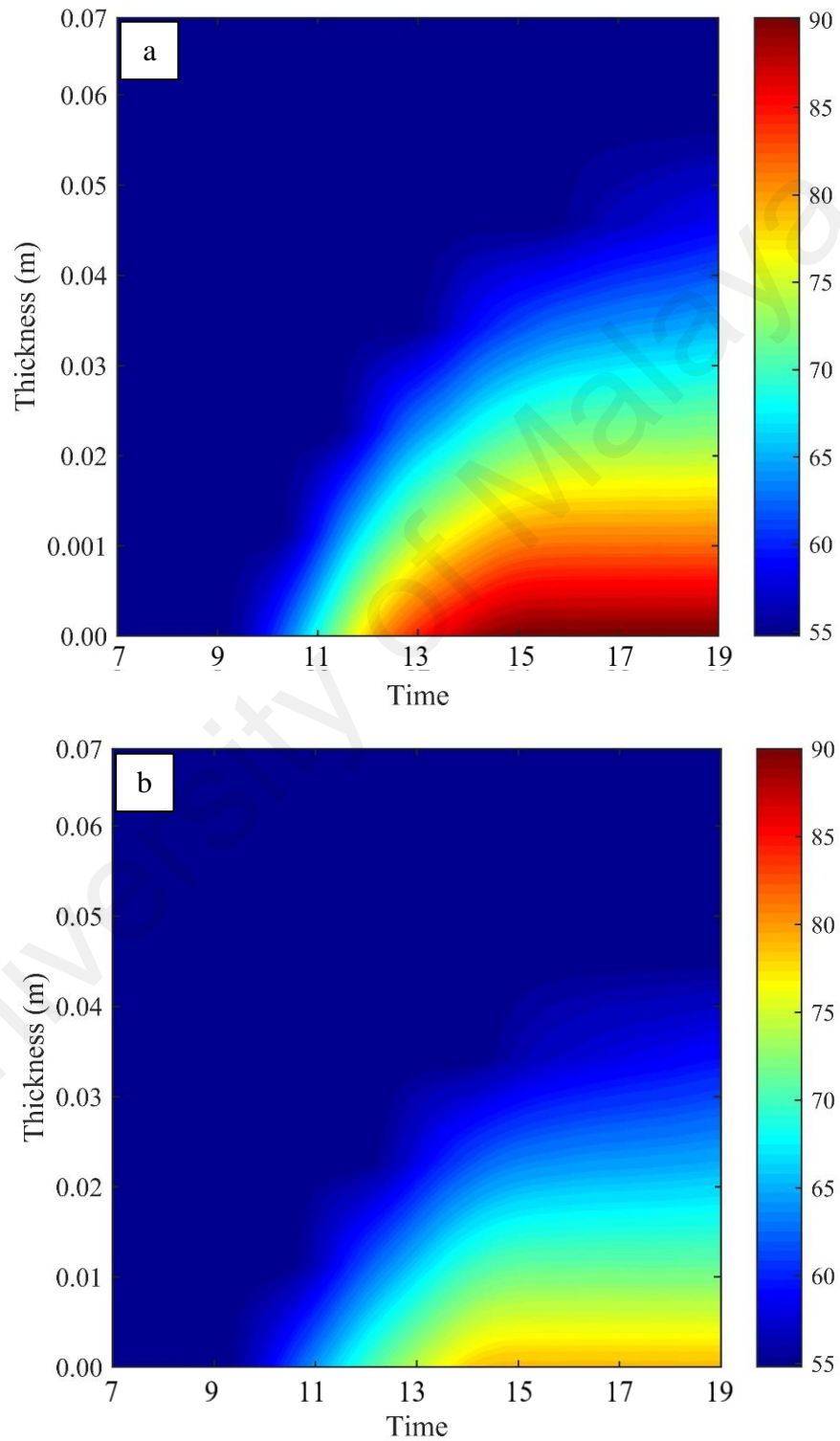


Figure 4.3: PCM temperature history for high (a) and low (b) daily solar radiation days.

As mentioned earlier, the system consists of 20 heat pipes. By considering this point that the equal heat transfers from every HPs and the LHS tank is in the standby mode, the thermocline and the interface location of the PCM in all slabs are the same. The liquid-solid interface movements for both days are shown in Figure 4.6. As soon as the HPC temperature increase to more than the temperature of the PCM the melting will starts. Around 07:00, the layer of the PCM adjacent to the HPC immediately starts to melt. At the end of the day, the melted thickness of the PCM in each side of the fin is ~57mm and ~48mm for high and low solar radiation days. The rate at which the interface progresses mainly depend on the availability of the solar radiation, and the PCM properties. It is observed that the interface progression rate is faster in the afternoon. This is attributed to two reasons. One is due to the higher temperature gradient between the condenser and the PCM during the morning heating up time and the other is the presence of liquid PCM around the fin with its inherent low convective heat transfer coefficient. Figure 4.7 shows the temperatures at the HPE and the HPC sections, and of the PCM 1cm away from the finned HPC and mean PCM temperature for both typical days. The mean PCM temperature is the average temperature of the PCM slab at the time. This Figure compares thermoclines of the HPE, HPC, PCM at 1cm distance form the fin and mean temperature

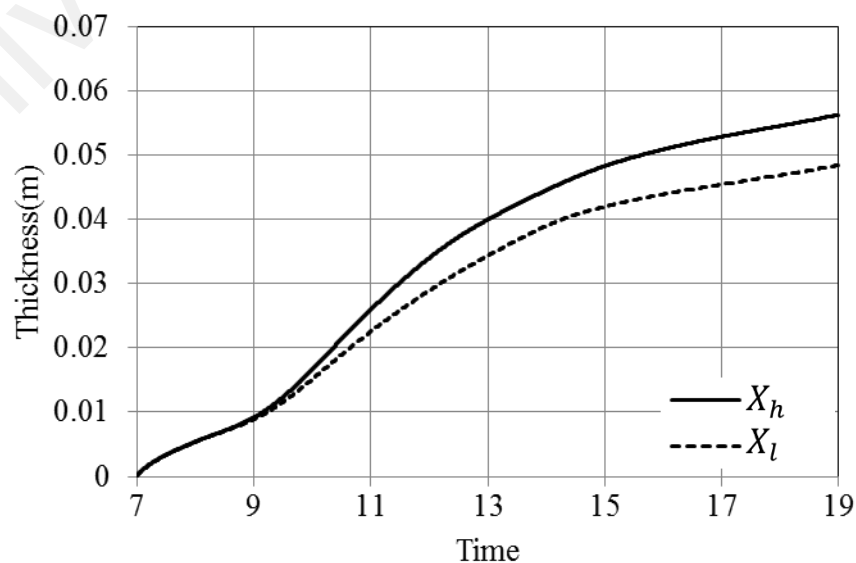


Figure 4.4: Liquid-solid interface in charging mode.

of PCM in whole thickness. In sunny day, the PCM temperature at the distance of 1cm reaches about 90°C while the mean PCM temperature is slightly over 66°C and the HPC highest temperature is a little over 100°C.

In the afternoon, at low solar radiation, the HPE and the HPC temperatures are almost equal due to the very low temperature difference between the HPC and the layer of the PCM in contact with it. The PCM mean temperature remains steady in the afternoon. A higher temperature of the front layer of the PCM causes the internal heat flux to the rear layer of the PCM; and with the lapse of time, there will be a smaller temperature gradient in the PCM. Due to the fact that the heat pipe heat transmission occurs only in one

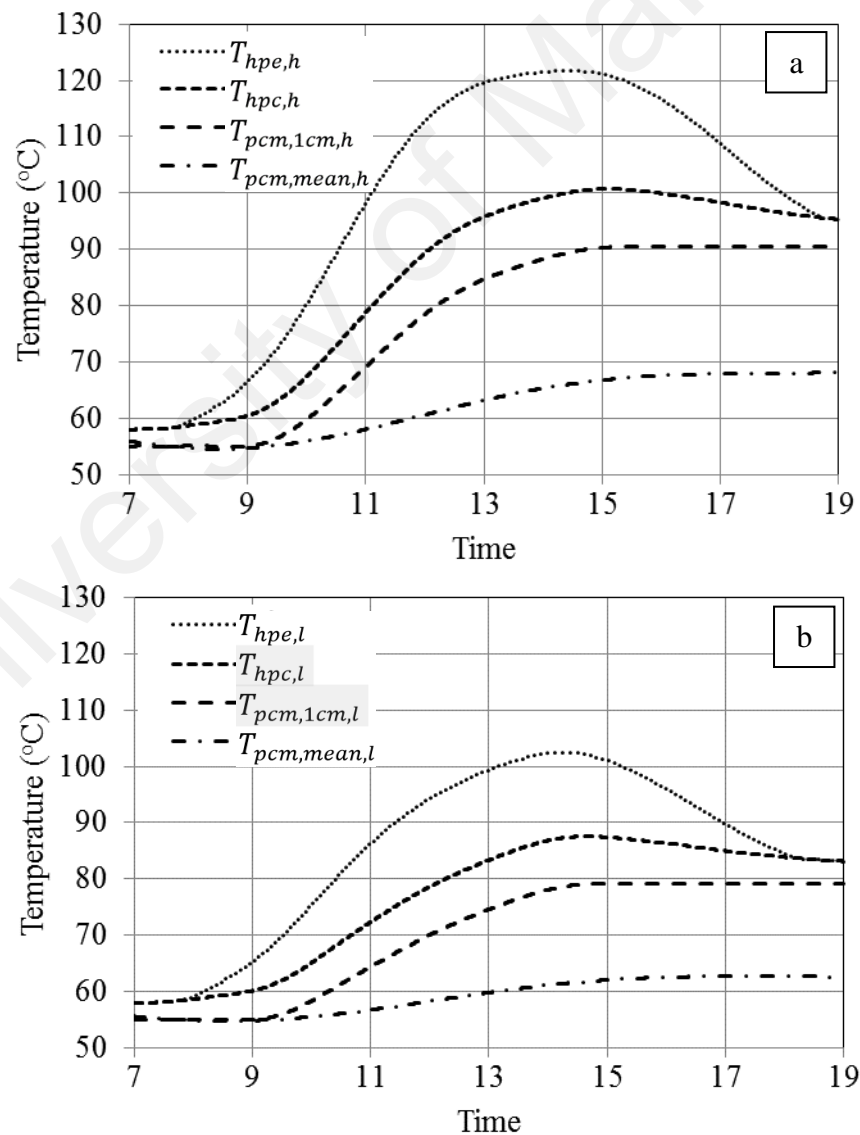


Figure 4.5: HPE, HPC and PCM temperatures.

direction from the HPE to the HPC (acts like a one way valve (Ward, 1981)), the stored energy would not be wasted out of the LHS tank.

4.6 Discharge mode

The discharge process starts after sunset when the controller lets the water pass through the pipe placed in the PCM tank. The direction of the heat transfer in the CHE mode is parallel to the x axis, while in the DHE mode it is parallel to the y axis (Figure 4.2). The discharge process is assumed to start after sunset when the controller allows the supply water to pass through the finned HWSHE pipe. By paying attention to the fact that in the DHE, convective heat transfer inside the pipe is coupled to the heat removal from the PCM, the most valuable parameters to observe in the storage tank are outlet water temperature and solid-liquid interface progression in different slabs of the storage tank.

The simulated results of outlet supply water temperature are shown in Figure 4.8 after 19:00 hour at three different flow rates of 50, 65 and 80 liter per hour (lph) for the mentioned two typical days. The inlet cold water inlet temperature is kept at 29°C. By increasing the flow rate, operating time of the system will decrease. The recommended operating temperature for domestic use is in the range of 38-41°C (Association, 2013). In this research, this value is assumed to be 39°C. Hence, the operating time of the system with outlet water temperature over 39°C degrades from over four hours to almost three hours. The highest outlet supply water temperature is 53°C for a flow rate of 50 lph, while this is about 47°C for 80 lph.

Refer to the explanation in section 3.3, in discharging mode, due to the increment of water temperature during passing through the finned HWSHE pipe, the phase change behavior of the PCM varies over the length of the storage tank. According to the Figure 3.3, the heat transfer from the melted PCM to the finned pipe is symmetric in both rectangular slabs. Figure 4.9 shows the progression of the solid-liquid interface in the

LHS tank during discharging mode for five slabs of the LHS tank at four different flow rates. The results indicate that earlier PCM slabs solidify sooner than later ones, because of the larger temperature difference of the inlet supply water and the PCM.

Due to the high temperature of the melted PCM at the end of the charging mode, refer to equation (3.20), a modified latent heat value of 229kJ/kg was used for the interface progression determination.

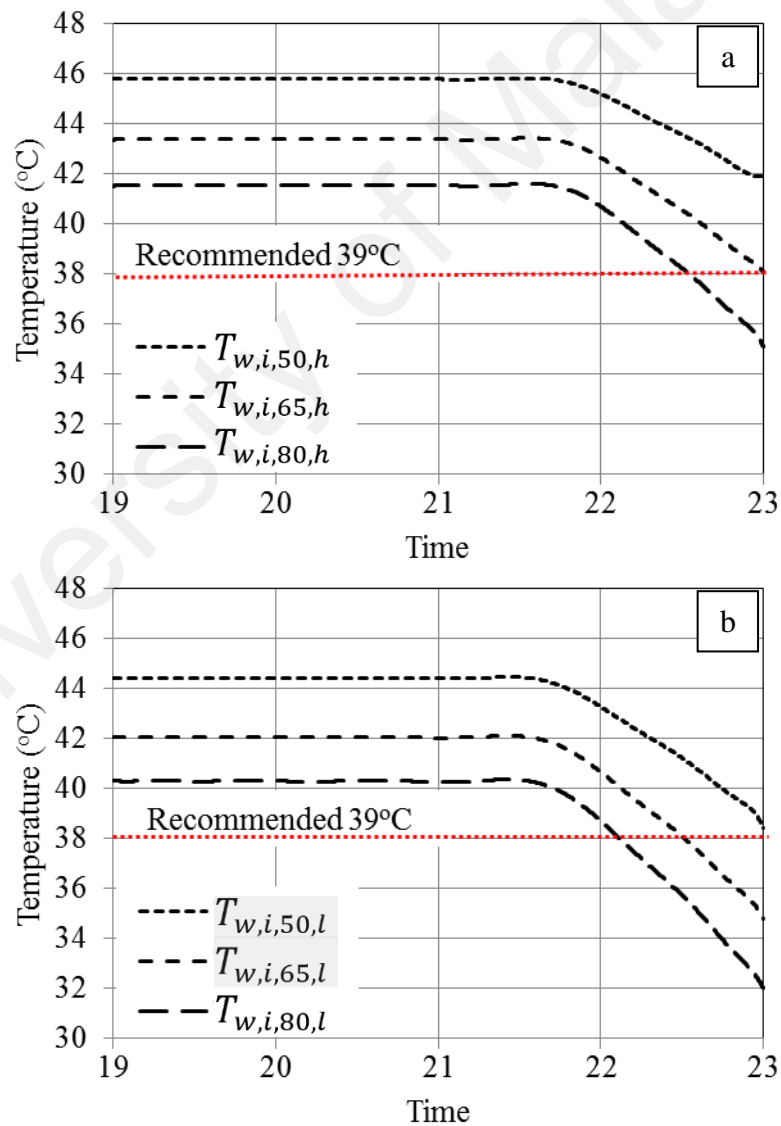


Figure 4.6: Outlet supply water temperature in HPSC-LHS design for different flow rates.

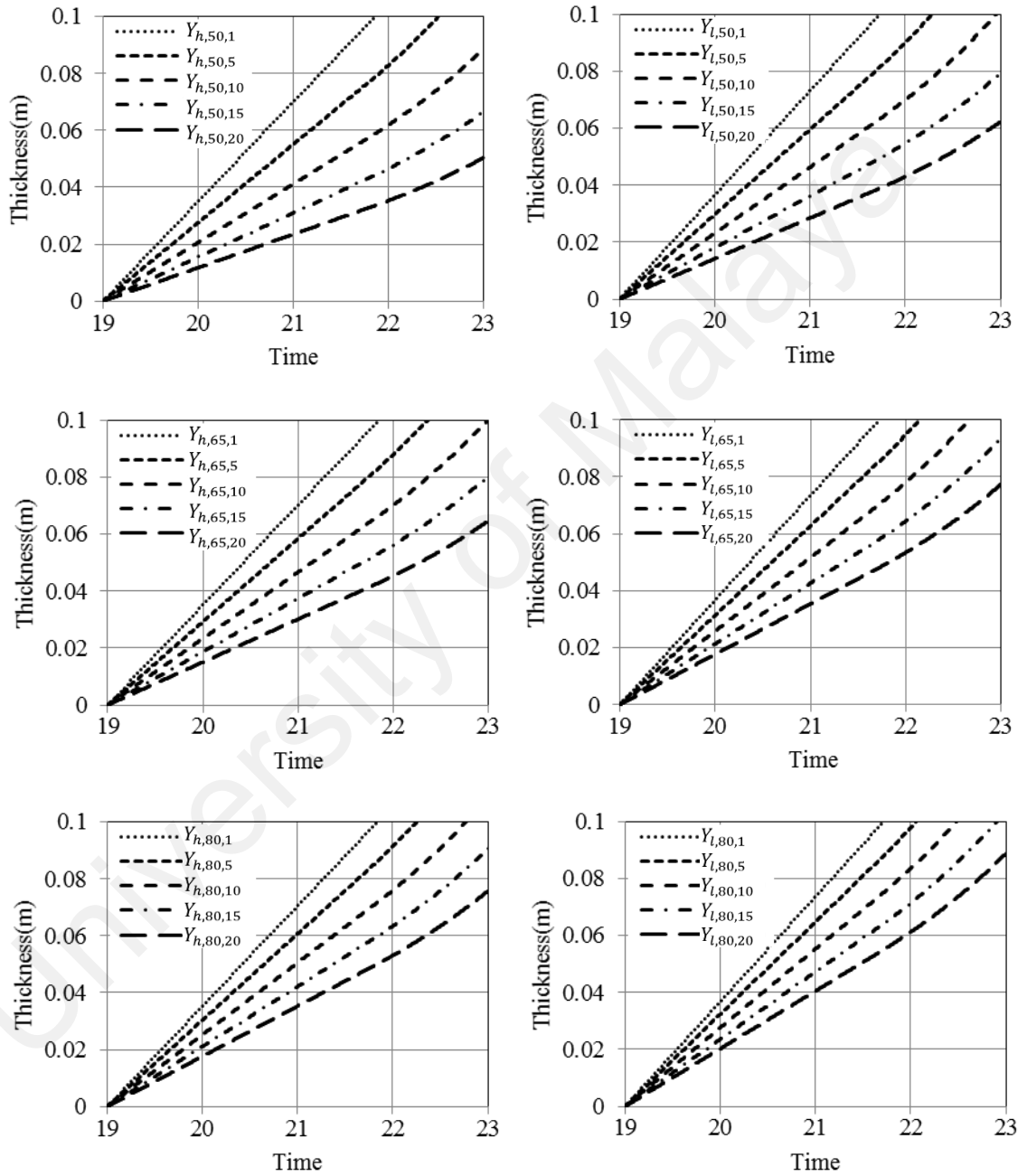


Figure 4.7: Progression of solid-liquid interface in slabs 1, 5, 10, 15 and 20 for different flowrates.

4.7 Comparison with baseline system

As described in section 3.3.5, to be able to compare the baseline and the innovative systems, it is assumed that the produced hot water is stored in the water tank until 19:00 and then release of the hot water starts at the same time as the PCM tank. While the outlet water temperature from the water tank is at a higher temperature than the operating temperature (39°C), it must be mixed with cold water (29°C) to reach to balance the temperature.

Figure 4.10 shows the outlet water temperature ($T_{w,b}$) simulated for a baseline HPSC system with 20 heat pipes for two typical days at different flow rates. The magnitude of

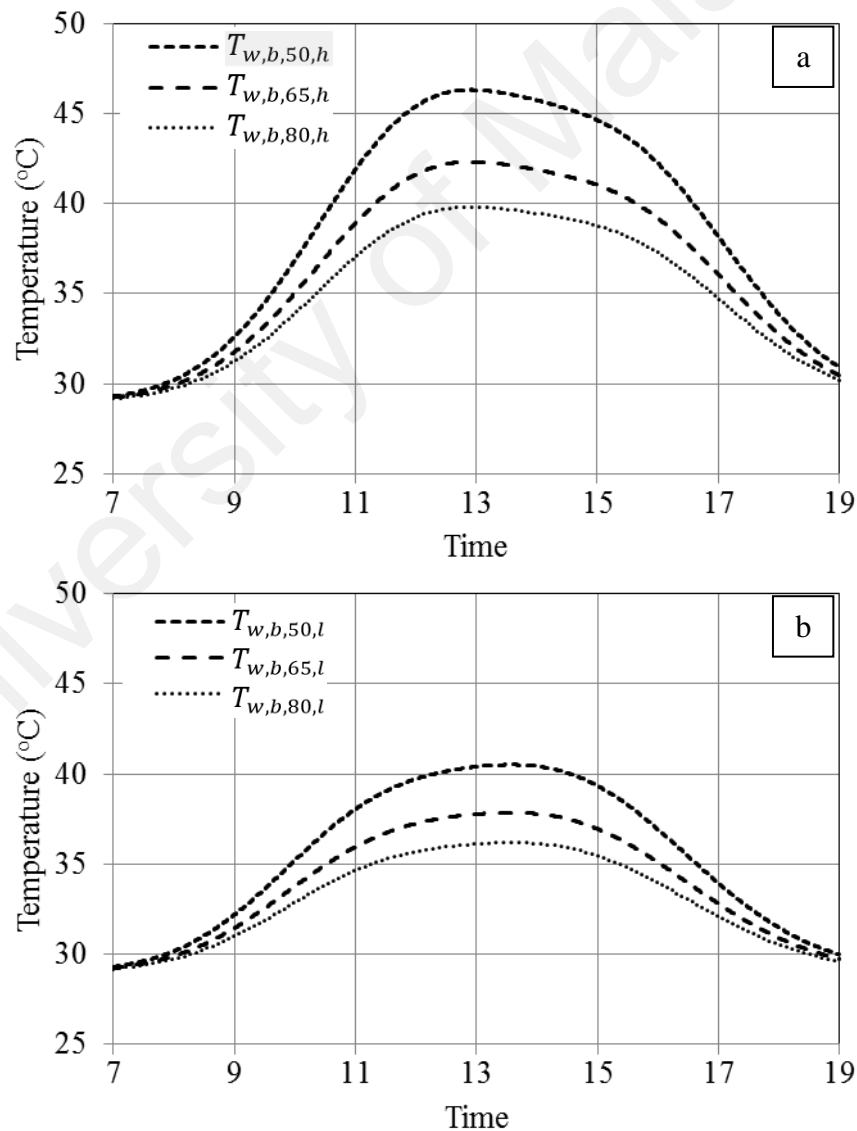


Figure 4.8: Outlet water temperature ($T_{w,b,o}$) for baseline HPSC system in days with high intensity (a) and low intensity (b).

the produced hot water at operating temperature and the total efficiency of the systems can be estimated by equations introduced in section 3.3.5. Figure 4.11 compares usable volume ($V_{u,r}$) and efficiency (η) between the innovative and baseline systems. Generally, the thermal performance of the baseline system decreases, when the draw-off flow rate increases. As a result, usable hot water volume decreases. In baseline system, when the solar radiation is weak, the efficiency of the system is less than 30%, while in the days with high intensity radiation, the efficiency is in the range of 50-60%. The thermal efficiency of the innovative system for both days are in the range of ~50%. The graphs indicate this point that the efficiency of the HPSC-LHS design does not drop significantly for different flow rates and different solar radiation pattern.

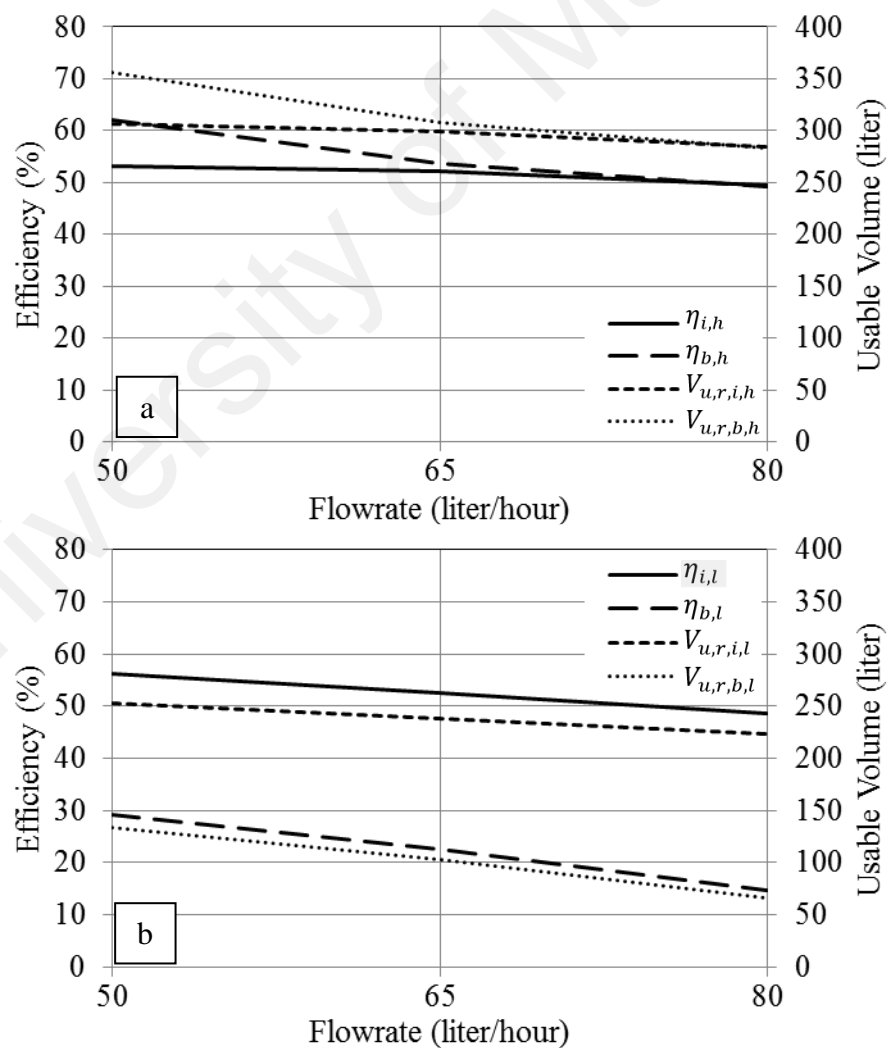


Figure 4.9: Comparison of efficiency and usable hot water volume for different flow rates in days with high intensity (a) and low intensity (b).

The average surface temperature of the HPE and the HPC of the baseline and proposed systems are compared for two typical days and different flow rates in Figure 4.12. The HPC maximum temperature in the HPSC-LHS system for high and low solar radiation days are over 100°C and less than the 90°C, respectively. Same data for baseline system when the flow rate is 50 lph is ~58°C and ~48°C, respectively.

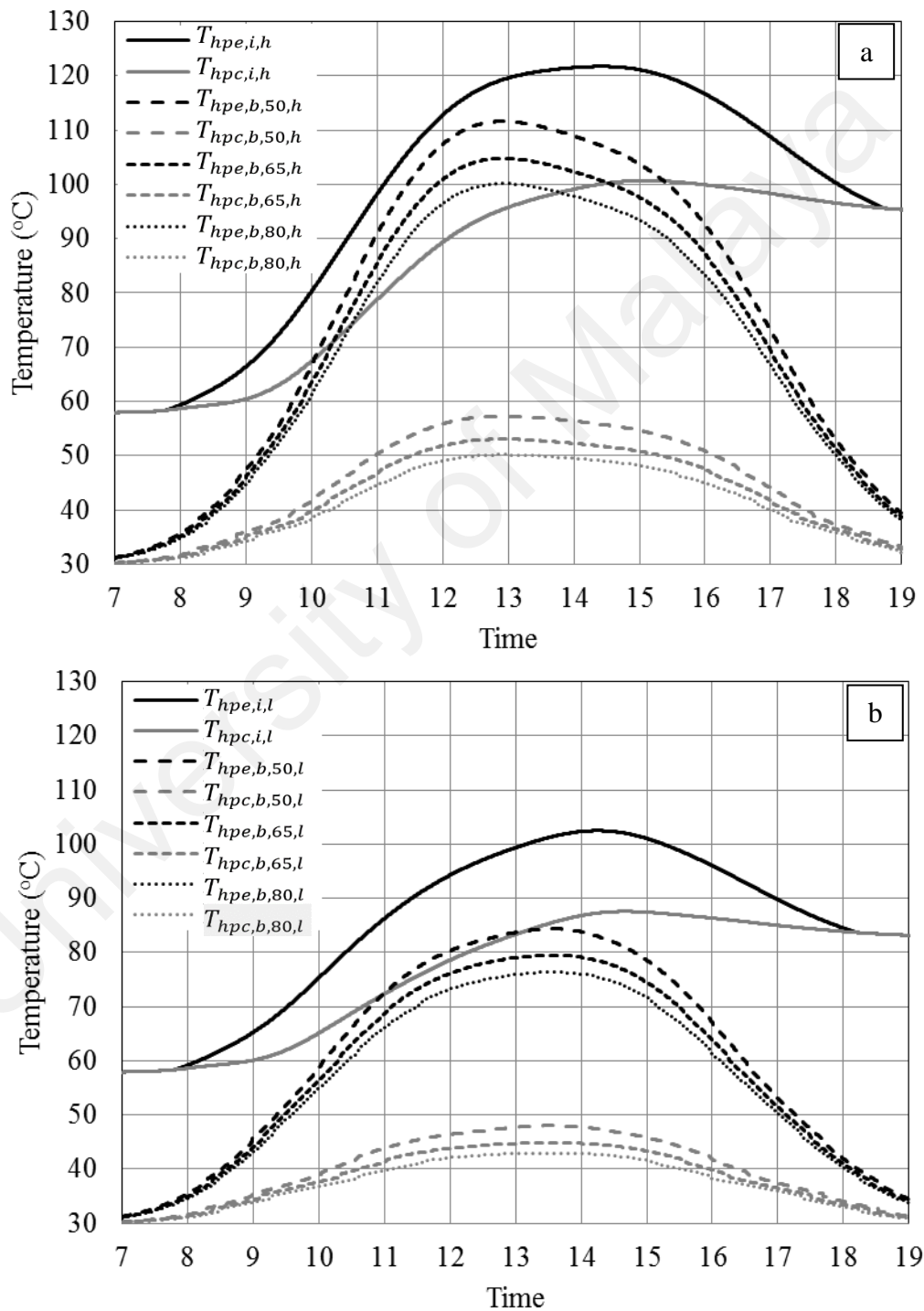


Figure 4.10: Comparison of HPE and the HPC temperature at two supply water flow rates in days with high intensity (a) and low intensity (b).

Based on two reasons, probably, the thermal efficiency of the HP in the baseline system is higher than the other one. First, the HPC surface temperature in the baseline system is much lower than the HPSC-LHS design, which is because in the baseline system, cold water passing through the manifold cools it down, while at the HPSC-LHS system the surrounding material is stationary which leads to low temperature difference between the finned HPC and the PCM. This low temperature difference causes to less heat transfer to the PCM. Second, the temperature difference of the HPE and HPC in baseline system is higher than the other one. Higher temperature difference causes to more heat transfer through the HP. According to the graphs, much higher temperature of the HPE in the HPSC-LHS system is because the absorbed solar energy in the HPE section is not removed in the HPC section and remained in the device.

Physically, when the HPE is heated above a certain temperature, all the working fluid in the HP vaporizes and the condensing process ceases in the HPC; in such conditions, the HP's thermal conductivity is effectively reduced to the heat conduction properties of its solid metal casing alone. As most HPs are constructed of copper, an overheated HP will generally continue to conduct heat at around 1/80 of the original flux via conduction only rather than conduction and evaporation (Faghri, 2014). This fact explains why the temperature of the HPE and the HPC meet each other at afternoon and also, indicate that the reverse heat transfer from the LHS tank through the HPs is not effective. Moreover, consideration of this point plays an important role in the selection of the proper PCM for such LHS systems.

4.8 Summary

In this chapter, the overall efficiency of the HPSC-LHS system in different conditions was determined and compared with a conventional (baseline) HPSC system. Based on the findings of this analysis, it could be concluded that this design is reasonably

practicable. The results showed that the thermal performance of the proposed system could be higher than a baseline system in certain conditions. The analysis also shows that the sensitivity of the efficiency of the proposed system to the supply water flow rate is less than the baseline system. Moreover, in the days with low solar radiation, this design may perform better than the baseline one.

University of Malaya

CHAPTER 5: EXPERIMENTAL STUDY

PART I: CHARGING ONLY AND DISCHARGING ONLY MODES

5.1 Introduction

According to the theoretical study of the conceptual design of the HPSC-LHS system in previous chapter, it was found that under specific conditions the thermal performance of the proposed system could be in the same range or even higher than the conventional HPSC system. To have a considerable understanding about the performance of such this design, the experimental field test were carried out. For this purpose, by considering the findings of previous research works on the PCM melting/solidification processes, effective fins designs and the most suitable practical configuration, the proposed system were prepared, as it was explained in section 3.5.

This part of the research plans to examine the solar heat absorption by evacuated glass tube solar collector, heat transfer by the HP, the stored heat in the LHS tank and the overall efficiency of the system under different weather conditions, supply water flow rates and discharge time.

5.2 Experimental investigation

5.2.1 The apparatus

The Schematic of experimental set-up the HPSWH-LHS is shown in Figure 3.13. A photograph of the experimental setup and the LHS tank are shown in Figure 3.14. The dimensions of the LHS tank and fins are almost same as the theoretical model, but with some changes. All the necessary specifications of the evacuated tube solar collector, dimensions and properties of the HP and thermal properties of the PCM are charted in Tables 3.1, 3.2 and 3.3, respectively. The dimensions of the experimental design of the fins and tank are charted in Table 5.1. The setup is located at the rooftop of the Faculty

of Engineering, in University of Malaya. The latitude and longitude of the site are 3.1° and 101.4° , respectively. Slope of solar collector is 20° . The number of the HPSCs (N_t) is 20 sets. The aperture area of an HPSC (total) is 0.089 m^2 (1.773 m^2). The LHS tank holds about 57 kg of paraffin wax as PCM. For low temperature solar applications, paraffin wax with melting temperature in the range of $50\text{-}60^\circ\text{C}$ is found to be the most suitable (Aydin et al., 2015; Karthick & Manivannan, 2015; Wang et al., 2015).

Table 5.1: Dimensions of the experimental setup.

Item	Value (mm)
LHS tank height	220
LHS tank width	200
LHS tank length	1725
Fin height (long) on the shell	130
Fin height (short) on the shell	80
Fin length on the shell	60
Fin thickness on shell	1
Distance between fins on shell	12
Pipe outer diameter	13
Fin height on pipe	9
Fin thickness on pipe	0.5
Fins pitch on pipe	5

Fins are provided to increase heat transfer rates to/from the PCM. Besides fin material there are three parameters that influence the performance of the fins, viz., fin orientation, fin length and fin spacing (distance between the fins). Details of the fin designs are provided in 3.5.1.

5.3 Results and discussion

During the *charging only* mode, solar radiation incidents on the HPSC and the heat is absorbed and transferred via the HPs to the LHS tank to melt the PCM. The heat stores in the PCM in both forms of the latent and the sensible heat. In this mode, the supply water does not pass through the LHS tank. During the *discharging only* mode, the supply

water circulate through the finned pipes and receives heat from the molten PCM. This mode starts when the solar radiation become very weak or after sunset.

Typical data discussed here were obtained over 12 days and tabulated in Table 5.2. Tests were carried out for two cases; draw off at 17:30 and 19:30. Days with total solar radiation less/more than 15 MJ/day are considered as low/high intensity days. The water draw off is done for three different flowrates 50, 65 and 80 lph. In the following, the data for water draw off at 17:30 will be presented and discussed and then the efficiency of the system will be compared with the case of water draw off at 19:30.

Table 5.2: Summary of the runs.

Run no.	Solar intensity category	Daily radiation (MJ/m ²)	Flowrate (lph)	Discharge time
1	Low	4.0	50	17:30
2	Low	13.3	65	17:30
3	Low	10.4	80	17:30
4	High	18.0	50	17:30
5	High	20.8	65	17:30
6	High	16.5	80	17:30
7	Low	12.7	50	19:30
8	Low	14.5	65	19:30
9	Low	13.4	80	19:30
10	High	20.0	50	19:30
11	High	23.1	65	19:30
12	High	22.2	80	19:30

Typical solar radiation and ambient temperature graphs observed for case 1 and 2 are shown in Figures 5.1 and 5.2, respectively. It can be seen that during low intensity days (cloudy/rainy), the radiation pattern has fluctuates dramatically throughout the day which is due to cloudiness or rain. During high intensity (sunny) days, the pattern is quite steady with peaks of around 1000 – 1200 W/m². The maximum ambient temperature in low and high solar intensity days are 35°C and 42°C, respectively.

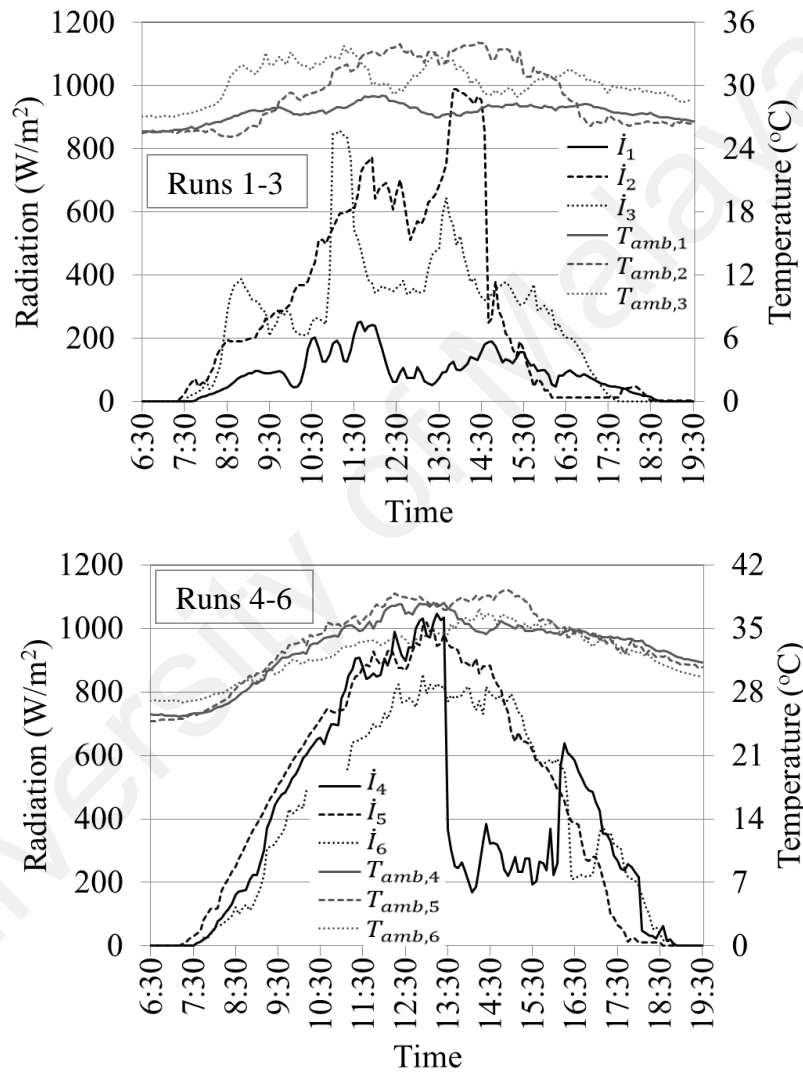


Figure 5.1: Solar radiation and ambient temperature in day time for runs in case 1.

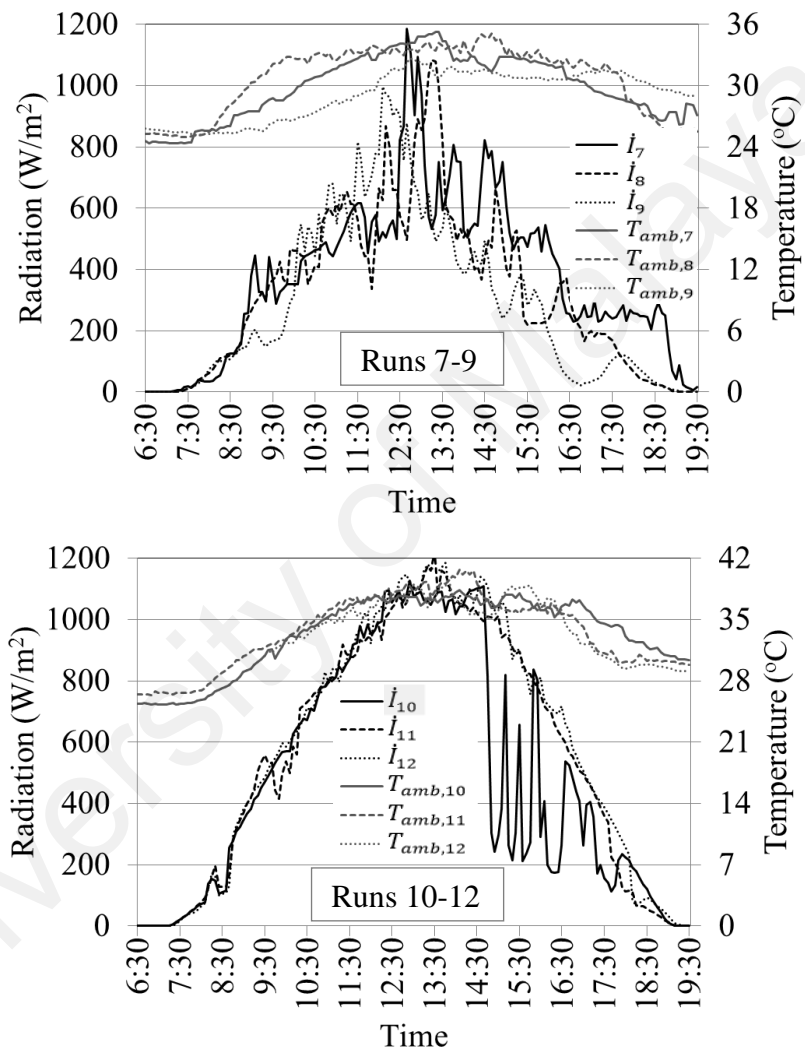


Figure 5.2: Solar radiation and ambient temperature in day time for runs in case 2.

5.3.1 Charging only mode

Figures 5.3 and 5.4 present the temperature progression of the PCM in the middle and the bottom of the LHS tank during charging for cases 1 and 2, respectively. One of the initial observations by TC1 to TC10 in middle of the tank and TC11 and TC12 in the bottom of the tank was that the PCM temperature along the tank is uniform. The temperature differences between the TCs are less than 4°C. That is because of equal heat flux to the tank by HPs. Therefore, in these two figures the average of temperature fluctuations of TC1-TC10 and TC11-TC12 are presented.

According to the graphs for PCM temperature progression, as soon as the wall temperature of the HP is equal to or higher than the melting point, the phase change process in the PCM starts, but it takes until about 9:30-10:00 before the PCM in the middle of the tank starts to getting over the melting point. Before melting takes place, the heat transfer through the PCM is pure conduction, and the temperature increases almost linearly with time. Low thermal conductivity of the PCM causes to quick increment of the PCM adjacent to the HP. On the days with low solar radiation, the PCM temperature in middle of the tank increases up to 110°C in the midday. However, according to the Figures, depends to the intensity and cloudiness level of the sky the highest temperature of the PCM varies in different runs in low intensity days. After this time, the melted PCM in the upper side of the tank conducts the heat to the lower side of the tank which still is remained in the solid form or is melted but in the lower temperature. In this time of the day, the solar radiation also becomes weaker and there will be less heat input to the PCM. For these two reasons, the temperature of the PCM in the middle of the tank dropped out after the 15:00-16:00. The influences of these two reasons are more observable in the same graph for discharge time at 19:30 (Figure 5.4). In the high intensity solar radiation days, the PCM temperature in the area near the finned shell reaches temperatures above 120-130°C and the bottom side of the PCM reaches the melting temperature at about

15:00. In opposite, in the low intensity solar radiation the lower layer of the PCM did not melt.

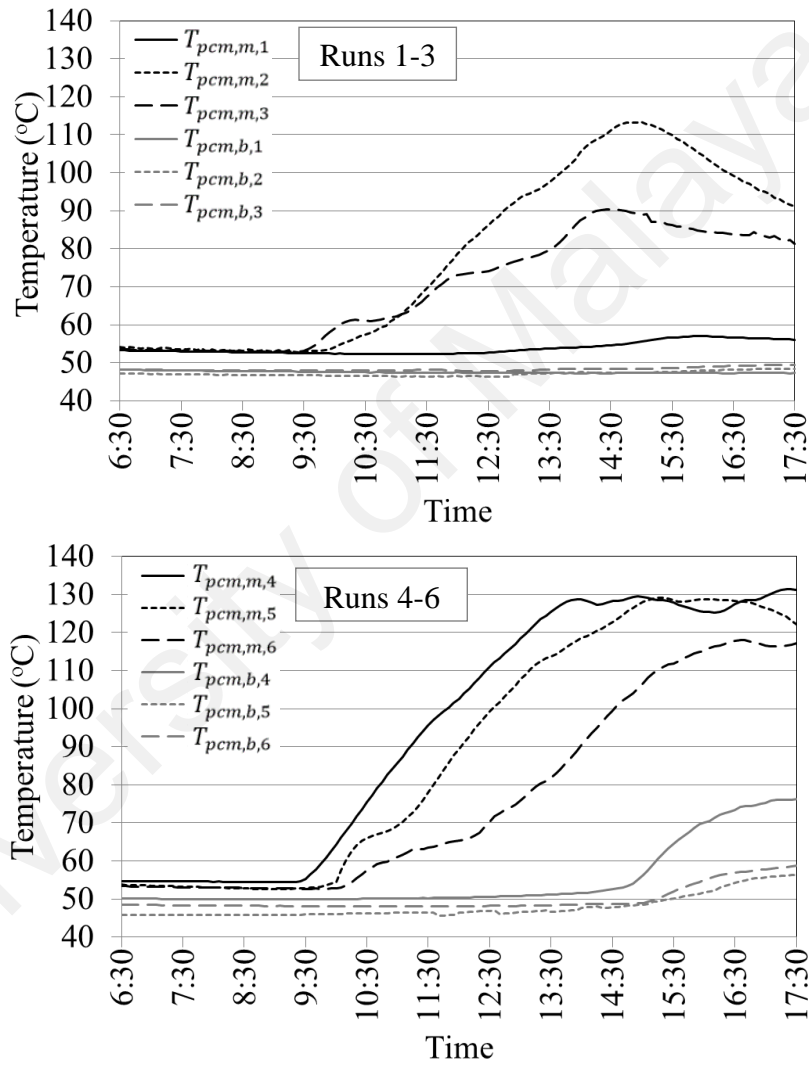


Figure 5.3: The PCM temperature increase in the middle and bottom of the tank in charging mode for runs 1-3 and 4-6.

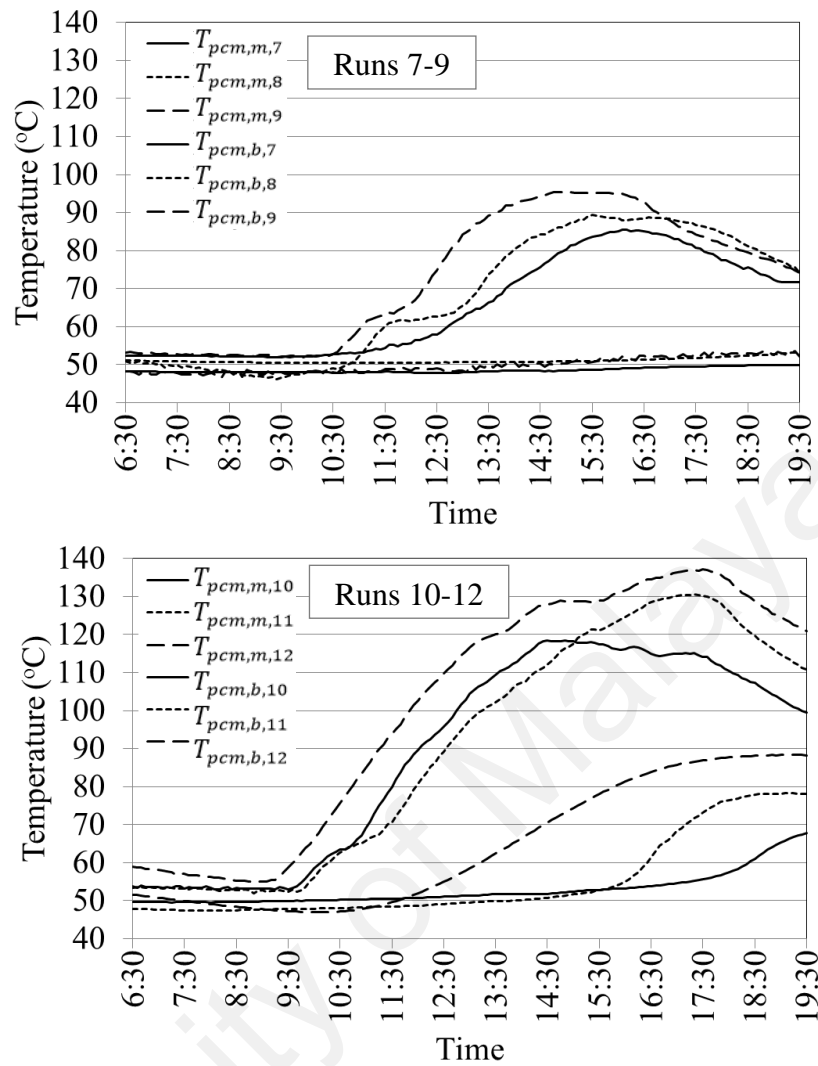


Figure 5.4: The PCM temperature growth in middle and bottom of the tank in charging mode for runs 7-9 and 10-12.

Observing the performance of the HP aids to understand their effect on the overall performance of the system. Figures 5.5 and 5.6 depict the recorded wall temperature fluctuation of the HP in all sections with time for both cases versus the PCM temperature in the middle of the tank. As mentioned in section 3.5.2, five of the HPs were selected to record the wall temperature of different sections. From the recorded data of the HPC (TC22-TC26), HPA (TC27-TC31) and HPE (TC32-TC36 and TC37-TC41) sections, the temperature differences between the HPs are less than 5°C. In addition, the two thermocouples placed on the evaporator section of each HP recorded uniform temperature along this section. According to these two points, average of the recorded data of the TCs on HPEs, HPAs and HPCs are presented for each time step.

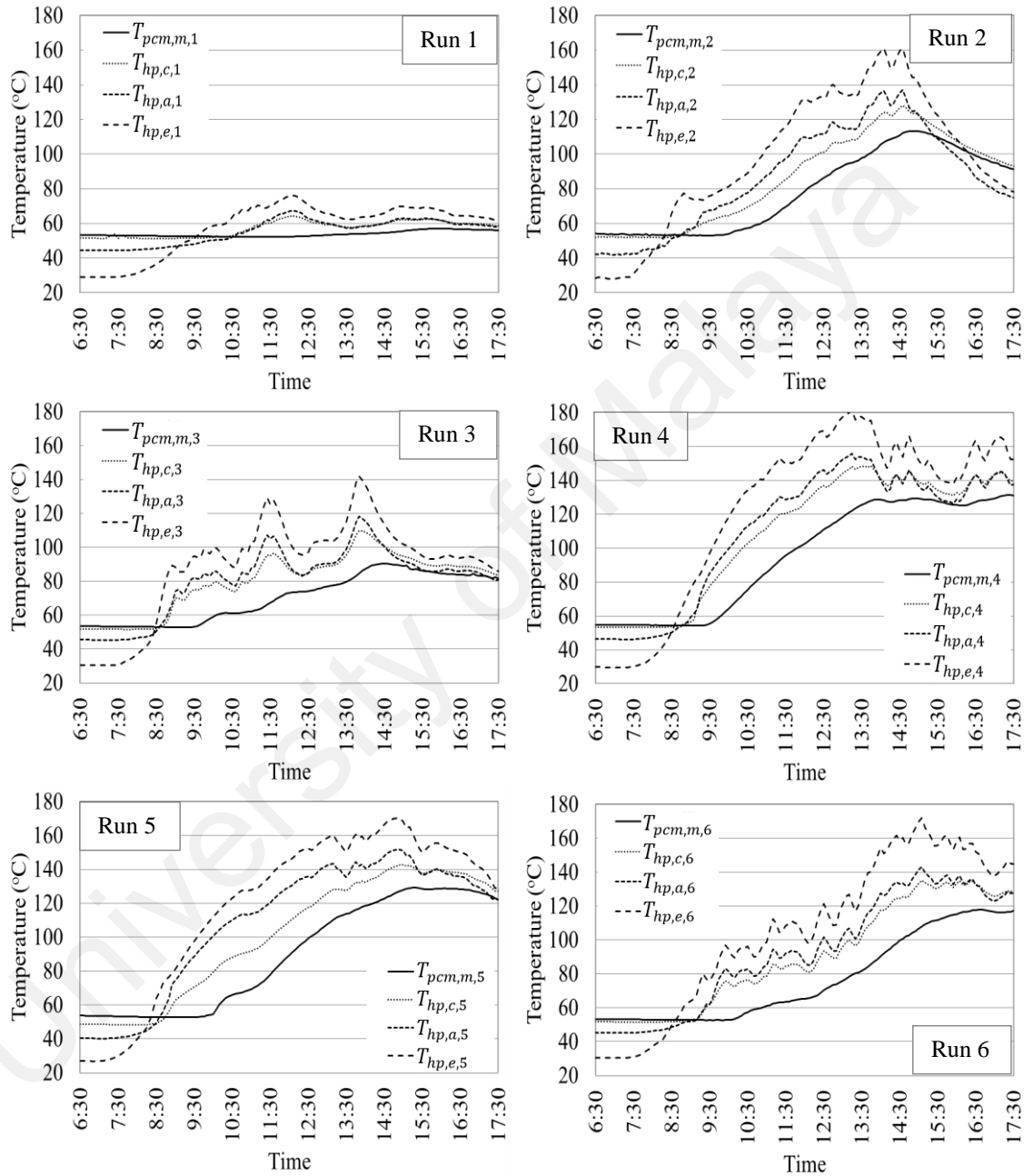


Figure 5.5: The HP sections wall temperatures versus the PCM temperature at the middle of the tank for runs 1-6.

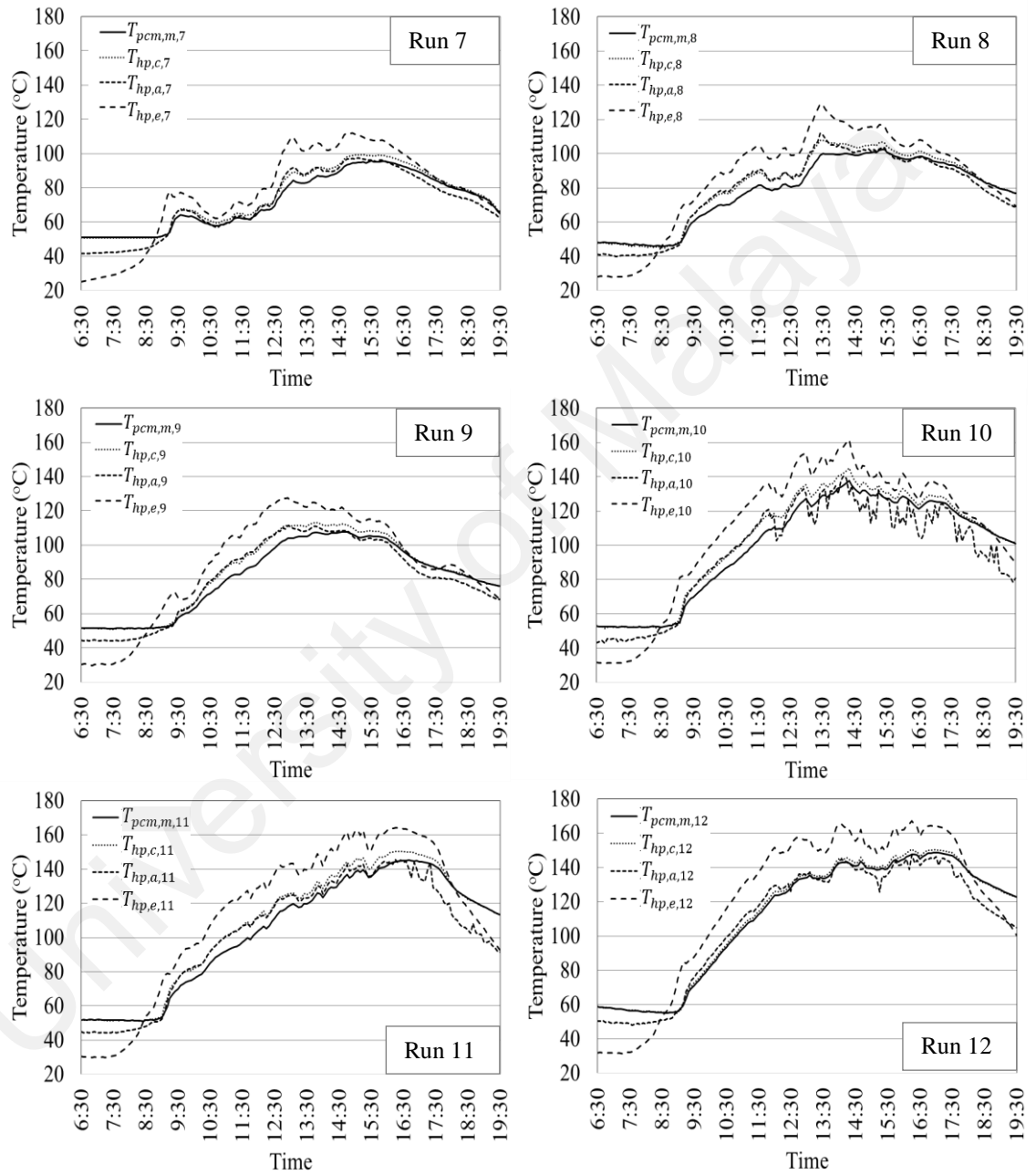


Figure 5.6: The HP sections wall temperatures versus the PCM temperature at the middle of the tank for runs 7-12.

From the graphs in the Figure 5.5, during the early stage of the charging process, the heat transmission from the glass tube to the HPE is mainly used to heat the wall of the HP. This step takes about 1 hour after sunrise. As soon as the HPC wall temperature is higher than the PCM temperature, the heat transfer between the HP and the PCM started. According to the theory, the HPE wall temperature is higher than it in the HPA. Depending on the intensity of the solar radiation, this temperature difference is up to 30°C. In the same manner, while the HP is operating, the HPA temperature is higher than the HPC. It is observed that at the time after midday when solar radiation lost its intensity, the temperature difference between the HPC and the PCM decreases to less than a certain degrees, the HP would not be able to transfer the absorbed heat to the PCM medium. At this time, the wall temperature of the HPA drops to the value close to the HPC. The temperature difference between the HPC and the PCM further decreases as the time passes in the evening.

5.3.2 Discharging only mode

The *discharging only* mode starts by flowing the water through the finned pipes and stops at 23:30 when the LHS tank lost its thermal inertia. Figures 5.7 and 5.8 represent the temperature of the outlet hot water from the tank for runs in both cases. According to the data the inlet cold water is in the range of the 27-29°C. Therefore, the average of the inlet cold water for runs 1-3, 4-6, 7-9 and 10-12 are also presented in the graphs. Obviously, for all of the flow rates, the runs with the low solar radiation produce lesser temperature increment of inlet water. Except the run 1, the temperature difference of the inlet and outlet water reach to less than 5 degree after almost two hours. In the run 1 the daily solar radiation is very low than other runs (fully rainy day). On the other hand, during the days with high intensity, the results are more considerable. For the run 4 (flow rate 50 lph), the cold and the hot temperature difference, even after 5 hours of discharging,

is more than 5°C. The corresponding time for 65 lph and 80 lph are 4 and 3.5 hours, respectively. For runs of case 2, hot water temperatures are very close together. This is because of daily solar radiation which varies for different runs and uncertainties of the setup which already explained.

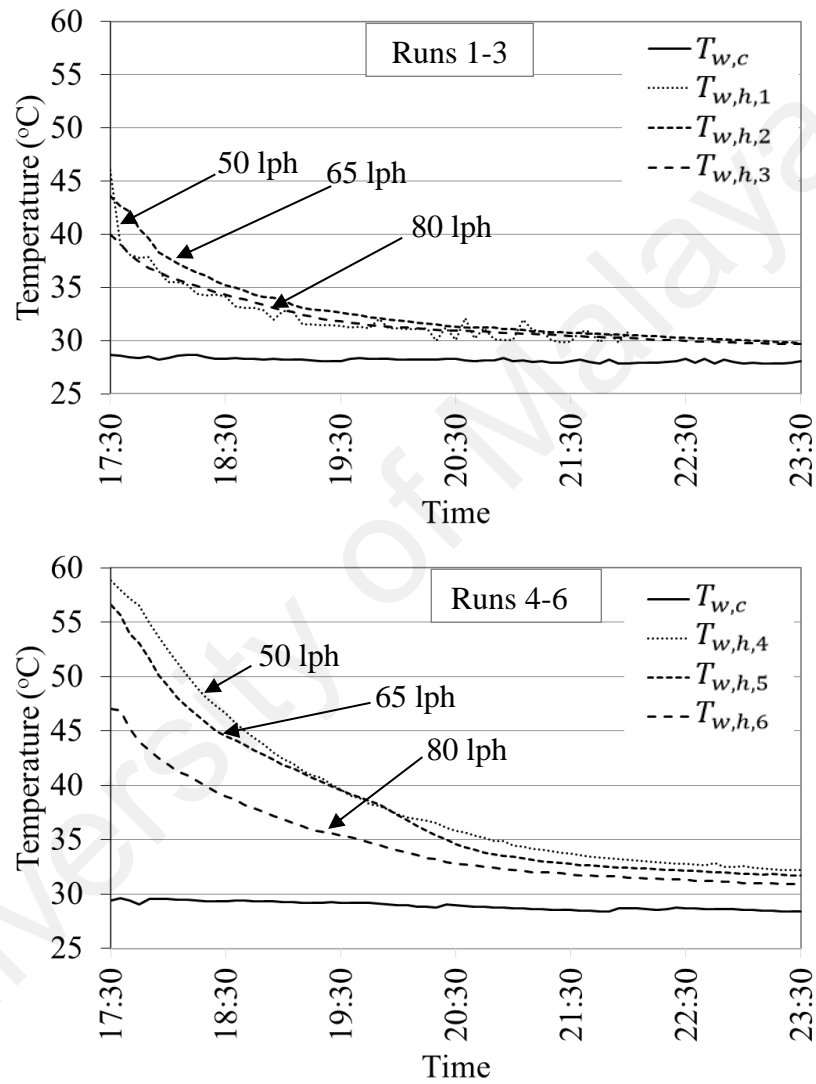


Figure 5.7: The hot water outlet temperature for three flow rates.

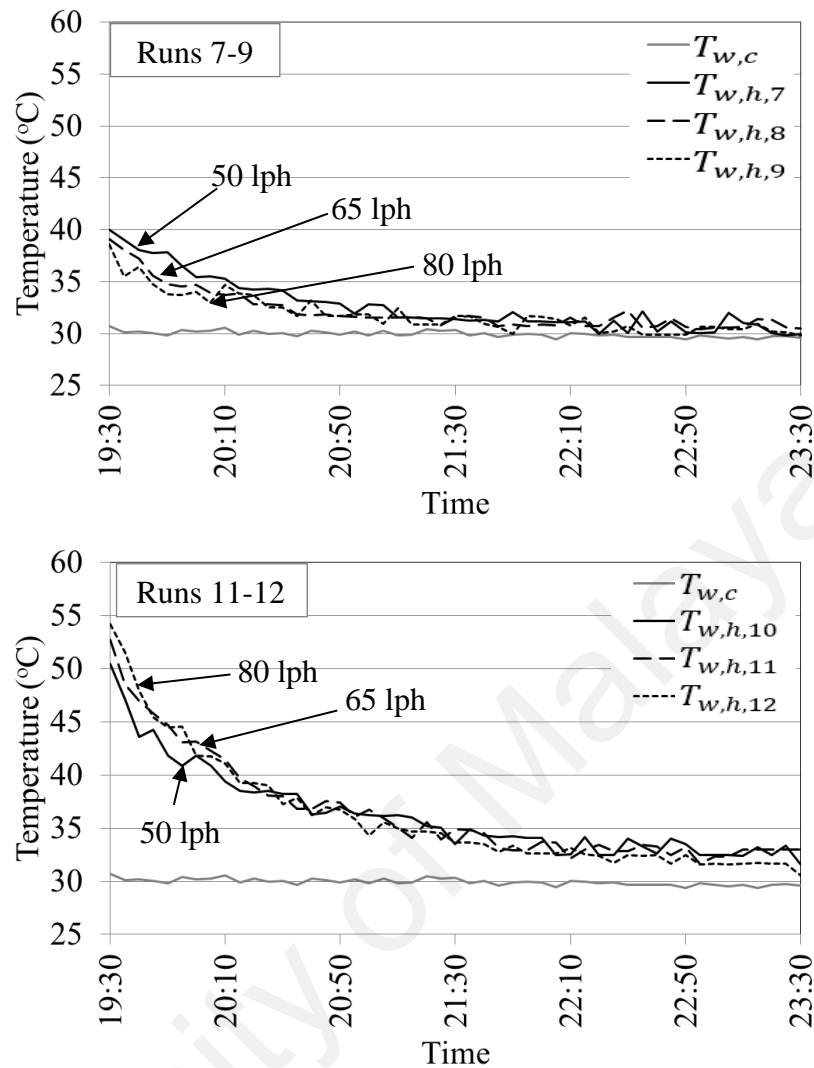


Figure 5.8: The hot water outlet temperature for three flow rates.

Figures 5.9 and 5.10 show the PCM temperature reductions in the middle of the tank during discharging in both cases. The stored heat in the LHS tank is a combination of the latent and sensible heats. By comparing the time of reduction of the hot water temperature and the PCM temperature, it could be understood that the PCM loses its temperature faster than the hot water, which is due to the PCM losing its stored sensible heat. In fact, the PCM loses the sensible heat much faster than the latent heat. The specific heat of PCM is low as compared to water thus the rate of temperature drop of PCM is higher than water. However, even after the PCM temperature drops to about the melting point, the water is still warming up for some degrees, because of the utilization of stored latent heat in PCM.

While, the thickness of the solidified PCM around the finned pipes is getting thicker, this process is getting slower, due to low thermal conductivity of the PCM in solid form.

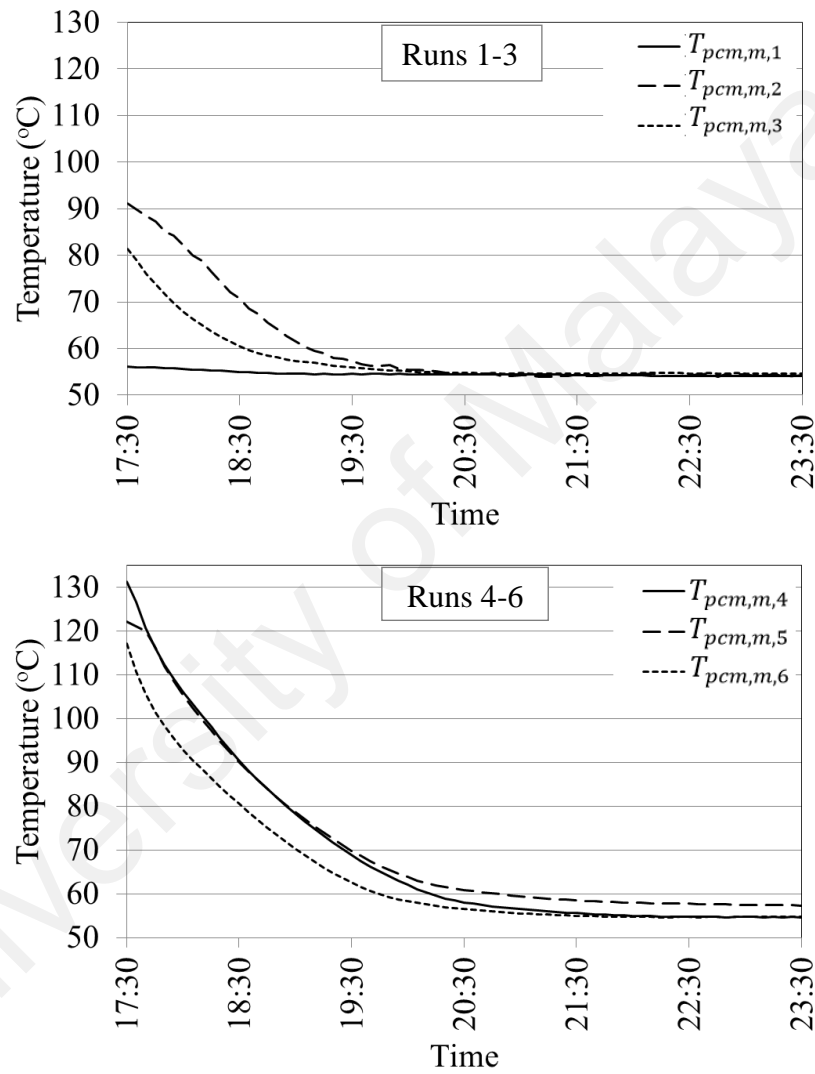


Figure 5.9: The PCM temperature change at the middle of the tank during the discharge operation.

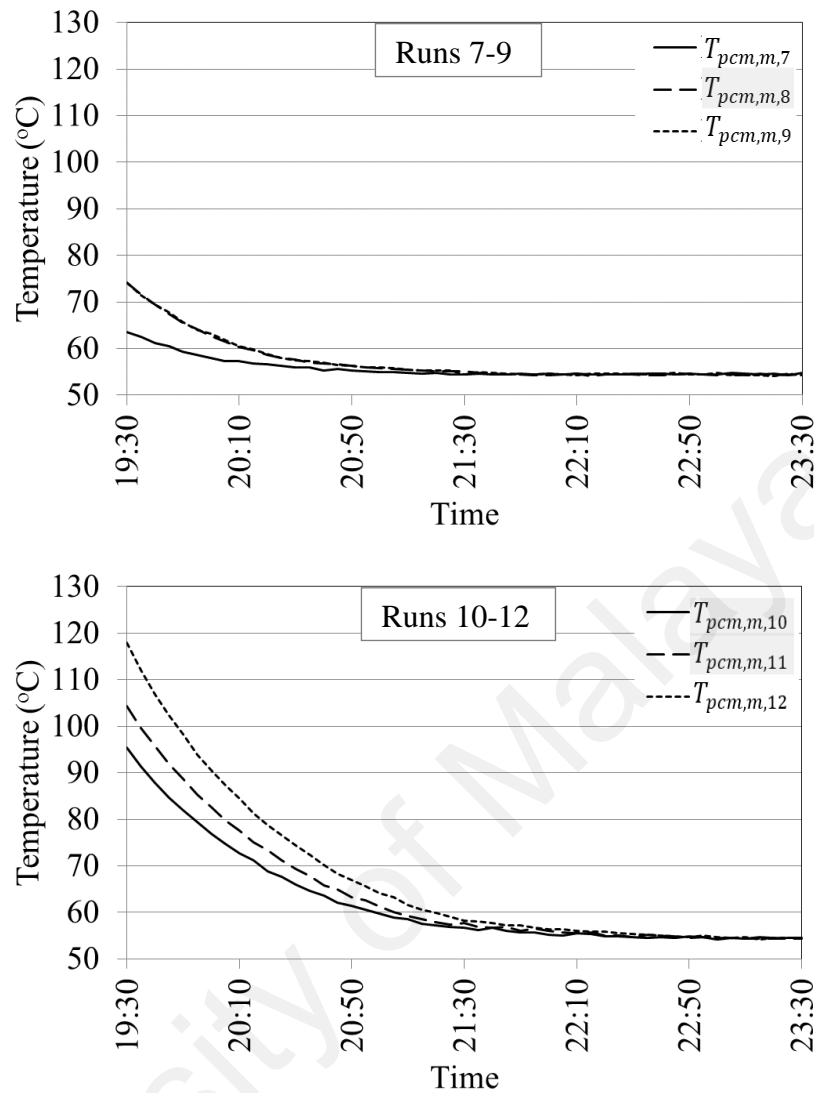


Figure 5.10: The PCM temperature change at the middle of the tank during discharging.

Figures 5.11 and 5.12 present the temperature fluctuations of the HP sections in comparison with the PCM temperature in discharging mode for both cases. According to the graphs for case 1, until 19:30, the temperature of the HPE is higher than the HPA at the same time. A similar pattern is found between HPA and HPC and between the HPC and the PCM adjacent to that. The main reason is that the sunset time is at about 19:30, thus the solar radiation intensity is getting weaker and the supply water draw off is already started. After 19:30, this pattern is reversed; due to unavailability of radiation to be absorbed by HPE. So, the temperature of HPE and HPA starts to drop to the ambient

temperature, whilst the HPC temperature follows the same pattern as that of the PCM temperature reduction.

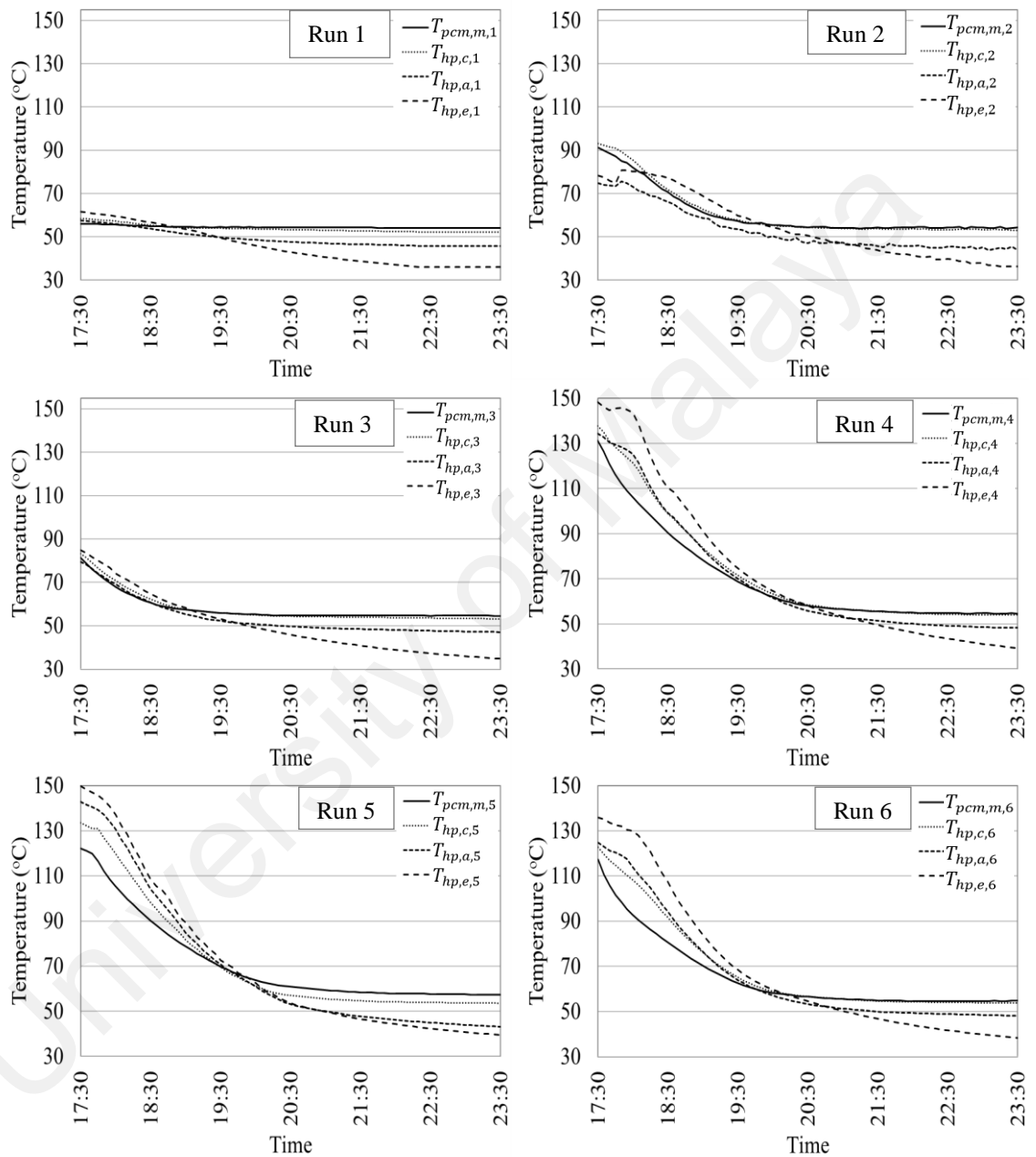


Figure 5.11: The HP sections wall temperatures versus the PCM temperature at the middle of the tank in discharging operation for runs 1-6.

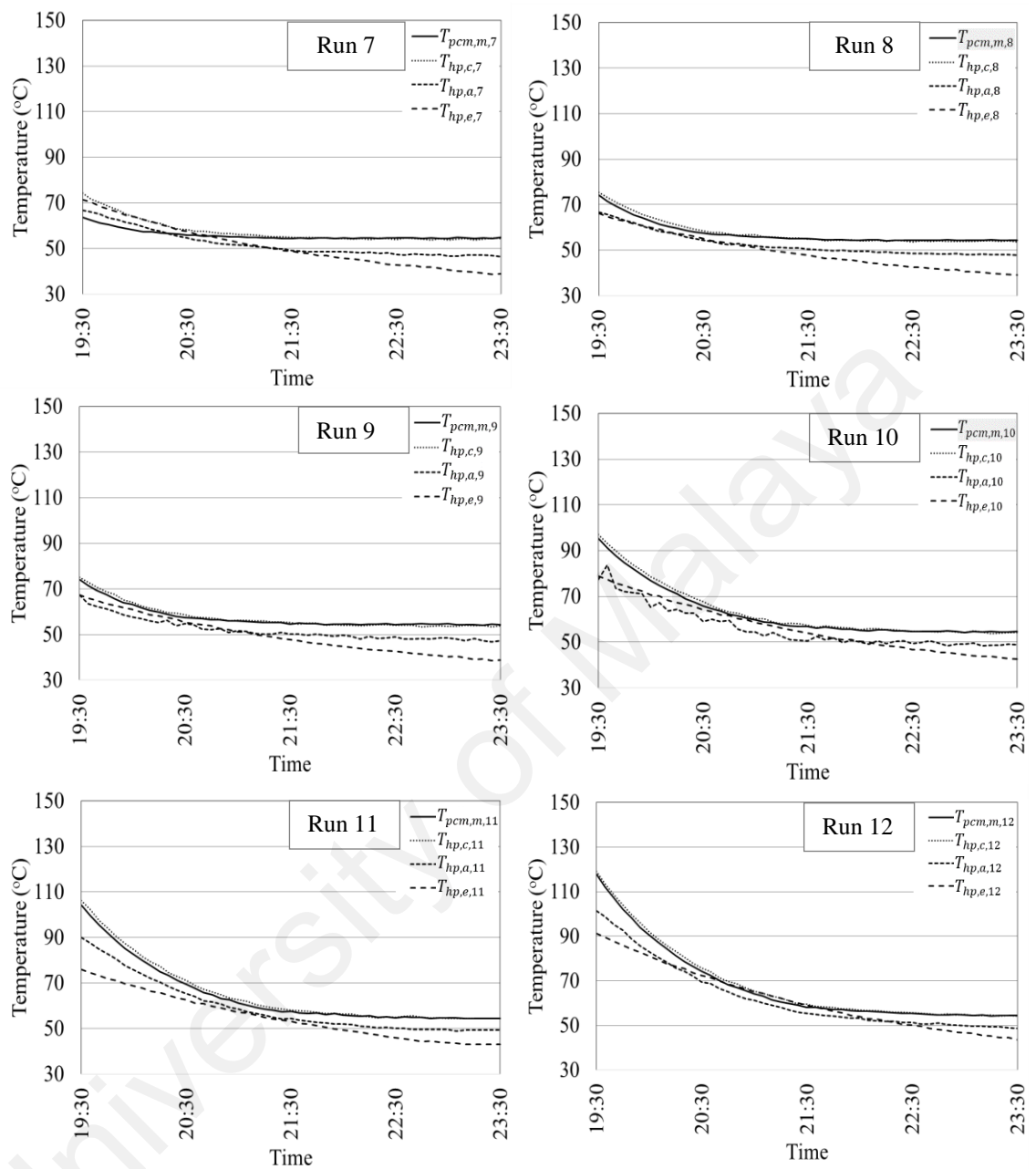


Figure 5.12: The HP sections wall temperatures versus the PCM temperature at the middle of the tank in discharging operation for runs 7-12.

5.4 System efficiency

The critical point to understand the performance of the system is studying the heat transfer and heat storage processes in the whole LHS tank. Regarding the design of the LHS tank, it is impossible to accurately observe the melt fraction of the PCM in the tank. However, an approximation method is used to estimate the molten fraction of the PCM

inside the tank by using the recorded data of the PCM temperature in the middle and the bottom of the tank. In the next step, the daily heat transmitted and thermal efficiencies of the system will be estimated.

5.4.1 Estimation of the melted fraction of the PCM

Table 5.3 charts the recorded daily solar radiation of some of the runs, initial and the maximum temperatures of the PCM in the middle and the bottom of the LHS tank. This data is used to find a correlation between the maximum temperature of the PCM in the middle and the bottom of the tank versus the total daily radiation. Then, by using this correlation the melting fraction will be estimated. According to the Figure 5.13, by interpolating a linear line between the data of the maximum temperature of the PCM in the bottom and the middle of the tank the following two equations could be extracted, having R-squared value of 0.99 and 0.84, respectively:

$$T_{pcm,m,max} = (5 \times 10^{-6}) \times \sum I + 36.3 \quad \text{for } 4 \leq \sum I \leq 18 \quad (5.1)$$

$$T_{pcm,b,max} = (9 \times 10^{-7}) \times \sum I + 42.4 \quad \text{for } 4 \leq \sum I \leq 18 \quad (5.2)$$

The unit of daily solar radiation ($\sum I$) in the equations is $MJ/m^2 \cdot day$. Then, by using the following equation the mean temperature of the whole PCM in the tank could be estimated:

$$\bar{T}_{pcm} = (T_{pcm,m} + T_{pcm,b})/2 \quad (5.3)$$

To estimate the melted fraction of the PCM in the tank, two points - as basic estimations - need to be taken into account. According to the Table 5.3, in a day with daily solar radiation about 4.0 MJ, the $T_{pcm,m,max} \approx 57^\circ C$, the tank is almost in solid form and only the PCM adjacent to the finned HPC is melted. With some simple calculations, the volume of the PCM in finned area around the HPC is computed, which is about 10% of the bulk of the PCM. Therefore, it could be estimated that in this day 10% of the whole PCM is melted ($F_{melt} \approx 10\%$). In a day with daily solar radiation about 16.5 MJ/m^2 , the

$T_{pcm,b,max} \approx 58.7^\circ\text{C}$, which means the whole PCM inside the tank is completely melted ($F_{melt} = 100\%$). With these two points and linear interpolation, the fraction of the melted PCM in other days could be estimated. The linear interpolation equations for F_{melt} is:

$$F_{melt} = (6.2 \times 10^{-8}) \times \sum I - 0.1427 \quad \text{for } 4 \leq \sum I \leq 18 \quad (5.4)$$

Figure 5.14 presents the graphs of the equations for the melted fraction of the PCM in the LHS tank and the PCM mean temperature.

Table 5.3: The PCM initial and maximum temperature.

$\sum I$	$T_{pcm,m,init}$	$T_{pcm,m,max}$	$T_{pcm,b,init}$	$T_{pcm,b,max}$
3.9	53.3	57.0	48.2	48.2
11.6	53.5	99.4	48.3	49.9
12.7	52.8	99.3	42.2	51.0
13.6	54.2	113.4	47.2	48.5
16.5	52.7	117.9	48.1	58.7
18.1	54.4	131.4	49.9	60.0

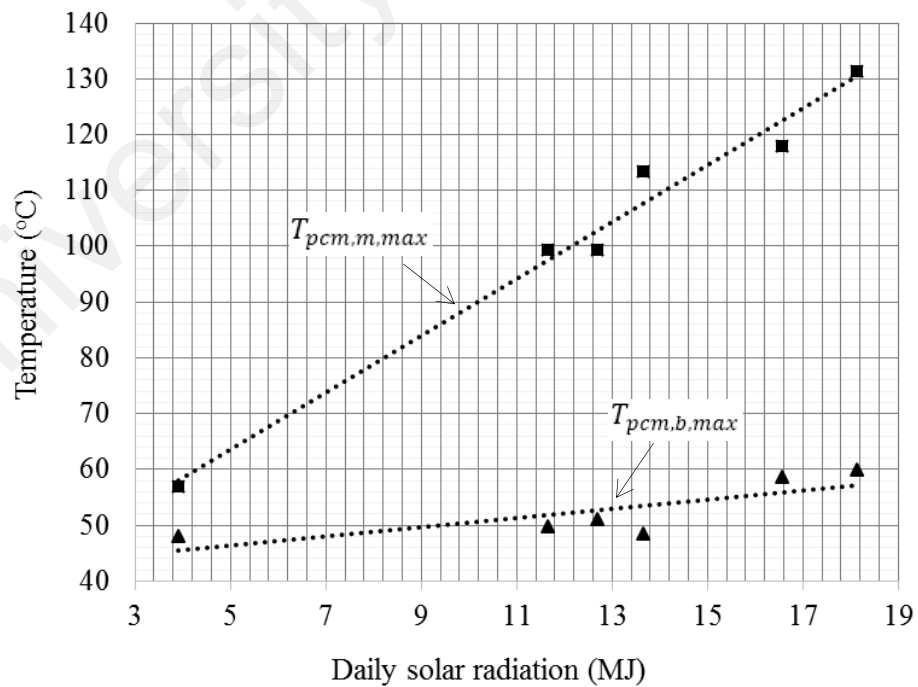


Figure 5.13: The PCM maximum temperature in the bottom and the middle of the tank versus total daily radiation.

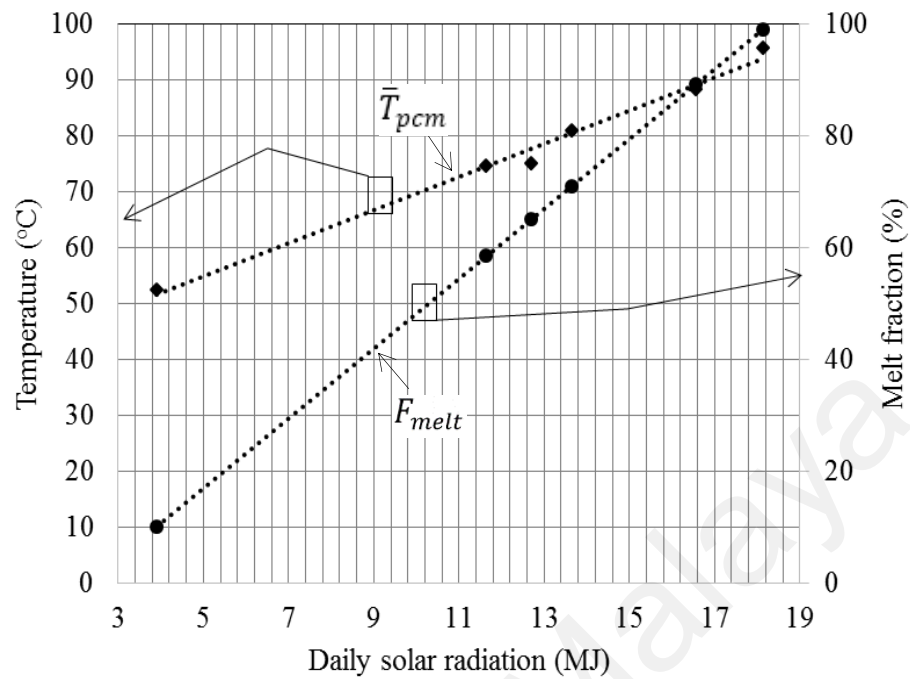


Figure 5.14: The PCM mean temperature and melted fraction.

5.4.2 System thermal efficiency

Tables 5.4 and 5.5 chart the recorded experimental and the computed data for total solar daily energy, cumulative energy stored in the PCM, thermal energy delivered to the supply water and the partial and overall efficiencies of the system for runs in case 1 and 2. The calculation of the absorbable solar radiation shows that with the physical properties of the solar collector, only ~60% of the recorded solar radiation is absorbable by the HPSCs. The absorbed energy is transferred by the HPSCs to the PCM tank through the HP. According to the recorded data of the surface temperature of the HPs in the HPA and the HPC and the thermo-physical properties of the HP, the total heat flux by the HP and efficiency of that for different runs are estimated. The highest efficiency of the HP is 55% while the average efficiency is ~50%. The same data for runs 7-12 are 57% and 52%, respectively. In runs 8 and 9 the HP efficiency is very close to the absorbable solar

radiation percentage, while for other runs there is a difference of 5-10%. This difference maybe causes because of the accuracy of the TCs data and actual performance of the HPs.

Table 5.4: Cumulative energy and efficiencies from runs 1-6.

Item	Run 1	Run 2	Run 3	Run 4	Run 5	Run 6
$\sum \dot{I}. A_{sc}$ (MJ/day)	6.9	23.6	18.4	32.0	36.9	29.4
$\sum \dot{S}. A_{sc}$ (MJ/day)	4.1	13.7	11.0	19.0	21.8	17.5
$\sum \dot{q}_{hp}$ (MJ/day)	3.8	11.7	8.9	16.1	18.0	14.6
F_{melt} (%)	19	75	58	100	100	95
$\sum \dot{q}_{lost}$ (MJ/day)	0.026	0.033	0.030	0.043	0.036	0.033
q_{pcm} (MJ/day)	3.1	10.5	7.8	15.4	16.6	12.8
$\sum \dot{q}_w$ (MJ/day)	2.4	8.45	6.9	13.9	15.0	12.6
η_s (%)	60	58	60	60	59	59
η_{hp} (%)	55	50	48	50	49	50
η_{pcm} (%)	46	45	42	48	45	44
η_w (%)	35	36	37	43	41	43

Table 5.5: Cumulative energy and efficiencies from runs 7-12.

Item	Run 7	Run 8	Run 9	Run 10	Run 11	Run 12
$\sum \dot{I}. A_{sc}$ (MJ/day)	22.6	25.7	23.7	35.4	41.0	39.5
$\sum \dot{S}. A_{sc}$ (MJ/day)	13.6	15.2	13.8	21.1	24.4	23.6
$\sum \dot{q}_{hp}$ (MJ/day)	11.3	14.7	13.1	17.6	20.0	18.0
F_{melt} (%)	72	82	76	100	100	100
$\sum \dot{q}_{lost}$ (MJ/day)	0.032	0.031	0.023	0.038	0.043	0.047
q_{pcm} (MJ/day)	8.7	11.0	10.2	16.1	17.9	17.6
$\sum \dot{q}_w$ (MJ/day)	7.1	9.3	9.3	11.2	16.0	16.8
η_s (%)	60	59	58	59	60	60
η_{hp} (%)	50	57	55	50	49	46
η_{pcm} (%)	39	43	43	45	44	45
η_w (%)	32	36	35	32	39	43

Using the recorded data for the PCM temperature at the middle and the bottom of the LHS tank and via equations 3.36, 3.37, 5.3 and 5.4, the heat lost, the stored energy in the PCM and the melted fraction are estimated. The approximation process of the melted fraction is already explained. The heat loss from the tank is less than ~1% of the total heat stored in duration of the day. The total heat stored and its efficiency are directly based on the earlier assumptions. Therefore, the numbers may not reveal the accurate magnitude

of the stored energy. The average percentage of the stored heat in the LHS tank for case 1 and 2 are 45% and 43%, respectively. Beside the heat loss from the tank walls, some other source of heat loss are finned pipe and heat conduction from the wall of the HPs after sunset. Although, the HP operates as a one-way valve, but when the temperature of the condenser is higher than the evaporator, there will be some heat conduction through the wall of the HP.

The total delivered energy to the supply water and its efficiency are determined based on the temperature difference between the inlet and the outlet temperatures of the water passing through the LHS tank. The overall efficiency of the system is determined by dividing the cumulative heat of the water to the recorded solar data. By comparing the efficiency of the hot water in different runs of cases 1 and 2, it can be seen that by increasing the flow rate from 50 to 80 lph the overall thermal efficiency of the system increased. In case 1, the efficiency of the system is above 42% in high intensity days,

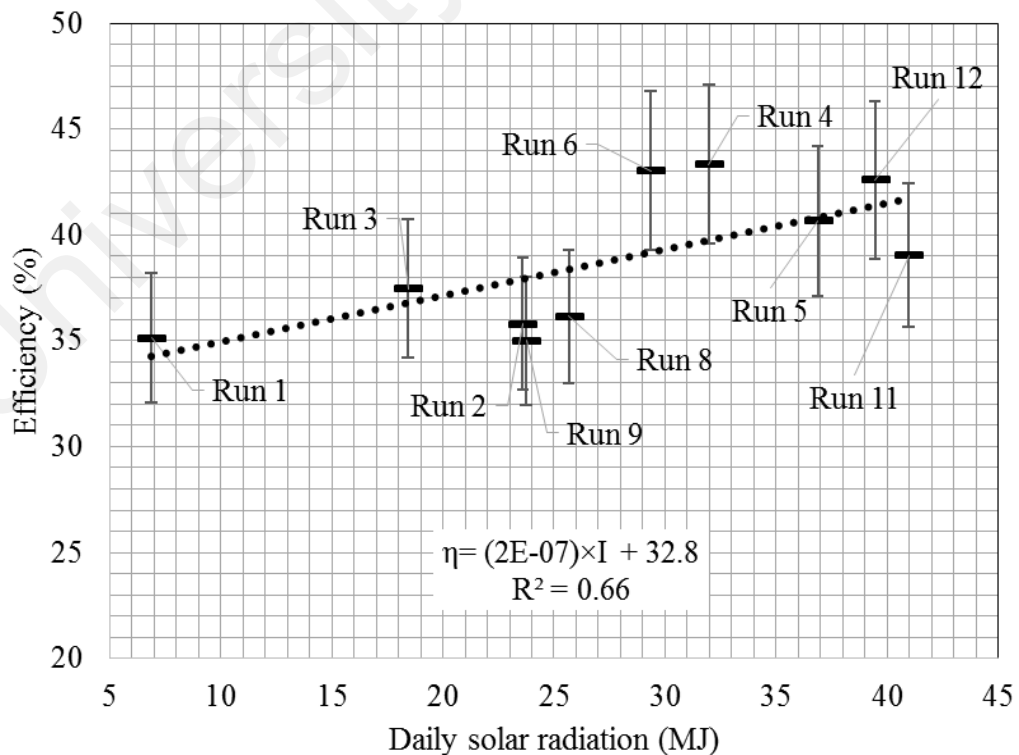


Figure 5.15: Overall thermal efficiency variations of the system with uncertainty range.

while in low intensity days this efficiency drop to about 36%. These efficiencies for low and high intensity days in case 2 is 34% and 38%, respectively.

In the Figure 5.15 the overall efficiency of the system in different runs are plotted against the recorded daily solar radiation. According to the uncertainty analysis in 3.5.4, the uncertainty of the overall thermal efficiency of the system can be determined to be about $\pm 8.7\%$. In general, by overviewing the results in cases 1 and 2, with respect to the uncertainty bars, the range of the changes on the efficiency of the system in different weather conditions and different flow rates is less than 10%, which indicates an almost steady efficiency. In addition, this fact could be extracted from the graphs that the discharge time does not have direct effect on the efficiency of the system.

5.5 Summary

The experimental investigation was carried out to determine the performance of the HPSC-LHS system in the charging only and discharging only mode. The objectives of this research were to evaluate the maximum possible heat storage in the LHS tank and the efficiency of the system by transferring the thermal energy to supply water. The results obtained from the tests indicated that this design is able to have considerable performance in different climatic and water draw off conditions.

CHAPTER 6: EXPERIMENTAL STUDY

PART II: SIMULTANEOUS CHARGING-DISCHARGING MODE

6.1 Introduction

In this chapter, the possibility of the simultaneous charging-discharging operation of the proposed HPSC-LHS design is examined. Tests in the chapter 5 were planned to identify the sectional and overall thermal performance of the system under different conditions. Based on two reasons it appears to be necessary to test the thermal behavior of the system in the simultaneous mode. One, the factual hot water demand pattern is in both day and night times. Second, the effect of the day time hot water withdrawal pattern on the solar energy absorption fraction. Therefore, in this chapter, first, the practicable hot water demand pattern will be introduced. Then, the results of the runs for this mode will be presented and at the end the effect of this test mode on the PCM and HP temperature fluctuations will be compared with those in the mode on no discharge at the day time.

6.2 Hot water load profile

There are several reports which tried to determine hot water consumption profile for households in different climates and conditions. Fairey and Parker (2004) reviewed the hot water consumption, delivery temperature and incoming cold feed temperature in residential domestic hot water systems for some cities in the USA. The mean household consumption has been found to be 122 liters/day, with a 95% confidence interval of ± 18 liters/day. Statistical analysis of the flow data from each dwelling has considered the impact of geographical region, boiler type, number of occupants, and the number of those occupants who are children. The mean energy content has been found to be 16.8 ± 2.2 MJ/day. The report by (Vine et al., 1987) examined few different houses in USA to find

the average profile in a year and then suggested a normalized profile for further researches. Hendron and Burch (2008) developed a standardized domestic hot water consumption schedules for residential buildings. Beside the general hot water profiles, several researchers focused on the hot water draw in SWH systems. Burch and Thornton (2012) outlined the current and the proposed draws and estimates typical ratings changes from draw specification changes for typical systems in four cities in USA. Baharuddin et al. (2009) studied the technical and economic feasibility of the domestic solar hot water heating systems in Malaysia.

A report by Zahedi et al. (2007) simulated a solar water heater in Malaysian climate for a house with 5 occupancies to produce 150 liter hot water daily. They used the profile suggested by Duffie and Beckman (2013) for their simulation. They reported that in terms of hot water consumption pattern, most families in Malaysia use hot water in evening and nights. A survey among 62 families (Kuala Lumpur) done in 2004 by Jabatan Kerja Raya (2004) indicated that most of the families use hot water just for shower in the morning and after 6 pm. In some cases, families use hot water in midday for washing and infants. Average number of family members in urban areas in Malaysia is 3-5 persons and for each person, 25-30 liter hot water is adequate. It means 100-150 liter/day per family should be enough as hot water consumption in Malaysia. Therefore, as presented in Figure 6.1, by comparing the hot water profiles, which was proposed in different reports two

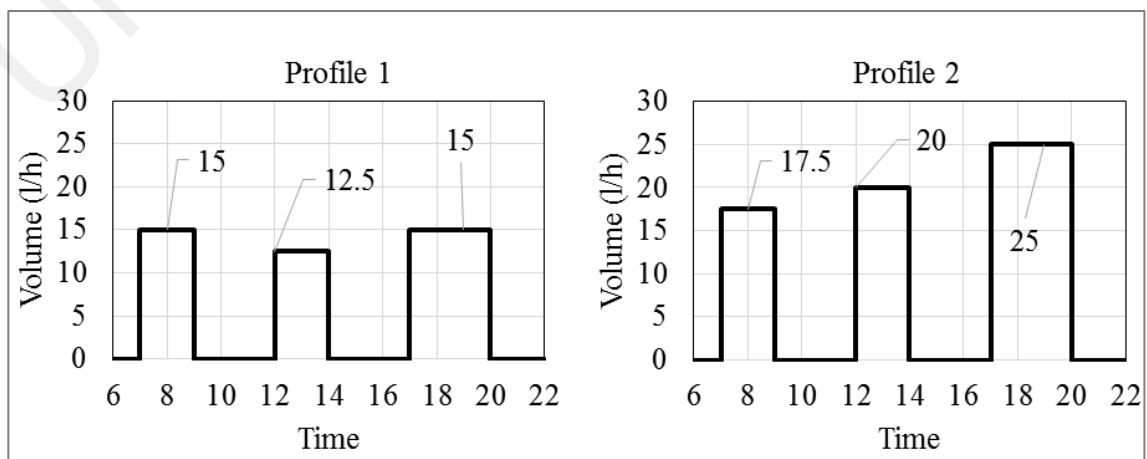


Figure 6.1: Hot water draw off profiles.

practical profiles for hot water draw off for two loads of 100 and 150 liter/day were considered. The water draw off steps are 07:00-09:00, 12:00-14:00 and 17:00-20:00. Data are recorded every 5 minutes. The magnitudes of the hot water draw off in each step are shown in the Figure 6.1. Typical data discussed here were obtained over 8 days and tabulated in Table 6.1. The experimental tests were carried out in simultaneous charging-discharging mode for different conditions of high/low daily solar radiation, hot water draw off profiles and consecutive/nonconsecutive discharged days. The last term is related to the cases when the day before taking the test the LHS tank is discharged or not.

Table 6.1: Summary of the runs.

Runs no.	Mode in the past day	Solar intensity category	Radiation (MJ/m ² .day)	Flowrate (lpd)	Run code
1	Not discharged	High	22.6	100	N-H-100
2	Not discharged	Low	5.4	100	N-L-100
3	Not discharged	High	18.0	150	N-H-150
4	Not discharged	Low	9.0	150	N-L-150
5	Discharged	High	21.5	100	Y-H-100
6	Discharged	Low	11.4	100	Y-L-100
7	Discharged	High	16.7	150	Y-H-150
8	Discharged	Low	13.5	150	Y-L-150

6.3 Results and discussion

Unlike the previous chapter, to get a better understanding about the proportions of all variables, for each run, data of the solar radiation, PCM temperature and hot water outlet are presented in a single Figure. Results will be studied in two sections; First, the runs for the nonconsecutive days and second, the runs for the consecutive days.

6.3.1 Nonconsecutive runs

Figure 6.2 depicts the experimental results for run N-H-100. According to the graph of the solar radiation, this day is a fully sunny day and the ambient temperature is in the range of 28-40°C. The inlet supply water is mostly in the range of 28-30°C. The PCM

temperature at the middle and bottom of the tank are about 58-60°C, which indicates that the bulk of the PCM is in liquid form. By starting water draw off from the LHS tank at 07:00, with flow rate of 15 lph, the outlet hot water temperature is over 40°C, while within the next hour it drops to about 37°C, but it increases again to about 39°C in 09:00. This is due to the higher solar intensity at this time, which leads to the PCM temperature increment. Next hot water draw off starts at 12:00 until 14:00. In this duration, when the flow rate is 12.5 lph, the hot water temperature is steadily in the range of 53-55°C. The PCM temperature in the middle of the tank drops from ~100°C to less than 90°C, in this duration. From 14:00 until 17:00 the LHS tank is in charging mode. In this period, the PCM temperature in the middle and bottom of the tank increase 130°C and 75°C, respectively, which shows that the bulk of the PCM is completely melted. The third draw off starts at 17:00 and continuous for three hours for flow rate 15 lph. The hot water temperature, initially, is over 65°C which is because of high sensible heat storage in the PCM. After this time, until 20:00, the hot water temperature drops to ~43°C which still is

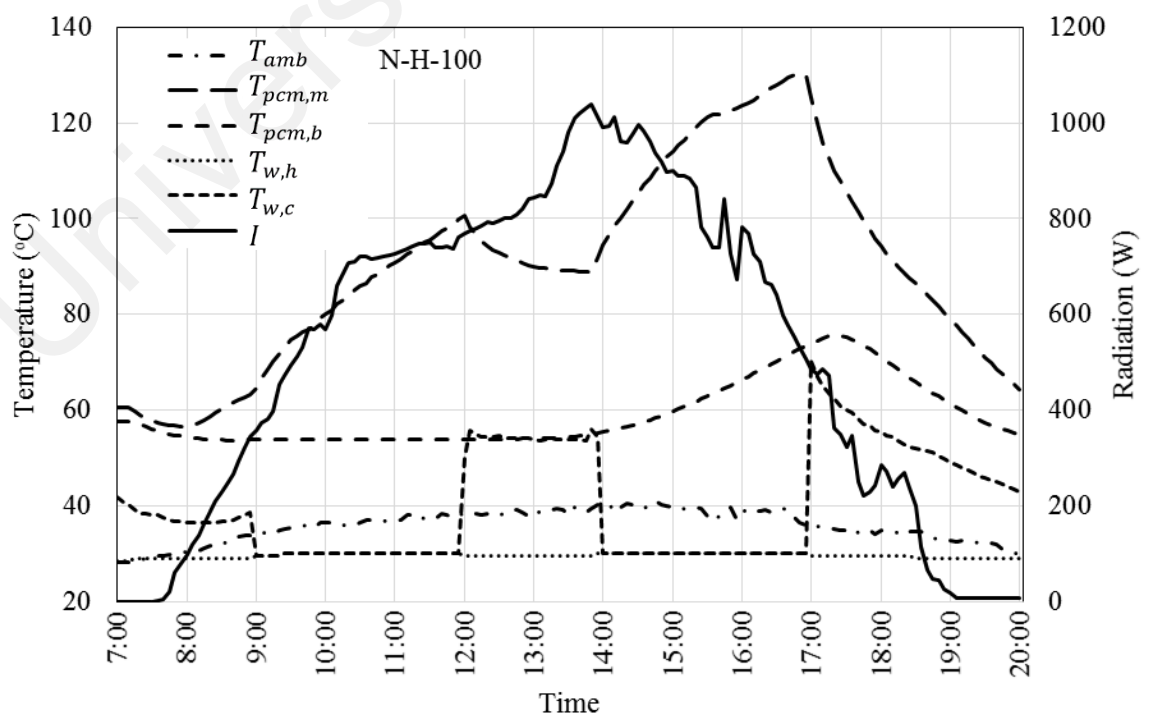


Figure 6.2: The experimental results for run N-H-100.

a high temperature. According to the observations of the test in the chapter 4, if the draw off continuous, the system is still able to provide more hot water for a while.

Figure 6.3 presents the data of run 2 for a complete rainy day in the situation that in the previous day the LHS tank was in in charging mode only. The PCM is initially fully melted in temperature range of 62-68°C. The tank is able to provide hot water in temperature range of 35-40°C in early morning. Regarding the low solar radiation the LHS tank is not charging rapidly in the time 09:00 to 12:00. Therefore, the temperature of the outlet water in the second time draw off does not exceed 37°C. Although, the PCM temperature in the middle of the tank reach to over 65°C in the afternoon, but the hot water temperature in third draw off drops fast from 40°C to about 30°C at 20:00. This case indicates that in such this situation the system needs an auxiliary heater to warm up the water to the operating temperature.

Figures 6.4 and 6.5 depicted results of the runs 3 and 4. These two runs are taken based on the profile 2 for high and low daily solar radiation in the case that the previous day was only in the charging mode. In run 3, the day was sunny until 15:00 and then rainy

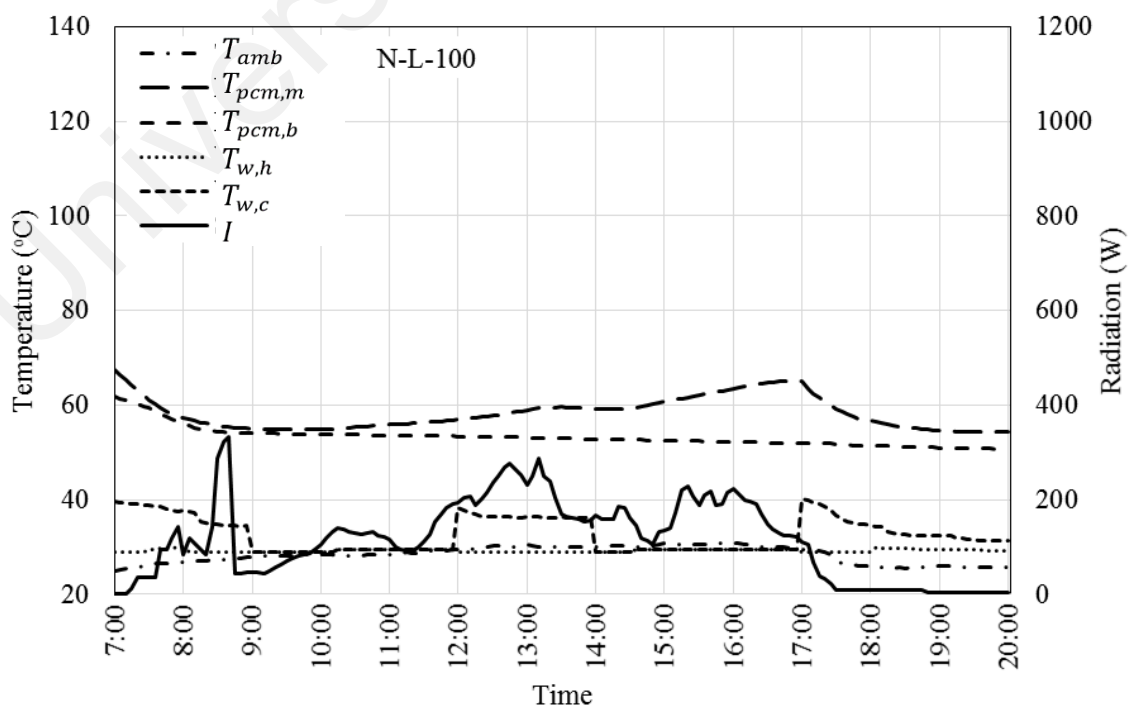


Figure 6.3: The experimental results for run N-L-100.

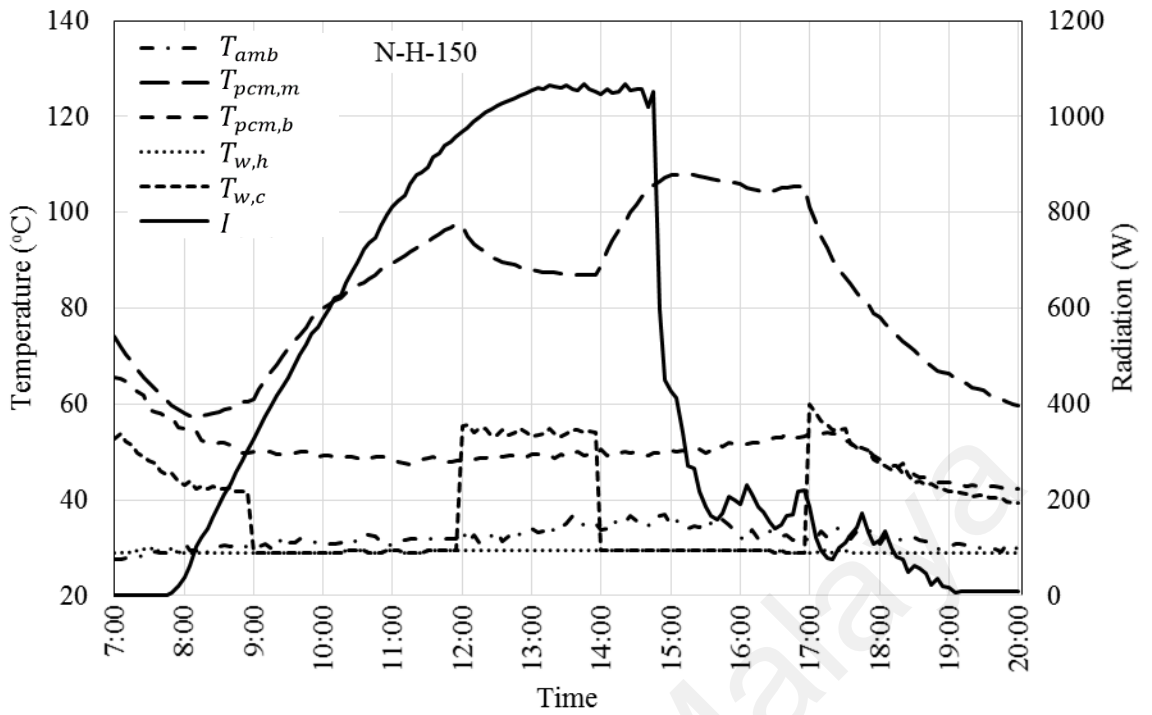


Figure 6.4: The experimental results for run N-H-150.

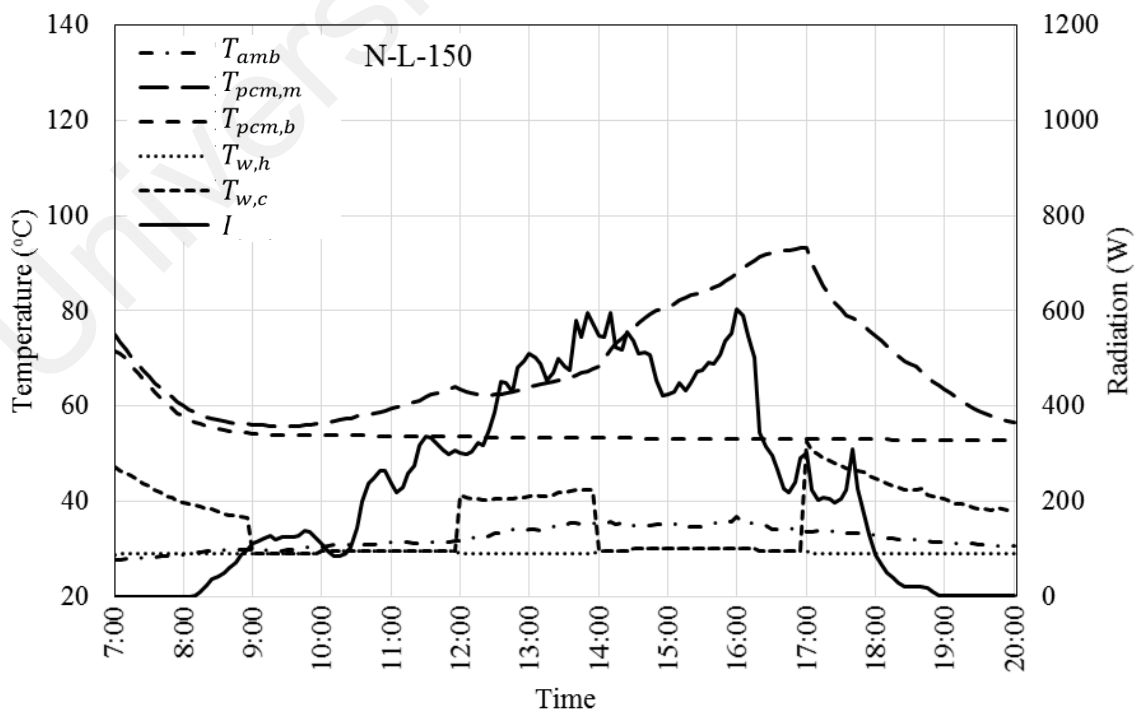


Figure 6.5: The experimental results for run N-L-150.

until night. The PCM is initially fully melted with temperature averagely about 70°C. The draw off flow rate in morning is 17.5 lph. The outlet hot water initially is ~53°C, then, it drops to 42°C at 09:00. The PCM temperature drops to about the melting temperature at this time, but, it rise up again dramatically until noon time to about 97°C. The supply water flow rate for the second draw off is 20 lph. Regarding the graph, the hot water temperature does not vary significantly in this duration and remain in the temperature about 54°C. In this period, the PCM temperature in the middle of the tank drops about 10°C, while the PCM temperature in the bottom of the tank remains in the solid form. The hot water temperature in the third draw off starts from 60°C, while the flow rate is 25 lph. After 3 hours the hot water temperature is still over 40°C. In the run 4, the solar radiation is weak in the whole day. The initial temperature of the PCM is averagely about 74°C. By comparing the hot water temperature range of all three steps in this run with run 3, this could be extracted that although the outlet water is not that much hot but the system is able to provide hot water over 38°C.

6.3.2 Consecutive runs

Runs 5-8 presents data for days which consecutively were charging and discharging according to the profiles 1 and 2.

Figure 6.6 presents the data for a sunny-cloudy day. The total daily solar radiation in this day is 21.6 MJ/m², which is close to the value of this term in run 1. The PCM temperature is initially in the range of the melting point. It seems that the tops side of the tank is melted, while the bottom side is solid. The hot water temperature in the morning starts from 36°C and drops to 32°C after two hours flowing with flow rate of 15 lph. Due to the high intensity of solar radiation until 12:00, the PCM temperature reaches to near 100°C. In the second draw off step, the hot water temperature fluctuates in the range of 53-55°C, while the PCM temperature in the middle of the tank drops to less than 90°C.

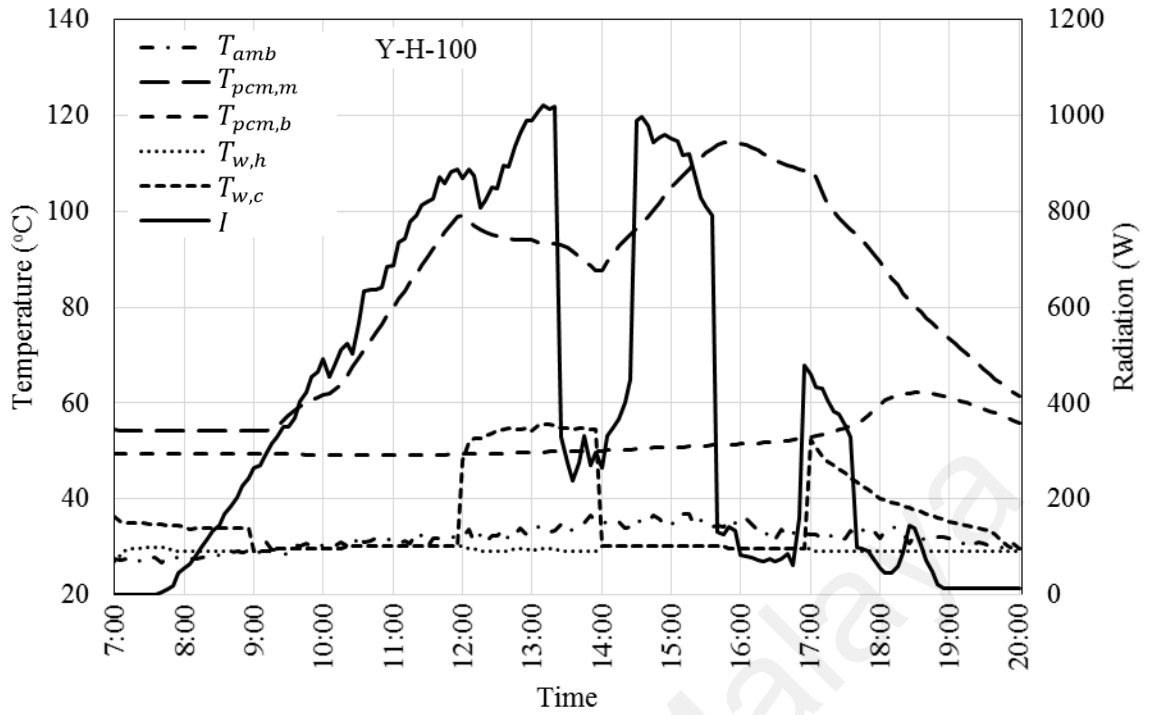


Figure 6.6: The experimental results for run Y-H-100.

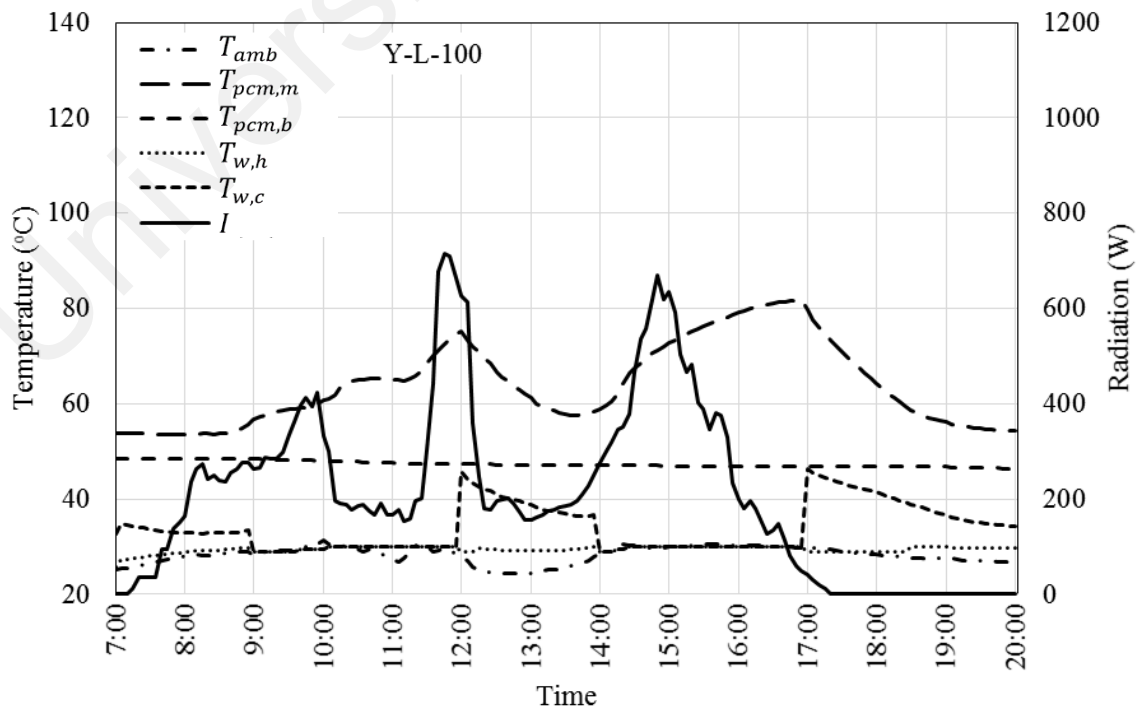


Figure 6.7: The experimental results for run Y-L-100.

Temperature of the PCM in the middle of the tank increases again up to 114°C, while the PCM in the bottom of the tank is slowly melting. After the time that the third draw off starts, the PCM temperature in the middle of the tank drops very fast due to two reasons, which are heat conduction to the PCM remained in the solid form and heat transfer to the supply water. Figure 6.7 presents data of the run 6 for a cloudy-rainy day with the PCM which some of the stored heat from the previous day is still remains on that. The temperature of the produced hot water in the first draw off step is in the range of 32-34°C, which is only 4-5°C above the inlet water. The hot water temperature in the beginning and end of the steps 2 and 3 are similarly 46°C and 34°C.

Figures 6.8 and 6.9 demonstrate the data of runs 7 and 8 which are taken based on the profile 2. Although, the PCM initial temperature in the runs 7 and 8 are same (~54°C) and the daily solar radiation of them are 16.7 MJ/m² and 13.5 MJ/m², respectively, the produced hot water in all 3 steps of both runs are in very close temperature ranges. This point indicates that the system is able to produce the demanded hot water volume in the all three steps of time. In the morning time the hot water temperature is in the operating temperature range, while in the midday and evening the produced hot water must be mixed with the cold water to reach to the usable temperature range.

6.4 Summary

Runs 1-4 reveals that if the LHS tank was not discharged in the previous day, the system is able to keep the stored heat for hot water production in the next day morning time. In the same way, the system is able to provide hot water for both draw off profiles even if the day is cloudy-rainy, but in lower temperature range, than the sunny days. According to the runs 5-8, except the fully rainy-cloudy days, the LHS tank is able to fulfil daytime demand of the moderate amounts of hot water withdrawn on sufficiently spaced time intervals.

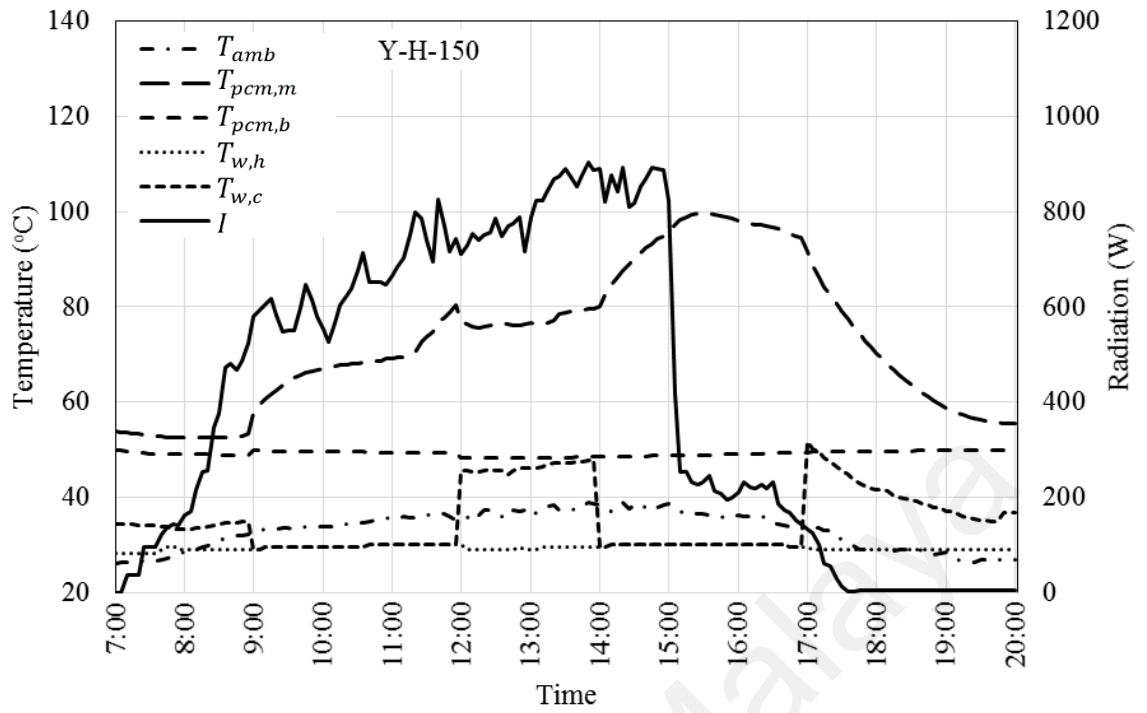


Figure 6.8: The experimental results for run Y-H-150.

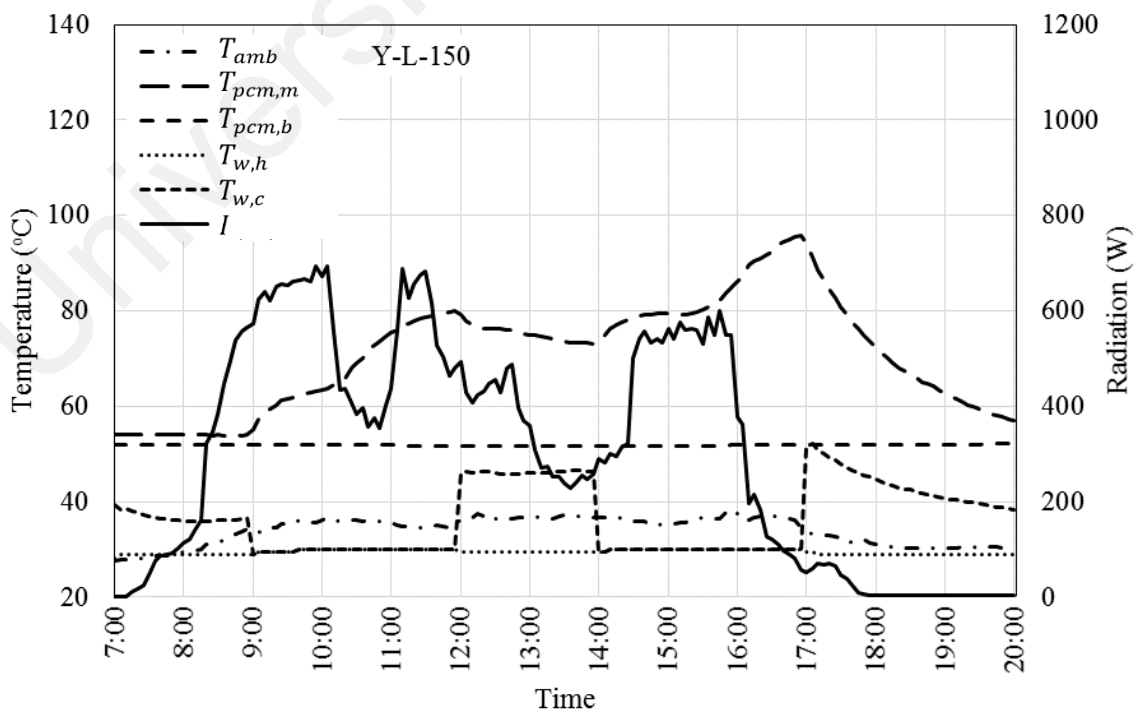


Figure 6.1: The experimental results for run Y-L-150.

CONCLUSIONS AND RECOMMENDATIONS

7.1 Conclusions

One of the main purposes of application based research is developing the theoretical and fundamental findings into new technologies. Today, the TES technics is one of the high-impact research topics at the sustainable renewable energy systems. Some of the most important challenges in this field are maximizing the solar energy absorption fraction, extending the operation time of the system, hot water production capacity and techno-economic optimization of the TES unit. As it was reviewed in the Chapter 2, the advantage of using the PCM as latent heat storage over the sensible heat storage is proven. Several configurations of the combined design of the solar water heater systems with PCM containers are studied. Most of the reports concluded that their model may be beneficial under certain conditions. The target of this research was to develop a new design for SWH with a LHS storage unit to perform efficiently in different climatic conditions and hot water load, while minimizing the weaknesses of the other similar systems.

For this purpose, after a vast study of the previous literatures, a new compact design for LHS tank in combination with a HPSC was proposed. Then, to obtain a primary understanding about the performance of this system, the thermal characteristics of the conceptual design of the HPSC-LHS system in different conditions was theoretical studied and compared with a conventional (baseline) HPSC system. Based on the findings from the theoretical modeling and the previous researches, a detailed design for the HPSC-LHS system for experimental tests was prepared. In the experimental step, a complete design of the proposed system was fabricated and tested under real conditions. Two modes of the tests were carried out. One charging only and discharging only; and the other one batch-wise simultaneous charging-discharging.

A combined mathematical algorithm and approximate solution were prepared to model the heat transfer processes in all sections of this system, which are solar collector, HP, PCM melting/solidification and outlet hot water temperature. The accuracy of the solution was already discussed. By comparing the results of the theoretical and experimental results and taking into account the necessary assumptions included to the calculations, it was observed that the theoretical results have generally acceptable agreement with the experimental results; although the design of the LHS tank varies in these two cases. Using actual characteristics for all parts of the system and calculations allows having minimum deviation from the real situation.

Based on the theoretical study, the feasibility of the new design was proven. It was demonstrated that the thermal performance of this design is reasonably practicable when it compared with the conventional system. The results showed that in sunny days, the thermal performance of the proposed system is comparable with the conventional one, while in cloudy/rainy days the new design have higher efficiency. In the conventional HPSC system, when the daily solar radiation is low, the efficiency of the system is less than 30%, while in the days with high daily solar radiation, the efficiency is in the range of 50-60%. The thermal efficiency of the HPSC-LHS system for both days are in the range of ~50%. The analysis also showed that the sensitivity of the efficiency of the proposed system to supply water flow rate is less than the baseline system. By comparing the efficiency of the hot water in experimental tests, it was illustrated that the flow rate has direct proportion on the overall efficiency of the system. The efficiency of the HPSC-LHS system in sunny days is in the range of the 38%-42%, while in cloudy-rainy days this efficiency drop to the range of 34%-36%. In general, by overviewing the findings of the first part of the experimental tests, with respect to the uncertainty of the system, the range of the changes on the efficiency of the system in different weather conditions and

different flow rates is less than 10%, which indicates an almost steady efficiency, which prove the results of the theoretical modeling.

One of the findings of this research was that the batch-wise discharging of hot water from the storage tank was best suited for applications where the requirement is intermittent for a tropical climatic region like Malaysia. The simultaneous charging-discharging tests proved that this design is able to provide over 150 liter hot water in the operating temperature every day, except fully rainy-cloudy days. It also found that this system is able to keep the stored heat from previous day to produce hot water in early morning for domestic usages such as showering.

From the experimental findings and comparing the characteristics of this design with other introduced SWH-LHS systems several advantages could be extracted:

- Overall, it is understood that beyond different PCM melting/solidification enhancement rate technics, HP is a reliable and manageable choice. Interestingly, advantages of the HP and PCM cover their disadvantages like overheating of the HP and low thermal conductivity of the PCM. The heat transmission from collector to the LHS tank by HP is fast and efficient.
- Using fins on HP increases heat transfer rate to the PCM and decreases temperature gradient in bulk of the PCM. Fins amplitude the heat transmission from the HP to the PCM medium.
- By a charged TES tank (molten PCM), it is possible to use the hot water at any time of night or next day early morning, when the solar radiation is still weak.
- High viscosity, less weight and lower volume of the PCM cause to less heat loss from the LHS tank in comparison with the SHS tank.
- The principle of thermal stratification in the SHS tank have very high importance to the efficiency of SWH systems. An advantage of the LHS tank is removing the stratification effect in the TES unit.

- The configuration leads to very low energy waste in the system. Therefore, by using advantages of HPs, fins, PCM and dual heat exchangers, it could be expected to achieve highest possible thermal efficiency in converting solar energy to hot water.
- The other problem is about growing legionella bacteria inside the hot water tank, which is naturally occurring organisms present in many hot water tanks. Indirect and instantaneous heating of the water in the LHS tank will lead to removing this problem too.
- Regarding the economic concerns, this compact design minimizes the required infrastructures on the buildings, such as piping works, hot water tank, base structure for hot water tank and de-stratification tools, which leads to a simple, cheap and reliable structure. In addition, this system is basically stationary and there is no moveable part in the structure. Therefore, it could causes to less maintenance in the future.
- Paraffin wax is cheap, with long term lifecycle and durability of the thermal properties. There are no associated risks with health and safety issues.
- This system could be a stand-alone system for night hot-water demands or part of a SWH configuration, which is combined with a conventional SWH systems.

7.2 Recommendations

The overall observations from the experimental field tests of the HPSC-LHS system and the findings of the previous research reports indicates that the performance of this system depends on various parameters such as the weather condition which fluctuates widely in this region, the thermal properties of the PCM, the geometric design of the LHS tank, the fin design on the HPC and the HWSHE pipe lines, supply water inlet temperature, flow rate and the water draw off time. According to these parameters, several new topics could be suggested for further researches and investigations:

- To reach to the maximum efficiency of the system and minimize the effect of the design and environmental parameters an optimization study must be carried out on the effective design of the finned shell on the HPC, the effective design of the finned HWSHE pipe line and the most appropriate thermal properties of the PCM.
- Simulation of the actual design of the LHS tank by softwares like ANSYS will help to be able to compare different configurations of the LHS design, PCM type, entry heat flux pattern and supply water piping system.
- Techno-economic evaluation and annual performance of this design is necessary to find out the impact of the new TES unit on the financial issues such as initial capital and payback periods for small/ large scales of this design.
- Earlier valuations of the proposed system were based on the first thermodynamic law. However, this kind of assessment cannot perfectly describe the performance of system, since the essence of energy utilization is to extract available energy as much as possible. So, it is necessary to evaluate the performance of the system based on the second thermodynamic law. Exergy analysis of this system is necessary to the maximum useful work possible during a process that brings the system into equilibrium with a heat reservoir.
- This research carried out in a tropical climatic region. It is necessary to evaluate the characteristics and performance of the HPSC-LHS design for other climatic conditions such as four seasons or cold weather regions.

REFERENCES

- Abhat, A. (1978). Performance studies of a finned heat pipe latent thermal energy storage system. Proceedings of International Solar Energy Congress (pp. 541-546), India.
- Abhat, A. (1980). Short term thermal energy storage. *Revue de physique appliquee*, 15(3), 477-501.
- Abhat, A. (1983). Low temperature latent heat thermal energy storage: heat storage materials. *Solar energy*, 30(4), 313-332.
- Akgün, M., Aydin, O., & Kaygusuz, K. (2007). Experimental study on melting/solidification characteristics of a paraffin as PCM. *Energy Conversion and Management*, 48(2), 669-678.
- Akhilesh, R., Narasimhan, A., & Balaji, C. (2005). Method to improve geometry for heat transfer enhancement in PCM composite heat sinks. *International Journal of Heat and Mass Transfer*, 48(13), 2759-2770.
- Al-Hinti, I., Al-Ghandoor, A., Maaly, A., Abu Naqera, I., Al-Khateeb, Z., & Al-Sheikh, O. (2010). Experimental investigation on the use of water-phase change material storage in conventional solar water heating systems. *Energy Conversion and Management*, 51(8), 1735-1740.
- Alexiades, V., & Solomon, A. D. (1993). *Mathematical Modeling of Melting and Freezing Processes*: Taylor & Francis Group.
- Armstrong, P., Ager, D., Thompson, I., & McCulloch, M. (2014a). Domestic hot water storage: Balancing thermal and sanitary performance. *Energy Policy*, 68, 334-339.
- Armstrong, P., Ager, D., Thompson, I., & McCulloch, M. (2014b). Improving the energy storage capability of hot water tanks through wall material specification. *Energy*, 78, 128-140.
- Association, T. M. V. M. (2013). Recommended Code of Practice for Safe Water Temperatures. London, England: BEAMA.
- Aydin, D., Utlü, Z., & Kincay, O. (2015). Thermal performance analysis of a solar energy sourced latent heat storage. *Renewable and Sustainable Energy Reviews*, 50, 1213-1225.
- Ayompe, L. M., Duffy, A., Mc Keever, M., Conlon, M., & McCormack, S. J. (2011). Comparative field performance study of flat plate and heat pipe evacuated tube

collectors (ETCs) for domestic water heating systems in a temperate climate. *Energy*, 36(5), 3370-3378.

Baharuddin, A., Kamaruzzaman, S., Mohamad, A., Mohd Yusof, O., Azami, Z., & Ahmad Mahir, R. (2009). Economics of domestic solar hot water heating systems in Malaysia. *European Journal of Scientific Research*, 26(1), 20-28.

Bauer, T. (2011). Approximate analytical solutions for the solidification of PCMs in fin geometries using effective thermophysical properties. *International Journal of Heat and Mass Transfer*, 54(23-24), 4923-4930.

Beckman, W. A., Klein, S. A., & Duffie, J. A. (1977). *Solar heating design, by the f-chart method*: Wiley.

Benli, H., & Durmuş, A. (2009). Performance analysis of a latent heat storage system with phase change material for new designed solar collectors in greenhouse heating. *Solar Energy*, 83(12), 2109-2119.

Bergman, T. L., & Incropera, F. P. (2011). *Introduction to Heat Transfer*: Wiley.

Blank, I. A., Korten, M. K., & Moore, C. N. (2007). Existence, uniqueness and regularity of the free boundary in the Hele-Shaw problem with a degenerate phase. *Contemporary Mathematics*, 428, 33.

Brahim, T., Dhaou, M. H., & Jemni, A. (2014). Theoretical and experimental investigation of plate screen mesh heat pipe solar collector. *Energy Conversion and Management*, 87, 428-438.

Briozzo, A. C., & Tarzia, D. A. (2010). Exact Solutions for Nonclassical Stefan Problems. *International Journal of Differential Equations*, 2010.

Buckles, W. E., & Klein, S. A. (1980). Analysis of solar domestic hot water heaters. *Solar Energy*, 25(5), 417-424.

Burch, J., & Thornton, J. (2012). A Realistic Hot Water Draw Specification for Rating Solar Water Heaters: National Renewable Energy Laboratory (NREL), Golden, CO.

Caldwell, J., & Chan, C. C. (1998). Numerical solutions of the Stefan problem by the enthalpy method and the heat balance integral method. *Numerical heat transfer*, 33(1), 99-117.

- Canbazoğlu, S., Şahinaslan, A., Ekmekyapar, A., Aksoy, Ý. G., & Akarsu, F. (2005). Enhancement of solar thermal energy storage performance using sodium thiosulfate pentahydrate of a conventional solar water-heating system. *Energy and Buildings*, 37(3), 235-242.
- Cheng, T.-F. (2000). Numerical analysis of nonlinear multiphase Stefan problems. *Computers & Structures*, 75(2), 225-233.
- Churchill, S., & Bernstein, M. (1977). A correlating equation for forced convection from gases and liquids to a circular cylinder in crossflow. *ASME Transactions Journal of Heat Transfer*, 99, 300-306.
- Crank, J. (1984). *Free and moving boundary problems*: Clarendon Press.
- Davis, G. B., & Hill, J. M. (1982). A moving boundary problem for the sphere. *IMA Journal of Applied Mathematics*, 29(1), 99-111.
- De Soto, W., Klein, S., & Beckman, W. (2006). Improvement and validation of a model for photovoltaic array performance. *Solar energy*, 80(1), 78-88.
- Duffie, J. A., & Beckman, W. A. (2013). *Solar Engineering of Thermal Processes*: Wiley.
- Eames, P. C., & Griffiths, P. W. (2006). Thermal behaviour of integrated solar collector/storage unit with 65°C phase change material. *Energy Conversion and Management*, 47(20), 3611-3618.
- El Qarnia, H., & Adine, H. A. (2010). Thermal behavior of a shell-and-tube heat storage unit using twophase change materials. *Computational Thermal Sciences*, 2(3), 249-268.
- Esen, M., Durmuş, A., & Durmuş, A. (1998). Geometric design of solar-aided latent heat store depending on various parameters and phase change materials. *Solar Energy*, 62(1), 19-28.
- Ettouney, H., El-Dessouky, H., & Al-Ali, A. (2005). Heat transfer during phase change of paraffin wax stored in spherical shells. *Journal of solar energy engineering*, 127(3), 357-365.
- Ettouney, H., El-Dessouky, H., & Al-Kandari, E. (2004). Heat transfer characteristics during melting and solidification of phase change energy storage process. *Industrial & engineering chemistry research*, 43(17), 5350-5357.

- Faghri, A. (2014). Heat Pipes: Review, Opportunities and Challenges. *Frontiers in Heat Pipes (FHP)*, 5(1).
- Fairey, P., & Parker, D. (2004). A review of hot water draw profiles used in performance analysis of residential domestic hot water systems. *Florida Solar Energy Center*, (2).
- Fernandez-Seara, J., Uhía, F. J., & Sieres, J. (2007). Experimental analysis of a domestic electric hot water storage tank. Part I: Static mode of operation. *Applied thermal engineering*, 27(1), 129-136.
- Gharebaghi, M., & Sezai, I. (2008). Enhancement of heat transfer in latent heat storage modules with internal fins. *Numerical Heat Transfer; Part A: Applications*, 53(7), 749-765.
- Günther, E., Mehling, H., & Hiebler, S. (2007). Modeling of subcooling and solidification of phase change materials. *Modelling and Simulation in Materials Science and Engineering*, 15(8), 879.
- Guo, C., & Zhang, W. (2008). Numerical simulation and parametric study on new type of high temperature latent heat thermal energy storage system. *Energy Conversion and Management*, 49(5), 919-927.
- Gupta, S. K., Kratz, D. P., Stackhouse Jr, P. W., & Wilber, A. C. (2001). *The Langley parameterized shortwave algorithm (LPSA) for surface radiation budget studies*: Citeseer.
- Hahn, D. W., & Ozisik, N. (2012). *Heat Conduction*: Wiley.
- Hasnain, S. (1998). Review on sustainable thermal energy storage technologies, Part I: heat storage materials and techniques. *Energy Conversion and Management*, 39(11), 1127-1138.
- Hendron, R., & Burch, J. (2008). *Development of standardized domestic hot water event schedules for residential buildings*: National Renewable Energy Laboratory.
- Hill, J. M. (1987). *One-dimensional Stefan problems: an introduction*: Longman Scientific & Technical.
- Hill, J. M., & Kucera, A. (1983). Freezing a saturated liquid inside a sphere. *International Journal of Heat and Mass Transfer*, 26(11), 1631-1637.

- Horbaniuc, B., Dumitrascu, G., & Popescu, A. (1999). Mathematical models for the study of solidification within a longitudinally finned heat pipe latent heat thermal storage system. *Energy Conversion and Management*, 40(15), 1765-1774.
- Horbaniuc, B., Popescu, A., & Dumitraşcu, G. (1996). The correlation between the number of fins and the discharge time for a finned heat pipe latent heat storage system. *Renewable Energy*, 9(1), 605-608.
- Huang, C. L., & Shih, Y. P. (1975). A perturbation method for spherical and cylindrical solidification. *Chemical Engineering Science*, 30(8), 897-906.
- Hussein, H. (2003). Optimization of a natural circulation two phase closed thermosyphon flat plate solar water heater. *Energy Conversion and Management*, 44(14), 2341-2352.
- Ibáñez, M., Cabeza, L. F., Solé, C., Roca, J., & Nogués, M. (2006). Modelization of a water tank including a PCM module. *Applied Thermal Engineering*, 26(11–12), 1328-1333.
- Iqbal, M. (1979). A study of Canadian diffuse and total solar radiation data—II Monthly average hourly horizontal radiation. *Solar Energy*, 22(1), 87-90.
- Jegadheeswaran, S., & Pohekar, S. D. (2009). Performance enhancement in latent heat thermal storage system: a review. *Renewable and Sustainable Energy Reviews*, 13(9), 2225-2244.
- Jegadheeswaran, S., Pohekar, S. D., & Kousksou, T. (2011). Performance Enhancement of Solar Latent Heat Thermal Storage System with Particle Dispersion - an Exergy Approach. *Clean - Soil, Air, Water*, 39(10), 964-971.
- JKR. (2004). standard specification for building works *Water Meter* (Vol. ISO 4064-1 : 2005). Malaysia: Jabatan Kerja Jaya.
- Jung, E. G., & Boo, J. H. (2014). Thermal analytical model of latent thermal storage with heat pipe heat exchanger for concentrated solar power. *Solar Energy*, 102, 318-332.
- Karthick, R., & Manivannan, A. (2015). Thermel energy storage in solar water heater using phase change material. *The International Daily journal Discovery*, 37(167), 28-36.
- Kaviany, M. (2002). *Principles of heat transfer*: Wiley.

- Khalifa, A. J. N., Suffer, K. H., & Mahmoud, M. S. (2013). A storage domestic solar hot water system with a back layer of phase change material. *Experimental Thermal and Fluid Science*, 44(0), 174-181.
- Kim, Y., & Seo, T. (2007). Thermal performances comparisons of the glass evacuated tube solar collectors with shapes of absorber tube. *Renewable Energy*, 32(5), 772-795.
- Koca, A., Oztop, H. F., Koyun, T., & Varol, Y. (2008). Energy and exergy analysis of a latent heat storage system with phase change material for a solar collector. *Renewable Energy*, 33(4), 567-574.
- Kousksou, T., Bruel, P., Cherreau, G., Leoussoff, V., & El Rhafiki, T. (2011). PCM storage for solar DHW: From an unfulfilled promise to a real benefit. *Solar Energy*, 85(9), 2033-2040.
- Kreith, F., & Romie, F. (2002). A study of the thermal diffusion equation with boundary conditions corresponding to solidification or melting of materials initially at the fusion temperature. *Proceedings of the Physical Society. Section B*, 68(5), 277.
- Lacroix, M. (1993). Study of the heat transfer behavior of a latent heat thermal energy storage unit with a finned tube. *International Journal of Heat and Mass Transfer*, 36(8), 2083-2092.
- Lacroix, M., & Benmadda, M. (1997). Numerical simulation of natural convection-dominated melting and solidification from a finned vertical wall. *Numerical Heat Transfer; Part A: Applications*, 31(1), 71-86.
- Lacroix, M., & Benmadda, M. (1998). Analysis of natural convection melting from a heated wall with vertically oriented fins. *International Journal of Numerical Methods for Heat and Fluid Flow*, 8(4), 465-478.
- Lamberg, P. (2003). *Mathematical modelling and experimental investigation of melting and solidification in a finned phase change material storage*: Helsinki University of Technology.
- Lamberg, P. (2004). Approximate analytical model for two-phase solidification problem in a finned phase-change material storage. *Applied Energy*, 77(2), 131-152.
- Lamberg, P., Lehtiniemi, R., & Henell, A. M. (2004). Numerical and experimental investigation of melting and freezing processes in phase change material storage. *International Journal of Thermal Sciences*, 43(3), 277-287.

- Lamberg, P., & Sirén, K. (2003). Approximate analytical model for solidification in a finite PCM storage with internal fins. *Applied Mathematical Modelling*, 27(7), 491-513.
- Langford, D. (1966). The freezing of spheres. *International Journal of Heat and Mass Transfer*, 9(8), 827-828.
- Lenel, U. R., & Mudd, P. R. (1984). A review of materials for solar heating systems for domestic hot water. *Solar Energy*, 32(1), 109-120.
- Li, N. Y. (1995). Thermomechanical stresses and some asymptotic behavior in castings with spherical solidification. *Journal of thermal stresses*, 18(2), 165-184.
- Lienhard, J. H. (2011). *A Heat Transfer Textbook*: Dover Publications.
- Liu, M., Saman, W., & Bruno, F. (2012). Review on storage materials and thermal performance enhancement techniques for high temperature phase change thermal storage systems. *Renewable and Sustainable Energy Reviews*, 16(4), 2118-2132.
- Liu, Z., Sun, X., & Ma, C. (2005). Experimental study of the characteristics of solidification of stearic acid in an annulus and its thermal conductivity enhancement. *Energy conversion and management*, 46(6), 971-984.
- Liu, Z., Wang, Z., & Ma, C. (2006a). An experimental study on heat transfer characteristics of heat pipe heat exchanger with latent heat storage. Part I: Charging only and discharging only modes. *Energy Conversion and Management*, 47(7-8), 944-966.
- Liu, Z., Wang, Z., & Ma, C. (2006b). An experimental study on the heat transfer characteristics of a heat pipe heat exchanger with latent heat storage. Part II: Simultaneous charging/discharging modes. *Energy Conversion and Management*, 47(7-8), 967-991.
- Mahjouri, F. (2004). Vacuum tube liquid-vapor (heat-pipe) collectors. Proceedings of Proceedings of the solar conference (pp. 341-346).
- Malvi, C. S., Dixon-Hardy, D. W., & Crook, R. (2011). Energy balance model of combined photovoltaic solar-thermal system incorporating phase change material. *Solar Energy*, 85(7), 1440-1446.
- Marshall, R. (1979). Experimental determination of heat transfer coefficients in a thermal store containing a phase change material-The rectangular cavity. Proceedings of International Conference on Future Energy Concepts (pp. 216-220).

- Mathur, A. (2011). High energy advanced thermal storage (heats)- energy (ARPA-E) (Vol. 1): ADVANCED RESEARCH PROJECTS AGENCY.
- Mauthner, F. (2012). Solar Heat Worldwide. *International Energy Agency, Solar Heating and Cooling Programme*.
- Mazman, M., Cabeza, L. F., Mehling, H., Nogues, M., Evliya, H., & Paksoy, H. Ö. (2009). Utilization of phase change materials in solar domestic hot water systems. *Renewable Energy*, 34(6), 1639-1643.
- Mosaffa, A. H., Talati, F., Basirat Tabrizi, H., & Rosen, M. A. (2012a). Analytical modeling of PCM solidification in a shell and tube finned thermal storage for air conditioning systems. *Energy and Buildings*, 49(0), 356-361.
- Mosaffa, A. H., Talati, F., Rosen, M. A., & Tabrizi, H. B. (2012b). Approximate analytical model for PCM solidification in a rectangular finned container with convective cooling boundaries. *International Communications in Heat and Mass Transfer*, 39(2), 318-324.
- Naaktgeboren, C. (2007). The zero-phase Stefan problem. *International Journal of Heat and Mass Transfer*, 50(23-24), 4614-4622.
- Nallusamy, N., Sampath, S., & Velraj, R. (2007). Experimental investigation on a combined sensible and latent heat storage system integrated with constant/varying (solar) heat sources. *Renewable Energy*, 32(7), 1206-1227.
- Nithyanandam, K., & Pitchumani, R. (2011). Analysis and optimization of a latent thermal energy storage system with embedded heat pipes. *International Journal of Heat and Mass Transfer*, 54(21-22), 4596-4610.
- Nkwetta, D. N., & Smyth, M. (2012). Performance analysis and comparison of concentrated evacuated tube heat pipe solar collectors. *Applied Energy*, 98(0), 22-32.
- Ozisik, M. N. (1993). *Heat conduction*: John Wiley & Sons.
- Özişik, M. N. (1993). *Heat conduction*: Wiley.
- Pedroso, R., & Domoto, G. (1973). Perturbation solutions for spherical solidification of saturated liquids. *Journal of Heat Transfer*, 95, 42.

- Peterson, G. P. (1994). An introduction to heat pipes. Modeling, testing, and applications. *Wiley Series in Thermal Management of Microelectronic and Electronic Systems*, New York, Chichester: Wiley, c1994, 1.
- Poots, G. (1962). On the application of integral-methods to the solution of problems involving the solidification of liquids initially at fusion temperature. *International Journal of Heat and Mass Transfer*, 5(6), 525-531.
- Reddy, K. S. (2007). Thermal modeling of PCM-based solar integrated collector storage water heating system. *Journal of Solar Energy Engineering, Transactions of the ASME*, 129(4), 458-464.
- Regin, A. F., Solanki, S. C., & Saini, J. S. (2008). Heat transfer characteristics of thermal energy storage system using PCM capsules: A review. *Renewable and Sustainable Energy Reviews*, 12(9), 2438-2451.
- Riley, D., Smith, F., & Poots, G. (1974). The inward solidification of spheres and circular cylinders. *International Journal of Heat and Mass Transfer*, 17(12), 1507-1516.
- Saman, W., Bruno, F., & Halawa, E. (2005). Thermal performance of PCM thermal storage unit for a roof integrated solar heating system. *Solar Energy*, 78(2), 341-349.
- Seeniraj, R., Velraj, R., & Narasimhan, N. L. (2002). Thermal analysis of a finned-tube LHTS module for a solar dynamic power system. *Heat and mass transfer*, 38(4-5), 409-417.
- Shabgard, H., Bergman, T. L., Sharifi, N., & Faghri, A. (2010). High temperature latent heat thermal energy storage using heat pipes. *International Journal of Heat and Mass Transfer*, 53(15-16), 2979-2988.
- Shabgard, H., Robak, C. W., Bergman, T. L., & Faghri, A. (2012). Heat transfer and exergy analysis of cascaded latent heat storage with gravity-assisted heat pipes for concentrating solar power applications. *Solar Energy*, 86(3), 816-830.
- Shah, R. K., & Bhatti, M. (1987). Laminar convective heat transfer in ducts. *Handbook of single-phase convective heat transfer*, 3.
- Sharifi, N., Bergman, T. L., Allen, M. J., & Faghri, A. (2014). Melting and solidification enhancement using a combined heat pipe, foil approach. *International Journal of Heat and Mass Transfer*, 78(0), 930-941.

- Sharifi, N., Faghri, A., Bergman, T. L., & Andraka, C. E. (2015). Simulation of heat pipe-assisted latent heat thermal energy storage with simultaneous charging and discharging. *International Journal of Heat and Mass Transfer*, 80(0), 170-179.
- Sharifi, N., Wang, S., Bergman, T. L., & Faghri, A. (2012). Heat pipe-assisted melting of a phase change material. *International Journal of Heat and Mass Transfer*, 55(13-14), 3458-3469.
- Sharma, A., Tyagi, V., Chen, C., & Buddhi, D. (2009). Review on thermal energy storage with phase change materials and applications. *Renewable and Sustainable energy reviews*, 13(2), 318-345.
- Sharma, S. D., Buddhi, D., Sawhney, R. L., & Sharma, A. (2000). Design, development and performance evaluation of a latent heat storage unit for evening cooking in a solar cooker. *Energy Conversion and Management*, 41(14), 1497-1508.
- Shatikian, V., Ziskind, G., & Letan, R. (2008). Numerical investigation of a PCM-based heat sink with internal fins: Constant heat flux. *International Journal of Heat and Mass Transfer*, 51(5-6), 1488-1493.
- Sobotka, V., Agazzi, A., Boyard, N., & Delaunay, D. (2013). Parametric model for the analytical determination of the solidification and cooling times of semi-crystalline polymers. *Applied Thermal Engineering*, 50(1), 416-421.
- Standard, B. (2013). In-situ formed dispensed rigid polyurethane and polyisocyanurate foam products *British Standard BS EN 14318-1 2013*: British Standards Institute.
- Stewartson, K., & Waechter, R. (1976). On Stefan's problem for spheres. *Proceedings of the Royal Society of London. A. Mathematical and Physical Sciences*, 348(1655), 415-426.
- Stritih, U. (2004). An experimental study of enhanced heat transfer in rectangular PCM thermal storage. *International Journal of Heat and Mass Transfer*, 47(12), 2841-2847.
- Talmatsky, E., & Kribus, A. (2008). PCM storage for solar DHW: An unfulfilled promise? *Solar Energy*, 82(10), 861-869.
- Tao, L. C. (1967). Generalized numerical solutions of freezing a saturated liquid in cylinders and spheres. *AIChE Journal*, 13(1), 165-169.
- Varol, Y., Koca, A., Oztop, H. F., & Avci, E. (2010). Forecasting of thermal energy storage performance of Phase Change Material in a solar collector using soft computing techniques. *Expert Systems with Applications*, 37(4), 2724-2732.

- Vine, E., Diamond, R., & Szydowski, R. (1987). Domestic hot water consumption in four low-income apartment buildings. *Energy*, 12(6), 459-467.
- Wang, Z., Qiu, F., Yang, W., & Zhao, X. (2015). Applications of solar water heating system with phase change material. *Renewable and Sustainable Energy Reviews*, 52, 645-652.
- Ward, D. S. (1981).
- Wei-Sheng, T. W.-L. O. K.-S. N. (2013). Performance of natural and forced convection heat pipe solar water heaters. Proceedings of 12th International Conference on Sustainable Energy Technologies (SET-2013) (pp.), Hong Kong.
- Wilson, D. G., Solomon, A. D., Boggs, P. T., Office, U. S. A. R., Mathematics, U. C. C., & Dept, S. R. (1978). *Moving boundary problems: proceedings of the Symposium and Workshop on Moving Boundary Problems, held at Gatlinburg, Tennessee on September 26-28, 1977*: Academic Press.
- Wrobel, L. C., & Brebbia, C. A. (1991). *Computational Modelling of Free and Moving Boundary Problems: Proceedings of the First International Conference, Held 2-4 July, 1991, Southampton, U.K*: WIT Press.
- Wrobel, L. C., & Brebbia, C. A. (1993). *Computational modelling of free and moving boundary problems II: Second International Conference on Computational Modelling of Free and Moving Boundary Problems 93*: Computational Mechanics Publications.
- Wu, S., & Fang, G. (2011). Dynamic performances of solar heat storage system with packed bed using myristic acid as phase change material. *Energy and Buildings*, 43(5), 1091-1096.
- Wu, T., Liaw, H. C., & Chen, Y. Z. (2002). Thermal effect of surface tension on the inward solidification of spheres. *International Journal of Heat and Mass Transfer*, 45(10), 2055-2065.
- Xiao, W., Wang, X., & Zhang, Y. (2009). Analytical optimization of interior PCM for energy storage in a lightweight passive solar room. *Applied Energy*, 86(10), 2013-2018.
- Zahedi, H., Adam, N., Sapuan, S., & Ahmad, M. (2007). Effect of storage tank geometry on performance of solar water heater. *Journal of Scientific and Industrial Research*, 66(2), 146.

- Zalba, B., Marín, J. M., Cabeza, L. F., & Mehling, H. (2003). Review on thermal energy storage with phase change: materials, heat transfer analysis and applications. *Applied thermal engineering*, 23(3), 251-283.
- Zambolin, E., & Del Col, D. (2010). Experimental analysis of thermal performance of flat plate and evacuated tube solar collectors in stationary standard and daily conditions. *Solar Energy*, 84(8), 1382-1396.
- Zeng, R. L., Wang, X., Zhang, Y. P., Di, H. F., & Zhang, Q. L. (2009). Numerical study of thermal performance of phase change material energy storage floor in solar water heating system. *Hunan Daxue Xuebao/Journal of Hunan University Natural Sciences*, 36(SUPPL.), 141-145.
- Zerroukat, M., & Chatwin, C. R. (1994). *Computational moving boundary problems*: Research Studies Press.
- Zhang, Y., & Faghri, A. (1996). Heat transfer enhancement in latent heat thermal energy storage system by using an external radial finned tube. *Journal of Enhanced Heat Transfer*, 3(2).
- Zhu, N., & Vafai, K. (1999). Analysis of cylindrical heat pipes incorporating the effects of liquid-vapor coupling and non-Darcian transport—a closed form solution. *International Journal of Heat and Mass Transfer*, 42(18), 3405-3418.
- Zongqin, Z., & Bejan, A. (1989). Melting in an enclosure heated at constant rate. *International journal of heat and mass transfer*, 32(6), 1063-1076.
- Zuo, Z. J., & Faghri, A. (1998). A network thermodynamic analysis of the heat pipe. *International Journal of Heat and Mass Transfer*, 41(11), 1473-1484.

LIST OF PUBLICATIONS AND PAPERS PRESENTED

Journal: Energy

Theoretical model of an evacuated tube heat pipe solar collector integrated with phase change material

Journal: Renewable and sustainable energy review

A state-of-the-art review on hybrid heat pipe latent heat storage

Journal: Energy (under review)

An experimental study on heat transfer characteristics of heat pipe solar collector integrated with latent heat storage tank (Part I: charging and discharging only modes)

Journal: Renewable Energy (under review)

An experimental study on heat transfer characteristics of heat pipe solar collector integrated with latent heat storage tank (Part II: charging and discharging only modes)

Conference: WSEAS Environmental Sciences and Renewable Energy (2013), Malaysia

Analytical thermal modeling of a heat pipe solar water heater system integrated with phase change material

Conference: ISES Solar world Congress (2015), South Korea

Performance of an evacuated tube heat pipe solar collector integrated with thermal energy storage tank in a tropic climate

Conference: ASME International Mechanical Engineering Congress (2015), USA

Introducing a new design of heat pipe solar collector integrated with latent heat storage unit

Patent: Solar water heat regulator (Under registration process)

APPENDIX A: ABSORBABLE SOLAR ENERGY CALCULATION

The radiation on the tilted surface was considered to include three components: direct, isotropic diffuse and ground reflected diffuse. In general, it is not possible to calculate the reflected energy term in detail. Therefore, standard practice is to assume that there is one surface, a horizontal, diffusely reflecting ground, large in extent, contributing to this term. When total incident radiation (I_T) is determined, the ratio of total radiation on the tilted surface to that on the horizontal surface can be determined. The total incident radiation on the absorber surface can be written as (Duffie & Beckman, 2013):

$$I_T = I_b R_b + I_d \left(\frac{1+\cos\beta}{2} \right) + I_g \rho_g \left(\frac{1-\cos\beta}{2} \right) \quad (A1)$$

where $\left(\frac{1+\cos\beta}{2} \right)$ and $\left(\frac{1-\cos\beta}{2} \right)$ are the view factors from the collector to the sky and from the collector to the ground, respectively. I_b is beam radiation, I_d is diffuse radiation, I_g is solar radiation diffusely reflected from the ground, R_b is the ratio of total radiation on the tilted surface to that on the horizontal surface, ρ_g is diffuse reflectance and β is slope of solar collector. Equation (2) is used to calculate absorbed solar radiation for a tilted collector (MJ/m^2):

$$S = I_b R_b (\tau\alpha)_b + I_d (\tau\alpha)_d \left(\frac{1+\cos\beta}{2} \right) + I_g \rho_g (\tau\alpha)_g \left(\frac{1-\cos\beta}{2} \right) \quad (A2)$$

which, S is the absorbable solar radiation. Suitable transmittance (τ) and absorptance (α) values are taken from Duffie and Beckman (2013). The ratio of total radiation on the tilted surface to that on the horizontal surface can be determined by:

$$R_b = \frac{\text{total radiation on tilted surfaced}}{\text{total radiation on horizontal surface}} = \frac{\cos\theta}{\cos\theta_z} \quad (A3)$$

where, θ angle between the beam radiation and the normal to the surface is determined from:

$$\begin{aligned} \cos\theta &= \sin\delta \sin\varphi \cos\beta - \sin\delta \cos\varphi \sin\beta \cos\gamma + \cos\delta \cos\varphi \cos\beta \cos\omega + \\ &\cos\delta \sin\varphi \sin\beta \cos\gamma \cos\omega + \cos\delta \sin\beta \sin\gamma \sin\omega \end{aligned} \quad (A4)$$

where, δ is declination, φ is latitude, β is slope angle between the plate of the surface, γ is surface azimuth angle and ω is hour angle (angular displacement of the sun). θ_z zenith angle (angle between the vertical and the line to the sun) was determined according to Gupta et al. (Gupta et al., 2001):

$$\cos \theta_z = \{f \cdot \cos^{-1}(-f/g) + g[1 - (f/g)^2]^{0.5}\} / \cos^{-1}(-f/g) \quad (A5)$$

where $f = \sin \delta \cdot \sin \varphi$ and $g = \cos \delta \cdot \cos \varphi$. The declination δ can be found from the equation which was given by Iqbal (Iqbal, 1979):

$$\delta = 0.006918 - 0.399912 \cos B + 0.070257 \sin B - 0.006758 \cos 2B + 0.000907 \sin 2B - 0.002679 \cos 3B + 0.00148 \sin 3B \quad (A6)$$

where $B = (n - 1) \frac{360}{365}$ and n is number of the day in year. An hourly clearness index k_T can also be defined:

$$k_T = \frac{I_T}{I_o} \quad (A7)$$

where, the value of I_o can be calculated by:

$$I_o = \frac{12 \times 3600}{\pi} \times G_{sc} \times \left(1 + 0.033 \cos \frac{360N}{365}\right) \times \left[\cos \varphi \cos \delta (\sin \omega_2 - \sin \omega_1) + \frac{\pi \times (\omega_2 - \omega_1)}{180} \sin \varphi \sin \delta\right] \quad (A8)$$

Then, the ratio of diffuse and beam radiations are calculated by:

$$\frac{I_d}{I_T} = \begin{cases} 1.0 - 0.09k_T, & (k_T \leq 0.22) \\ 0.9511 - 0.1604k_T + 4.388k_T^2 - 16.638k_T^3 \\ \quad + 12.336k_T^4, & (0.22 < k_T \leq 0.80) \\ 0.165, & (k_T > 0.8) \end{cases} \quad (A9)$$

And

$$I_b = \left(1 - \frac{I_d}{I_T}\right) \times I_T \quad (A10)$$

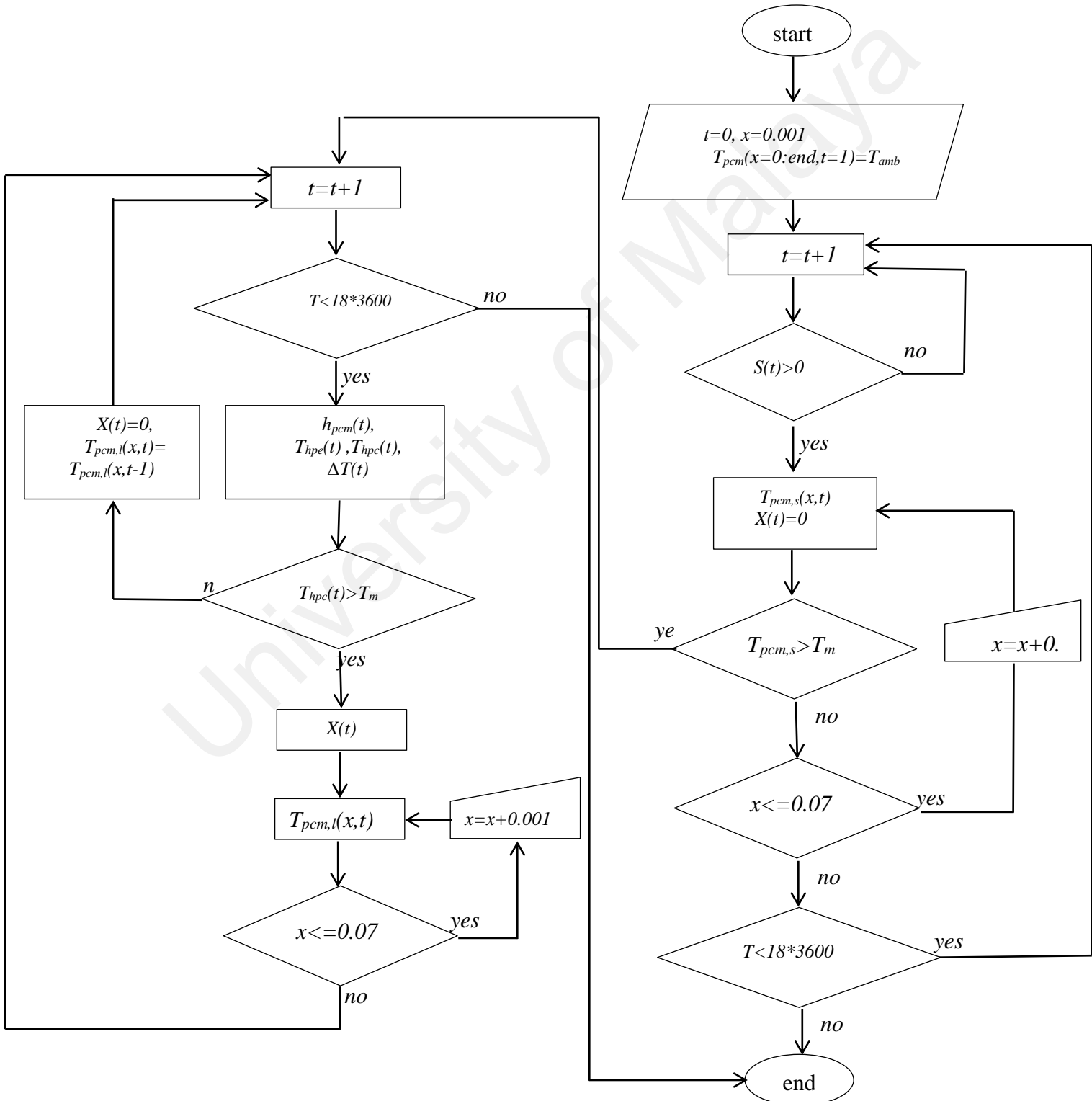
It is considered that the a portion of solar radiation reflected by the absorber plate leaves the system and due to the evacuation of the tubes and that convection does not occur between the glass cover and the absorber plate.

APPENDIX B: THEORETICAL SOLUTION ALGORITHM

Flowchart diagrams of solution processes are prepared in this section:

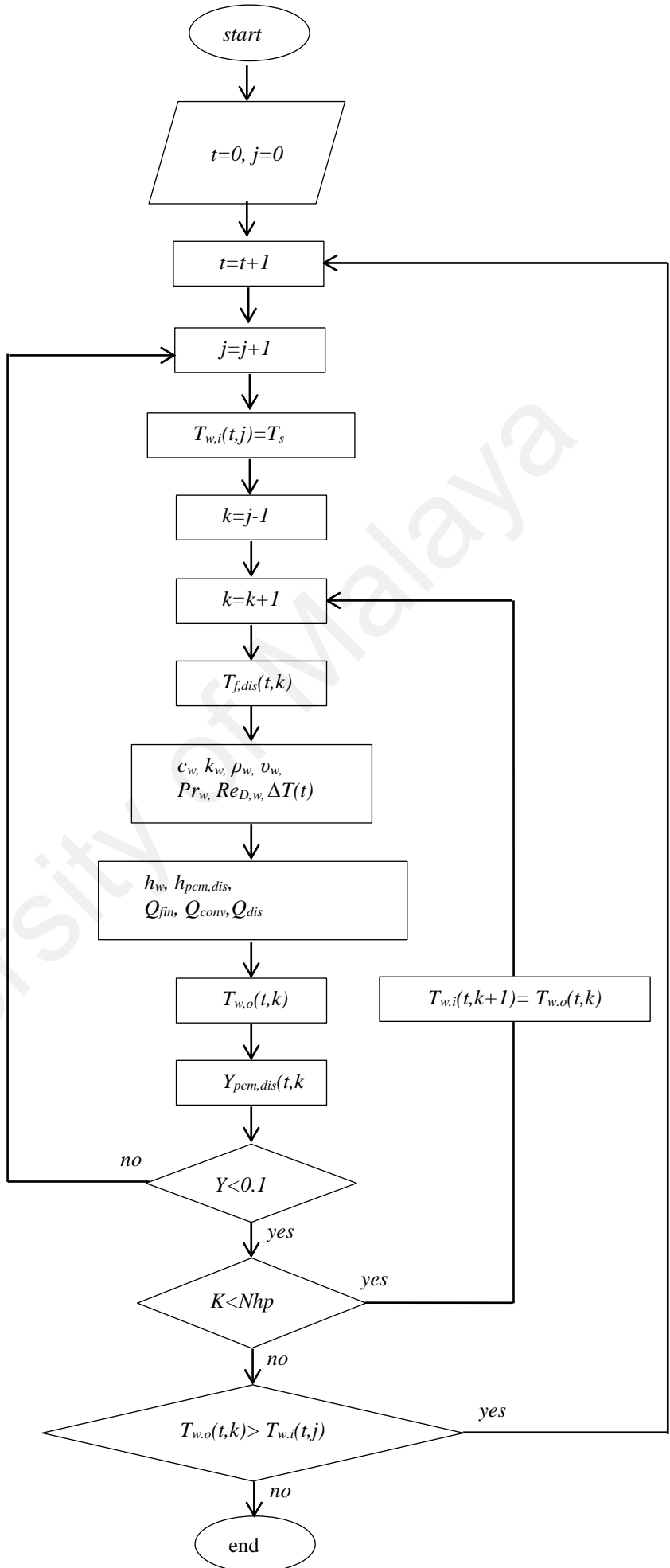
B.1. HPSC-PCM system – Charging mode

t , x , represent time and position at depth of the PCM, respectively.



B.2. HPSC-PCM system – discharging model

j represents number of the PCM slab that are completely solidified. k is number of the heat pipe. Y is solid-liquid interface location. Properties of the water are calculated at $T_f = (T_{w,i} + T_m)/2$.

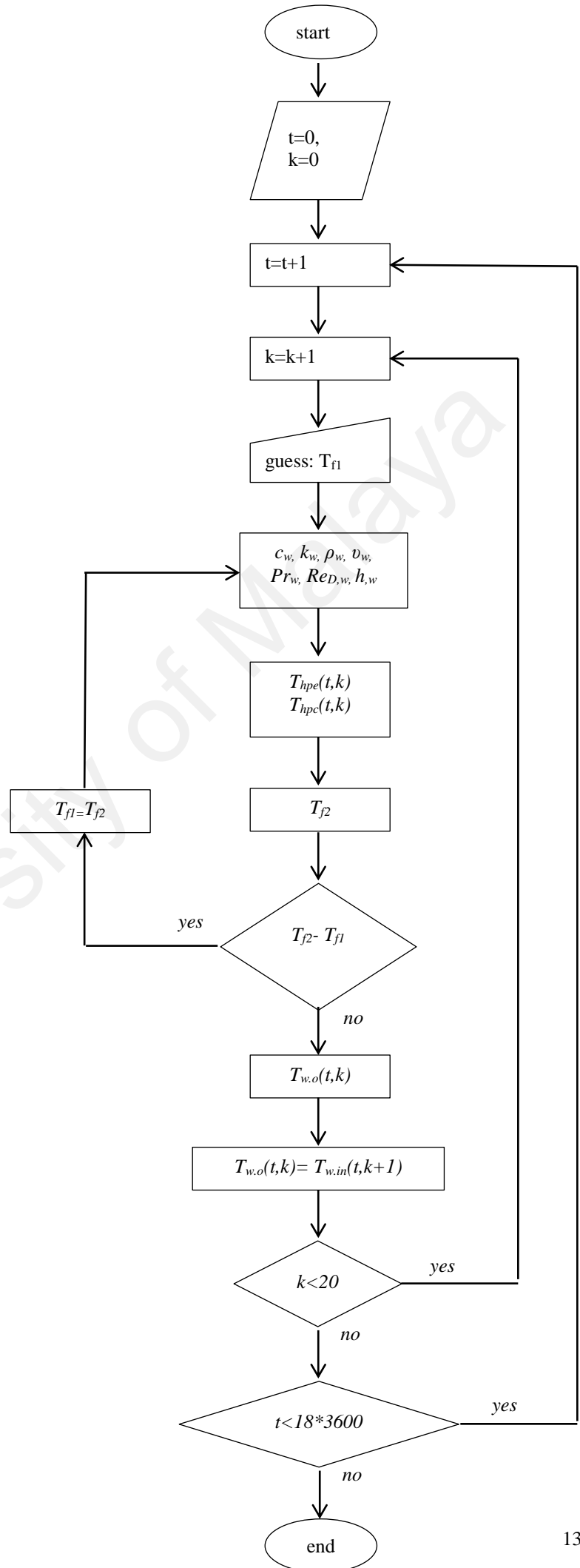


B.3. Baseline HPSC

system

Properties of the water are calculated at $T_f = (T_{w,in} + T_{hpc})/2$.

T_f need to be find by trial and error method.



APPENDIX C: MATLAB CODE FOR THEORETICAL ANALYSIS

```
%% Initialization
clf
close all
clear
clc
tic

%% Solar Constants
lat=3.117755;
slope=20; % Degree (C)
azimuth=180; % Degree (C)
gsc=1367; % (W/m^2)
nalpha=0.95;
Tdew=22.2; %Degree (C)
rog=0.30;
g=9.88; % Gravity (m/s^2)

%% Paraffin properties
Tm=55;
Lmpcm=164; % Melting process, Heat of Fusion (Latent heat) (kj/kg)
kspcmf=0.349; % Thermal conductive coefficient (W/mC)=(j/msC)
klpcmf=0.167; % Thermal conductive coefficient (W/mC)=(j/msC)
rhoipcmf=916; % Density (kg/m^3)
rhoipcmf=990; % Density (kg/m^3)
clpcmf=2760; % Specific heat of PCM (J/kgC)
cspcmf=2480; % Specific heat of PCM (J/kgC)
betapcmf=293*(10^(-6)); % Volume expansion at ?T=20°C, (%)
vispcmf=0.00385; % Dynamic viscosity (m) kgm-1s-1
alpl=klpcmf/(rhoipcmf*clpcmf);

%% Heat pipe characteristics
Nhp=20; % Number of HeatPipes
Npcmslab=Nhp*2; % Number of PCM slabs, which is twice of heat pipe number
lhpe=1.675; % length of evaporator (m)
lhpa=0.030; % length of adiabatic region (m)
lhpc=0.070; % length of condenser (m)
twhp=0.0005;
Roe=0.004; % Outer radius of heat pipe evaporature (m)
Rie=Roe-twhp; % Inner radius of heat pipe (m)
Roa=0.004; % Outer radius of heat pipe adiabatic (m)
Ria=Roa-twhp;
Roc=0.012; % Outer radius of heat pipe condenser (m)
Ric=Roc-twhp;
Row=0.003; % cross-sectional radius of the vapor core (m)
Riw=Row-0.0005; % Effective pore radius r(c,e) (m)
Khp=1.5*10^(-11); % Permeability
kwall=385; % thermal conductivity of solid (W/mK)
ltube=lhpe+lhpa; % length of the absorbr plate (m)
doet=0.058; % Outer diameter of evacuated tube (m)
```

```

Atube=ltube*doet;
% (Multiple wire mesh screens)
d=0.1*10^(-3); % Thickness of the fiber
ke=0.668; % thermal conductivity of liquid
ks=kwall; % thermal conductivity of solid
N2=200; % Mesh number per unit length
eps=1-(1.05*pi*N2*d)/4; % porosity
keff=1*((ke*(ke+ks-(1-eps)*(ke-ks)))/(ke+ks+(1-eps)*(ke-ks)));

%% Water flow rates & Pipe sizes
Ts=29;
Tu=40;
rhow=995; % (kg/m3)
rp=0.009; % Radius pipe

vf=0.05486; % m/s
Flow=vf*pi*(rp^2); % m^3/s
massw=rhow*Flow; % mass flow rate (kg/s)
Flowrate=massw*3600 % mass flow rate (kg/h)

%% Fins specifications
% ***FIN ON HEAT PIPE DIMENSION***
kfin=180; % Thermal conductive coefficient (W/mK)
cpfin=960; % Specific heat (cp) (J/kgK)
rowfin=2713; % Density (kg/m3)
tfin=0.002; % Thinckness of the fin (m)
dfin=tfin/2; % Half thickness of the fin (m)
h1fin=0.200; % Height of the fin (m)
h2fin=0.100; % Half height of the fin (m)
lfinhp=0.200; % length of the fin (m)
lhp=0.142; % Distance between two heat pipe (m)
Afinhpc=lfinhp*h1fin;
A2fin=lfinhp*h2fin;
Afinpipe=h1fin*lhp;
lpcm=(lhp-tfin)/2; % PCM depth that must be charged by heat pipe (cm)
% ***FIN ON PIPE AND PCM DIMENSIONS***
hfinp=0.100; % Height of fin on pipe
wfinp=lhp-tfin; % Width of PCM
tfinp=0.002; % Thinckness of the fin (m)
kfinp=380; % Thermal conductive coefficient copper (W/mK)
deppcmD=0.5*lfinhp; % PCM depth in discharging process

%% System dimensions

xx=0.001:0.001:lpcm;
[mx,nx]=size(xx);

yy=0.001:0.001:deppcmD;
[my,ny]=size(yy);

timeS=1:(12*3600);
timeS=timeS';

```

```

timef=(3600*6+1):(3600*18); % Time defining
timef=timef';

timeD=linspace(0,4,3600*4)';

%% Insertion of data from excel file
exl = actxserver('excel.application');
exlWkbk = exl.Workbooks;
exlFile = exlWkbk.Open('D:\GoogleD\Research\Matlab\analyticalthesis\data.xlsx');
exldata = exlFile.Sheets.Item('H');
robj = exldata.Columns.End(4); % Find the end of the column
numrows = robj.row; % And determine what row it is
dat_range = ['A1:B' num2str(numrows)]; % Read to the last row
rngObj = exldata.Range(dat_range);
data = rngObj.Value;
[m,n]=size(data(1:end,:));
Quit(exl);
delete(exl);

%

for i=1:m
    x(i)=isnan(data(JKR, 2004));
    if x(i)==0
        solinit(i,1)=data{i,1}*((1000*1000)/3600);
    else
        solinit(i,1)=1;
    end
end

for i=1:m
    for j=1+(i-1)*3600:3600+(i-1)*3600
        solinit1(j,1)=solinit(i,1);
    end
end

for i=7:18
    for j=(1+(i-7)*3600):(3600+(i-7)*3600)
        solinit2(j,1)=solinit1((6*3600)+j,1);
    end
end

y1=createFitsolariH(timeS, solinit2);
solifit=feval(y1,timeS);

%

day=1;

for i=2:(m+1)
    dec(i-1,1)=23.45*sin(2*pi*((284+day)/365));
end

```

```

omega(1,1)=-180;
for i=2:m
    omega(i,1)=omega(i-1,1)+0.46153846153846153846153846153846;
end
for i=1:m
    ff(i,1)=sin(lat*(pi/180))*sin(dec(i,1)*(pi/180));
    gg(i,1)=cos(lat*(pi/180))*cos(dec(i,1)*(pi/180));
    costetaz(i,1)=(ff(i,1)*acos(-(ff(i,1)/gg(i,1)))+gg(i,1)*(1-
(ff(i,1)/gg(i,1))^2)^0.5)/acos(-(ff(i,1)/gg(i,1)));
    tetaz(i,1)=acos(costetaz(i,1))*(180/pi);
end

for i=1:m
    if omega(i,1)<0
        aa=-1;
    else
        aa=1;
    end

azimuths(i,1)=aa*acos((cos(tetaz(i,1)*(pi/180))*sin(lat*(pi/180)))/(sin(tetaz(i,1)*(pi/180))*cos(lat*(pi/180))))*(180/pi);
end

for i=1:m

cosTeta(i,1)=cos(tetaz(i,1)*(pi/180))*cos(slope*(pi/180))+sin(tetaz(i,1)*(pi/180))*sin(slope*(pi/180))*cos((azimuths(i,1)-azimuth)*(pi/180));
    ratio(i,1)=cosTeta(i,1)/costetaz(i,1);
end

for i=1:m
    tetab(i,1)=tetaz(i,1);
    alphab(i,1)=nalpha*(1-1.5879*(10^(-3))*tetab(i,1)+2.7314*(10^(-4))*tetab(i,1)^2-2.3026*(10^(-5))*tetab(i,1)^3+9.0244*(10^(-7))*tetab(i,1)^4-1.8*(10^(-8))*tetab(i,1)^5+1.7734*(10^(-10))*tetab(i,1)^6-6.9937*(10^(-13))*tetab(i,1)^7);
    taub=0.82;
    tab(i,1)=1.01*alphab(i,1)*taub;
end
tetad=59.7-0.1388*slope+0.001497*slope^2;
tetag=90-0.5788*slope+0.002693*slope^2;
alphad=nalpha*(1-1.5879*(10^(-3))*tetad+2.7314*(10^(-4))*tetad^2-2.3026*(10^(-5))*tetad^3+9.0244*(10^(-7))*tetad^4-1.8*(10^(-8))*tetad^5+1.7734*(10^(-10))*tetad^6-6.9937*(10^(-13))*tetad^7);
alphag=nalpha*(1-1.5879*(10^(-3))*tetag+2.7314*(10^(-4))*tetag^2-2.3026*(10^(-5))*tetag^3+9.0244*(10^(-7))*tetag^4-1.8*(10^(-8))*tetag^5+1.7734*(10^(-10))*tetag^6-6.9937*(10^(-13))*tetag^7);
taud=0.83;
taug=0.68;
tad=1.01*alphad*taud;
tag=1.01*alphag*taug;

a1(1,1)=((24*3600)/pi)*gsc*(1+0.033*cos((2*pi*day)/365));

```

```

a2(1,1)=cos(lat*(pi/180))*cos(dec(1,1)*(pi/180))*(sin(omega(2,1)*(pi/180))-
sin(omega(1,1)*(pi/180))) ;
a3(1,1)=((pi*(omega(2,1)-omega(1,1)))/180)*sin(lat*(pi/180))*sin(dec(1,1)*(pi/180)) ;
solio(1,1)=(a1(1,1)*(a2(1,1)+a3(1,1)));
for i=3:(m+1)
    a1(i-1,1)=((24*3600)/pi)*gsc*(1+0.033*cos((2*pi*day)/365)) ;
    a2(i-1,1)=cos(lat*(pi/180))*cos(dec(i-1,1)*(pi/180))*(sin(omega(i-1,1)*(pi/180))-
sin(omega(i-2,1)*(pi/180))) ;
    a3(i-1,1)=((pi*(omega(i-1,1)-omega(i-2,1)))/180)*sin(lat*(pi/180))*sin(dec(i-
1,1)*(pi/180)) ;
    solio(i-1,1)=(a1(i-1,1)*(a2(i-1,1)+a3(i-1,1)));
end
for i=1:m
    if solio(i,1)<0
        solio(i,1)=0.0000001;
    end
end

for i=1:m
    kt(i,1)=solinit(i,1)/solio(i,1);
end

for i=1:m
    if kt(i,1)<=0.22
        solid(i,1)=solinit(i,1)*(1.0-0.09*kt(i,1));
    elseif kt(i,1)<=0.80
        solid(i,1)=solinit(i,1)*(0.9511-0.1604*kt(i,1)+4.388*kt(i,1)^2-
16.638*kt(i,1)^3+12.336*kt(i,1)^4);
    else
        solid(i,1)=solinit(i,1)*0.165;
    end
    solib(i,1)=(1-(solid(i,1)/solinit(i,1)))*solinit(i,1);
end

%

for i=1:m

solstemp(i,1)=(solib(i,1)*ratio(i,1)*tab(i,1)+solid(i,1)*tad*((1+cos(slope))/2)+solinit(i,1
)*rog*tag*((1-cos(slope))/2))*Atube*0.5;
    for j=1+(i-1)*3600:3600+(i-1)*3600
        solstemp1(j,1)=solstemp(i,1);
    end
end

for i=7:18
    for j=(1+(i-7)*3600):(3600+(i-7)*3600)
        solsstemp2(j,1)=solstemp1((6*3600)+j,1);
    end
end
y2=createFitsolarsH(timeS,solsstemp2);
solsfit=feval(y2,timeS);

```

```

solaract=solsfit*2*(1/Atube);

solar=zeros(3600*18,1);
for t=(6*3600+1):(18*3600)
    solar(t,1)=solsfit(t-6*3600,1);
end
solaritot=sum(solifit);
solarstot=sum(solsfit);
solarb=solar*2;
solartotact=sum(solar)*2*Nhp;

%% Tambinet curve fitting

for i=1:m
    tambtemp(i,1)=data{i,2};
    for j=1+(i-1)*3600:3600+(i-1)*3600
        Tamb(j,1)=tambtemp(i,1);
    end
end
for i=7:18
    for j=(1+(i-7)*3600):(3600+(i-7)*3600)
        Tambtemp2(j)=Tamb((6*3600)+j,1);
    end
end
Tambtemp2=Tambtemp2';
y2=createFitTamb(timeS, Tambtemp2);
Tambfit=feval(y2,timeS);
for t=1:(18*3600)
    if t<(6*3600+1)
        Tamb(t,1)=Tambfit(1);
    else
        Tamb(t,1)=Tambfit(t-6*3600);
    end
end

xlswrite('solar.xlsx',solifit,1,'A1:A43200');
xlswrite('solar.xlsx',solaract,1,'B1:B43200');
xlswrite('solar.xlsx',Tamb(3600*6+1:3600*18),1,'C1:C43200');

toc

%% Heat Pipe Evacuated tube basic design

% 20 tubes

tic

for k=1:Nhp
    Thpeb(1,k)=Tamb(1);
    Thpab(1,k)=Tamb(1);
    Thpcb(1,k)=Tamb(1);

```

```

Tfib(1,k)=Ts;
Tfeb(1,k)=Tfib(1,k);
end

for t=2:(18*3600+1)
    Tfib(t-1,1)=Ts;
    for k=1:Nhp
        aq=5;
        Tfm0(t-1,k)=Tfib(t-1,k)+3;
        while aq>0.5
            if Tfm0(t-1,k)>95
                Tfm0(t-1,k)=95;
            else
                Tfm0(t-1,k)=Tfm0(t-1,k);
            end
            cpwb(t-1,k)=(4.214-2.286*10^(-3)*Tfm0(t-1,k)+4.991*10^(-5)*Tfm0(t-1,k)^2-
4.519*10^(-7)*Tfm0(t-1,k)^3+1.857*10^(-9)*Tfm0(t-1,k)^4)*1000; % Water specific heat
capacity as a function of temperature (p = 1 bar)
            ktcwb(t-1,k)=0.5636+1.946*10^(-3)*Tfm0(t-1,k)-8.151*10^(-6)*Tfm0(t-1,k)^2; %
Water thermal conductivity as a function of temperature (p = 1 bar)
            rhowb(t-1,k)=1001.1-0.0867*Tfm0(t-1,k)-0.0035*Tfm0(t-1,k)^2; % Water density as a
function of temperature (p = 1 bar)
            visdwb(t-1,k)=1.684*10^(-3)-4.264*10^(-5)*Tfm0(t-1,k)+5.062*10^(-
7)*Tfm0(t-1,k)^2-2.244*10^(-9)*Tfm0(t-1,k)^3; % Water dynamic viscosity as a function of
temperature (p = 1 bar)

            Prwb(t-1,k)=((cpwb(t-1,k)*visdwb(t-1,k))/ktcwb(t-1,k));
            ReDb(t-1,k)=(rhowb(t-1,k)*vf*2*rp)/visdwb(t-1,k);
            if ReDb(t-1,k)<2
                ReDb(t-1,k)=2;
            end
            hfwb(t-1,k)=(ktcwb(t-1,k)/(Roc*2))*(0.3+((0.62*ReDb(t-1,k))^(1/2)*Prwb(t-
1,k)^(1/3))/(1+(0.4/Prwb(t-1,k))^(2/3))^(3/4))*(1+(ReDb(t-1,k)/282000)^(5/8))^(4/5));

            Thpeb(t-1,k)=Tfm0(t-1,k)+(solarb(t-
1,1)/(2*pi*lhpc))*(((log(Roe/Rie)/kwall)+(log(Row/Riw)/keff))*(1+(lhpc/lhpe))+(1/(hf
wb(t-1,k)*Roe)));
            Thpab(t-1,k)=Tfm0(t-1,k)+(solarb(t-
1,1)/(2*pi*lhpc))*(((log(Roa/Ria)/kwall)+(log(Row/Riw)/keff)+(1/(hfwb(t-1,k)*Roa)));
            Thpcb(t-1,k)=Tfm0(t-1,k)+(solarb(t-1,1)/(2*pi*hfwb(t-1,k)*Roc*lhpc));

            Tfm00(t-1,k)=(Tfib(t-1,k)+Thpcb(t-1,k))/2;
            aq=abs(Tfm00(t-1,k)-Tfm0(t-1,k));
            Tfm0(t-1,k)=Tfm00(t-1,k);
        end

        Qmfb(t-1,k)=hfwb(t-1,k)*pi*Roc*2*lhpc*(Thpcb(t-1,k)-Tfib(t-1,k));
        if Qmfb(t-1,k)>solarb(t-1,1)
            Qmfb(t-1,k)=solarb(t-1,1);
        end
        Tfeb(t-1,k)=((0.95*Qmfb(t-1,k))/(massw*cpwb(t-1,k)))+Tfib(t-1,k);
        Tfib(t-1,k+1)=Tfeb(t-1,k);
    end
end

```

```

end
end

toc

xlswrite('Twatbasis.xlsx',Tfeb(3600*6+1:3600*18,20),1,'A1:A43200');

%% PCM Charging process

tic

hpcmfinC=ones(3600*6,1)*0.01;
Thpe=ones(3600*6,1)*Tm;
Thpa=ones(3600*6,1)*Tm;
Thpc=ones(3600*6,1)*Tm;
X1=zeros(3600*18,1);
deltaTC=ones(3600*6,1);

for x=1:(nx/10)
    for t=1:(3600*6)
        TpcmC(t,x)=Tm;
    end
end

for t=(3600*6+1):(3600*18)

    hpcmfinC(t,1)=1000*0.072*(((g*deltaTC(t-
1,1)*0.5*(rhoIpcmf^2)*clpcmf*((klpcmf*(10^(-3)))^2)*betapcmf)/vispcmf)^(1/3));
    Thpe(t,1)=TpcmC(t-
1,1)+(solar(t,1)/(2*pi*lhpc))*(((log(Roe/Rie)/kwall)+(log(Rie/Row)/keff))*(1+(lhpc/lhp
e)))+(1/(hpcmfinC(t,1)*Roe)));
    Thpa(t,1)=TpcmC(t-
1,1)+(solar(t,1)/(2*pi*lhpc))*((log(Roa/Rie)/kwall)+(log(Rie/Row)/keff)+(1/(hpcmfinC
(t,1)*Roa)));
    Thpc(t,1)=0.95*1.1*(TpcmC(t-1,1)+(solar(t,1)/(2*pi*hpcmfinC(t,1)*Roc*lhpc)));

    deltaTC(t,1)=abs(Thpc(t,1)-Tm);
    if deltaTC(t,1)<3
        deltaTC(t,1)=1;
    end

    StlC(t,1)=(clpcmf*(10^(-3))*deltaTC(t,1))/Lmpcm;
    landa(t,1)=0.706*sqrt(StlC(t,1))*(1-0.21*(0.5642*StlC(t,1))^(0.93-0.15*StlC(t,1)));
    if landa(t,1)==0
        landa(t,1)=0.001;
    end

    if Thpc(t,1)<Tm
        tmelt=t;
    else
        tmelt=3600*6;
    end
end

```

```

    X1(t,1)=2*landa(t,1)*sqrt(alpl*(t-tmelt)); % Exact solution one-phase interface
location
end

    for x=1:(nx/10) % Temperature distribution based on one-phase exact solution
        TpcmC(t,x)=Thpc(t,1)-(deltaTC(t,1)*((erf(xx(x*10)/(2*sqrt(alpl*(t-
(3600*6))))))/erf(landa(t,1))));
        if TpcmC(t,x)<TpcmC(t-1,x)
            TpcmC(t,x)=TpcmC(t-1,x);
        end
    end
    TpcmCmean(t,1)=mean(TpcmC(t,:));
end

for t=(3600*6+1):(3600*18)
    if X1(t)<=lpcm
        X1(t)=X1(t);
    else
        X1(t)=X1(t-1);
    end
end

% Matrix defining

X2=X1((3600*6+1):(3600*18));
Thpe1=Thpe((3600*6+1):(3600*18),1);
Thpc1=Thpc((3600*6+1):(3600*18),1);
Tpcm1=TpcmC((3600*6+1):(3600*18),1);
Tpcm2=TpcmC((3600*6+1):(3600*18),2);
Tpcm3=TpcmC((3600*6+1):(3600*18),3);
Tpcm4=TpcmC((3600*6+1):(3600*18),4);
Tpcm5=TpcmC((3600*6+1):(3600*18),5);
Tpcm6=TpcmC((3600*6+1):(3600*18),6);
Tpcm7=TpcmC((3600*6+1):(3600*18),7);
TpcmCm=TpcmCmean((3600*6+1):(3600*18),1);

% Curve fitting

y3=createFitX(timef, X2);
y4=createFitThpe(timef, Thpe1);
y5=createFitThpc(timef, Thpc1);
y6=createFitTpcm1(timef, Tpcm1);
y7=createFitTpcm2(timef, Tpcm2);
y8=createFitTpcm3(timef, Tpcm3);
y9=createFitTpcm4(timef, Tpcm4);
y10=createFitTpcm5(timef, Tpcm5);
y11=createFitTpcm6(timef, Tpcm6);
y12=createFitTpcm7(timef, Tpcm7);
y13=createFitTpcmCmean(timef, TpcmCm);

% Tranfering data

```

```

X3=feval(y3,timef);
Thpe1=feval(y4,timef);
Thpc1=feval(y5,timef);
TpcmCf(:,1)=feval(y6,timef);
TpcmCf(:,2)=feval(y7,timef);
TpcmCf(:,3)=feval(y8,timef);
TpcmCf(:,4)=feval(y9,timef);
TpcmCf(:,5)=feval(y10,timef);
TpcmCf(:,6)=feval(y11,timef);
TpcmCf(:,7)=feval(y12,timef);
TpcmCfm(:,1)=feval(y13,timef);

toc

figure; contourf(TpcmCf,100,'LineStyle','none'); colormap(jet); colorbar
xlim([0 43200]);
set(gca,'XTick',0:7200:43200);
set(gca,'XTickLabel',{'6','8','10','12','14','16','18'});

%% PCM Discharging process

tic

wfinp=2*X1(end);
Acfin=wfinp*tfinp;
Affin=wfinp*hfinp;
pfin=2*tfinp+2*wfinp;
Abpipe=2*pi*rp*wfinp-2*Acfin;

Tpcmaveend=mean(TpcmCf(end,:));
LeffD=-1000*1.1*(Lmpcm+0.5*clpcmf*0.001*(Tpcmaveend-Tm)); % (j/kg) Effective
latent heat

visdwatwall=1.684*10^(-3)-4.264*10^(-5)*Tm+5.062*10^(-7)*Tm^2-2.244*10^(-
9)*Tm^3; % (kg/ms) Water dynamic viscosity at pipe wall temperature

tD=3600*4;

i=1;
for t=1:tD
    Twi(t,i)=Ts;
    for k=i:Nhp

        deltaTD(t,k)=Twi(t,k)-Tm;

        cpwat(t,k)=(4.214-2.286*10^(-3)*Twi(t,k)+4.991*10^(-5)*Twi(t,k)^2-4.519*10^(-
7)*Twi(t,k)^3+1.857*10^(-9)*Twi(t,k)^4)*1000; % Water specific heat
        kwat(t,k)=0.5636+1.946*10^(-3)*Twi(t,k)-8.151*10^(-6)*Twi(t,k)^2; % Water
thermal conductivity
        rhowat(t,k)=1001.1-0.0867*Twi(t,k)-0.0035*Twi(t,k)^2; % Water density
        visdwat(t,k)=1.684*10^(-3)-4.264*10^(-5)*Twi(t,k)+5.062*10^(-7)*Twi(t,k)^2-
2.244*10^(-9)*Twi(t,k)^3; % Water dynamic viscosity

```

```

Prwat(t,k)=(cpwat(t,k)*visdwat(t,k)/kwat(t,k));
ReDwat(t,k)=(rhowat(t,k)*vf*2*rp)/visdwat(t,k);

if ReDwat(t,k)<=2500 % For laminar flow
    Gz(t,k)=(ReDwat(t,k)*Prwat(t,k)*2*rp)/wfinp;
    NuD(t,k)=3.657+((0.0018*(Gz(t,k)^(1/3)))/(0.04+(Gz(t,k)^(-2/3))));
else % For Turbulant flow
    fNuDt(t,k)=(1/((1.82*log10(ReDwat(t,k))-1.64)^2))*(7-
(visdwat(t,k)/visdwatwall))*(1/6);
    NuD(t,k)=(((fNuDt(t,k)/8)*(ReDwat(t,k)-
1000)*Prwat(t,k))/(1+12.7*sqrt(fNuDt(t,k)/8)*((Prwat(t,k)^(2/3))-
1)))*((visdwat(t,k)/visdwatwall)^(0.11));
end
hwat(t,k)=(1.05*NuD(t,k)*(kwat(t,k))/(2*rp));
Qconv(t,k)=hwat(t,k)*Abpipe*deltaTD(t,k);

hpcmfinD(t,k)=0.072*(((g*(-
1)*deltaTD(t,k)*0.5*(rhoIpcmf^2)*clpcmf*(klpcmf^2)*betapcmf)/vispcmf)^(1/3));

Bi(t,k)=(hpcmfinD(t,k)*deppcmD)/kspcmf;
StlD(t,k)=(clpcmf*deltaTD(t,k))/LeffD;
landaD(t,k)=0.706*sqrt(StlD(t,k))*(1-0.21*(0.5642*StlD(t,k))^(0.93-
0.15*StlD(t,k)));
Bis=2/((StlD(t,k)/(2*(landaD(t,k)^2)))-1);

Qfin(t,k)=(sqrt(hpcmfinD(t,k)*pfin*kfinp*Acfin))*(tanh(((hpcmfinD(t,k)*pfin)/(kfinp*
Acfin))*hfinp))*deltaTD(t,k);

Qdis(t,k)=(Qconv(t,k)+2*0.95*Qfin(t,k))*1.05;

Two(t,k)=(Twi(t,k)+(-1)*(Qdis(t,k)/(massw*cpwat(t,k))));

Qimp(t,k)=(1/4)*Qdis(t,k);
if t==1
    XqDtemp(t,k)=((Qimp(t,k)/Affin)/(rhoIpcmf*LeffD));
    for x=10:10:ny
        if yy(x)<=XqDtemp(t,k)
            TpcmD(x/10,t,k)=Tm+((Qimp(t,k)/Affin)/klpcmf)*(XqDtemp(t,k)-0);
        else
            TpcmD(x/10,t,k)=Tm;
        end
    end
else
    XqDtemp(t,k)=XqDtemp(t-1,k)+((Qimp(t,k)/Affin)/(rhoIpcmf*LeffD));
    for x=10:10:ny
        if yy(x)<=XqDtemp(t,k)
            TpcmD(x/10,t,k)=Tm+((Qimp(t,k)/Affin)/klpcmf)*(XqDtemp(t,k)-
XqDtemp(t-1,k));
        else
            TpcmD(x/10,t,k)=Tm;
        end
    end
end

```

```

        end
    end
end

if XqDtemp(t,k)<=deppcmD
    XqD(t,k)=XqDtemp(t,k);
else
    XqD(t,k)=XqD(t-1,k);
end

Twi(t,k+1)=Two(t,k);

end

if i>1
    for k=1:i-1
        Twi(t,k)=Ts;
        Two(t,k)=Ts;
        hwat(t,k)=0;
        Qconv(t,k)=0;
        hpcmfinD(t,k)=0;
        Qfin(t,k)=0;
        for x=10:10:ny
            TpcmD(x/10,t,k)=TpcmD(x/10,t-1,k);
        end
    end
end

for k=i:Nhp
    if XqDtemp(t,k)>=deppcmD
        i=i+1;
        t;
        Two(t,end)
    end
end

end

y14=createFitTwo(timeD, Two(:,20));
TwoD(:,1)=feval(y14,timeD);

toc

%% Energy & Efficiency

for i=1:12
    Tfebmean(i)=mean(Tfeb(((3600*6)+3600*(i-1)+1):((3600*6)+3600*i),20));
    if Tfebmean(i)>=Tu
        Vub(i)=Flowrate*((Tfebmean(i)-Ts)/(Tu-Ts));
        Vudb(i)=Vub(i)*(0.03*(12-i));
    else
        Vub(i)=0;
    end
end

```

```

        Vudb(i)=0;
    end
    Vurb(i)=Vub(i)-Vudb(i);
end
Vubtot=sum(Vub);
Vudbtot=sum(Vudb);
Vurbtot=sum(Vurb);
cpwbmean=mean(cpwb((3600*6+1):(3600*18),20));
Ebtot=Vurbtot*cpwbmean*(Tu-Ts); % Watt
Effb=Ebtot/solartotact

for i=1:tD
    if TwoD(i,1)>=Tu
        Vui(i)=massw*((TwoD(i,1)-Ts)/(Tu-Ts));
    else
        Vui(i)=0;
    end
end
Vuitot=sum(Vui);
cpwatmean=mean(cpwat(:,20));
Eitot=Vuitot*cpwatmean*(Tu-Ts); % Watt
Effi=Eitot/solartotact

EffVu=[Vubtot,Vudbtot,Vurbtot;solartotact,Ebtot,Effb;Vuitot,Eitot,Effi];
xlswrite('EffVu.xlsx',EffVu,1,'A4:C6');

%% % Excels

xlswrite('Interface.xlsx',X3,1,'A1:A43200');

xlswrite('Tcharge.xlsx',Thpe1,1,'A1:A43200');
xlswrite('Tcharge.xlsx',Thpc1,1,'B1:B43200');
xlswrite('Tcharge.xlsx',TpcmCf(:,1),1,'C1:C43200');
xlswrite('Tcharge.xlsx',TpcmCfm(:,1),1,'D1:D43200');

xlswrite('XqD.xlsx',XqD(:,1),1,'A1:A14400');
xlswrite('XqD.xlsx',XqD(:,5),1,'B1:B14400');
xlswrite('XqD.xlsx',XqD(:,10),1,'C1:C14400');
xlswrite('XqD.xlsx',XqD(:,15),1,'D1:D14400');
xlswrite('XqD.xlsx',XqD(:,20),1,'E1:E14400');

xlswrite('Twatimp.xlsx',TwoD(:,1),1,'A1:A14400');

xlswrite('Twatbasis.xlsx',Tfeb((3600*6+1):(3600*18),20),1,'A1:A43200');

xlswrite('TpcmC.xlsx',TpcmCf,1);

xlswrite('TpcmD.xlsx',TpcmD(:,1),1);
xlswrite('TpcmD.xlsx',TpcmD(:,5),2);
xlswrite('TpcmD.xlsx',TpcmD(:,10),3);
xlswrite('TpcmD.xlsx',TpcmD(:,15),4);

```

```
xlswrite('TpcmD.xlsx',TpcmD(:,20),5);
```

```
xlswrite('TpcmD.xlsx',TpcmD(:,1),1);  
xlswrite('TpcmD.xlsx',TpcmD(:,5),2);  
xlswrite('TpcmD.xlsx',TpcmD(:,10),3);  
xlswrite('TpcmD.xlsx',TpcmD(:,15),4);  
xlswrite('TpcmD.xlsx',TpcmD(:,20),5);
```

```
xlswrite('Thp.xlsx',Thpe1(:,1),1,'A1:A43200');  
xlswrite('Thp.xlsx',Thpc1(:,1),1,'B1:B43200');  
xlswrite('Thp.xlsx',Thpeb(3600*6+1:3600*18,1),1,'C1:C43200');  
xlswrite('Thp.xlsx',Thpcb(3600*6+1:3600*18,1),1,'D1:D43200');  
xlswrite('Thp.xlsx',Thpeb(3600*6+1:3600*18,5),1,'E1:E43200');  
xlswrite('Thp.xlsx',Thpcb(3600*6+1:3600*18,5),1,'F1:F43200');  
xlswrite('Thp.xlsx',Thpeb(3600*6+1:3600*18,10),1,'G1:G43200');  
xlswrite('Thp.xlsx',Thpcb(3600*6+1:3600*18,10),1,'H1:H43200');  
xlswrite('Thp.xlsx',Thpeb(3600*6+1:3600*18,15),1,'I1:I43200');  
xlswrite('Thp.xlsx',Thpcb(3600*6+1:3600*18,15),1,'J1:J43200');  
xlswrite('Thp.xlsx',Thpeb(3600*6+1:3600*18,20),1,'K1:K43200');  
xlswrite('Thp.xlsx',Thpcb(3600*6+1:3600*18,20),1,'L1:L43200');
```

```
xlswrite('hpcmCharge.xlsx',hpcmfinC(:,1),1,'A1:A64800');  
xlswrite('hpcmDischarge.xlsx',hpcmfinD(:,1),1);  
xlswrite('hwatDischarge.xlsx',hwat(:,1),1);
```

APPENDIX D: CAD DRAWINGS OF FINS AND LHS TANK

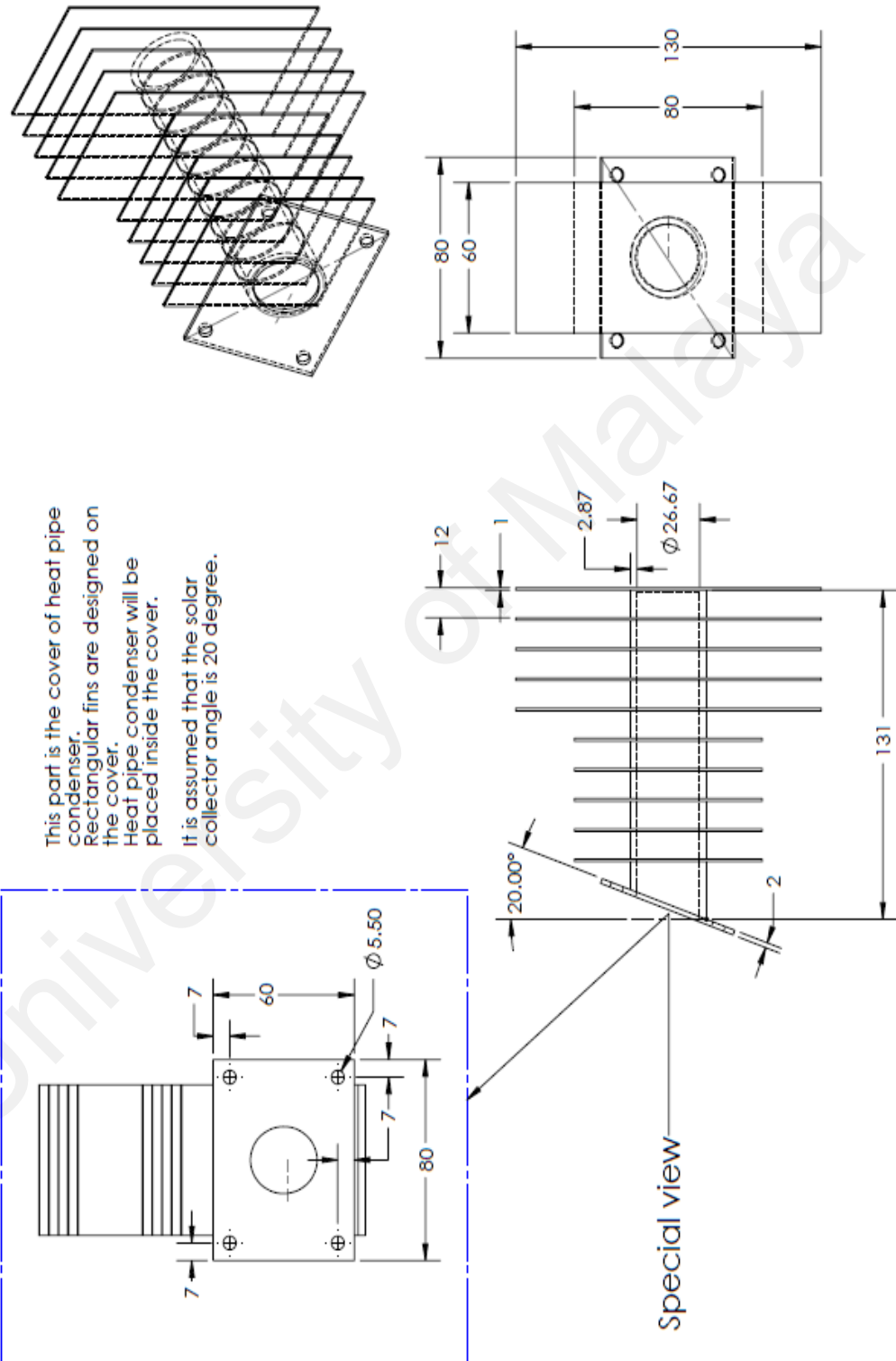


Figure D.1: CAD design of the fin shell, which HP condenser will be inserted into that.

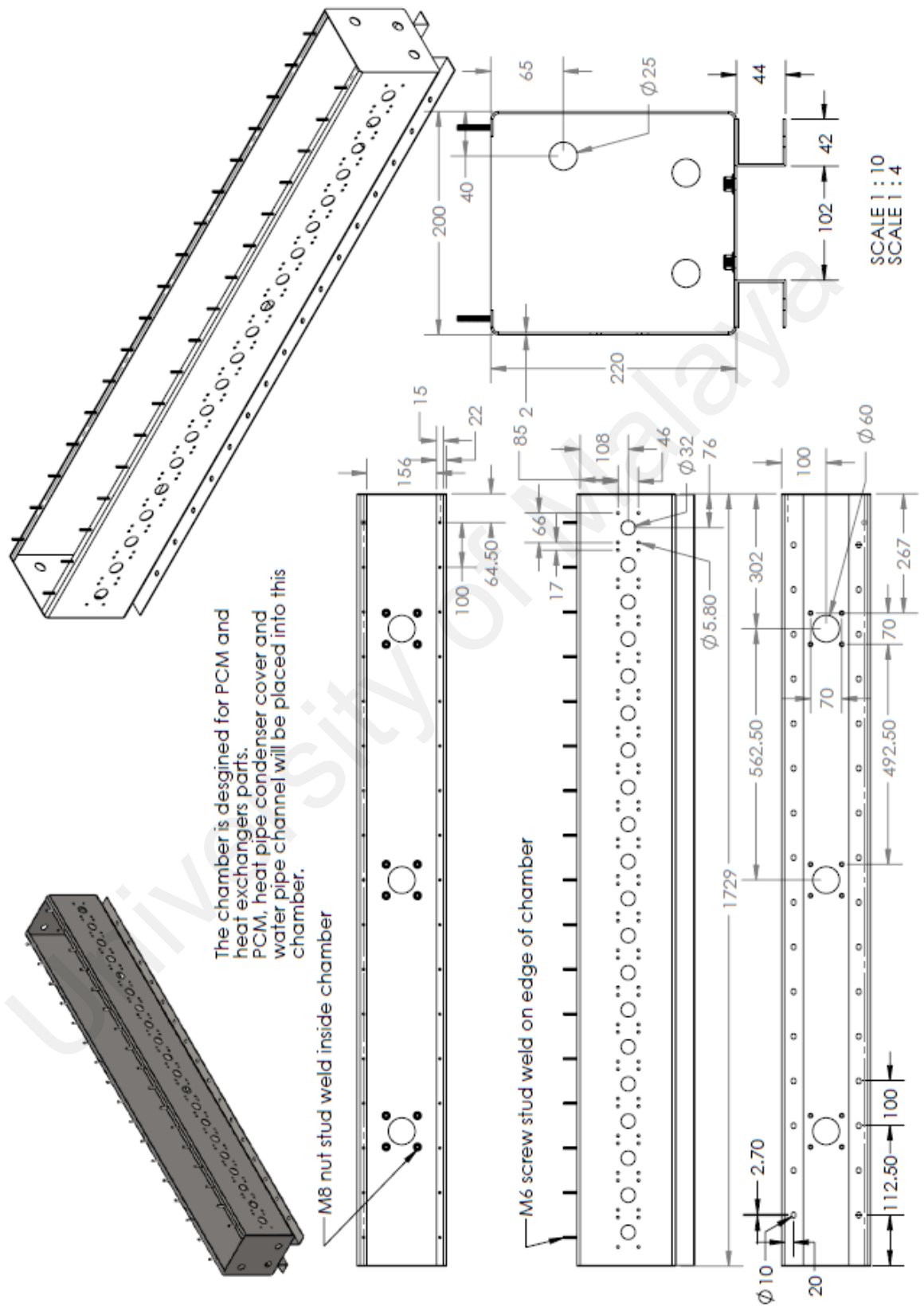


Figure D.2: CAD drawing of the LHS tank.

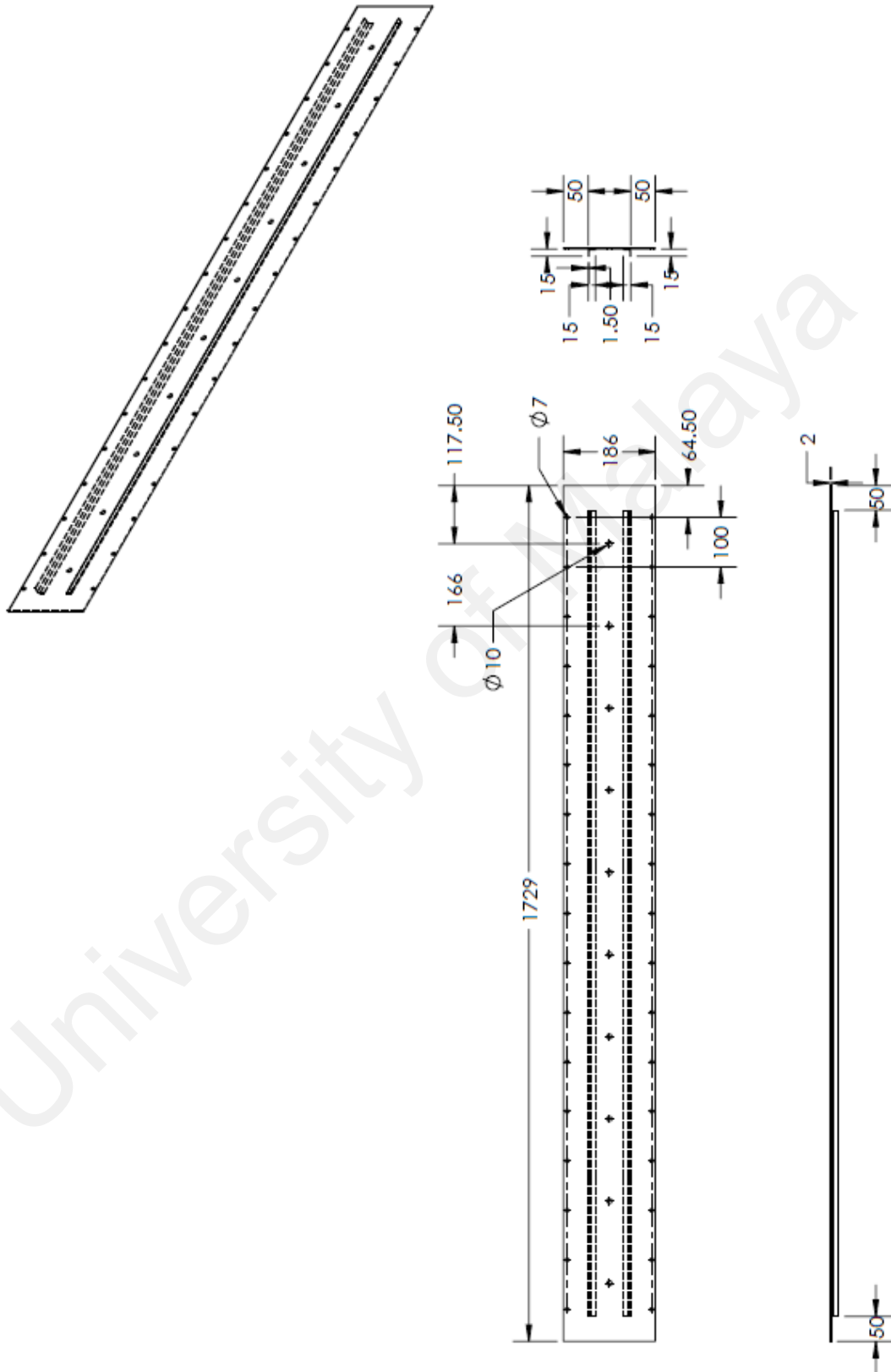


Figure D.3: CAD drawing of the LHS tank cover.

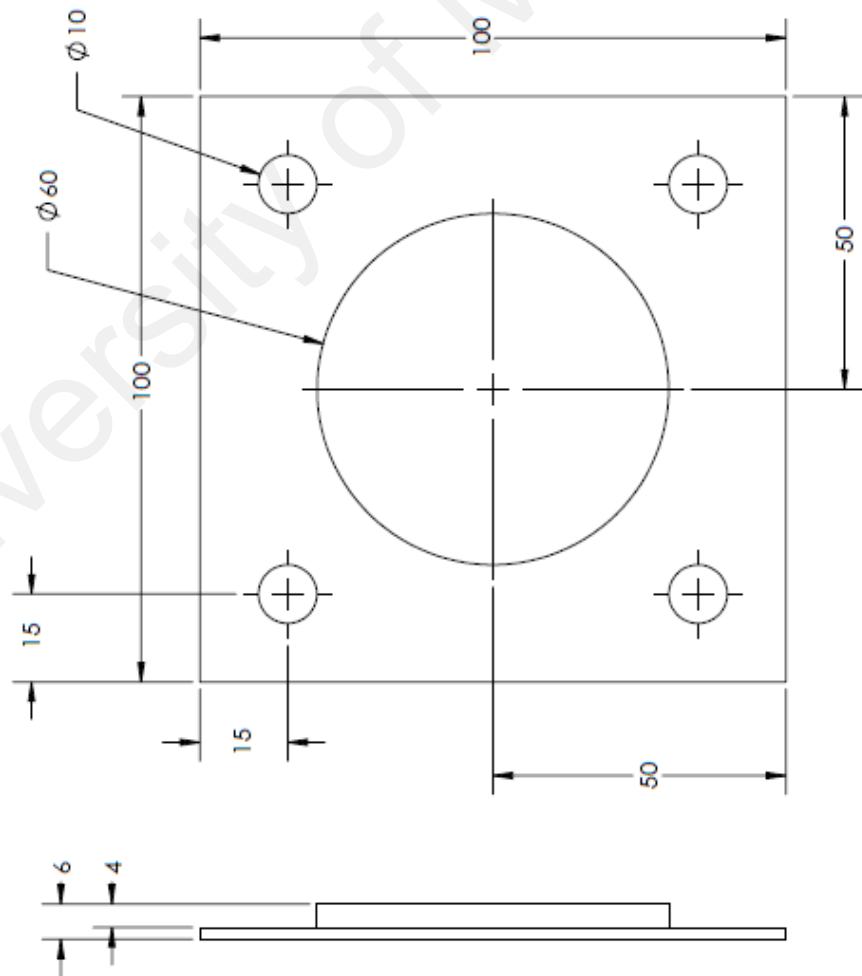
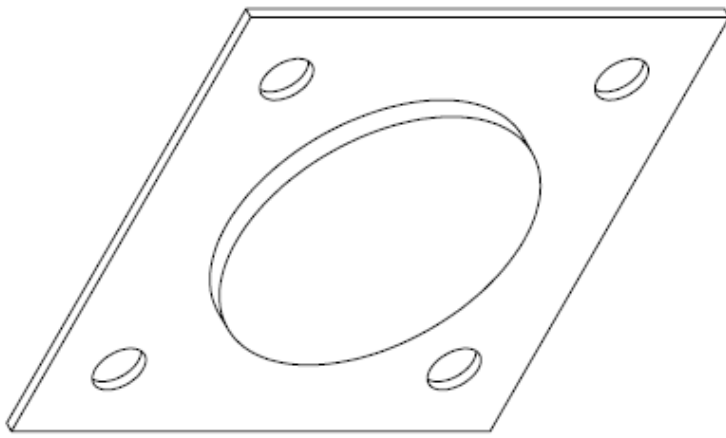


Figure D.4: CAD drawing of the discharging valve cover.

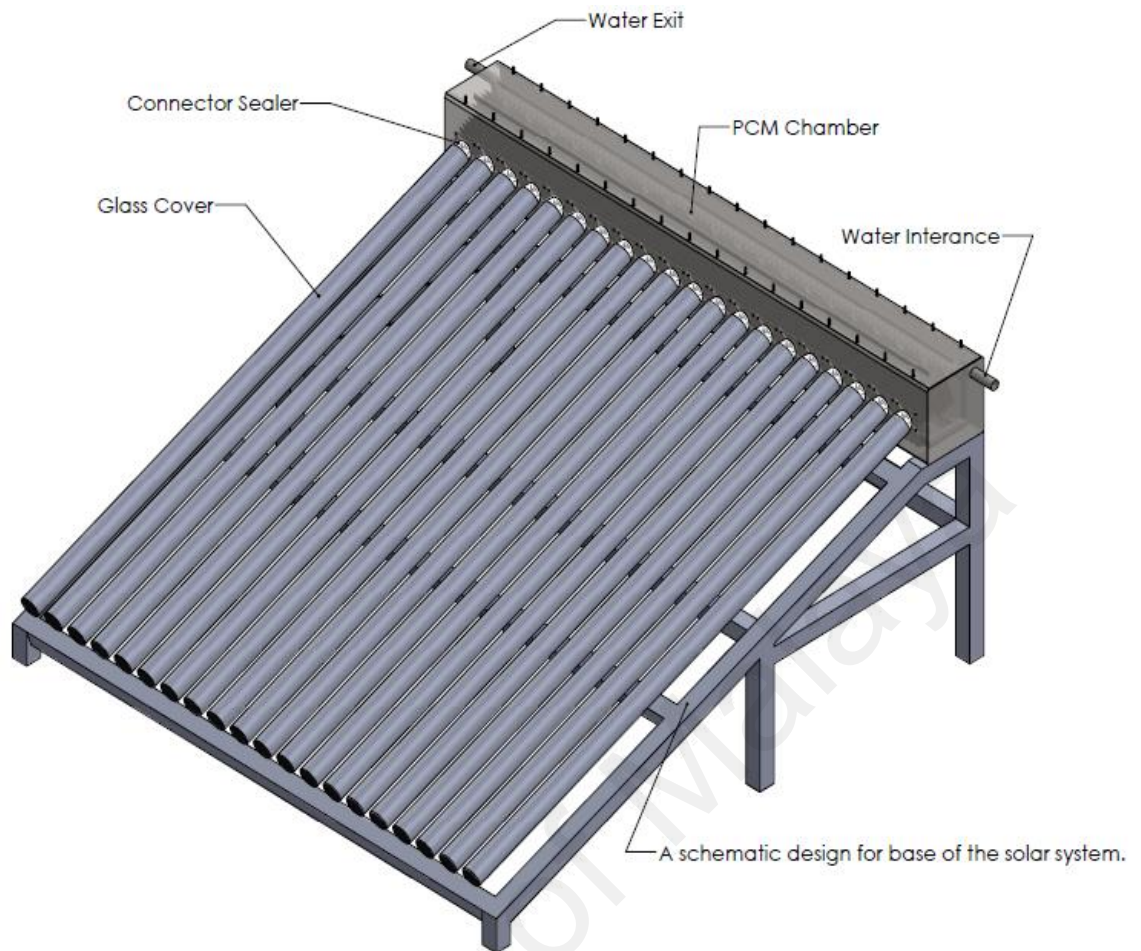


Figure D. 5: Isotropic view of the HPSC-LHS system.

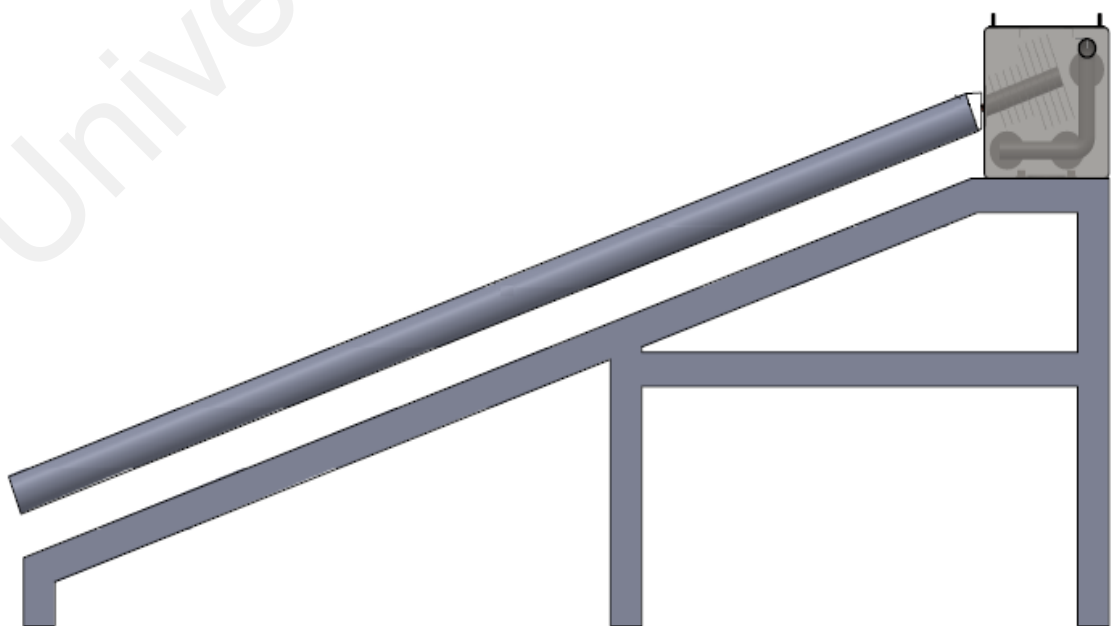


Figure D. 6: side view of the HPSC-LHS system.

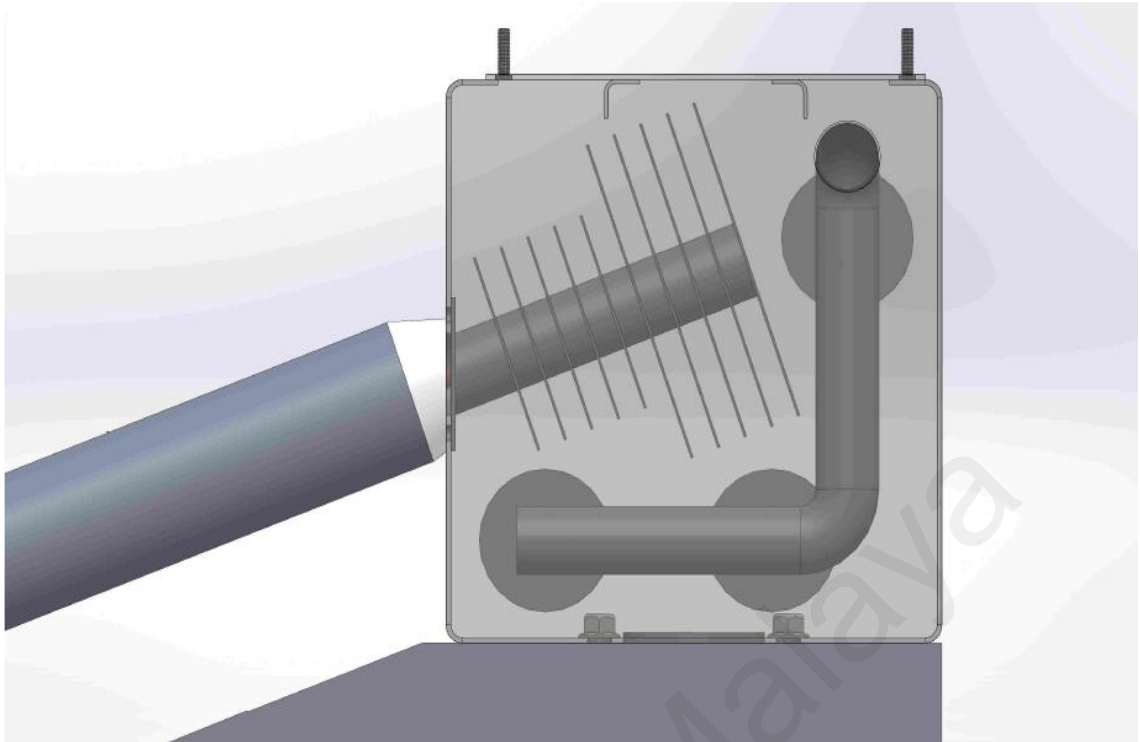


Figure D. 7: Heat exchange arrangement of the TES tank of the HPSC-LHS system (Side view).

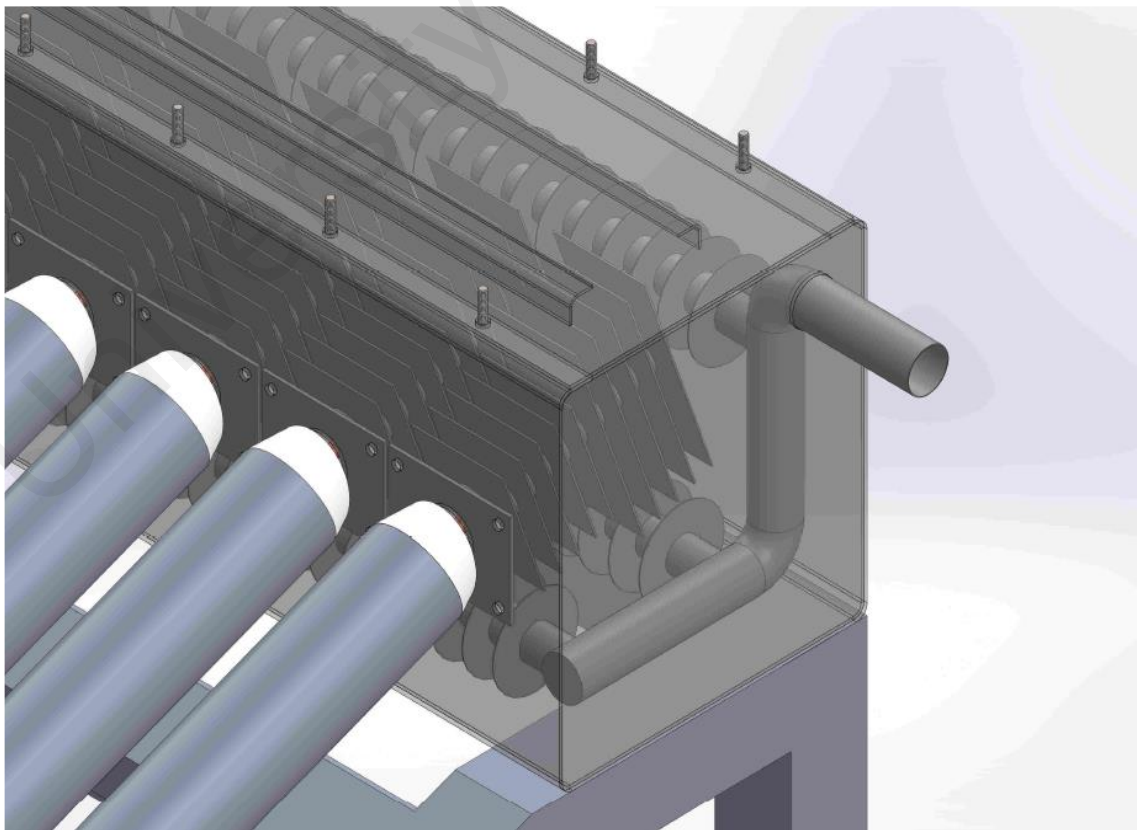


Figure D. 8: Heat exchange arrangement of the TES tank of the HPSC-LHS system (Isotropic view).

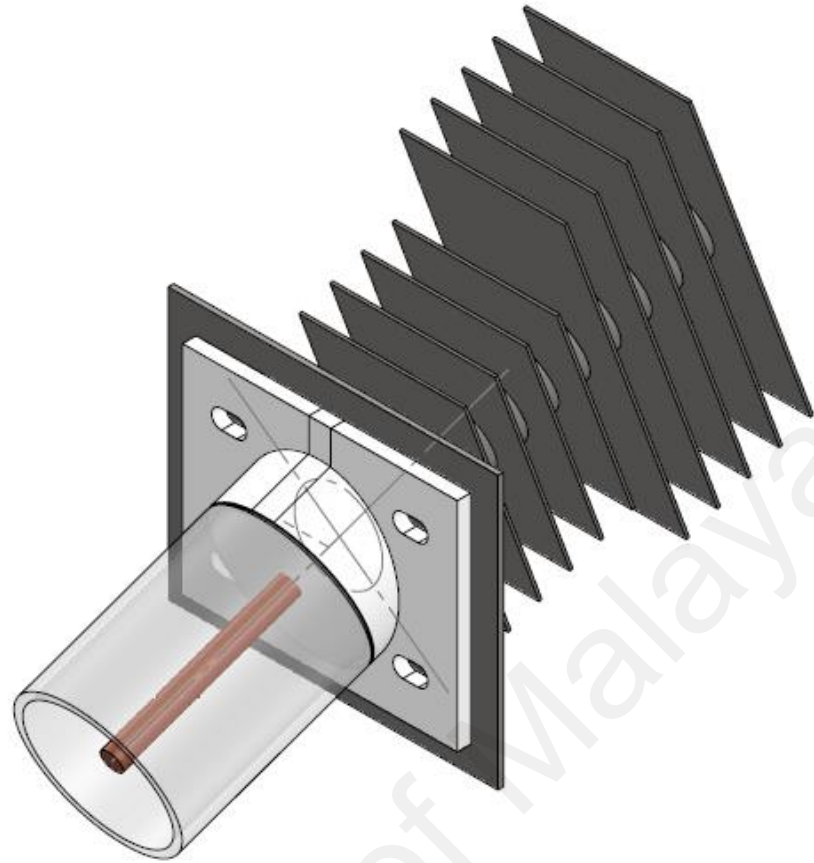


Figure D. 9: Heat pipe and its fin shell arrangement in the heat pipe condenser side heat exchanger (Isotropic view).

APPENDIX E: TABLES OF DATA OF CHAPTER 5

Table E. 1: Data of run 1.

<i>Time</i>	<i>I</i>	<i>T_{PCM}</i>	<i>T_{HPE}</i>	<i>T_{HPA}</i>	<i>T_{HPC}</i>	<i>T_{w,in}</i>	<i>T_{w,out}</i>
6:30	0.0	53.3	29.1	44.6	51.5		
6:45	0.0	53.2	29.0	44.6	51.4		
7:00	0.0	53.1	29.0	44.5	51.4		
7:15	0.0	53.1	28.9	44.5	52.3		
7:30	0.0	53.0	29.1	44.5	51.3		
7:45	2.0	52.9	29.8	44.6	51.7		
8:00	17.3	52.9	31.5	44.8	51.4		
8:15	29.1	52.8	33.7	45.2	51.3		
8:30	45.5	52.8	36.5	45.5	51.4		
8:45	71.9	52.7	40.3	46.1	51.4		
9:00	88.3	52.6	45.1	46.9	51.3		
9:15	56.7	52.6	49.1	47.5	51.5		
9:30	74.2	52.5	51.7	48.0	51.5		
9:45	96.6	52.5	55.8	49.4	51.7		
10:00	52.7	52.4	58.6	50.4	52.1		
10:15	61.0	52.4	59.3	50.6	52.2		
10:30	198.9	52.3	63.8	52.1	52.9		
10:45	126.1	52.3	68.0	54.4	54.9		
11:00	182.2	52.3	69.3	56.2	56.8		
11:15	128.6	52.3	70.0	58.7	59.3		
11:30	210.1	52.3	70.6	61.6	60.1		
11:45	224.0	52.3	73.3	65.2	62.6		
12:00	239.1	52.4	75.8	67.0	64.0		
12:15	120.8	52.5	74.9	66.6	63.8		
12:30	61.4	52.7	70.9	62.7	61.3		
12:45	73.7	53.0	67.6	61.4	60.3		
13:00	108.8	53.3	65.6	59.9	59.3		
13:15	57.6	53.5	64.2	58.8	58.7		
13:30	75.0	53.8	62.5	57.4	57.8		
13:45	117.0	53.9	62.7	57.6	58.0		
14:00	98.8	54.1	63.7	58.2	58.6		
14:15	140.8	54.3	64.6	59.0	59.1		
14:30	159.6	54.6	66.1	60.1	59.9		
14:45	191.7	55.0	68.9	62.1	61.5		
15:00	124.3	55.6	69.9	62.9	62.2		
15:15	121.1	56.3	69.0	62.5	62.1		
15:30	156.6	56.6	69.3	62.7	62.3		
15:45	117.7	56.9	68.9	62.7	62.3		
16:00	100.3	57.0	67.5	61.6	61.7		
16:15	47.5	56.9	65.2	60.1	60.6		

16:30	93.1	56.6	64.3	59.4	60.0		
16:45	82.6	56.5	64.3	59.4	60.0		
17:00	83.1	56.4	63.7	59.1	59.6		
17:15	62.1	56.3	62.9	58.5	59.2		
17:30	54.0	56.1	61.7	57.7	58.5	29.6	35.9
17:45		55.9	60.6	56.8	57.9	28.3	32.7
18:00		55.6	59.5	55.9	57.2	28.3	31.2
18:15		55.3	58.1	54.9	56.4	28.3	30.8
18:30		55.0	56.7	53.9	55.5	28.3	30.6
18:45		54.7	55.2	52.6	54.7	28.2	30.3
19:00		54.6	53.6	51.5	54.1	28.2	30.2
19:15		54.5	51.7	50.6	54.1	28.1	30.0
19:30		54.5	49.6	49.8	54.0	28.0	29.9
19:45		54.5	47.6	49.2	53.8	28.0	29.8
20:00		54.5	45.9	48.7	53.7	27.9	29.8
20:15		54.5	44.4	48.1	53.5	27.9	29.6
20:30		54.5	43.0	47.8	53.4	27.8	29.5
20:45		54.4	41.8	47.4	53.2	27.8	29.5
21:00		54.4	40.6	47.0	53.1	27.7	29.4
21:15		54.4	39.7	46.8	53.0	27.7	29.4
21:30		54.3	38.7	46.6	52.8	27.7	29.3
21:45		54.2	37.8	46.3	52.7	27.6	29.2
22:00		54.2	37.1	46.2	52.5	27.6	29.2
22:15		54.1	36.4	46.0	52.4	27.6	29.1
22:30		54.1	36.1	45.9	52.3	27.6	29.1
22:45		54.1	36.1	45.9	52.3	27.6	29.1
23:00		54.1	36.1	45.9	52.3	27.6	29.1
23:15		54.1	36.1	45.9	52.3	27.6	29.1
23:30		54.1	36.1	45.9	52.3	27.6	29.1

Table E. 2: Data of run 2.

<i>Time</i>	<i>I</i>	<i>T_{PCM}</i>	<i>T_{HPE}</i>	<i>T_{HPA}</i>	<i>T_{HPC}</i>	<i>T_{w,in}</i>	<i>T_{w,out}</i>
6:30	0.0	54.2	28.4	42.3	52.1		
6:45	0.0	53.9	28.6	42.5	52.3		
7:00	0.0	53.7	27.8	41.9	52.2		
7:15	0.0	53.9	29.0	42.0	51.9		
7:30	23.8	53.6	31.1	42.7	52.1		
7:45	71.5	53.3	37.8	44.7	52.0		
8:00	59.6	53.6	43.7	44.9	51.9		
8:15	143.0	53.3	49.8	47.3	51.7		
8:30	309.9	53.2	65.0	51.4	52.5		
8:45	166.9	53.1	75.6	53.0	53.5		
9:00	178.8	53.0	74.4	56.5	56.4		
9:15	226.5	53.2	73.8	63.3	59.2		
9:30	262.2	53.0	75.9	67.6	62.0		
9:45	286.1	53.2	78.5	70.3	63.4		
10:00	309.9	54.1	81.4	71.4	64.5		
10:15	369.5	55.8	85.4	74.4	66.5		
10:30	417.2	57.4	89.0	77.5	69.3		
10:45	512.5	59.2	95.9	82.6	72.5		
11:00	548.3	61.7	103.6	87.6	76.6		
11:15	595.9	65.3	109.2	92.9	80.9		
11:30	607.9	69.5	115.2	97.4	85.1		
11:45	750.9	74.0	124.8	104.4	90.4		
12:00	643.6	78.7	131.9	110.0	96.1		
12:15	691.3	82.6	131.1	110.2	98.5		
12:30	595.9	86.2	132.4	111.6	101.2		
12:45	572.1	89.9	140.3	118.5	106.4		
13:00	572.1	93.2	134.7	115.2	106.7		
13:15	631.7	95.2	134.5	114.9	108.5		
13:30	786.7	97.6	140.2	120.0	111.6		
13:45	870.1	100.9	149.4	128.1	117.1		
14:00	345.6	105.4	159.1	135.0	122.8		
14:15	309.9	108.6	150.0	128.1	122.4		
14:30	953.5	111.0	159.7	135.5	126.8		
14:45	262.2	113.2	147.9	127.2	124.8		
15:00	262.2	113.4	140.5	122.2	122.5		
15:15	166.9	112.0	130.3	115.3	118.8		
15:30	166.9	109.8	122.5	108.8	115.1		
15:45	47.7	107.2	114.5	103.8	111.2		
16:00	35.8	104.5	108.5	98.9	107.5		
16:15	11.9	101.7	102.1	94.2	104.5		
16:30	11.9	99.2	95.4	86.7	101.8		
16:45	11.9	97.2	89.0	83.1	99.5		
17:00	11.9	95.0	85.1	79.3	97.3		

17:15	11.9	93.1	81.1	77.1	95.1		
17:30	11.9	91.2	78.4	74.8	93.0	28.7	39.5
17:45		89.4	74.8	73.4	91.1	28.1	39.7
18:00		84.2	80.4	73.2	85.7	28.1	42.2
18:15		76.5	79.2	68.9	78.2	28.9	38.0
18:30		70.7	77.4	66.2	71.9	28.1	36.4
18:45		65.5	73.2	61.3	66.8	28.3	35.7
19:00		61.5	68.8	58.6	62.8	28.2	35.6
19:15		58.9	64.4	54.6	59.5	28.3	34.7
19:30		57.2	59.8	53.7	57.8	28.2	32.9
19:45		56.2	56.5	51.9	56.3	28.2	32.8
20:00		55.4	54.4	50.3	55.3	28.1	32.2
20:15		55.1	51.6	48.5	54.9	28.2	31.3
20:30		54.5	50.7	47.2	54.4	28.4	30.4
20:45		54.6	48.7	47.1	54.0	28.1	30.6
21:00		54.2	46.9	47.3	53.8	27.9	30.3
21:15		53.9	45.7	46.9	53.7	28.2	30.3
21:30		54.4	43.9	45.9	54.0	28.2	31.1
21:45		54.3	42.3	45.9	53.6	27.7	31.1
22:00		54.4	41.6	45.8	53.8	27.8	31.1
22:15		54.1	41.0	44.9	53.4	27.7	30.2
22:30		54.3	39.8	45.5	53.3	28.8	31.1
22:45		53.9	38.9	44.9	53.5	27.8	29.4
23:00		54.4	37.9	45.1	53.4	27.8	29.4
23:15		54.6	36.4	45.0	53.2	27.7	31.0
23:30		54.3	36.4	44.0	53.1	28.4	30.8

Table E. 3: Data of run 3.

<i>Time</i>	<i>I</i>	<i>T_{PCM}</i>	<i>T_{HPE}</i>	<i>T_{HPA}</i>	<i>T_{HPC}</i>	<i>T_{w,in}</i>	<i>T_{w,out}</i>
6:30	0.0	53.5	30.4	45.5	51.8		
6:45	0.0	53.4	30.4	45.5	51.8		
7:00	0.0	53.4	30.3	45.4	51.7		
7:15	0.0	53.3	30.3	45.3	51.7		
7:30	3.8	53.2	30.9	45.4	51.6		
7:45	24.0	53.2	33.3	45.7	51.6		
8:00	69.3	53.1	36.9	46.5	51.7		
8:15	78.4	53.0	41.7	47.3	51.8		
8:30	281.4	53.0	54.5	50.3	52.0		
8:45	377.2	53.0	80.8	57.8	54.9		
9:00	278.5	53.0	88.2	74.2	70.0		
9:15	315.1	52.9	85.5	73.7	69.1		
9:30	208.8	53.2	95.0	82.0	75.3		
9:45	343.8	55.7	98.7	84.5	77.6		
10:00	627.8	59.1	99.7	85.4	78.9		
10:15	210.2	61.2	94.6	82.2	77.4		
10:30	162.5	61.1	88.6	77.9	74.3		
10:45	314.4	61.4	99.4	85.4	79.5		
11:00	847.9	62.3	103.0	87.6	81.3		
11:15	842.7	64.0	118.1	98.8	89.3		
11:30	416.1	67.4	125.6	105.1	95.0		
11:45	278.5	70.9	119.1	100.1	93.6		
12:00	144.0	73.1	103.3	88.9	86.8		
12:15	185.8	73.7	96.2	84.3	83.9		
12:30	359.6	74.1	97.4	85.0	84.6		
12:45	339.0	75.6	103.6	89.6	88.1		
13:00	301.0	76.9	104.1	90.6	88.9		
13:15	420.8	78.1	105.4	91.9	90.1		
13:30	484.5	79.8	115.3	99.2	95.6		
13:45	1114.1	83.0	138.2	114.9	107.2		
14:00	523.2	87.4	136.8	115.4	109.1		
14:15	178.3	89.9	123.7	107.0	104.7		
14:30	131.7	90.4	113.5	100.4	100.5		
14:45	141.9	89.8	105.8	94.8	96.9		
15:00	170.9	88.9	101.9	91.9	94.7		
15:15	146.3	87.0	99.0	90.0	93.1		
15:30	109.7	86.1	94.7	86.7	90.6		
15:45	171.7	85.5	93.0	85.6	89.2		
16:00	204.8	84.7	94.1	86.3	89.2		
16:15	130.3	84.3	94.8	86.8	89.4		
16:30	204.1	83.8	93.8	86.0	88.6		
16:45	179.7	83.5	94.4	86.4	88.6		
17:00	119.3	83.3	92.5	84.8	87.5		

17:15	67.0	82.6	89.0	82.3	85.6		
17:30	32.4	81.3	85.0	79.5	83.1	31.2	36.0
17:45		73.7	80.2	74.3	76.6	28.7	37.4
18:00		68.0	74.1	69.3	70.8	28.6	36.0
18:15		63.8	69.6	64.3	66.0	28.7	35.1
18:30		60.6	64.6	60.8	62.2	28.6	34.3
18:45		58.5	61.0	57.7	59.4	28.4	33.6
19:00		57.4	58.2	55.4	57.5	28.3	32.8
19:15		56.6	55.4	53.5	56.7	28.1	32.2
19:30		55.9	53.0	52.3	56.0	28.0	31.8
19:45		55.5	51.1	51.3	55.3	28.9	31.5
20:00		55.2	49.1	50.7	55.0	28.8	31.3
20:15		54.9	47.4	50.1	54.6	28.7	31.1
20:30		54.7	45.8	49.7	54.4	28.6	30.9
20:45		54.7	44.4	49.3	54.2	28.5	30.8
21:00		54.7	43.2	49.0	54.1	28.4	30.7
21:15		54.7	41.9	48.7	54.0	28.3	30.6
21:30		54.6	40.9	48.5	54.0	28.3	30.4
21:45		54.7	39.8	48.3	53.8	28.2	30.3
22:00		54.7	38.9	48.0	53.7	28.1	30.3
22:15		54.7	38.0	47.8	53.7	28.5	30.1
22:30		54.6	37.3	47.7	53.6	28.4	30.0
22:45		54.7	36.6	47.5	53.5	28.3	29.9
23:00		54.7	35.9	47.3	53.4	28.2	29.8
23:15		54.7	35.4	47.2	53.3	28.2	29.7
23:30		54.6	34.9	47.1	53.2	28.1	29.7

Table E. 4: Data of run 4.

<i>Time</i>	<i>I</i>	<i>T_{PCM}</i>	<i>T_{HPE}</i>	<i>T_{HPA}</i>	<i>T_{HPC}</i>	<i>T_{w,in}</i>	<i>T_{w,out}</i>
6:30	0.0	54.6	29.8	46.4	53.4		
6:45	0.0	54.7	29.8	46.4	53.4		
7:00	0.0	54.6	29.6	46.3	53.4		
7:15	0.0	54.6	29.6	46.2	53.3		
7:30	0.1	54.6	30.2	46.2	53.3		
7:45	21.1	54.6	32.0	46.7	53.3		
8:00	52.5	54.5	35.3	47.3	53.3		
8:15	101.9	54.5	41.5	48.7	53.4		
8:30	161.4	54.5	50.4	50.3	53.6		
8:45	177.6	54.5	63.8	54.1	54.6		
9:00	252.9	54.5	75.7	59.3	56.5		
9:15	371.3	54.4	84.8	72.1	69.4		
9:30	459.5	55.3	96.8	85.1	77.3		
9:45	504.1	59.1	108.2	92.8	84.2		
10:00	563.1	64.3	118.4	99.8	90.7		
10:15	622.1	69.9	127.3	106.7	97.1		
10:30	655.2	75.5	134.1	112.8	102.9		
10:45	697.6	80.8	139.1	117.5	107.8		
11:00	779.4	85.8	143.2	121.5	112.0		
11:15	871.8	90.8	150.3	127.8	117.8		
11:30	580.5	95.6	150.0	128.7	120.5		
11:45	758.4	99.3	151.4	130.5	122.9		
12:00	904.2	102.6	156.7	135.0	126.8		
12:15	988.2	106.7	165.1	141.9	132.6		
12:30	896.8	111.0	169.4	146.2	137.0		
12:45	999.7	114.5	169.2	146.3	138.6		
13:00	975.8	118.3	177.4	152.4	144.2		
13:15	1047.2	122.3	181.8	156.0	148.2		
13:30	366.5	125.5	177.5	153.8	148.4		
13:45	245.2	128.0	175.5	152.4	148.8		
14:00	198.9	128.6	156.5	140.0	141.2		
14:15	1046.8	127.3	150.3	135.0	137.4		
14:30	221.3	128.3	157.8	140.7	141.6		
14:45	293.5	129.0	166.2	146.2	145.3		
15:00	243.5	129.4	152.1	137.0	139.5		
15:15	232.9	128.6	152.1	136.5	139.1		
15:30	193.8	127.8	142.2	130.1	134.4		
15:45	259.4	126.4	139.1	127.7	132.3		
16:00	223.4	125.5	141.9	129.0	132.8		
16:15	638.1	125.4	148.4	133.1	135.1		
16:30	585.0	127.4	163.8	143.6	143.0		
16:45	502.9	128.5	151.4	135.7	138.0		
17:00	454.1	129.5	163.4	143.6	143.4		

17:15	192.6	131.2	163.8	144.5	144.3		
17:30	105.1	131.2	148.3	134.5	137.8	31.4	38.5
17:45		116.2	145.6	129.5	128.4	29.8	56.5
18:00		106.1	143.6	125.3	121.5	29.8	52.5
18:15		98.1	124.7	111.0	109.2	29.6	49.0
18:30		90.5	110.4	99.3	98.9	29.5	46.6
18:45		84.0	101.9	91.5	91.4	29.5	44.3
19:00		78.4	91.3	83.1	83.8	29.4	42.4
19:15		73.3	81.9	75.8	77.1	29.2	40.9
19:30		68.9	74.7	70.1	71.5	29.2	39.6
19:45		65.0	69.0	65.4	67.0	29.1	38.2
20:00		62.0	64.5	61.5	63.3	29.2	37.3
20:15		59.6	61.1	58.3	60.4	29.4	36.7
20:30		58.0	58.1	55.9	58.5	29.4	35.8
20:45		57.1	55.6	54.3	57.5	29.4	35.2
21:00		56.5	53.4	53.0	56.7	29.3	34.4
21:15		56.0	51.4	52.1	56.1	29.2	34.0
21:30		55.6	49.5	51.3	55.6	29.1	33.7
21:45		55.2	47.8	50.7	55.1	28.9	33.4
22:00		55.0	46.2	50.1	54.7	28.9	33.2
22:15		54.8	44.8	49.6	54.5	28.8	32.9
22:30		54.7	43.5	49.2	54.3	28.7	32.8
22:45		54.7	42.3	48.9	54.1	28.6	32.9
23:00		54.7	41.2	48.6	54.0	28.5	32.6
23:15		54.7	40.2	48.4	53.9	28.4	32.3
23:30		54.6	39.3	48.2	53.9	28.4	32.2

Table E. 5: Data of run 5.

<i>Time</i>	<i>I</i>	<i>T_{PCM}</i>	<i>T_{HPE}</i>	<i>T_{HPA}</i>	<i>T_{HPC}</i>	<i>T_{w,in}</i>	<i>T_{w,out}</i>
6:30	0	50.7	26.9	40.4	48.8		
6:45	0	50.6	26.8	40.3	48.7		
7:00	0	50.5	26.9	40.2	48.6		
7:15	6.377	50.4	27.7	40.2	48.5		
7:30	30.8	50.3	30	40.7	48.4		
7:45	83.32	50.1	33.8	41.5	48.3		
8:00	115.4	50	39.8	42.7	48.3		
8:15	194.2	49.9	46.6	45	48.4		
8:30	250.4	49.8	64.2	49.1	49.3		
8:45	319.3	49.7	74.8	59.7	53.2		
9:00	385.2	49.6	81.1	74.4	62.8		
9:15	445.8	49.7	89.5	82.2	67		
9:30	506.4	49.8	97.7	88.6	70.6		
9:45	561	50.2	105	94.9	74.3		
10:00	614.2	54.5	112	101	79.4		
10:15	667	62.6	118	106	85		
10:30	713.5	66	123	110	88.1		
10:45	738.7	67.4	127	114	90.5		
11:00	741.1	69.3	128	114	91.9		
11:15	829.5	72.8	131	116	94.9		
11:30	875.7	77.9	136	120	99.6		
11:45	928.6	84	142	126	105		
12:00	896.4	89.4	146	130	109		
12:15	909	94.5	150	134	114		
12:30	869	99.2	152	136	118		
12:45	954.2	103	155	139	121		
13:00	1019	108	159	142	126		
13:15	944.2	112	157	141	128		
13:30	852.3	114	150	136	128		
13:45	609.3	116	161	144	132		
14:00	345.8	119	156	141	133		
14:15	758.8	120	160	144	135		
14:30	883.5	123	167	148	138		
14:45	805.8	126	170	151	141		
15:00	372.4	128	168	151	143		
15:15	303.6	129	161	145	141		
15:30	546.4	128	150	136	138		
15:45	561.3	128	155	139	139		
16:00	523.5	129	154	139	139		
16:15	455.7	129	152	138	139		
16:30	388.2	128	150	136	138		
16:45	271.8	128	146	133	136		
17:00	279.5	126	141	129	134		

17:15	170	125	136	125	131		
17:30	66.34	122.2	125.7	119.8	125.7	34.2	53.9
17:45		116.5	123.2	115.0	122.0	28.2	50.6
18:00		105.4	117.8	112.0	119.9	29.7	46.8
18:15		97.3	112.5	109.0	108.8	29.5	44.3
18:30		90.2	107.2	104.1	98.2	29.5	42.4
18:45		84.0	100.5	94.8	89.6	29.9	41.2
19:00		78.7	89.4	84.8	81.6	29.7	39.9
19:15		74.0	80.6	76.9	75.0	29.7	38.8
19:30		69.8	72.6	70.6	69.6	29.5	37.7
19:45		66.4	67.0	65.6	65.1	29.4	36.7
20:00		63.8	62.5	60.8	61.2	29.0	35.4
20:15		62.0	57.5	56.6	58.3	28.3	34.1
20:30		60.8	53.8	53.3	57.1	28.8	33.0
20:45		60.0	51.4	51.3	56.2	28.6	32.2
21:00		59.4	49.8	50.0	55.5	28.5	31.8
21:15		58.9	48.0	48.7	55.1	28.3	31.4
21:30		58.5	46.6	47.7	54.6	28.2	31.2
21:45		58.1	45.4	46.9	54.3	28.2	31.0
22:00		57.9	44.3	46.2	54.1	28.1	30.9
22:15		57.8	43.3	45.5	54.0	28.0	30.7
22:30		57.7	42.4	44.9	53.9	28.5	30.6
22:45		57.5	41.5	44.5	53.8	28.4	30.5
23:00		57.5	40.8	44.0	53.7	28.3	30.3
23:15		57.4	40.1	43.6	53.7	28.3	30.3
23:30		57.3	39.5	43.2	53.6	28.2	30.2

Table E. 6: Data of run 6.

<i>Time</i>	<i>I</i>	<i>T_{PCM}</i>	<i>T_{HPE}</i>	<i>T_{HPA}</i>	<i>T_{HPC}</i>	<i>T_{w,in}</i>	<i>T_{w,out}</i>
6:30	0.0	53.4	30.5	45.4	51.7		
6:45	0.0	53.3	30.4	45.3	51.7		
7:00	0.0	53.2	30.3	45.3	51.6		
7:15	0.0	53.2	30.4	45.2	51.6		
7:30	2.2	53.1	31.1	45.3	51.5		
7:45	32.1	53.0	33.3	45.7	51.5		
8:00	73.2	53.0	37.2	46.4	51.5		
8:15	59.1	52.9	41.0	47.0	51.6		
8:30	150.6	52.9	49.3	48.6	51.8		
8:45	158.5	52.8	57.6	50.7	52.1		
9:00	86.0	52.8	63.9	52.0	53.0		
9:15	379.2	52.7	75.7	56.5	54.8		
9:30	214.3	52.7	75.9	62.3	62.3		
9:45	532.5	52.7	89.0	77.2	71.3		
10:00	151.8	52.8	94.6	81.6	74.8		
10:15	315.2	54.4	93.9	80.9	74.5		
10:30	253.7	57.5	96.3	82.9	76.6		
10:45	546.3	59.5	90.5	79.0	74.4		
11:00	606.7	61.1	98.8	84.9	78.9		
11:15	190.4	63.0	109.7	93.0	85.3		
11:30	364.9	63.5	108.5	92.0	84.5		
11:45	864.4	64.4	109.9	93.1	85.5		
12:00	208.7	65.4	101.1	87.1	82.2		
12:15	685.4	66.5	103.4	88.4	83.6		
12:30	444.8	70.3	121.5	101.6	93.5		
12:45	288.5	73.4	108.7	93.6	89.3		
13:00	361.9	75.9	121.2	102.2	96.0		
13:15	244.7	79.5	122.1	103.9	98.4		
13:30	950.1	81.8	128.2	107.9	102.0		
13:45	339.9	85.8	140.5	117.7	109.7		
14:00	1008.7	90.4	154.4	127.6	117.8		
14:15	953.7	95.0	156.8	130.3	121.2		
14:30	289.4	99.6	158.9	133.0	124.6		
14:45	977.9	103.0	157.6	132.5	125.8		
15:00	978.9	106.7	169.7	141.3	133.1		
15:15	893.0	110.2	163.7	137.9	132.8		
15:30	781.3	111.9	156.0	133.5	130.6		
15:45	166.9	113.9	161.8	138.2	134.3		
16:00	710.5	115.2	158.4	136.2	133.6		
16:15	682.2	116.6	153.7	133.2	132.3		
16:30	210.8	117.8	151.9	132.5	132.7		
16:45	387.5	117.6	142.3	126.2	128.5		
17:00	340.3	116.6	138.0	123.0	126.0		

17:15	427.5	116.3	143.4	126.3	127.8		
17:30	198.0	117.2	130.7	118.4	122.8	30.8	63.2
17:45		101.7	132.5	116.4	114.6	29.0	44.0
18:00		92.9	130.0	112.5	108.3	29.0	41.9
18:15		86.4	121.0	104.9	100.6	29.0	40.4
18:30		80.6	107.4	94.3	91.7	28.8	39.0
18:45		75.2	94.6	84.5	83.3	28.7	37.9
19:00		70.4	84.1	76.4	76.2	28.7	36.9
19:15		66.1	75.2	69.4	70.0	28.6	35.9
19:30		62.6	68.4	63.8	65.1	28.9	35.4
19:45		59.9	63.3	59.9	61.4	28.9	34.7
20:00		58.3	59.6	57.0	58.9	28.8	34.0
20:15		57.3	56.9	54.8	57.4	28.7	33.3
20:30		56.5	54.5	53.3	56.7	28.6	32.8
20:45		56.0	52.3	52.2	56.1	28.5	32.5
21:00		55.5	50.2	51.3	55.5	28.4	32.2
21:15		55.2	48.5	50.6	55.0	28.3	32.0
21:30		54.9	46.8	50.0	54.6	28.2	31.8
21:45		54.8	45.3	49.6	54.4	28.1	31.6
22:00		54.7	44.0	49.3	54.3	29.0	31.5
22:15		54.6	42.8	49.1	54.2	28.9	31.4
22:30		54.7	41.7	48.8	54.1	28.9	31.3
22:45		54.7	40.7	48.7	54.0	28.8	31.2
23:00		54.7	39.8	48.4	53.9	28.7	31.0
23:15		54.7	39.0	48.3	53.8	28.6	31.0
23:30		54.7	38.3	48.2	53.8	28.6	30.9

Table E. 7: Data of run 7.

<i>Time</i>	<i>I</i>	<i>T_{PCM}</i>	<i>T_{HPE}</i>	<i>T_{HPA}</i>	<i>T_{HPC}</i>	<i>T_{w,in}</i>	<i>T_{w,out}</i>
6:30	1.67	51.2	50.8	41.6	25.0		
6:45	1.67	51.2	50.8	41.8	26.0		
7:00	1.67	51.2	50.8	42.0	27.1		
7:15	5.35	51.2	50.8	42.2	28.1		
7:30	18.37	51.2	50.8	42.4	29.2		
7:45	38.62	51.1	50.8	42.7	30.9		
8:00	34.80	51.1	50.7	43.2	33.1		
8:15	54.11	51.1	50.7	43.7	35.3		
8:30	126.22	51.1	50.7	44.7	40.9		
8:45	155.78	51.1	50.7	46.5	48.9		
9:00	380.45	51.7	51.7	49.6	61.6		
9:15	326.34	54.0	53.4	55.1	78.0		
9:30	364.36	63.2	66.5	66.4	76.5		
9:45	335.58	63.6	67.3	67.0	75.6		
10:00	350.75	62.9	66.5	65.7	73.7		
10:15	442.45	60.3	63.3	61.5	67.7		
10:30	464.23	58.6	60.9	58.8	63.9		
10:45	488.35	57.7	59.5	57.2	62.3		
11:00	473.58	59.5	61.2	59.1	65.5		
11:15	554.23	62.1	64.6	63.3	71.1		
11:30	616.63	62.2	65.0	64.0	71.1		
11:45	452.56	61.7	64.2	62.0	70.5		
12:00	492.73	65.8	68.5	68.4	77.9		
12:15	542.35	67.1	70.9	70.3	79.4		
12:30	822.05	69.7	73.0	73.8	84.8		
12:45	1104.05	77.8	83.1	85.1	101.0		
13:00	968.89	82.8	88.6	91.2	109.1		
13:15	531.70	83.0	88.1	89.4	104.2		
13:30	594.02	83.2	87.9	88.4	102.3		
13:45	805.96	86.1	90.9	91.7	105.7		
14:00	526.58	86.9	91.8	89.9	103.8		
14:15	550.42	87.3	91.3	89.5	102.7		
14:30	822.05	89.5	93.4	91.9	105.7		
14:45	666.42	93.4	98.3	96.8	111.9		
15:00	604.02	94.5	99.4	96.8	111.3		
15:15	492.49	95.1	99.5	96.8	109.6		
15:30	475.09	95.8	98.9	96.2	107.9		
15:45	538.14	95.3	99.1	96.3	107.7		
16:00	497.57	95.3	98.3	95.0	106.4		
16:15	402.27	94.0	97.2	92.8	102.9		
16:30	254.95	92.6	95.1	90.5	99.8		
16:45	247.72	90.9	93.6	88.3	96.7		
17:00	246.60	88.9	90.8	85.6	92.8		

17:15	235.03	86.6	88.2	82.5	89.4		
17:30	240.17	84.4	85.4	79.6	85.8		
17:45	283.12	82.5	83.6	77.6	83.2		
18:00	257.08	80.5	81.7	76.2	81.0		
18:15	247.92	79.1	80.3	74.7	80.6		
18:30	264.57	77.8	78.8	73.2	78.3		
18:45	251.01	76.0	76.7	71.1	75.9		
19:00	42.60	74.3	74.9	68.3	72.8		
19:15	16.48	70.1	71.2	65.7	69.5		
19:30	15.49	63.6	74.2	66.8	71.3	28.6	46.0
19:45		60.6	68.4	63.3	67.3	27.7	37.8
20:00		57.9	63.8	60.6	63.8	28.0	35.5
20:15		56.8	60.8	57.5	60.4	28.4	34.4
20:30		55.9	58.2	54.6	57.4	28.9	34.2
20:45		55.6	57.1	52.4	55.0	27.7	33.1
21:00		55.0	56.1	51.4	52.5	28.6	32.8
21:15		54.6	55.3	50.5	50.4	28.5	31.5
21:30		54.5	54.8	49.0	48.7	28.3	31.4
21:45		54.5	54.6	48.7	47.0	27.6	31.2
22:00		54.6	54.4	48.5	45.7	27.5	31.1
22:15		54.5	53.9	48.3	44.6	28.8	31.2
22:30		54.6	53.9	47.3	42.8	27.8	30.1
22:45		54.5	54.3	47.5	41.9	28.0	31.1
23:00		54.5	53.7	46.7	40.5	27.9	30.1
23:15		54.5	53.6	47.0	39.7	27.7	30.9
23:30		54.8	54.3	46.3	38.9	27.8	29.9

Table E. 8: Data of run 8.

<i>Time</i>	<i>I</i>	<i>T_{PCM}</i>	<i>T_{HPE}</i>	<i>T_{HPA}</i>	<i>T_{HPC}</i>	<i>T_{w,in}</i>	<i>T_{w,out}</i>
6:30	1.67	48.2	47.7	41.0	27.9		
6:45	1.67	48.1	47.9	41.2	28.2		
7:00	1.67	47.8	47.4	40.6	27.7		
7:15	1.67	47.3	46.8	40.4	28.0		
7:30	11.80	47.0	46.0	40.6	28.8		
7:45	38.88	47.0	46.7	40.2	30.6		
8:00	62.36	46.4	45.6	40.9	33.8		
8:15	111.42	46.0	45.3	41.4	38.7		
8:30	120.58	45.9	45.1	42.4	46.0		
8:45	167.60	46.4	46.0	44.4	51.7		
9:00	265.41	47.6	48.1	46.1	63.6		
9:15	327.39	53.7	56.6	58.1	70.3		
9:30	366.37	60.7	65.1	64.4	72.8		
9:45	369.96	64.0	69.1	69.4	78.6		
10:00	462.34	66.6	72.5	73.8	83.3		
10:15	441.51	69.6	76.0	77.4	88.4		
10:30	411.69	70.1	77.0	78.7	89.1		
10:45	584.06	72.1	79.3	81.4	92.5		
11:00	614.51	75.9	84.0	85.1	98.7		
11:15	653.15	78.6	86.5	87.2	101.4		
11:30	560.37	81.4	89.0	90.7	104.4		
11:45	443.97	79.5	86.0	87.0	98.3		
12:00	664.80	79.2	85.3	85.4	97.6		
12:15	796.08	81.9	88.5	88.1	103.1		
12:30	575.35	80.6	86.7	86.2	99.0		
12:45	641.97	81.2	87.1	86.4	99.7		
13:00	854.60	87.9	95.5	96.3	111.7		
13:15	1083.77	94.7	103.3	105.6	122.4		
13:30	812.75	99.9	107.7	111.0	128.3		
13:45	560.42	99.6	106.3	105.0	122.5		
14:00	504.37	99.5	105.6	105.0	119.1		
14:15	398.91	99.9	105.3	103.1	117.3		
14:30	440.41	99.0	103.7	100.7	113.7		
14:45	663.47	100.0	104.5	102.4	115.6		
15:00	403.55	100.9	105.2	101.5	115.9		
15:15	527.84	102.0	106.5	102.8	116.8		
15:30	220.13	100.8	104.2	100.7	112.8		
15:45	225.36	98.4	101.3	96.7	107.3		
16:00	238.44	96.9	99.1	95.6	104.5		
16:15	354.57	96.9	99.2	95.9	104.6		
16:30	309.69	98.4	101.6	97.7	108.1		
16:45	209.38	97.2	99.7	96.3	105.4		
17:00	198.76	95.3	97.4	93.7	101.9		

17:15	190.15	94.5	96.4	92.3	99.9		
17:30	169.85	93.4	95.0	91.2	98.2		
17:45	108.30	91.5	93.0	88.8	95.5		
18:00	68.41	89.0	90.0	86.8	91.5		
18:15	39.62	86.3	86.9	82.6	87.5		
18:30	23.69	83.7	84.0	78.7	83.5		
18:45	16.57	81.5	81.1	75.9	80.2		
19:00	0.37	79.7	79.8	72.8	76.9		
19:15	0.37	78.4	78.4	70.4	73.3		
19:30	0.37	74.1	75.5	66.7	66.1	27.6	39.1
19:45		67.4	69.2	63.0	62.8	28.2	35.6
20:00		62.7	64.4	59.5	60.0	28.4	34.7
20:15		59.7	61.1	56.9	57.3	28.5	33.9
20:30		57.6	58.4	54.3	55.1	28.0	32.7
20:45		56.7	57.1	52.5	53.0	28.3	31.9
21:00		55.8	56.7	52.0	51.2	27.8	31.5
21:15		55.3	55.7	51.1	49.2	28.1	31.7
21:30		55.1	54.9	50.5	47.8	28.1	31.5
21:45		54.5	54.4	49.8	46.3	28.1	30.8
22:00		54.3	54.2	49.4	45.2	28.8	30.9
22:15		54.1	53.8	49.2	43.6	28.0	30.7
22:30		54.4	53.7	48.5	42.4	28.1	32.2
22:45		54.4	54.2	48.4	41.8	28.4	31.5
23:00		54.4	53.9	48.2	40.7	28.5	30.6
23:15		54.5	54.2	48.1	39.8	28.5	31.4
23:30		54.3	53.7	47.8	39.2	28.2	30.5

Table E. 9: Data of run 9.

<i>Time</i>	<i>I</i>	<i>T_{PCM}</i>	<i>T_{HPE}</i>	<i>T_{HPA}</i>	<i>T_{HPC}</i>	<i>T_{w,in}</i>	<i>T_{w,out}</i>
6:30	1.67	51.7	51.5	44.4	30.5		
6:45	1.67	51.6	51.4	44.2	30.2		
7:00	1.67	51.4	51.1	44.1	30.3		
7:15	1.67	51.5	51.3	44.3	30.4		
7:30	12.93	51.3	50.9	43.9	30.8		
7:45	28.75	51.4	51.3	44.3	32.3		
8:00	73.64	51.4	51.3	44.6	35.4		
8:15	103.41	51.5	51.4	45.5	41.4		
8:30	107.05	51.4	51.2	46.9	47.8		
8:45	145.57	51.6	51.3	48.8	54.4		
9:00	187.08	52.0	52.1	50.5	62.2		
9:15	161.62	52.7	53.7	52.3	70.1		
9:30	168.61	57.6	61.0	60.9	69.4		
9:45	197.09	60.2	63.3	62.3	68.7		
10:00	317.11	62.8	66.2	66.0	72.8		
10:15	459.10	67.9	72.8	73.1	82.7		
10:30	442.48	71.7	77.6	79.1	89.7		
10:45	592.98	75.1	81.7	83.3	94.9		
11:00	547.60	79.7	87.0	87.7	102.5		
11:15	584.13	82.8	89.9	91.2	105.6		
11:30	817.20	83.7	90.9	92.1	106.5		
11:45	664.23	87.1	94.6	96.0	111.7		
12:00	776.17	89.4	97.3	99.2	114.6		
12:15	960.70	94.1	102.2	103.9	120.8		
12:30	900.66	98.3	107.1	106.0	124.3		
12:45	751.10	102.3	110.6	110.2	127.4		
13:00	563.40	104.0	111.1	110.6	125.9		
13:15	556.54	104.9	111.3	109.0	124.5		
13:30	536.09	105.1	110.8	108.2	122.3		
13:45	484.81	107.3	113.1	111.1	125.0		
14:00	384.84	106.8	111.8	109.0	122.1		
14:15	458.97	106.9	111.6	108.1	120.7		
14:30	494.03	107.4	111.8	108.4	120.9		
14:45	310.55	107.7	111.9	108.3	119.6		
15:00	257.15	105.7	109.0	104.2	115.1		
15:15	353.26	104.7	107.8	103.1	113.9		
15:30	284.49	105.2	108.4	104.0	115.0		
15:45	302.46	104.9	108.2	102.9	114.0		
16:00	191.49	103.6	106.4	101.5	111.3		
16:15	96.15	100.3	102.4	97.1	105.4		
16:30	44.05	96.4	97.5	92.0	98.7		
16:45	22.16	93.0	93.3	87.1	93.1		
17:00	33.75	90.1	90.2	83.6	89.0		

17:15	55.11	88.4	88.4	81.3	86.6		
17:30	106.54	86.7	87.0	81.0	85.9		
17:45	121.25	85.6	85.9	80.7	87.4		
18:00	93.94	84.5	84.9	80.1	88.6		
18:15	61.79	82.9	83.6	78.4	85.8		
18:30	32.65	81.5	81.8	76.7	82.7		
18:45	13.78	79.8	79.6	74.8	79.5		
19:00	6.06	78.3	78.3	72.4	75.4		
19:15	0.57	77.1	77.0	70.1	71.8		
19:30	0.57	74.1	75.2	67.5	67.3	28.2	40.6
19:45		67.7	68.8	61.4	63.6	28.7	34.8
20:00		63.2	64.3	57.6	61.0	28.4	34.0
20:15		59.9	60.9	55.3	58.3	28.1	33.8
20:30		57.5	58.6	54.7	55.3	28.5	32.5
20:45		56.4	57.2	52.2	53.7	28.0	31.7
21:00		55.9	56.1	51.6	51.1	29.0	31.9
21:15		55.2	55.9	50.1	49.6	28.3	30.9
21:30		54.5	55.3	50.3	47.8	28.3	31.7
21:45		54.7	55.1	50.1	46.0	27.7	30.6
22:00		54.6	54.1	49.7	45.0	28.6	31.6
22:15		54.6	54.0	49.3	43.4	27.7	31.6
22:30		54.4	54.0	49.0	42.6	27.7	30.7
22:45		54.8	53.3	48.2	41.5	28.0	29.9
23:00		54.7	53.5	48.5	40.2	28.6	30.7
23:15		54.3	53.8	48.4	39.2	28.3	31.0
23:30		54.2	53.7	47.3	38.8	28.1	29.9

Table E. 10: Data of run 10.

<i>Time</i>	<i>I</i>	<i>T_{PCM}</i>	<i>T_{HPE}</i>	<i>T_{HPA}</i>	<i>T_{HPC}</i>	<i>T_{w,in}</i>	<i>T_{w,out}</i>
6:30	1.67	52.8	53.3	43.2	31.8		
6:45	1.67	52.4	51.6	42.8	31.0		
7:00	1.67	52.5	52.4	45.4	31.3		
7:15	0.09	52.5	52.8	45.2	31.3		
7:30	20.83	52.3	52.4	45.1	32.5		
7:45	46.61	52.2	52.3	46.0	34.7		
8:00	71.08	52.4	52.2	46.0	38.7		
8:15	152.97	52.7	52.4	47.5	44.0		
8:30	109.72	52.3	52.3	48.9	52.5		
8:45	278.26	53.1	53.3	50.8	59.0		
9:00	344.89	54.3	54.9	53.4	74.8		
9:15	413.15	64.8	70.3	68.3	82.1		
9:30	471.32	69.8	75.6	75.7	85.8		
9:45	532.58	74.3	80.2	81.3	92.6		
10:00	570.26	78.6	84.0	86.2	99.0		
10:15	647.49	82.5	88.6	90.5	104.3		
10:30	671.93	86.5	93.0	93.3	109.9		
10:45	746.89	89.2	96.6	98.0	114.2		
11:00	804.29	93.6	101.8	101.2	120.0		
11:15	846.00	98.2	106.2	106.1	124.9		
11:30	872.20	102.8	111.3	112.3	129.9		
11:45	978.94	108.2	117.0	120.0	135.2		
12:00	954.30	110.4	118.5	117.3	134.8		
12:15	993.83	109.6	116.3	105.8	128.3		
12:30	1056.18	115.0	123.2	122.2	138.5		
12:45	1055.78	122.9	131.7	130.0	150.2		
13:00	1075.00	127.3	135.3	129.9	153.7		
13:15	1062.86	123.9	129.8	112.2	143.1		
13:30	1072.23	129.1	136.1	131.4	152.0		
13:45	1025.50	129.8	136.1	131.6	149.9		
14:00	1016.67	133.4	140.3	130.1	156.0		
14:15	1078.17	136.2	143.6	139.0	159.8		
14:30	1100.83	132.9	137.7	125.8	149.1		
14:45	815.57	131.8	136.6	124.1	146.5		
15:00	294.50	128.9	132.3	113.0	138.9		
15:15	262.05	130.6	134.9	132.5	143.8		
15:30	656.38	127.1	130.3	127.0	136.4		
15:45	273.53	124.8	127.4	110.4	131.8		
16:00	289.75	128.8	133.1	116.5	141.9		
16:15	175.27	125.5	127.9	116.5	133.5		
16:30	262.44	121.3	123.3	105.3	126.7		
16:45	487.52	125.1	128.2	121.0	135.7		
17:00	263.83	125.6	128.6	123.3	136.6		

17:15	356.46	125.0	128.1	123.9	135.4		
17:30	154.97	121.7	123.9	118.7	128.3		
17:45	133.55	117.4	118.9	111.8	121.1		
18:00	224.31	115.1	116.1	109.5	118.5		
18:15	179.00	113.0	113.8	96.3	115.7		
18:30	119.04	110.5	111.0	94.7	111.9		
18:45	61.24	107.6	108.1	100.3	107.4		
19:00	10.29	104.8	104.7	84.8	102.1		
19:15	0.15	103.2	103.1	82.8	95.8		
19:30	0.15	95.4	97.0	77.3	78.8	28.3	62.4
19:45		84.6	86.6	72.2	74.7	27.8	44.3
20:00		76.9	78.5	65.2	70.7	27.7	41.8
20:15		71.1	72.2	64.3	67.2	28.2	38.5
20:30		65.9	67.6	59.0	64.2	27.5	38.2
20:45		62.1	63.1	59.6	61.8	28.4	36.5
21:00		59.7	60.2	54.3	58.6	27.8	36.2
21:15		57.5	58.0	52.5	56.2	28.4	36.0
21:30		56.7	57.4	50.6	54.0	28.1	33.5
21:45		56.1	56.7	51.8	51.6	28.2	34.2
22:00		55.2	55.3	50.1	50.3	28.0	34.1
22:15		55.3	55.3	49.3	48.2	28.3	34.2
22:30		54.7	54.7	49.4	46.6	28.2	34.0
22:45		54.6	54.4	49.6	45.3	28.3	34.0
23:00		54.2	54.2	49.0	44.6	28.3	32.5
23:15		54.7	53.8	48.6	43.8	28.4	33.2
23:30		54.5	54.2	48.9	42.6	28.0	31.6

Table E. 11: Data of run 11.

<i>Time</i>	<i>I</i>	<i>T_{PCM}</i>	<i>T_{HPE}</i>	<i>T_{HPA}</i>	<i>T_{HPC}</i>	<i>T_{w,in}</i>	<i>T_{w,out}</i>
6:30	1.67	51.8	51.8	44.8	30.4		
6:45	1.67	52.0	51.7	44.3	30.1		
7:00	1.67	51.9	51.8	44.2	30.0		
7:15	1.67	51.7	51.5	44.1	29.9		
7:30	19.58	51.6	51.5	44.9	30.8		
7:45	46.26	51.6	51.8	45.0	33.5		
8:00	78.20	51.4	51.3	45.7	37.6		
8:15	163.17	51.5	51.5	46.6	43.3		
8:30	128.01	51.8	52.1	48.0	53.7		
8:45	284.07	51.8	52.0	50.7	59.0		
9:00	366.85	53.0	53.6	52.4	73.7		
9:15	445.61	64.5	70.0	67.8	78.5		
9:30	557.41	69.8	75.7	76.0	87.0		
9:45	443.94	74.0	80.2	80.8	93.3		
10:00	536.87	76.1	81.9	83.1	95.5		
10:15	560.86	78.7	84.4	84.3	97.4		
10:30	730.68	85.1	91.7	91.8	107.3		
10:45	765.91	89.3	96.7	96.9	114.3		
11:00	796.15	92.1	100.8	101.1	118.9		
11:15	856.80	94.4	103.6	103.6	121.9		
11:30	877.99	97.1	106.6	106.9	124.9		
11:45	933.05	98.8	106.7	106.3	122.7		
12:00	942.99	103.8	112.3	111.7	129.2		
12:15	934.25	105.2	112.4	111.6	127.9		
12:30	1038.80	111.4	119.7	118.5	137.4		
12:45	1038.99	115.7	124.0	122.5	141.4		
13:00	1106.00	118.9	125.7	124.5	143.3		
13:15	1142.42	117.7	123.1	121.4	136.9		
13:30	1220.88	119.8	125.0	123.1	139.6		
13:45	1149.10	123.8	130.2	126.8	145.4		
14:00	1070.78	123.5	128.9	125.5	141.4		
14:15	1043.53	129.4	136.4	133.0	152.1		
14:30	1022.09	131.4	138.3	134.8	154.0		
14:45	1009.25	136.8	144.3	142.5	161.9		
15:00	1011.37	138.1	145.3	139.9	162.0		
15:15	938.07	139.6	146.8	143.0	162.7		
15:30	896.25	135.4	140.2	136.0	150.7		
15:45	821.45	140.5	147.1	141.9	160.9		
16:00	754.55	142.3	148.3	143.7	162.7		
16:15	694.92	144.2	150.2	145.7	164.2		
16:30	617.84	145.0	150.3	143.9	163.5		
16:45	554.30	145.1	149.9	134.9	162.1		
17:00	497.07	144.2	148.2	134.3	160.2		

17:15	437.56	143.6	147.0	140.1	158.0		
17:30	360.18	141.7	145.0	128.5	153.7		
17:45	205.02	136.7	138.7	120.8	142.7		
18:00	112.21	130.5	130.9	113.8	131.3		
18:15	67.89	126.1	126.1	107.5	123.0		
18:30	56.78	122.9	122.6	104.4	117.1		
18:45	35.18	120.5	120.4	102.9	111.2		
19:00	12.39	118.0	117.5	97.3	105.2		
19:15	1.01	115.6	115.7	95.5	98.9		
19:30	1.01	104.4	106.1	89.9	76.1	27.9	52.7
19:45		91.9	94.2	82.7	71.9	28.0	45.8
20:00		82.6	84.7	75.8	68.8	27.9	43.2
20:15		75.0	77.5	70.5	65.9	27.8	39.7
20:30		69.3	71.2	65.3	62.6	27.7	38.0
20:45		64.9	66.0	61.8	59.8	28.1	37.6
21:00		61.3	62.6	58.4	57.2	28.3	36.8
21:15		58.6	59.7	55.8	55.0	28.4	34.1
21:30		57.6	58.1	54.5	53.1	28.0	34.9
21:45		56.8	57.1	52.7	51.3	27.9	33.1
22:00		56.0	56.4	52.1	49.3	28.0	33.7
22:15		55.6	55.2	50.7	47.8	27.5	33.0
22:30		54.7	54.8	50.2	46.0	27.7	32.9
22:45		54.9	54.8	49.7	44.4	28.2	32.5
23:00		54.6	54.4	49.6	43.7	28.2	32.3
23:15		54.4	54.5	49.4	43.0	28.1	33.0
23:30		54.4	54.5	49.4	43.0	28.1	33.0

Table E. 12: Data of run 12.

<i>Time</i>	<i>I</i>	<i>T_{PCM}</i>	<i>T_{HPE}</i>	<i>T_{HPA}</i>	<i>T_{HPC}</i>	<i>T_{w,in}</i>	<i>T_{w,out}</i>
6:30	1.67	58.6	59.0	50.4	32.0		
6:45	1.67	58.2	58.6	49.8	31.9		
7:00	1.67	57.6	57.9	49.0	31.8		
7:15	1.67	57.3	57.5	49.3	31.4		
7:30	16.26	56.5	56.8	49.0	32.2		
7:45	40.32	56.4	56.4	48.9	34.5		
8:00	63.30	55.7	56.0	48.8	37.7		
8:15	174.79	55.7	55.6	50.0	43.1		
8:30	104.18	55.5	55.7	51.1	53.0		
8:45	296.68	55.4	55.8	51.7	58.5		
9:00	380.30	55.9	56.4	55.1	75.2		
9:15	443.17	63.5	66.4	67.9	84.0		
9:30	484.19	71.3	72.8	76.1	88.0		
9:45	548.11	76.6	77.7	81.3	94.7		
10:00	585.87	82.5	84.1	88.0	102.2		
10:15	632.93	88.0	89.2	93.9	108.7		
10:30	712.05	93.4	94.9	99.4	115.9		
10:45	763.14	98.9	100.3	104.3	122.5		
11:00	793.36	104.2	106.0	110.1	129.4		
11:15	797.52	108.5	110.4	114.6	133.2		
11:30	898.25	112.5	114.4	117.6	137.1		
11:45	967.11	118.0	120.3	124.2	144.7		
12:00	921.32	123.7	126.3	129.5	151.7		
12:15	1043.22	124.8	126.1	127.8	149.1		
12:30	1078.75	128.1	130.0	126.2	152.4		
12:45	1140.06	133.1	134.4	136.2	157.3		
13:00	1100.07	134.3	136.0	135.5	156.1		
13:15	1156.50	133.9	135.4	133.3	152.0		
13:30	1160.19	133.5	134.6	131.9	148.6		
13:45	1184.54	136.2	137.9	134.3	153.4		
14:00	1048.74	142.7	145.2	144.1	165.5		
14:15	1076.30	143.3	145.5	142.8	163.8		
14:30	1075.20	140.9	142.6	138.4	155.5		
14:45	1108.68	141.8	143.3	139.3	155.9		
15:00	1038.52	139.4	140.6	135.8	150.4		
15:15	966.29	138.8	140.3	125.7	150.1		
15:30	900.58	139.3	141.2	135.7	152.2		
15:45	756.60	144.6	146.9	143.5	163.0		
16:00	811.98	145.1	147.2	142.7	162.3		
16:15	709.38	147.8	150.5	147.4	167.1		
16:30	716.81	145.0	146.4	141.4	158.0		
16:45	579.09	148.2	150.1	144.6	164.0		
17:00	507.22	148.5	150.2	146.1	164.5		

17:15	442.35	148.1	149.5	145.2	162.7		
17:30	386.91	146.9	148.5	140.9	159.1		
17:45	323.47	143.3	143.9	136.7	149.8		
18:00	257.27	137.6	137.2	129.2	138.9		
18:15	63.28	134.3	134.1	121.6	130.7		
18:30	91.58	131.5	131.3	117.7	124.6		
18:45	64.84	129.2	128.8	114.1	119.7		
19:00	34.39	127.2	126.6	111.0	114.3		
19:15	5.46	124.8	124.4	107.3	107.5		
19:30	0.46	118.0	119.1	101.3	91.4	27.8	56.2
19:45		102.3	104.1	92.7	85.9	28.4	45.4
20:00		90.5	92.1	83.0	81.0	28.4	41.8
20:15		81.3	83.4	75.8	76.6	28.2	39.3
20:30		74.3	75.7	69.5	72.3	28.1	37.3
20:45		68.4	69.8	65.1	68.6	27.6	37.0
21:00		64.1	65.3	61.2	65.2	27.5	34.3
21:15		60.6	62.2	58.0	62.1	28.1	34.7
21:30		58.2	59.6	55.5	59.0	27.6	33.7
21:45		57.1	58.1	54.1	56.3	27.8	32.8
22:00		56.4	57.0	53.2	54.1	27.5	32.6
22:15		55.9	56.2	51.7	52.0	28.3	32.6
22:30		55.4	55.6	51.3	50.1	27.5	32.5
22:45		54.8	54.8	51.0	48.1	27.5	31.7
23:00		54.7	54.9	49.9	46.7	28.4	31.7
23:15		54.2	54.7	49.4	45.4	28.4	31.7
23:30		54.5	54.1	48.7	43.6	28.2	30.5

APPENDIX F: TABLES OF DATA OF CHAPTER 6

Table F. 1: Data for run 1.

<i>Time</i>	<i>I</i>	<i>T_{amb}</i>	<i>T_{pcm,m}</i>	<i>T_{pcm,b}</i>	<i>T_{w,i}</i>	<i>T_{w,o}</i>
7:00	0.0	28.2	60.4	57.5	28.5	41.7
7:15	0.0	28.5	59.7	57.4	29.0	39.1
7:30	0.0	29.2	57.8	56.1	29.0	38.1
7:45	21.3	29.7	56.8	55.0	29.0	37.0
8:00	98.1	30.4	56.6	54.3	29.0	36.5
8:15	162.3	31.1	57.9	53.9	29.0	36.4
8:30	229.7	31.9	60.2	53.7	29.0	36.6
8:45	293.1	33.5	62.1	53.7	29.0	37.5
9:00	356.7	33.6	64.5	53.8	29.5	29.5
9:15	397.5	34.2	70.2	53.8		
9:30	494.8	35.3	74.7	53.8		
9:45	572.2	35.6	77.0	53.8		
10:00	569.0	36.5	80.0	53.8		
10:15	686.1	36.0	83.0	53.8		
10:30	720.0	36.5	85.8	53.8		
10:45	718.0	36.9	88.4	53.8		
11:00	725.0	37.0	90.9	53.8		
11:15	742.8	38.2	93.3	53.8		
11:30	750.0	37.3	95.7	53.8		
11:45	741.7	38.1	98.0	53.8		
12:00	770.0	38.0	100.6	53.8	29.5	50.0
12:15	785.0	38.1	95.4	53.8	29.5	54.5
12:30	795.0	37.9	92.9	53.9	29.5	54.7
12:45	810.0	39.2	91.2	54.0	29.5	54.1
13:00	844.0	39.0	90.0	54.1	29.5	53.8
13:15	873.9	39.3	89.4	54.2	29.5	54.0
13:30	980.0	38.2	89.1	54.3	29.5	53.9
13:45	1030.6	38.7	88.8	54.7	29.5	53.5
14:00	991.6	40.5	94.4	55.5		
14:15	961.0	39.7	100.2	56.3		
14:30	995.1	39.4	105.4	57.2		
14:45	938.5	41.0	110.1	58.3		
15:00	900.0	39.8	114.1	59.7		
15:15	882.7	39.6	117.8	61.2		
15:30	760.0	37.8	121.2	62.8		
15:45	841.4	38.4	122.1	64.5		

16:00	782.3	38.6	123.6	66.4		
16:15	711.5	39.0	125.7	68.3		
16:30	641.5	39.2	128.0	70.3		
16:45	552.5	37.6	130.2	72.2		
17:00	484.5	35.2	125.2	74.0	29.5	70.2
17:15	473.3	35.3	112.8	75.4	29.5	63.4
17:30	323.7	34.8	105.6	75.3	29.5	60.0
17:45	220.0	34.3	99.6	73.5	29.5	57.2
18:00	285.9	34.8	94.2	71.1	29.5	55.3
18:15	256.7	34.3	90.0	68.5	29.5	53.6
18:30	199.0	34.6	86.4	65.9	29.0	52.0
18:45	47.4	33.3	82.9	63.6	29.0	51.1
19:00	17.7	32.7	79.0	61.3	29.0	49.1
19:15	8.0	32.6	74.9	59.2	29.0	47.3
19:30	8.0	32.4	71.1	57.4	29.0	45.7
19:45	8.0	30.8	67.4	56.0	29.0	44.4
20:00	8.0	29.9	64.3	55.0	29.0	42.9

University of Malaya

Table F. 2: Data for run 2.

<i>Time</i>	<i>I</i>	<i>T_{amb}</i>	<i>T_{pcm,m}</i>	<i>T_{pcm,b}</i>	<i>T_{w,i}</i>	<i>T_{w,o}</i>
7:00	0.0	25.0	67.5	61.8	29.1	39.5
7:15	11.9	25.6	64.3	60.6	29.1	39.1
7:30	35.8	26.2	61.2	59.3	29.4	38.8
7:45	95.4	26.5	58.6	57.5	29.7	38.1
8:00	83.4	26.8	57.2	56.0	30.0	37.7
8:15	95.4	27.1	56.3	55.0	29.0	35.3
8:30	286.1	27.3	55.7	54.4	29.0	34.7
8:45	43.0	27.6	55.2	54.1	29.0	34.5
9:00	47.0	27.9	55.0	54.0		
9:15	49.1	28.1	54.9	54.0		
9:30	70.6	28.1	54.9	53.9		
9:45	84.8	28.3	54.9	53.9		
10:00	105.3	28.3	55.0	53.8		
10:15	140.5	28.3	55.1	53.8		
10:30	130.1	28.3	55.4	53.7		
10:45	131.4	28.4	55.7	53.6		
11:00	115.3	28.5	55.9	53.6		
11:15	91.1	28.8	56.1	53.5		
11:30	111.7	29.0	56.3	53.5		
11:45	170.3	29.3	56.6	53.4		
12:00	195.0	29.4	56.9	53.4	29.0	38.3
12:15	188.1	29.8	57.4	53.3	29.0	36.9
12:30	237.5	30.2	57.8	53.3	29.0	36.5
12:45	275.9	30.0	58.3	53.2	29.0	36.3
13:00	231.3	30.5	58.8	53.2	29.0	36.3
13:15	250.0	30.1	59.5	53.0	29.0	36.2
13:30	170.6	30.0	59.6	53.0	29.0	36.3
13:45	159.8	29.9	59.4	52.9	29.0	36.1
14:00	167.6	30.1	59.2	52.8		
14:15	158.1	30.3	59.2	52.7		
14:30	163.0	30.0	59.2	52.7		
14:45	114.4	30.2	60.0	52.6		
15:00	136.0	30.7	60.7	52.5		
15:15	219.2	30.6	61.4	52.4		
15:30	188.5	30.6	62.2	52.4		
15:45	187.5	30.8	62.8	52.3		
16:00	223.9	30.7	63.5	52.2		
16:15	197.6	30.4	64.3	52.2		
16:30	149.4	30.1	64.8	52.1		
16:45	123.1	30.1	65.0	52.0		
17:00	111.2	29.4	64.9	51.9	29.0	40.3

17:15	39.7	29.2	61.6	51.8	29.0	39.0
17:30	9.0	27.1	59.2	51.7	29.0	36.8
17:45	9.0	26.2	57.5	51.5	29.0	35.1
18:00	9.0	26.0	56.8	51.4	29.0	34.6
18:15	9.0	25.5	56.0	51.3	29.8	33.2
18:30	9.0	25.5	55.3	51.1	29.7	32.6
18:45	9.0	25.8	54.9	51.1	29.6	32.4
19:00	2.5	25.9	54.6	51.0	29.5	32.4
19:15	2.5	26.0	54.5	50.9	29.5	31.8
19:30	2.5	25.8	54.3	50.9	29.4	31.6
19:45	2.5	25.7	54.3	50.8	29.3	31.4
20:00	2.5	25.6	54.3	50.7	29.3	31.3

University of Malaysia

Table F. 3: Data for run 3.

<i>Time</i>	<i>I</i>	<i>T_{amb}</i>	<i>T_{pcm,m}</i>	<i>T_{pcm,b}</i>	<i>T_{w,i}</i>	<i>T_{w,o}</i>
7:00	0.0	27.6	74.1	65.6	28.8	52.7
7:15	0.0	28.0	68.7	63.4	29.0	51.2
7:30	0.0	28.8	64.4	58.9	29.7	48.2
7:45	0.0	29.0	60.7	57.3	29.0	45.3
8:00	37.9	31.1	58.0	54.7	29.0	43.0
8:15	121.0	28.1	57.5	52.4	29.0	42.8
8:30	189.5	30.2	58.4	51.9	29.0	42.4
8:45	256.7	30.7	59.9	50.7	29.0	41.7
9:00	328.4	30.4	61.1	50.0		
9:15	393.0	30.0	66.6	50.1		
9:30	456.0	31.0	71.7	49.8		
9:45	526.0	31.9	76.0	50.2		
10:00	578.0	30.7	80.0	49.2		
10:15	626.6	31.2	82.3	48.7		
10:30	695.9	31.9	84.7	48.6		
10:45	747.0	32.4	87.1	49.0		
11:00	812.4	30.9	89.4	48.4		
11:15	859.4	31.7	91.7	47.4		
11:30	895.4	32.0	94.0	48.7		
11:45	940.6	32.0	96.2	47.9		
12:00	968.0	33.6	97.0	48.2	29.5	55.5
12:15	997.6	31.1	92.7	48.6	29.5	55.0
12:30	1023.2	33.5	90.2	49.3	29.5	53.6
12:45	1037.7	33.7	89.0	49.1	29.5	53.9
13:00	1053.5	34.0	88.1	49.5	29.5	53.2
13:15	1063.9	34.7	87.4	49.4	29.5	54.9
13:30	1066.2	35.0	87.0	48.8	29.5	53.7
13:45	1069.1	34.8	87.1	49.3	29.5	54.2
14:00	1045.6	33.8	88.7	50.5		
14:15	1052.1	34.9	96.4	49.8		
14:30	1056.4	35.6	101.6	50.1		
14:45	1051.6	36.5	105.7	49.6		
15:00	426.7	34.5	107.8	50.2		
15:15	269.9	34.0	108.2	50.1		
15:30	184.4	35.8	107.4	49.9		
15:45	173.2	35.8	106.5	51.1		
16:00	191.3	32.2	105.9	51.8		
16:15	184.5	31.9	104.6	51.8		
16:30	139.0	32.7	104.6	52.9		
16:45	168.5	31.6	105.3	53.0		
17:00	184.3	31.2	101.2	53.8	29.0	59.8

17:15	79.4	32.2	92.5	53.9	29.5	55.7
17:30	111.2	33.2	86.4	52.4	29.5	54.7
17:45	170.9	34.1	81.9	50.2	29.0	50.9
18:00	115.9	30.7	78.0	48.5	29.0	47.8
18:15	80.3	31.7	74.4	47.1	29.0	46.6
18:30	61.3	32.0	71.2	45.1	29.0	43.7
18:45	21.9	31.1	68.1	43.9	29.0	43.3
19:00	15.8	30.3	66.3	43.6	29.0	41.8
19:15	7.7	30.6	64.3	42.8	29.0	41.2
19:30	7.7	29.9	62.8	42.5	29.0	40.9
19:45	7.7	29.3	61.0	42.5	29.0	40.4
20:00	7.7	29.7	59.6	42.3	29.0	39.3

University of Malaysia

Table F. 4: Data for run 4.

<i>Time</i>	<i>I</i>	<i>T_{amb}</i>	<i>T_{pcm,m}</i>	<i>T_{pcm,b}</i>	<i>T_{w,i}</i>	<i>T_{w,o}</i>
7:00	0.0	27.7	75.1	71.5	28.7	47.4
7:15	0.0	27.8	70.2	68.5	29.0	45.2
7:30	0.0	28.2	66.2	64.3	29.0	43.1
7:45	0.0	28.5	62.8	60.5	29.0	41.1
8:00	0.0	28.9	60.1	57.8	29.0	39.8
8:15	11.1	29.3	58.1	56.3	29.0	38.9
8:30	41.9	29.4	57.0	55.3	29.0	37.8
8:45	72.2	29.8	56.4	54.7	29.0	37.0
9:00	112.8	29.7	56.1	54.2		
9:15	128.0	29.5	55.8	54.0		
9:30	126.4	29.9	55.8	53.9		
9:45	139.2	30.4	56.0	53.9		
10:00	111.6	30.4	56.4	53.9		
10:15	84.5	31.0	57.1	53.8		
10:30	145.2	31.0	57.8	53.8		
10:45	248.2	31.0	58.5	53.8		
11:00	237.9	31.3	59.6	53.7		
11:15	258.2	31.3	60.7	53.7		
11:30	337.4	31.3	61.8	53.7		
11:45	306.8	31.6	62.9	53.6		
12:00	300.4	31.6	63.7	53.6	29.0	41.4
12:15	322.0	32.0	62.5	53.5	29.0	40.4
12:30	387.3	33.2	62.4	53.5	29.0	40.4
12:45	431.2	34.1	63.0	53.5	29.0	40.6
13:00	509.2	34.1	63.9	53.5	29.0	41.1
13:15	455.5	34.1	64.9	53.4	29.0	41.0
13:30	483.4	34.9	65.7	53.4	29.0	42.0
13:45	545.1	35.2	66.9	53.4	29.0	42.5
14:00	549.0	35.3	68.3	53.4		
14:15	523.3	35.1	73.0	53.3		
14:30	537.9	34.9	76.5	53.3		
14:45	507.8	34.9	79.2	53.2		
15:00	425.2	35.1	80.8	53.2		
15:15	433.2	34.7	82.8	53.1		
15:30	476.5	34.6	83.8	53.1		
15:45	508.1	35.5	85.5	53.1		
16:00	603.6	36.7	87.9	53.1		
16:15	501.6	35.3	90.6	53.1		
16:30	297.5	34.1	92.2	53.1		
16:45	219.4	34.3	92.8	53.0		
17:00	300.8	33.7	93.1	53.0	29.5	52.6

17:15	209.4	33.7	85.2	53.1	29.0	49.2
17:30	206.6	33.8	80.3	53.1	29.0	47.5
17:45	227.4	33.4	78.0	53.0	29.0	46.5
18:00	88.5	32.7	74.8	53.0	29.0	44.9
18:15	40.9	32.2	71.5	53.0	29.0	43.2
18:30	20.8	31.9	68.8	52.9	29.0	42.4
18:45	16.9	31.6	66.2	52.9	29.0	41.4
19:00	2.4	31.5	63.5	52.8	29.0	40.5
19:15	2.4	31.2	61.1	52.8	29.0	39.4
19:30	2.4	31.0	58.9	52.8	29.0	38.5
19:45	2.4	30.7	57.4	52.8	29.0	38.8
20:00	2.4	30.6	56.5	52.7	29.0	37.8

University of Malaysia

Table F. 5: Data for run 5.

<i>Time</i>	<i>I</i>	<i>T_{amb}</i>	<i>T_{pcm,m}</i>	<i>T_{pcm,b}</i>	<i>T_{w,i}</i>	<i>T_{w,o}</i>
7:00	0.0	27.4	54.3	49.3	27.0	36.2
7:15	0.0	27.8	54.3	49.3	29.6	35.1
7:30	0.0	27.8	54.3	49.3	29.8	34.8
7:45	10.3	27.8	54.2	49.3	30.0	34.5
8:00	56.5	27.7	54.3	49.3	29.0	34.0
8:15	97.3	27.6	54.2	49.3	29.0	33.8
8:30	144.8	28.3	54.2	49.3	29.0	33.9
8:45	203.6	29.1	54.2	49.3	29.0	33.8
9:00	263.6	29.2	54.2	49.3		
9:15	315.9	29.4	54.4	49.3		
9:30	351.2	29.2	57.3	49.3		
9:45	421.3	30.6	60.1	49.2		
10:00	491.2	30.2	61.6	49.2		
10:15	511.3	30.9	63.8	49.1		
10:30	565.4	32.5	69.4	49.2		
10:45	637.1	31.8	74.7	49.1		
11:00	685.8	30.8	79.9	49.1		
11:15	778.1	30.8	85.2	49.1		
11:30	821.0	30.1	90.5	49.2		
11:45	859.0	32.0	95.6	49.2		
12:00	869.0	31.9	99.2	49.3	30.0	48.1
12:15	806.2	32.6	96.3	49.4	29.0	52.6
12:30	848.4	32.3	94.7	49.4	29.0	54.1
12:45	935.2	32.5	94.1	49.6	29.5	54.4
13:00	990.0	33.6	94.0	49.7	29.0	54.3
13:15	1013.3	33.2	93.3	49.8	29.5	55.5
13:30	275.7	33.1	92.5	49.9	29.0	54.6
13:45	331.1	35.0	89.6	50.0	29.0	54.7
14:00	265.4	35.3	87.7	50.0		
14:15	365.4	35.1	92.7	50.2		
14:30	989.4	35.8	96.4	50.4		
14:45	942.4	36.7	100.3	50.6		
15:00	952.4	34.5	105.0	50.8		
15:15	920.7	36.8	108.8	50.9		
15:30	810.0	35.4	112.2	51.1		
15:45	126.6	34.2	114.3	51.3		
16:00	83.8	34.5	114.2	51.4		
16:15	72.0	33.4	112.7	51.6		
16:30	69.4	31.5	110.6	51.9		
16:45	62.4	32.8	109.2	52.3		
17:00	459.0	32.5	108.7	52.9	29.5	52.5

17:15	405.0	32.5	101.6	53.7	29.0	47.9
17:30	352.7	31.8	97.3	54.7	29.0	45.3
17:45	95.3	33.3	94.0	56.4	29.0	42.7
18:00	57.0	31.8	89.4	59.6	29.0	40.1
18:15	58.3	33.8	84.6	61.5	29.0	38.9
18:30	138.3	32.3	80.2	62.2	29.0	37.7
18:45	47.1	31.6	76.8	62.0	29.0	36.5
19:00	14.2	31.6	73.5	61.2	29.0	35.3
19:15	14.2	29.8	70.2	60.0	29.0	34.5
19:30	14.2	30.6	67.0	58.8	29.0	33.6
19:45	14.2	30.0	64.0	57.3	29.0	32.1
20:00	14.2	29.7	61.3	55.9	29.0	30.5

University of Malaysia

Table F. 6: Data for run 6.

<i>Time</i>	<i>I</i>	<i>T_{amb}</i>	<i>T_{pcm,m}</i>	<i>T_{pcm,b}</i>	<i>T_{w,i}</i>	<i>T_{w,o}</i>
7:00	0.0	25.3	53.8	48.5	25.8	32.8
7:15	11.9	25.8	53.7	48.5	27.6	34.3
7:30	35.8	26.6	53.6	48.5	28.0	33.5
7:45	95.4	27.3	53.7	48.5	28.5	33.2
8:00	164.4	28.0	53.6	48.5	28.9	32.8
8:15	273.6	28.2	53.7	48.5	29.1	32.8
8:30	240.0	28.5	53.7	48.5	29.3	32.8
8:45	262.6	28.9	54.2	48.4	29.6	33.0
9:00	264.0	28.2	56.8	48.4		
9:15	285.2	28.8	57.9	48.3		
9:30	335.2	29.1	58.8	48.1		
9:45	413.0	30.1	59.1	48.1		
10:00	332.3	31.3	60.7	48.0		
10:15	190.0	30.2	63.4	47.9		
10:30	185.2	29.5	65.0	47.8		
10:45	166.2	29.2	65.4	47.7		
11:00	167.4	27.2	65.1	47.5		
11:15	159.7	28.9	65.2	47.4		
11:30	303.1	30.2	68.5	47.5		
11:45	714.1	29.8	72.5	47.5		
12:00	625.7	28.0	75.2	47.5	29.0	45.9
12:15	247.3	25.2	70.8	47.4	29.8	42.6
12:30	195.3	24.3	66.6	47.2	29.3	40.9
12:45	190.3	24.5	63.8	47.2	29.3	39.9
13:00	156.8	24.4	61.4	47.2	29.2	38.8
13:15	174.1	25.1	59.0	47.2	29.2	37.6
13:30	184.2	25.5	57.9	47.2	29.3	37.0
13:45	209.2	26.6	57.8	47.1	29.6	36.4
14:00	276.5	28.6	58.8	47.1		
14:15	345.9	29.8	62.0	47.0		
14:30	465.7	30.2	67.5	47.0		
14:45	618.9	29.7	70.5	47.0		
15:00	634.8	29.9	72.7	47.0		
15:15	465.1	30.1	74.6	46.9		
15:30	388.2	30.5	76.2	46.9		
15:45	375.3	30.5	77.7	46.9		
16:00	198.2	30.3	79.1	46.9		
16:15	180.7	30.3	80.3	46.9		
16:30	135.5	30.1	81.1	46.9		
16:45	80.2	30.0	81.6	46.8		
17:00	39.9	28.9	79.6	46.8	29.0	46.4

17:15	12.7	29.6	74.6	46.8	29.0	44.5
17:30	1.6	28.9	70.8	46.9	29.0	43.4
17:45	1.6	28.6	67.4	46.9	29.0	42.3
18:00	1.6	28.3	64.2	46.9	29.0	41.4
18:15	1.6	28.1	61.3	46.8	29.0	40.1
18:30	1.6	27.7	58.7	46.8	30.0	38.9
18:45	1.6	27.4	57.1	46.8	30.0	37.7
19:00	1.6	27.3	56.1	46.7	29.9	36.6
19:15	1.6	27.2	55.3	46.7	29.8	35.6
19:30	1.6	27.2	54.8	46.6	29.8	35.0
19:45	1.6	26.9	54.4	46.5	29.7	34.6
20:00	1.6	26.7	54.3	46.4	29.7	34.3

University of Malaysia

Table F. 7: Data for run 7.

<i>Time</i>	<i>I</i>	<i>T_{amb}</i>	<i>T_{pcm,m}</i>	<i>T_{pcm,b}</i>	<i>T_{w,i}</i>	<i>T_{w,o}</i>
7:00	0.0	26.2	54.0	49.9	28.2	34.5
7:15	35.8	26.5	53.5	49.5	28.2	34.3
7:30	95.4	26.7	53.0	49.2	28.2	34.1
7:45	135.7	27.2	52.6	49.0	29.5	33.8
8:00	163.6	28.5	52.7	49.1	29.0	33.3
8:15	252.6	29.7	52.6	49.0	29.0	33.7
8:30	376.1	30.9	52.7	49.0	29.0	34.3
8:45	467.1	32.0	52.8	48.9	29.0	34.8
9:00	580.4	32.5	57.6	49.8		
9:15	616.0	33.2	61.6	49.7		
9:30	549.8	33.5	64.2	49.7		
9:45	647.4	34.0	66.1	49.6		
10:00	553.3	33.9	67.1	49.6		
10:15	603.9	34.0	67.8	49.6		
10:30	676.6	34.7	68.2	49.5		
10:45	652.4	35.2	68.6	49.5		
11:00	666.2	35.5	69.2	49.4		
11:15	751.0	35.8	70.0	49.4		
11:30	739.9	36.3	73.7	49.3		
11:45	770.9	36.4	77.8	49.3		
12:00	710.0	35.3	76.9	48.3	30.0	45.6
12:15	740.6	36.2	75.7	48.3	29.0	45.5
12:30	784.8	36.6	76.4	48.3	29.0	45.6
12:45	776.3	37.4	76.1	48.2	29.0	45.5
13:00	789.1	35.9	76.6	48.3	29.0	46.2
13:15	845.9	38.2	76.7	48.3	29.5	46.9
13:30	889.3	37.5	78.8	48.4	29.5	47.3
13:45	878.0	38.2	79.3	48.5	29.5	47.6
14:00	888.9	38.5	80.0	48.6		
14:15	843.0	38.3	86.3	48.6		
14:30	818.5	38.4	90.2	48.7		
14:45	892.9	37.4	93.3	48.7		
15:00	823.9	38.6	96.0	48.8		
15:15	254.8	36.7	98.9	48.9		
15:30	232.0	36.6	99.7	48.9		
15:45	208.6	35.8	99.0	49.0		
16:00	211.5	36.2	98.1	49.1		
16:15	218.0	36.2	97.3	49.2		
16:30	231.5	34.7	96.7	49.4		
16:45	167.2	33.8	95.3	49.4		
17:00	133.2	34.0	91.6	49.5	29.5	51.7

17:15	62.0	33.1	84.3	49.6	29.0	48.4
17:30	14.2	31.3	79.0	49.7	29.0	45.7
17:45	6.2	29.1	74.4	49.6	29.0	42.9
18:00	6.2	29.0	70.3	49.6	29.0	41.6
18:15	6.2	28.7	66.7	49.7	29.0	40.2
18:30	6.2	29.0	63.7	49.8	29.0	39.4
18:45	6.2	28.5	61.1	49.9	29.0	38.4
19:00	6.2	28.5	58.9	50.0	29.0	37.0
19:15	6.2	26.7	57.3	50.0	29.0	36.0
19:30	6.2	26.9	56.4	50.0	29.0	35.1
19:45	6.2	26.9	55.8	50.0	29.0	35.0
20:00	6.2	27.0	55.6	50.0	29.0	36.8

University of Malaysia

Table F. 8: Data for run 8.

<i>Time</i>	<i>I</i>	<i>T_{amb}</i>	<i>T_{pcm,m}</i>	<i>T_{pcm,b}</i>	<i>T_{w,i}</i>	<i>T_{w,o}</i>
7:00	0.0	27.7	54.0	51.9	28.0	39.4
7:15	11.9	27.9	54.0	51.9	29.0	38.0
7:30	45.8	28.3	54.0	51.9	29.0	36.9
7:45	90.4	28.7	53.9	51.9	29.0	36.3
8:00	113.4	29.3	54.0	51.9	29.0	35.9
8:15	160.6	30.1	53.9	51.9	29.0	35.8
8:30	383.6	31.6	53.9	51.8	29.0	36.0
8:45	539.4	33.3	53.9	51.9	29.0	36.3
9:00	572.8	33.4	55.1	51.9		
9:15	621.8	34.5	59.4	51.9		
9:30	654.4	35.3	61.5	51.9		
9:45	666.1	35.9	62.5	51.9		
10:00	670.8	36.1	63.4	51.9		
10:15	432.9	35.9	65.2	51.9		
10:30	384.4	36.0	69.0	51.8		
10:45	376.3	36.0	72.7	51.8		
11:00	438.1	35.5	75.3	51.8		
11:15	625.4	34.7	77.4	51.7		
11:30	682.3	34.7	78.6	51.7		
11:45	504.2	34.7	79.5	51.6		
12:00	493.9	36.3	79.1	51.6	29.5	46.0
12:15	424.2	37.5	76.5	51.7	29.5	46.3
12:30	456.0	36.5	76.3	51.7	29.5	45.9
12:45	486.7	36.3	75.9	51.7	29.5	45.9
13:00	359.4	36.5	74.9	51.7	29.5	46.1
13:15	274.5	36.6	74.3	51.7	29.5	46.0
13:30	239.7	37.3	73.5	51.7	29.5	46.4
13:45	255.8	36.9	73.3	51.7	29.5	46.4
14:00	288.6	36.7	73.5	51.6		
14:15	294.3	36.5	77.0	51.6		
14:30	500.0	35.9	78.6	51.6		
14:45	533.2	35.1	79.3	51.6		
15:00	562.4	35.2	79.4	51.5		
15:15	560.7	35.6	79.3	51.5		
15:30	531.1	36.7	80.1	51.6		
15:45	599.3	36.3	82.1	51.7		
16:00	378.1	37.6	86.0	51.8		
16:15	215.6	36.7	90.3	51.8		
16:30	120.6	36.8	92.4	51.9		
16:45	88.7	36.5	95.1	51.9		
17:00	52.1	33.8	94.3	51.9	29.5	51.5

17:15	68.8	32.9	86.4	51.9	29.0	50.0
17:30	47.1	32.3	80.9	51.9	29.0	48.0
17:45	7.9	31.9	76.2	51.9	29.0	46.0
18:00	3.6	31.0	72.3	51.9	29.0	44.6
18:15	3.6	30.4	69.0	51.9	29.0	43.4
18:30	3.6	30.3	67.0	51.9	29.0	42.5
18:45	3.6	30.2	64.6	51.9	29.0	41.5
19:00	3.6	30.1	62.5	52.0	29.0	40.6
19:15	3.6	30.5	60.9	52.0	29.0	40.1
19:30	3.6	30.4	59.4	52.0	29.0	39.6
19:45	3.6	30.4	58.0	52.1	29.0	38.9
20:00	3.6	30.4	57.0	52.1	29.0	38.2

University of Malaysia